Université Fédérale
Toulouse Midi-Pyrénées

THÈSE

En vue de l'obtention du

DOCTORAT DE L'UNIVERSITÉ DE TOULOUSE

Délivré par :

Université Toulouse 3 Paul Sabatier (UT3 Paul Sabatier)

Si vous êtes en cotutelle internationale, remplissez ce champs en notant : Cotutelle internationale avec "nom de l'établissement", sinon effacer ce texte pour qu'il n'apparaisse pas à l'impression

---

Présentée et soutenue par :
Ana TRAPAIDZE

le mercredi 25 février 2015

Titre :

Integration of thrombin-binding aptamers in point-of-care devices for continuous monitoring of thrombin in plasma

---

École doctorale et discipline ou spécialité :
ED GEET : Micro et Nanosystèmes

Unité de recherche :
LAAS - CNRS

Directeur/trice(s) de Thèse :

Mme Anne-Marie Gué, Dr LAAS-CNRS

Jury :
Mme A. Varenne , Prof. ParisTech (Rapporteur)
MM T. Hianik , Prof. Comenius University in Bratislava (Rapporteur)
F. Couderc, Prof. Université P. Sabatier
J.M. Herbert, Dr, SANOFI
A. Bancaud, Dr LAAS-CNRS

"Life is journey, not a destination."
Ralph Waldo Emerson

"What matters in life is not what happens to you but what you remember and how you remember it."
Gabriel García Marquez

Acknowledgements

I would like to express my gratitude to my thesis director Dr. Anne-Marie GUE for offering me the opportunity to undertake this extremely interesting and challenging project at the honorable laboratory of LAAS-CNRS. I thank her for supervising my research work, for her valuable guidance, encouragement and trust.

I sincerely thank Dr. Aurelien BANCAUD for taking active part in my supervision, his constant and efficient presence, continuous support, motivation, enthusiasm, constructive guidelines throughout my thesis. I learned much from him.

I am immensely grateful to Marie BRUT for her contribution to this project, help in modeling experiments, fruitful discussions and support.

I wish to also thank the permanent members of N2IS group Anne HEMERYCK, George LANDA, Mehdi JAFARI, Alain ESTEVE, Carole ROSSI, Pier JOSEPH for providing with professionally enriching and welcoming atmosphere. Especially I would like to acknowledge Daniel ESTEVE for his brave vision, organizing inspiring meetings and outstanding managerial skills.

My gratitude is also for the staff of the laboratory, especially to Charline BLATCHE, Sandrine SOULEILLE and group TEAM for sharing their knowledge, their help and guidance with the equipment and clean room processes.

I would like to show great appreciation to all the colleagues at IPBS, LCC, CHU Rangueil, ITAV, Sanofi, University Paul Sabatier who provided to me scientific and technical assistance to carry out experiments at their facilities and helped to enrich my professional experiences.

I would like to thank my colleagues and friends Hubert RANCHON, Sebastian CARGOU, Sebastian MEANCE, Vincent PICOT, Marc FOUET, Cloe LANTHONY, Mehdi BAHRAMI, Ayse BERBER for their valuable discussions, encouragement, help, time and memorable moments in Toulouse.

Special thanks go to my dear friends Basudhara RANA and Yasmina GEHA for always being there for me, sharing sweetest and hardest moments, making every day an adventure. I think of them as my sisters.

I owe my deepest gratitude to my family for their unconditional love, support and care. I wouldn't have made this far without them. I thank my mother and father for inspiring me, shaping my individuality, believing in me and supporting me at each important stage of my life. I cannot find words to express my gratitude to my dearest friend and spouse Tornike MCHEDLISHVILI. Tornike has been true and great supporter and has unconditionally loved me during my good and bad times. His faith in me and my intellect gave me the force, confidence and determination to attain the goal. I thank Tornike for giving the most amazing present of my life: our wonderful daughter Katerina, who made our life even more joyful and colorful. I love you so much! Thank you for being part of my journey!!!

I dedicate this thesis
to my mother and father,
to my husband and daughter.

Integration of thrombin-binding aptamers in point-of-care devices for continuous monitoring of thrombin in plasma

Abstract of the PhD Thesis

Thrombin is the central enzyme in the process of hemostasis, being at the cross-roads of coagulation and platelet reactions. Normally, in vivo concentration of thrombin is rigorously regulated; however, clinically impaired or unregulated thrombin generation predisposes patients either to hemorrhagic or thromboembolic complications, the major causes of mortally in the US and Europe. Monitoring thrombin in real-time is therefore needed to enable rapid and accurate determination of drug administration strategy for patients under vital threat.

Aptamers, short single-stranded oligonucleotide ligands, selected for their high affinity and specificity, represent promising candidates as biorecognition elements for new-generation biosensors. Several aptamers have been developed for thrombin sensing. These aptamers are known to bind distinct exosites of thrombin that gives an advantage of building different assays involving simultaneous targeting two different binding sites. The aim of this PhD work therefore is to investigate different solutions for the integration of thrombin-binding aptamers in point-of-care devices for continuous monitoring of thrombin in plasma.

First the kinetics of aptamer interaction with thrombin and specificity towards prothrombin and thrombin – inhibitor complexes was rigorously investigated using Surface Plasmon Resonance. These experiments unveiled the complex character of interaction of the HD1 a 15-bp aptamer with thrombin, confirming nonspecific interactions with prothrombin, natural inhibitors of thrombin, serum albumin and some of other plasma proteins, whereas another 29-bp aptamer HD22 proved to be highly affine and specific towards thrombin. On the other hand we explored aptamer integration options. In order to find optimal surface functionalization conditions for aptamers sensing, different supports such as gold, polystyrene, polycarbonate and appropriate protocols were used. We found that the easiest and the most efficient functionalization strategy is grafting thiol-modified aptamers on the gold surface. Furthermore to achieve nanoscale control of functional aptamer density, we showed advantage of ordered immobilization of already DNA-capped nanoparticles and well-characterized on the desired solid support through convective assembly. Aptamer-modified Gold NP-s were also used to validate thrombin detection principle through hydrodynamic assay involving aggregation of NPs in the presence of the thrombin. With this assay, we validated the principle and at the same managed to detect different concentrations of thrombin (5-500 nM) with good precision, study the thermal stability of the aptamers and their complex with thrombin and specificity of aptamers towards thrombin in buffer. In diluted plasma, however aggregation of nanoparticles occurred even in the absence of thrombin, suggesting the presence of nonspecific interactions with aptamers that cannot be controlled or neglected in aggregation assay.

We finally proposed a novel approach to increase sensitivity and specificity for thrombin detection based on the engineering of aptadimer structures bearing aptamers HD1and HD22 interconnected with a nucleic acid spacer. This spacer forms a hairpin of 4 to 9 bp, and fluorophore and quencher couple is embedded within hairpin. In the absence of target, the fluorophore remains quenched, whereas upon capturing a target, fluorescent signal is triggered. Since this strategy requires simultaneous targeting of both binding-sites, it provides an efficient solution for improved thrombin detection, by increasing specificity, selectivity and affinity, and decreasing non-specific interactions. Preliminary tests gave promising results in specific detection for thrombin and opened new perspectives for development specific aptamer-based fluosensor both for the surface and the volume measurements.

L'étude de différentes solutions d'intégration des aptameres dans des dispositifs de diagnostic type « point of care » pour le suivi en continu de la thrombine dans le plasma

Résumé

La thrombine est l'enzyme principale dans le processus d'hémostase, étant impliquée dans la coagulation et les réactions plaquettaires. Les dérèglements de la concentration de thrombine en raison d'un trouble clinique prédisposent les patients à des complications hémorragiques ou thromboemboliques qui sont une cause de mortalité majeure en Europe et aux Etats-Unis. Le suivi en temps réel de la thrombine dans le sang est donc nécessaire pour améliorer le traitement de patients en état critique.

Les aptamères, qui sont de courts nucléotides monobrins, sélectionnés pour leur grande affinité et spécificité vers des cibles déterminées, semblent constituer des candidats prometteurs pour la reconnaissance moléculaire dans des biocapteurs de nouvelle génération. Plusieurs aptamères ont été développés pour la détection de la thrombine. L'objectif de ces travaux est l'étude de différentes solutions d'intégration des aptamères dans des dispositifs de diagnostic de type «point of care» (au chevet du patient) pour le suivi en continu de la thrombine dans le plasma.

Dans un premier temps, la cinétique d'interaction des aptamères avec la thrombine et leur spécificité vis-à-vis de la prothrombine et des inhibiteurs de la thrombine ont été étudiés rigoureusement par résonance par plasmons de surface (SPR). Ces travaux ont démontré la faible spécificité de l'aptamère HD1, qui un nucléotide de 15 bases, vis-à-vis de la thrombine, et ont confirmé le présence d'interactions non-spécifiques avec la prothrombine, les inhibiteurs naturels de la thrombine, l'albumine de bœuf et d'autres protéines plasmatiques. Inversement, nous avons observé une bonne affinité de l'aptamère HD22 avec la même liste de cible. Parallèlement, nous avons évalué des stratégies d'intégration d'aptamères dans des dispositifs d'analyse. Nous montrons en particulier que la technique le plus simple et le plus efficace de fonctionnalisations de surface par des aptamères est fondée sur le couplage de fonctions thiol sur des surfaces d'or. Le principe de reconnaissance a ensuite été validé par des expériences d'agrégation en régime hydrodynamique. Celles-ci ont montré la possibilité de détecter la thrombine dans des gammes de concentration de 5 à 500nM. Toutefois, dans du plasma, l'agrégation des nanoparticules a été observée en absence de thrombine suggérant la présence d'interactions non spécifiques.

Enfin, afin d'augmenter la spécificité de la détection de la thrombine, nous avons proposé une nouvelle approche basée sur l'ingénierie de structures dimères interconnectant HD1 et HD22. Le lien entre ces deux aptamères peut se replier suivant une structure en tête d'épingle, ce qui met à proximité un fluorophore et son absorbeur de fluorescence. En l'absence de cible, le fluorophore est éteint en raison de la proximité l'absorbeur, alors qu'après capture de la cible, le signal de fluorescence est augmenté. Des tests préliminaires ont donné des résultats encourageants pour la détection spécifique de la thrombine, même dans le plasma.

List of abbreviations

2D	*Two dimensional*
3D	*Three dimensional*
A2M	*Alpha 2 Macroglobulin*
aPTT	*Activated partial thromboplastin time*
ATIII	*Antithrombin III*
Au	*Gold*
AuNP	*Gold nanoparticle*
bp	*Base pair*
BQH	*Black hole quencher*
BSA	*Bovine serum albumin*
DLS	*Dynamic light scattering*
DNA	*Deoxyribonucleic acid*
dsDNA	*Double-stranded DNA*
DTT	*dithiothreitol*
DVT	*Deep vein thrombosis*
ELISA	*Enzyme-linked immunosorbent assay*
F	*Coagulation factor*
F1+2	*Prothrombin fragment 1+2*
FII	*Coagulation factor II, Prothrombin*
FIIa	*Activated coagulation factor II, Thrombin*
FPA	*Fibrinopeptide A*
FRET	*Forster resonance energy transfer*
FX	*Coagulation factor X*
FXa	*Activated coagulation factor X*
HCII	*Heparin cofactor II*
k_a	*Association rate constant*
K_d	*Dissociation constant*
k_d	*Dissociation rate constant*
kDa	*Kilo Dalton*
LOD	*Limit of detection*
MI	*Myocardial infarction*
mM	*millimolar concentration*
MW	*Molecular weight*
nM	*nanomolar concentration*
NMR	*Nuclear magnetic resonance*
NP	*Nanoparticle*
NSBr	*Nonspecific binding reducer*

nt	*nucleotide*
O.D.	*Optical density*
PBS	*Phosphate buffered saline*
PC	*Polycarbonate*
PCR	*Polymerase chain reaction*
PE	*Pulmonary embolism*
pM	*Picomolar concentration*
ProT	*Prothrombin*
PS	*Polystyrene*
PT	*Prothrombin time*
QCM	*Quartz crystal microbalance*
QD	*Quantum dot*
RNA	*Ribonucleic acid*
RT-PCR	*Reverse transcription PCR*
RU	*Response unit*
SELEX	*Systematic evolution of ligands by Exponential Enrichment*
SEM	*Scanning electron microscope*
SPR	*Surface plasmon resonance*
ssDNA	*Single-stranded DNA*
TAT	*Thrombin-antithrombin complex*
Thr	*Thrombin*
UV-Vis	*Ultraviolet-visible*
VTE	*Venous thromboembolism*
µM	*micromolar concentration*

Table of contents

CHAPTER 1. GENERAL INTRODUCTION

1.1 Hemostasis, thrombosis and bleeding – all pivots around thrombin

Hemostasis is the body's normal physiological response for the prevention and stopping of bleeding at a site of injury. Congenital or clinically caused abnormalities in hemostasis may lead to thrombosis or to hemorrhage. Thrombosis in its various manifestations together with embolism, accounts for significant mortality and morbidity, as well as the cost of medical care. Many, if not most cases of thrombosis can be avoided and almost all recurrent episodes can be prevented by choosing appropriate antithrombotic therapy. But if a treatment is not tailored to the particular needs of patient it may lead to the blood loss. The successful and prompt medical decision-making for appropriate drug administration strategy requires defining etiology/predisposing factors and the close monitoring of hemostatic state of the patient. In this section we will discuss about disorders resulting from the abnormalities in the hemostasis, their risk factors, underlying mechanisms and the central role of thrombin, dictating normal or pathologic outcome.

1.1.1 Hemostasis

Normally, blood remains in the closed high-pressure circulatory system inside the blood vessels. When the blood vessel or tissue gets injured and starts bleeding, body's instinctive physiological response is hemostasis - quick, localized and tightly regulated process of clotting for stopping loss of blood to maintain the integrity of circulatory system.

In response to injury damaged blood vessel constricts (vascular spasm) so that blood flows out more slowly and outside the blood vessel an accumulating pool of blood (a hematoma) presses against the vessel, helping prevent further bleeding.

Almost instantly, starts as well clot formation. Exposed collagen initiates series of reactions for platelet activation and accumulation at the site of injury, in process called primary hemostasis. Von Willebrand's factor, produced by the cells of the vessel wall, acting as glue holds platelets to seal the break in the disrupted endothelium. As platelets accumulate at the site, they change shape from round to spiny, form a mesh that plugs the injury and release proteins entrapping more platelets and clotting proteins in the plug that becomes a blood clot.

At the same time exposure of the blood to tissue factor induces sequential activation of blood clotting (coagulation) factors, called secondary hemostasis or coagulation that culminates into generation of thrombin. Thrombin converts fibrinogen, a blood clotting factor that is normally dissolved in blood, into long strands of fibrin that radiate from the clumped platelets and form a net that entraps more platelets and blood cells. The fibrin strands add bulk to the developing clot and help hold it in place to keep the vessel wall plugged.

Primary and secondary hemostasis are related events: activated platelets release some clotting factors, whereas some clotting factors – thrombin, fibrinogen, play a role in platelet plug formation; these events occur concomitantly, and under normal conditions, regulatory

mechanisms contain thrombus formation temporally and spatially (Marieb and Hoehn, 2012; Roderique and Wynands, 1967).

Hemostasis is a dynamic process. The reactions that result in the formation of a blood clot are balanced by other reactions that slow down or stop the clotting process and dissolve the clot in a process called fibrinolysis when the injury site is healed.

1.1.2 Blood coagulation

The coagulation process is the important part of hemostasis, involving a complex set of stepwise protease reactions that transform circulating blood into a gel.

Several coagulation cascade models have been proposed, including the intrinsic and extrinsic pathway models and the more recent cell-based and tissue factor-based models.

1.1.2.1 The Intrinsic and extrinsic pathway model

In the 1960s the process of blood coagulation was regarded as a cascade or waterfall model, where one activated protein leads to the activation of an additional "downstream" protein (Davie and Ratnoff, 1964; Macfarlane, 1964). The coagulation reactions were divided into two pathways so called intrinsic and extrinsic. Both pathways fuse in a common pathway to generate the enzyme thrombin, which subsequently converts fibrinogen into fibrin (Fig.1.1).

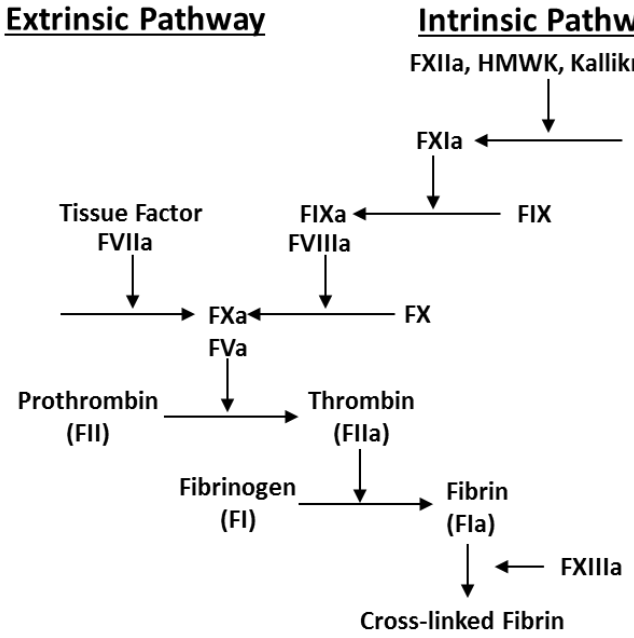

FIGURE 1.1 The extrinsic and intrinsic pathways in the cascade model of coagulation. These pathways are assayed clinically using the prothrombin time (PT) and activated partial thromboplastin time (aPTT), respectively.

The intrinsic pathway begins with contact activation, involving coagulation factors XII and XI (FXII and FXI respectively), prekallikrein (PK) and high molecular weight kininogen (HMWK). These four contact factors do not require the presence of the calcium for their reaction and are all readily absorbed onto negatively charged surfaces. After complex of HMWK, PK and FXII is formed, FXII and prekallikrein become activated to FXIIa and kallikrein. In the presence of cofactor HMWK FXIIa takes part in activation of FXI, which then activates FIX in the presence of calcium. The process continues with formation of FVIIIa/FIXa complex which activates FX.

The extrinsic pathway begins with trauma to tissue, causing exposure of tissue factor (TF) and activation of factor VII in the presence of calcium. The complex of TF/FVIIa then activates FX. Thus intrinsic and extrinsic pathways converge at activation of FX. FXa with FV will form prothrombinase complex that converts prothrombin into thrombin, which in its turn converts fibrinogen into fibrin to form a clot, and also, activated by thrombin, factor XIII stabilizes the fibrin.

Though these cascade models were a major advance in the field of coagulation, they stem from *in vitro* testing and thus are unable to fully explain hemostasis *in vivo.* The intrinsic and extrinsic systems could not operate *in vivo* as independent and redundant pathways as the models implied. These two branches of cascade do not have equal importance. For example deficiencies in HMWK, PK and FXII do not cause bleeding disorders, indicating that they are not essential to hemostasis. However, activation of factor X by TF-FVIIa of the extrinsic pathway cannot compensate for deficiencies in FVIII and FIX in patients with hemophilia (Osterud and Rapaport, 1977). For these reasons, a model of coagulation that better paired *in vivo* observations was proposed by Hoffman (Hoffman and Monroe, 2001).

1.1.2.2 The cell-based model of coagulation

The revised model of blood coagulation, called cell-based model, assumes that coagulation is more regulated by the cellular surfaces upon which activation of the coagulation proteins occurs, than by the kinetics and levels of the factors themselves. TF rather than "contact" factors is of central importance in the initiation of coagulation. In this model, coagulation occurs in three semi-concurrent phases: initiation, amplification, and propagation (Fig.1.2) (Hoffman and Monroe, 2001, 2007; Smith, 2009).

The initiation stage begins on the surface of TF-bearing cell (monocyte or fibroblast). Its exposure to circulating VII induces activation of FVII and complex formation. The complex of whose catalyzes the formation of activated FIX and FX. FXa activates and joins with FV to form the prothrombinase complex, which forms a small amount of thrombin on the TF-bearing cell surface. Now that amount of thrombin is enough to catalyze several additional reactions, forming the amplification stage of coagulation.

During **amplification stage**, platelets that were recruited to the site of vascular injury through platelet receptors glycoprotein VI (GPVI) and glycoprotein Ib-V-IX (GP Ib-V-IX) binding to the exposed extracellular matrix proteins collagen and von Willebrand factor (vWF), serve as the next cellular surface upon which coagulation proceeds. Once activated, platelets release alpha granules that contain factor V. FVIII binds to platelets in complex with vWF. The small amount of thrombin, generated during the initiation phase on the surface of TF-bearing cells, diffuses and activates these platelets through the cleavage of PAR1, and catalyzes the activation of factors XI, V, and VIII. Upon activation of FVIII thrombin by thrombin, the bond between FVIII and vWF is broken, but FVIIIa remains on the platelet surface.

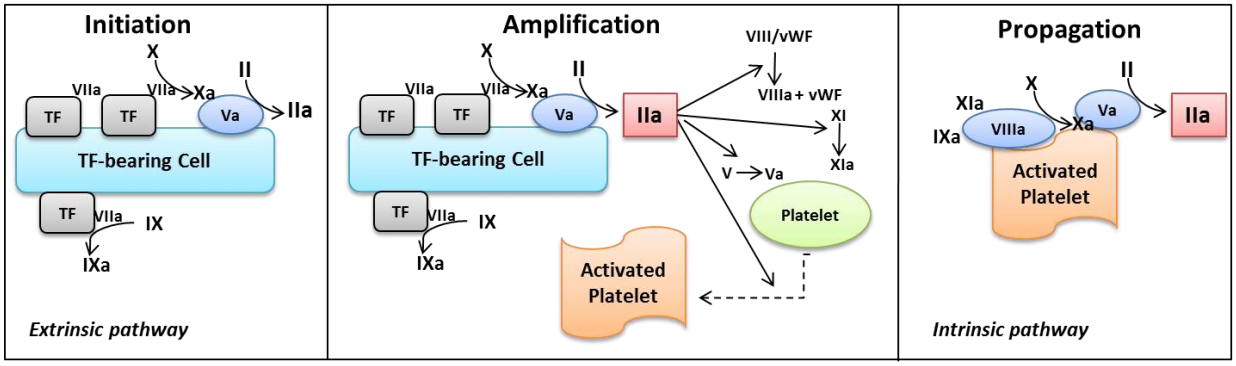

FIGURE 1.3 Steps in a cell-based model of coagulation. Initiation occurs on the TF-bearing cell as activated FX combines with its cofactor, FVa, to activate small amounts of thrombin. The small amount of thrombin generated on the TF-bearing cell amplifies the procoagulant response by activating cofactors, factor XI, and platelets. Finally, the large burst of thrombin required for effective hemostasis is formed on the platelet surface during the propagation phase.

During **propagation stage** FIXa diffuses from TF-bearing cell to activated platelet surface and there interaction with cofactor FVIIIa forms the tenase complex, which in its turn activates FX. Freshly formed FXa on the surface of activated platelet combines with the platelet-bound FVa to form the prothrombinase complex, which generates the "thrombin burst" necessary for fibrin formation. The clotting process (fibrin formation) occurs at the inception of the propagation phase, when only 5-10 nM thrombin has been produced. At the end of propagation phase thrombin concentration locally might reach several hundred nM (Fig.1.3) (Brummel et al., 2002; Mann, 2003a).

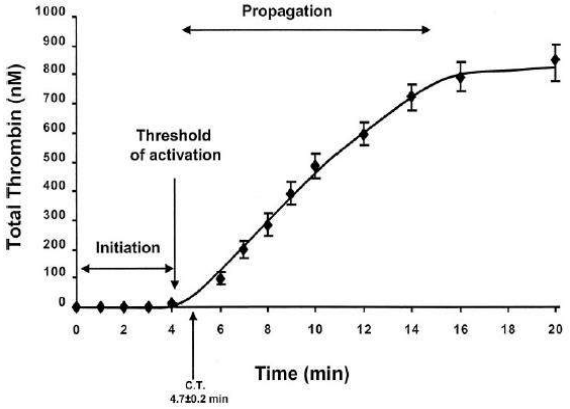

FIGURE 1.2 Thrombin concentrations at different stages of coagulation (reprinted from Mann, 2003a)

The cell-based model of coagulation hence shows us that the extrinsic and intrinsic pathways are not redundant. The extrinsic pathway operates on the TF-bearing cell to initiate and amplify coagulation. By contrast, the intrinsic pathway operates on the activated platelet surface to produce the burst of thrombin that causes formation and stabilization of the fibrin clot (Hoffman and Monroe, 2007).

1.1.2.3 Tissue Factor- based model

Expanding upon the cell-based model of hemostasis, recent studies proposed a new view of coagulation. This model primarily highlighting the role of tissue factor, hypothesizes that coagulation is initiated not solely by tissue factor exposed by vascular injury but also by activation of encrypted tissue factor by protein disulfide isomerase (PDI) (Furie and Furie, 2008). According to this model, tissue factor circulates in blood in encrypted form, bound to so-called microparticles (MPs). These complex vesicular structures, shed from activated or apoptotic endothelial cells, platelets, monocytes and, in certain disease states, from granulocytes and erythrocytes, are less than 1000 nm in diameter and display proteins similar to those found on their parent cell (e.g. ultra large vWF monomers on endothelial cell-derived MPs, P-selectin on platelet-derived MPs, TF on monocyte-derived MPs). MP-bound tissue factor in its encrypted form is not capable of initiating coagulation. But when platelets exposed to area of vascular injury

become activated by collagen and express P-selectin, then the circulating microparticles bind to it through P-selectin glycoprotein ligand-1. Consequently encrypted tissue factor gets activated by PDI, which was secreted by activated platelets, and is sequestered to the area of injury, ready to promote coagulation (Cho et al., 2008b).

1.1.2.4 Inhibition of coagulation

The attenuation of the coagulation system is as important as the procoagulant process and involves both stoichiometric and dynamic regulators. Tissue factor pathway inhibitor (TFPI) and Antithrombin III (ATIII) are the main stoichiometric inhibitors of the process. TFPI, neutralizing tissue factor-FVIIa-FXa complex, is the principal regulator of the initiation phase of thrombin generation, whereas ATIII, inhibiting FIIa, FIX, FX and FXI, acts to diminish thrombin activity and its generation. The dynamic regulator–activated protein C (APC), depends on thrombin generation, as the activation of the zymogen protein C is accomplished by thrombomodulin-bound thrombin. APC competes with FXa and FIXa for binding FVa and FVIIIa, ultimately proteolytically inactivating FVa and FVIIIa. Thus, its influence is mostly associated with quenching the propagation phase of thrombin generation (Mann et al., 2003).

1.1.3 Fibrinolysis

The fibrinolytic system is being initiated to disrupt fibrin clot as soon it starts being formed (Hoffman and Monroe, 2007). Fibrin is cleaved into soluble degradation products by plasmin, the protein activated from the inactive precursor plasminogen by action of urokinase–type plasminogen activator (uPA) and tissue plasminogen activator (tPA). The release of tPA from endothelial cells is provoked by thrombin and venous occlusion. Degraded fibrin exposes C-terminal lysines and, acting as cofactor, facilitates plasminogen activation. But PAs are down-regulated by plasminogen activator inhibitors (PAIs). Down-regulation of fibrinolysis is also performed by thrombin-activatable inhibitor of fibrinolysis (TAFI) that removes C-terminal lysines from fibrin and prevents its degradation.

Thus, hemostasis and fibrinolysis are conjugated processes, finely tuned to balance each other and well regulated to confine reactions locally and temporally. Alterations of the balance, either due to the absence or abnormality of specific hemostatic elements, lead to thrombosis or to bleeding.

1.1.4 Thrombosis

Thrombosis is the formation of an undesired blood clot (thrombus) inside a blood vessel, obstructing the normal flow of blood through the circulatory system. It happens when the pathologic processes overwhelm the regulatory mechanisms of hemostasis, therefore the formation of the hemostatic plug and the thrombotic process have several characteristics in common. However, there are certain principal differences between the development of thrombus and hemostatic plug formation.

Thrombosis is multifactorial, though abnormalities that are characteristic to thrombosis can be postulated in three types known as Virchow's triad. Particularly: (I) abnormalities of endothelium/endocardium – "abnormal vessel wall"; (II) abnormalities of hemorheology,

turbulence and stasis – “abnormal blood flow”; (III) abnormalities in platelets, the coagulation and fibrinolytic pathways “abnormal blood constituents” (Chung and Lip, 2003).

Thrombus formation can happen both in vein and artery and, depending on the location, causes, composition, risk factors and complications are different. With arterial thrombosis, blood vessel wall damage is required for thrombosis formation, as it initiates coagulation (López and Chen, 2009), but the majority of venous thrombus form without any injured epithelium (Martinelli et al., 2010). Thrombus is red with predominant fibrin in venous thrombosis, and white due to the higher proportion of platelets in the arterial thrombosis (Sobieszczyk et al., 2002). The main complication of thrombosis - embolism, which occurs if the thrombus breaks off and, carried by circulation, can induce local clogging at a site distant from its point of origin, is as dangerous and life threatening as the unwanted blood clotting in circulatory system.

The formation of venous thrombosis is associated with stasis and hypercoagulability. The most commonly occurring venous thrombosis is the deep venous thrombosis (DVT), which concerns the deep veins of legs or in the pelvic veins. It is associated with serious complications and the high risk of embolism affecting lungs - pulmonary embolism (PE). This life threatening combination is called venous thromboembolism (VTE) (Anderson and Spencer, 2003). VTE can also lead to serious long-term complications, including post-thrombotic syndrome (PTS) and chronic thromboembolic pulmonary hypertension (CTPH).

Arterial thrombosis is the formation of the thrombus within an artery mostly following the rupture of the atheroma, an accumulation of degenerative material of artery walls, or caused by atrial fibrillation. Arterial thrombosis is mainly associated with heightened platelet reactivity and damage to the vessel wall. Arterial thrombosis is not only blocking blood supply to major organs (heart and brain) but is also a major cause of arterial. Together, these factors manifest in following serious problems: Stroke – disturbance in blood flow to brain caused either by hemorrhage or ischemia, which on its own follows from arterial thrombosis or embolism (Deb et al., 2010); Patients with stroke have a relatively high risk of deep vein thrombosis (DVT) because of immobility and increased prothrombotic activity (Kappelle, 2011). Myocardial infarction (MI) - restriction of blood supply to the heart due to abstraction of the coronary artery by thrombus (Gawaz, 2004); When arterial flow is interrupted, tissue necrosis and gangrene are also possible (Ouriel, 2001).

The risk factors for venous and arterial thrombosis are mostly distinct, though age, inflammation and metabolic syndrome represent shared risk factors (Martinelli et al., 2010). The risk of both thrombosis in patients above 40 years of age is significantly increased compared to younger patients, and it approximately doubles with each subsequent decade (Bick and Kaplan, 1998). **Predisposing factors for VTE are**: age, pregnancy and postpartum period, obesity, immobility, dehydration, use of estrogen oral contraceptives, hormone replacement therapy, inherited and acquired hematological conditions, previous VTE and travel. **Whereas exposing factors for VTE include**: surgery, including major trauma, multiple trauma, hip fracture, or lower extremity paralysis because of spinal cord injury, orthopedic surgery, and abdominal surgery, active cancer or cancer therapy, respiratory or heart failure, acute medical illness, venous compression (e.g. by tumor, hematoma, arterial abnormality), recent MI or stroke, metabolic, endocrine or respiratory pathologies, central venous catheterization, inflammatory bowel disease,

severe infection, general care including duration and type of anesthesia, pre- and post-operative immobilization, level of hydration and the presence of sepsis (Anderson and Spencer, 2003; Martinelli et al., 2010). The presence of a residual thrombus after a first episode of deep vein thrombosis is an independent risk factor for recurrence. A potential mechanism by which the residual thrombus increases the risk of recurrence is impaired by venous outflow, resulting in blood stasis and clot formation. **Predisposing factors of arterial thrombosis** include**:** advanced age, family history smoking, hypertension, diabetes, obesity, sedentary lifestyle, stress, and metabolic syndrome, hyperlipidemia, and blood serum lipid abnormalities (Martinelli et al., 2010).

Both, the venous and arterial thrombosis, together with embolism represent clearly the most common cause of death in developed countries. Affecting up to 15 in 1000 people, about 2 million individuals die each year from an arterial or venous thrombosis or the following consequences in the USA, which is 4 times as prevalent as fatality due to malignancy. The morbidity rate occurring due to both arterial and venous thrombotic events has the same scale as the mortality (Bick and Haas, 2003). Table 1.1 shows the statistics of the morbidity and mortality due to several major types of thrombosis in US.

Table 1.1Incidence of thrombosis in United States

Disease	U.S. Incidence/100 000	Total cases in US/ Year
Deep Vein Thrombosis (DVT)	**159/100 000**	**450 000**
Pulmonary embolus (PE)	**139/100 000**	**355 000**
Fatal pulmonary embolus	**94/100 000**	**240 000**
Myocardial infarction (AMI)	**600/100 000**	**1 500 000**
Fatal Myocardial infarction	**300/100 000**	**750 000**
Cerebrovascular thrombosis (CVT)	**600/100 000**	**1 500 000**
Fatal cerebrovascular thrombosis	**396/100 000**	**990 000**
Total thrombosis in US	**1498/100 000**	**5 785 000**
Total Deaths in from above thrombosis	**790/100 000**	**1 990 000**
All cancer in US 1996	**544/100 000**	**1 359 150**
Cancer deaths in US 1996	**222/100 000**	**554 740**

In order to avoid development or recurrence of thrombosis and its complications after surgeries, stroke, myocardial infarction and other exposing factors, adequate anticoagulant treatment and prophylaxis is required (Bick and Haas, 2003).

Depending on the causes of the forming blood clots some patients at risk may be given medications that reduce the stickiness of platelets, so that they will not clump together to block a blood vessel. Aspirin, ticlopidine, clopidogrel, abciximab and tirofiban are examples of drugs that interfere with the activity of platelets. Other patients will receive an anticoagulant, a drug that inhibits the action of clotting factors. Commonly used anticoagulants are warfarin, heparin, rivaroxaben, hirudin, hirulog, fonfraparinux. Existing blood clots can be dissolved by thrombolytic drugs, which include streptokinase, urokinase, anistreplase etc. (Fenton et al., 1998; Ofosu, 2006). However, drugs that are designed to inhibit thrombosis by selectively attacking one single enzyme may in practice work out completely different than expected. These drugs may save lives, but by introducing misbalance in circulatory system, they can also put the person at

risk of severe bleeding (Levine et al., 2004). Therefore, close medical supervision and monitoring of patients hemostatic state is the curial part of thrombosis management (Blann et al., 2003).

1.1.5 Bleeding

The inability to form a proper blood clot leads to bleeding. Improper clotting can be caused by congenital or acquired deficiency or mutation of platelets (disorder of primary hemostasis) and/or coagulation factors (disorder of secondary hemostasis) (Triplett, 2000).

Bleeding associated with coagulation abnormalities is characterized by the formation of large hematomas, hemarthrosis, large single ecchymosis (either spontaneous or following minor trauma) or prolonged bleeding following injury, trauma, surgical or dental procedures, and menstruation. Major bleeding occurring intracranial, intraspinal or retroperitoneal might lead to death and therefore require transfusion or hospital admission.

Acquired bleeding disorders (coagulopathy) are more common in hospitalized patients and can be life-threatening. Causes of coagulopathic bleeding include consumption of coagulation factors and platelets, excessive fibrinolysis, hypothermia, and acidosis (Hoffman and Monroe, 2007). The hallmark of coagulopathy is microvascular bleeding, which means oozing from cut surfaces and minor sites of trauma, such as needle sticks. Microvascular bleeding can lead to massive blood loss. Acquired bleeding are often developed during medical conditions such as acute and chronic disseminated intravascular coagulation (DIC), anemia, cirrhosis of the liver, HIV, leukemia and vitamin K deficiency, or following surgical or accidental trauma, when the use of either fluid for volume replacement (in trauma patients), massive blood transfusion or an anticoagulant therapy is administered (Hoffman and Monroe, 2007).

Anticoagulant therapy including aspirin, heparin and warfarin is the main cause of clinical bleeding (Cuthbert, 1999). Therefore, because of increasing clinical use of potent antithrombotic drugs, perioperative bleeding is a major challenge. The risk of bleeding is related to the intensity and duration of an anticoagulant therapy and it can be markedly increased by combinations of antithrombotic drugs or during switching between different antithrombotic drugs. Although major hemorrhage is infrequent (up to 5% of patients receiving therapeutic doses of heparin may experience major bleeding episodes), management can be difficult especially with antithrombotic agents for which there are no specific reversal agents. Bleeding during antithrombotic therapy is associated with high morbidity and mortality. Especially due to increasing number of elderly population prevalence of thrombosis-related complications and bleeding associated with thrombotic treatment is also constantly rising (Schulman et al., 2008).

1.1.6 Balancing thrombosis and bleeding risks

In normal conditions there is a fine balance in the body ensuring that there is not too much blood clotting or bleeding. Given the challenge of balancing bleeding and clotting in patients, hemostatic management must be tailored to each patient. With every approach to reduce thrombosis, there is an accompanying risk of increasing bleeding complications; conversely reducing bleeding complications may increase thrombotic events. Hence, balancing both ends of the spectrum represents an essential problem. It should take into account patient's genetic and acquired risk factors and acute disturbances in bleeding and clotting caused by

surgical intervention or other predisposing and risk factors. At the same time it must consider the risk for development thrombotic event and bleeding relative to the risks and benefits (Makris et al., 2013). Individual approach relays on precise adjustment of the length and the type (dose and drug combination) of therapy.

Significant advances in the management of normal hemostasis in susceptible patients might be achieved by introduction of novel hemostatic and antithrombotic drugs. Though it is challenging to make drugs that prevent thrombosis without causing a hemorrhagic diathesis and the therapeutic window of such agents tends to be narrow, however ideal agent would have specific antithrombotic activity to prevent pathological activation of hemostasis yet would produce negligible global anticoagulant activity so that the hemostatic system could respond appropriately to physiological pro-coagulant stimuli (Cuthbert, 1999).

However therapeutic decision making, anticoagulant drug trials and subsequent tailoring of the treatment require monitoring of patients coagulation behavior. Observing the dynamics of hemostatic processes has an utmost importance to detect the propensity of patient to develop thrombotic or hemorrhagic disorders and to monitor the effectiveness of the combination and the dosage of a medication. Self-management of the dose of own anticoagulants, reducing incidence of bleeding and thrombosis complications, also require home monitoring. Developments of new, more rational antithrombotic strategies thus require tools to assess the state of patient for dose adjustment and safety.

Nevertheless, the “hemostatic state of patient” bears very global meaning. There are various laboratory tests available to assess different profiles and parameters of the hemostasis, but which parameter can define the risk of thrombosis or bleeding? Both mechanisms are so interconnected that they must have common denominator that is a key in mechanism of thrombosis and hemorrhage and thus acting on it and monitoring of which will be crucial.

Thrombin, playing important role at all stages of hemostasis and fibrinolysis has a potential to be considered as such denominator, as it is non-duplicated enzyme lying on the final common path of all coagulation and fibrinolysis reactions.

1.1.7 The first law of thrombosis and hemostasis

Prof. Hemker and his group, researching since long time connection between thrombin generation and the thrombotic and bleeding risks, identified thrombin generation (level) to be the hinge on which all the problems around thrombosis pivot on. Amount of generated thrombin dictates bleeding of thrombotic tendency. Based on this, he postulated following as the first law of thrombosis and hemostasis:

“More thrombin means more thrombosis and less bleeding, less thrombin means less thrombosis but more bleeding” (Hemker et al., 2004).

Indeed results of his extensive studies support this postulate to hold true for congenital and acquired tendencies to venous and arterial thrombosis, as well as for bleeding and under all variants of antithrombotic treatment (Al Dieri et al., 2012).

Furthermore the clear argument in support of driving role of thrombin in thrombosis is the clinical effectiveness of drugs, used to treat both venous and arterial thrombosis, which either

inhibit prothrombin activation into thrombin, or directly inhibit thrombin or accelerate thrombin inhibition (Ofosu, 2006).

In order to see in more details the importance of thrombin in various reactions will be described in the following paragraph.

1.1.8 The central importance of thrombin

Thrombin is a trypsin-like serine protease, activated by FXa or prothrombinase complex (FXa+FVa) from its zymogen precursor protein prothrombin as the ultimate enzyme of coagulation cascade (mechanism of activation is described in chapter 3).

Thrombin exerting a multitude of highly regulated action on the blood, the vessel wall and large variety of cells, is involved in diverse important physiological and pathological processes including procoagulant, anticoagulant, inflammation and cell-signaling and-activation.

1.1.8.1 Master enzyme of hemostasis

Thrombin is often seen as the end-product of the coagulation cascade and as such responsible for the final step, the conversion of the soluble protein fibrinogen into the insoluble fibrin clot. However thrombin has many more important functions in whole coagulation. It takes part in paradoxically opposite games of procoagulant and anticoagulant pathways (Griffin, 1995).

As procoagulant thrombin acts when it converts fibrinogen into an insoluble fibrin gel by ordered two step-cleavage processes, which is the non-duplicated reaction in coagulation cascade. The fibrin matrix is further strengthened through cross-linking reaction mediated by factor XIII, a transglutaminase also activated by thrombin (Dahlbäck, 2000). Into stable, cross-linked fibrin plug thrombin-activated platelets are recruited and aggregated (Vu et al., 1991). Thrombin mainly activates platelets by interacting and cleaving protease activated receptors (PARS), however there is also another mechanism of thrombin mediated platelet-activation involving proteolysis of glycoprotein V, part of the GpIb-IX-V complex on circulating platelet surface. This in turn yields hyper-responsive platelets with enhanced fibrinogen binding and aggregation (Ramakrishnan et al., 1999). Although the exact mechanism is still not clear, thrombin interaction with GpIbα also activates platelets and GpIb-IX –thrombin complex facilitates fibrin binding to Integrin (Ramakrishnan et al., 2001).

Moreover, thrombin maintains and amplifies its own production via positive feedback mechanism involving thrombin-activated factors V, VIII (Mann et al., 1988) and XI (Gailani and Broze, 1991). Factor V, when activated, associates with activated factor X and cleaves prothrombin to thrombin at 20 000 times higher rate. Factor VIII, when activated, associates with activated factor IX and activates factor X. Factor XI, when activated, activates factor IX. Thus once the initial stimulus of coagulation cascade is "turned off", it is thrombin that governs the perpetuation of clotting stimulus[1] (Narayanan, 1999).

To complement the role of thrombin in clot formation, thrombin also plays a part in **inhibition of lysis** of that clot. This action is carried out by thrombin-mediated activation of

[1] Ability of thrombin to stimulate and amplify its own production, allows initiation of undesired coagulation even without vascular damage, if it escapes inhibition at the injury site.

“thrombin-activatable fibrinolysis inhibitor" (TAFI) and stimulation plasminogen activator inhibitor-1 (PAI-1) synthesis (Villamediana et al., 1990). Activated TAFI inhibits fibrinolysis by cleavage of carboxy-terminal lysine residues on the fibrin polymers, which are needed for assembling of the fibrinolytic system (Tilburg et al., 2000). PAI-1 functions as the principal inhibitor of tissue plasminogen activator (tPA) and urokinase (uPA), the activators of plasminogen and hence fibrinolysis (Nilsson et al., 1985).

Furthermore, thrombin regulates its own production by being part of an inhibitory system. **Thrombin function as anticoagulant** is achieved via binding to a vascular endothelial cell protein called thrombomodulin. This leads to the activation of anticoagulant protein C, causing inactivation of coagulation factors V and VIII and thus down-regulation of thrombin generation, and inhibition of thrombin's ability to form fibrin and activate factor XIII, platelets and coagulation feedback stimulatory proteins (Esmon, 2000).

Interestingly, thrombin also plays a role in **degradation of the fibrin clot** by activating tissue plasminogen activator (t-PA), which in turn activates plasminogen into plasmin. Plasmin on one hand degrades its main target fibrin and on the other hand down-regulates thrombin generation by digestion of prothrombin and clotting factors V, VIII and XII (Fenton et al., 1998; Omar and Mann, 1987). Thrombin is a chemo-attractant for neutrophils, which take part in degradation of the fibrin clot (Sonne, 1988). Thrombin interaction with PAI-1 yields reciprocal inhibition of each partner (Ehrlich et al., 1991; Meijer et al., 1997).

Thus, the role of thrombin as the key arbiter of complicated web of positive and negative feedback loops governing procoagulant and anticoagulant pathways and their balance is clearly impressive. Thrombin indeed deserves the title of the master enzyme of hemostasis. Thrombin, however, also has many biological effects that are much more complex than merely hemostatic ones.

1.1.8.2 Non-hemostatic functions

Apart from thrombin role in hemostasis, fibrinolysis and platelet activation thrombin also takes an important part in cell activation, modulation and signaling, and in mitogenic, pleiotropic, inflammatory processes through interaction with specific cell surface receptors (Frenkel et al., 2005). Almost every cell type tested in vitro (except erythrocytes) was responsive to thrombin (Fenton et al., 1998). Most of the cellular effects elicited by thrombin are mediated through activation and subsequent signal transduction cascades of members of the PAR family. Thrombin activates PAR1, PAR3 and PAR4 (Siller-Matula et al., 2011).

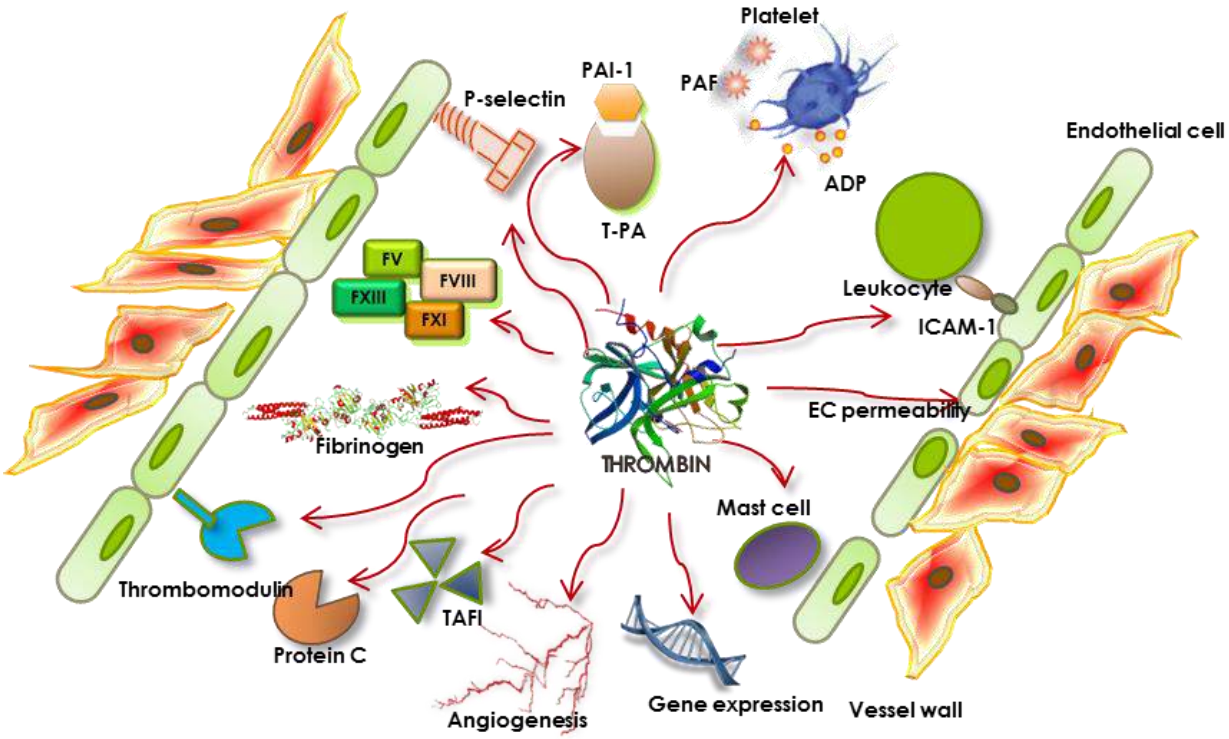

FIGURE 1.4 Multiple roles of thrombin. Thrombin is involved in coagulant, anticoagulant, fibrinolytic, anti-fibrinolytic and pleiotropic processes as well as angiogenesis and gene expression.

As we've seen above thrombin influences platelet activation in many ways. It also has complex effects on the endothelial cells, with the release of a variety of biologic mediators, including expression of ICAM-1, which promotes leukocyte adhesion on the endothelial cells (Rahman et al., 2001) and thromboplastin (Galdal et al., 1985). Thrombin modulates multiple processes in the vascular system including vascular permeability, vascular tone, inflammation and formation of neovessel. Thrombin interaction with PAR1 on the surface of endothelial cells, induces a chain of reactions causing the reversible change of endothelial cell shape thus creating gaps and increasing vascular permeability (Garcia et al., 1986). Thrombin-exposed endothelial cells reversibly lose their ability to adhere to collagen, they can migrate to a distal sites and start thrombin-facilitated proliferation and formation of new vessel (Maragoudakis et al., 2002). Thrombin also potentiates vascular endothelial growth factor (VEGF)-induced endothelial cell proliferation. This process is accompanied by up-regulation of the expression of VEGF receptors. In addition, thrombin increases the mRNA and protein levels of alphaV/beta3 integrin and it can bind to this receptor. This implies the role of thrombin in angiogenesis, a process that is essential in tumor growth and metastasis. Furthermore, thrombin indirectly up-regulates the transcription of VEGF by inducing the production of reactive oxygen species and the expression of the hypoxia-inducible factor 1 (Dupuy et al., 2003).

Thrombin also activates numerous cells involved in the inflammatory and reparative responses, including monocytes, T lymphocytes and mast cells. It affects leukocyte migration, edema formation, and other processes related to tissue repair (Rickles et al., 2003; Siller-Matula et al., 2011). One of the thrombin actions involves the stimulation of chemotaxis[1] of white blood cells (neutrophils and monocytes) at the site of injury and generation and release by them chemokine

[1] chemo-attraction induces the objects (cells) to move down to a chemical gradient

and cytokine (Becker and Spencer, 1998; Frenkel et al., 2005). Moreover, thrombin plays an important role in cellular proliferation including smooth muscle cells, macrophages, endothelial cells and fibroblast. This function of thrombin causes it to be implicated in the disease process of atherosclerosis and the build-up of the atherosclerotic plaque which contains many macrophages and smooth muscle cells (Borissoff et al., 2009).

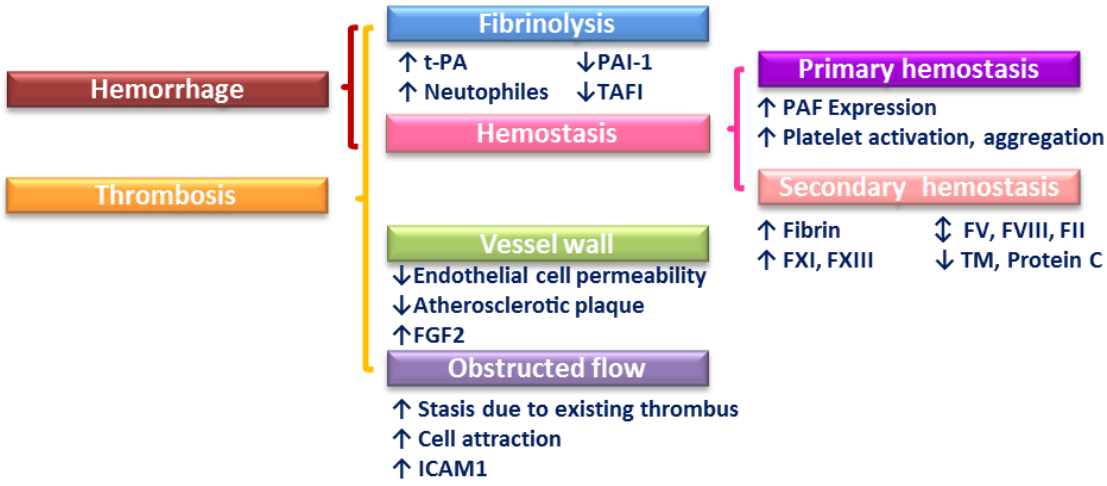

FIGURE 1.5 Role of thrombin in development of hemorrhage and thrombosis. Thrombin involved in hemostatic and cellular interactions has impact on fibrinolysis and hemostasis as well as on vessel walls and blood flow. On one hand thrombin-mediated down-regulated hemostasis, increased fibrinolysis and decreased vascular integrity lead to hemorrhage. On the other hand, up-regulated hemostasis and down-regulated fibrinolysis, together or separately with alterations of vessel wall and obstructed flow (Virchow triad), cause thrombosis. Arrows indicate whether thrombin action (↑) up- or (↓) down- regulates or acts both ways (↕) on corresponding process

To summarize, non-hemostatic effects being independent form hemostasis also complement thrombin's importance in development of normal, hemorrhagic or thrombotic conditions. Thrombin interactions with various molecules and cells and consequent functions of thrombin demonstrate that thrombin has an impact on each and every parameter, factor determining course of normal hemostasis and fibrinolysis or pathological thrombosis and hemorrhage. Fig.1.4 summarizes most important functions of thrombin, whereas Fig.1.5 depicts schematically the actions of thrombin at each hemorrhage- and thrombosis-related pathologic process.

Thus thrombin's hemostatic and non-hemostatic functions prove the first part of "the first law of hemostasis" emphasizing the pivotal role of thrombin.

1.1.8.3 Why does more thrombin lead to thrombosis and less thrombin to bleeding?

In the following part, we will try to gather the evidence for answering the question, why and how does the amount of thrombin dictate the risk of thrombosis or bleeding and thus to provide the molecular proof for credibility of the first law of thrombosis.

We've seen how hemostasis and fibrinolysis are interconnected with diverse positive and negative feedback loops, directly or indirectly influenced by thrombin. Domination of one or another process thus depends on developing thrombin concentration. How well thrombin is generated, how well it exerts its actions and how well it is inhibited-defines the extent of a hemostatic plug or a thrombotic or bleeding process (Hemker et al., 2004).

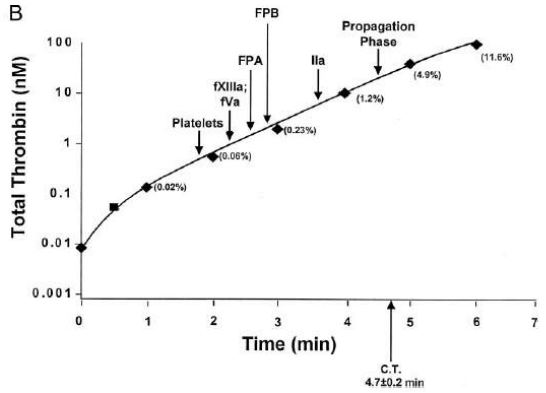

FIGURE 1.6 Thrombin concentration during thrombin generation and initial points of detection thrombin action products. (Reprinted from Mann 2003)

Obviously, the bleeding risk arises if at the site of injury not enough thrombin is available/generated leading to unsuccessful hemostasis. This can be caused by the malfunctioning of the clotting factors or too much inhibition of either thrombin or clotting factors. On other hand, low levels of thrombin are not sufficient to activate fibrinolysis inhibitor (TAFI) and uninhibited, accelerated fibrinolysis can lead to bleeding from the destabilized healing wound (Hemker et al., 2006).

But there is more about low thrombin levels. In fact, thrombin is a Janus-headed allosteric protein, existing in anti-coagulant and procoagulant conformations (Bode, 2006; Dang et al., 1995). Thrombin allosterity is regulated by the coordination of Na+. Na+ free thrombin, so-called "slow thrombin" is considered as anticoagulant, since it prefers to bind thrombomodulin. Thrombomodulin, on one hand, blocks thrombin's active site preventing its action on procoagulant substrates and explosive generation of thrombin, and, on the other hand, accelerates activation of protein C, which shuts down the propagation of thrombin-generating cascade. Whereas Na+ bound thrombin, "fast thrombin", upon Na+ binding undergoes allosteric change and gets improved affinity for procoagulant substrates and reduces affinity for protein C. Yet, distribution of the "slow" and "fast" thrombins depend on thrombin level, due to the affinity of the Na+ which is in the range of 110 mM at 37 °C. Thus physiologic NaCl concentration of 140 mM is not sufficient for saturation of all thrombin with Na+. At the early onset of the thrombin generation, thrombin concentration is low and mostly Na+-free. But in the middle of thrombin generation the ratio of slow/fast thrombin is about 2/3, to maintain the equilibrium between up- and down-regulation (Di Cera, 2007). Thus, thrombin's character as anticoagulant or procoagulant depends on its structure, which in turn depends on the concentration of the thrombin. Studies carried out on animals, involving intravenous infusion of various thrombin concentrations also confirmed that slow infusion of low concentration thrombin induced bleeding instead of thrombosis, indicating that without damage of endothelium or alterations in the vessel wall, the fibrinolytic and anticoagulant properties of thrombin prevail (Siller-Matula et al., 2011).

Now, there remains the question about the amount of thrombin that can be considered as low (anticoagulant) and high (procoagulant) level. Non-hemostatic functions of thrombin, described above, highlight that thrombin can function and thus be generated independently to its hemostatic purposes, i.e. vessel injury. And since many of these cellular processes get regulated by sub-nanomolar concentrations of thrombin (Vu et al., 1991), we can assume that several pM concentration of free non-hemostatic (not necessarily pathologic) thrombin should be circulating in blood. This amount of thrombin is necessary as well for keeping coagulation in state of low-level activation but constantly poised to instantaneously respond to injury with a burst of thrombin generation at the site of vascular damage. This circulating thrombin level, to say so, is negligible to be considered as procoagulant or coagulant. The range of the "negligible" circulating

thrombin level obviously has a certain threshold. This threshold should be adjacent with the concentration initiating inhibitory pathway i.e. anticoagulation. Due to technical reasons direct detection of free circulating thrombin is not yet possible to determine exact ranges of "negligible" and "anticoagulant" levels of thrombin and hence to correlate thrombin levels to predisposition for development bleeding of thrombotic disorder. Though, the level of the free (uninhibited) thrombin that can lead to thrombotic development of scenario can be already about 5 nM. This is the thrombin concentration which can initiate thrombin burst. Detection level of free thrombin in concentration range of 5 to 20 nM in patients' blood must indicate the high risk of thrombosis. And concentration above that indicates the presence of thrombosis. Thus, all cases of thrombin generation exceeding this negligible threshold have to be regulated to confine thrombin in time and space in order to keep balance in non-pathologic thrombin activities in whole organism.

Normally thrombin, escaped inhibition by thombomodulin at the site of generation, gets deactivated and removed from circulation by natural inhibitors of thrombin - ATIII, HCII and A2M forming irreversible 1:1 complex. Nevertheless, despite rigorous regulation, the risk of development of pathologic outcomes due to uncontrolled free thrombin outbreak still exists. The main sources of impaired thrombin can be: (i) existence of the non-hemostatic trigger, which could act on low concentration of **existing free circulating thrombin** to up-regulate thrombin production; (ii) **uninhibited thrombin escaping a site of injury**; (iii) **thrombin,** which was **entrapped** in its active form within fibrin mesh and got **released** following the fibrin degradation by plasmin. One can imagine that the extra thrombin generated after coagulation *in vivo* can diffuse from the site of coagulation and act in a hemostatic and/or prothrombotic manner (Kessels et al., 1994).

Thus description of thrombin concentration in time could be used for monitoring patients' state. Ability to detect free thrombin level thus could significantly improve determination of risk factors for bleeding in the preoperative patients and risk factors for recurrent thrombosis and help managing successful therapy.

Following section covers the current laboratory methods available to indirectly measure thrombin concentration.

1.2 Monitoring of hemostatic state

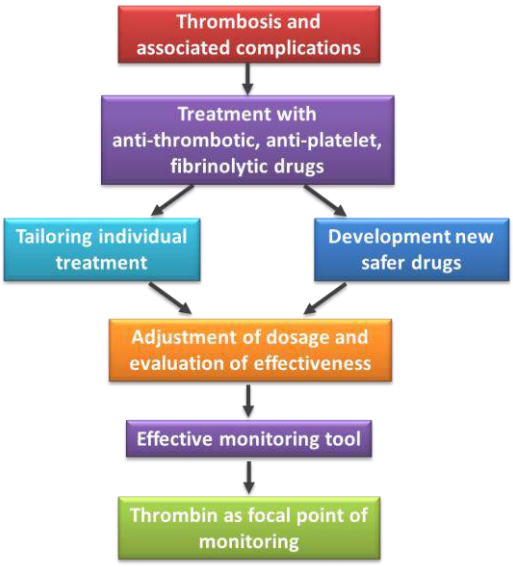

FIGURE 1.7 Monitoring of thrombin as the focal point

In order to assess the hemostatic state of the patient for identifying hemostatic defects, diagnosing underlying causes, predicting and avoiding development of pathology, making individual treatment decision, evaluating the success of initial treatment modalities, providing guidance for supplemental therapeutic interventions, monitoring new anticoagulant therapy and epidemiology there are several methods and test developed for clinical use or in trial.

In this section will be described some of the main methods available in routine clinical use and the test that have potential to provide detailed information on hemostatic state, based on indirect and direct assessment of thrombin generation, activity and inhibition.

1.2.1 Routine blood tests

Routine tests of blood coagulation frequently ordered to assess clotting function in patients are *in vitro* screening assays prothrombin time (PT) and activated partial thromboplastin time (aPTT). These tests measure clotting times (time needed to form a fibrin clot) of recalcified whole blood or platelet poor plasma. Assessing only the time taken to form a clot, which occurs when only around 5% of all physiologically relevant thrombin is formed (Hemker and Beguin, 1995), these tests do not entirely reflect global hemostatic balance. They permit only identification of connectivity between plasma levels of soluble coagulation factors required for hemostasis and give an indication of specific deficiencies, which do not always closely correlate with the clinical phenotype. These screening tests are abnormal when there is a deficiency of one or more of the soluble coagulation factors but they do not tell us what the risk for clinical bleeding will be and also are insensitive to prothrombotic states. However apart from their application as screening assays, these methods serve as the backbone of all the specialized clot-based assays for factor activities, for the indirect measurement of inhibitory antithrombin and protein C activities and also for the measurement of the effect of treatment with an anticoagulant drug or a combination of drugs during pathological conditions (Tripodi, 2008).

Prothrombin Time measures the time needed to form a clot after reagent containing a phospholipid-protein extract of tissue (thromboplastin) and access of calcium is added to blood or plasma sample. Thromboplastin leads to clot formation through activation extrinsic and common pathways, thus allowing assessment of functionality of FVII, FV, FX and FII clotting factors and fibrinogen. It is used to detect inherited or acquired coagulation defects related to the extrinsic pathway of coagulation, to monitor warfarin therapy and to evaluate liver damage and vitamin K status (Kitchen and Preston, 1999).

Activated Partial Thromboplastin Time is the time taken to the formation of a fibrin clot after addition of calcium in the plasma incubated with phospholipid (cephalin) and contact activator (e.g. Kaolin, micronized silica or ellagic acid). In this method fibrin clotting is induced by activation of intrinsic pathway and therefore reflecting function of intrinsic factors such as FVIII, FIX, FXI, FXII, vWf, prekallikrein. The principal clinical use of aPTTs include the detection of hereditary or acquired deficiencies or defects of the intrinsic coagulation factors, monitoring heparin anticoagulant therapy, the detection of coagulation inhibitors (i.e., lupus anticoagulant), and to monitor coagulation factor replacement therapy (Korte et al., 2000).

Both essays depend on detection of a fibrin clot as the endpoint. **Detection of clot formation** is performed mostly on automated instruments employing mechanical and optical methods. **Mechanical detection** comprises electro-mechanical method, based on completion of an electrical circuit by a fibrin strand; and electromagnetic-mechanical approach, based on an increase in plasma viscosity as fibrin forms. **Optical detection** include photo-optical method, which observes the phenomenon of light scattering upon fibrin strand formation and photometric approach based on absorbency change of monochromatic light.

For monitoring of oral anticoagulation therapy (warfarin) there are commercial portable instruments already available for self-testing PT (CoaguChek® XS system), which have proven self-testing to be as good clinically as visiting the anticoagulation clinic and even shown that self-testing patients have less thrombotic and hemorrhagic events than those who visit anticoagulation clinics as their only form of monitoring (Heneghan et al., 2012). However when coagulation assays are performed for other, above-described purposes, despite automation, the presence of highly qualified and trained medical personal is required for blood and plasma collection, treatment, analysis and result interpretation. While these tests have proven useful in identifying bleeding risk, they have limited utility when applied to the evaluation of thrombotic risk (Mann, 2003b).

1.2.2 Thrombin generation assay

Prothrombin time (PT) and activated partial thromboplastin time (aPTT) do not incorporate cellular elements and provide data only on isolated components of the coagulation cascade. Since clotting times only represent the lag phase before thrombin generation starts, they not always mirror pathologies associated with bleeding or thrombosis (Hemker and Beguin, 1995). The extent of hemostatic-thrombotic reaction is also critically determined by the amount of thrombin that forms and by the time it remains active. The end result of one's capacity to generate thrombin captures the interaction between proteases and their inhibitors and is therefore potentially more useful as a reflection of a thrombotic or hemorrhagic phenotype (van Veen et al., 2008).

Thrombin formation in plasma can be measured by the thrombin generation potential in plasma *in vitro* after the activating stimulus, or by measuring the *in vivo* markers of thrombin generation, inhibition and activity. *In vivo* markers are discussed in the next paragraph.

Thrombin generation assay is based on thrombin generation in recalcified plasma (Hemker et al., 2006) or blood (Tappenden et al., 2007) triggered by tissue factor in the presence of phospholipids. Generated thrombin causes the cleavage of a chromogenic (defibrinated,

platelet poor plasma) or fluorogenic (platelet rich plasma, whole blood) substrate of thrombin. Derivation of the thrombin concentration in the plasma from the rate of substrate conversion produces a characteristic pattern of thrombin generation in time (Baglin, 2005).

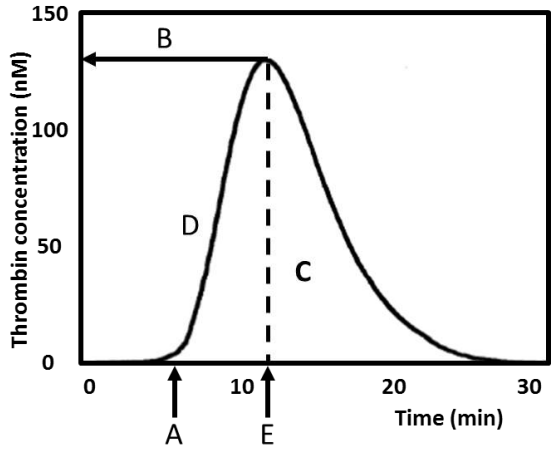

FIGURE 1.8 Thrombogram, showing (A) lag time (min); (B)Peak height (nM) (C) Endogenous thrombin potential(area under the curve) (D) maximal raising slope (nM/min) (E)time to peak (min)

The curve obtained is called thrombogram (Fig. 1.8), showing the four main parameters: lag time (A), time to peak (B), peak thrombin (C) and endogenous thrombin potential (area under the curve). During an initiation phase, or lag time, small amounts of thrombin are formed. This is followed by a propagation phase, a thrombin burst, which reaches its peak and afterwards declines to the baseline upon the activation of inhibitors (Hemker et al., 2004). The amount of thrombin formed reflects the function of the hemostatic system much better than the clotting time does. Thrombogram measures both low and high reactivity of the clotting system, hence thrombin generation potential may correlate more closely with a hyper- or hypocoagulable phenotype and is sensitive to the action of all types of antithrombotic drugs or a combination of pathological conditions (Berntorp and Salvagno, 2008; Al Dieri et al., 2012).

Thrombin generation has been automated to run several samples together (Hemker et al., 2002) and also miniaturized in microfluidic system, to decrease the volume of reagents and to investigate thrombin generation in constrained environment more alike to blood vessels (Koch et al., 2009). However the application of thrombin generation assays to clinical decision-making remains still hampered by standardization problems (Castoldi and Rosing, 2011).

1.2.3 Markers of thrombin formation

While routine blood tests look how fast fibrin clot is formed i.e. how well is thrombin activated, they don't tell how much thrombin was in blood before coagulation and how much was generated. Current state of thrombin levels can be assessed indirectly by measuring the *in vivo* markers of thrombin generation, activity and inhibition in plasma. These include prothrombin fragment F1+2 representing a measure of thrombin generated (Pelzer et al., 1991), FPA, reflecting thrombin activity towards fibrin (Nossel et al., 1974) and thrombin-antithrombin complexes; indicating the amount of thrombin inhibited (Pelzer et al., 1988).

Identification of these molecular markers is being done by means of, specific antibodies prepared against them (LIA or ELISA methods). Measured marker levels show the effect of coagulation factor levels on thrombin generation and function, and thus indicate ongoing physiological or abnormal process related to clot formation, thrombosis, vascular damage, or drug effect (Quinn et al., 2000).

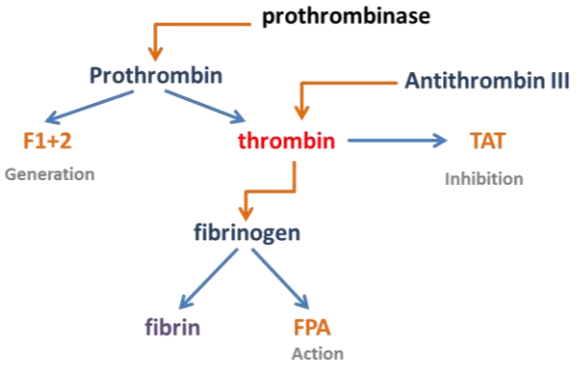

FIGURE 1.9 Molecular markers of thrombin generation, action and inhibition

Prothrombin fragment F1+2 or just F1+2 is the fragment of prothrombin formed during prothrombin activation by FXa in amounts equimolar to the thrombin generated with half-life of 90 min (Bauer, 1993; Pelzer et al., 1991). Prothrombin fragment 1+2 is a quantitative marker to assess the degree to which the coagulation system has been activated. F1+2 levels have been used to assess thrombotic risk and monitor the lowest dose of warfarin needed to prevent a thrombotic event in those patients on oral anticoagulant therapy. Elevated levels are observed in inherited thrombophilia (protein C deficiency, protein S deficiency, and antithrombin deficiency). Increased levels occur in thrombosis, pulmonary embolism, DIC, trauma, septicemia and complications of pregnancy. Patients on oral anticoagulant therapy have reduced levels of F1+2 (Pelzer et al., 1991).

Fibrinopeptide A or FPA is a peptide of 16 amino acids obtained from cleavage of the two A chains of fibrinogen by thrombin, thus concentration of it is a specific index of thrombin action in which only active, non-inhibited thrombin plays important role. Short half-life of 3-5 min makes FPA reliable marker for actual blood clotting activation (Nossel et al., 1974). Elevated FPA levels in plasma are shown to be associated with disorders such as disseminated intravascular coagulation, deep venous thrombosis, arterial thrombosis, coronary artery thrombosis and malignancy (Eisenberg et al., 1985).

Thrombin-Antithrombin complex or TAT is complex of thrombin irreversibly inhibited by the main natural inhibitor of thrombin ATIII. The half-life of TAT is less than 15 min (Pelzer et al., 1988). Elevated concentrations of TAT are found in persons predisposed to thrombosis as well as in patients with: multiple trauma, liver dysfunction, septicemia, or preeclampsia (López et al., 1999). TAT is complementary to FPA assay as they are related to different steps. TAT complexes indicate thrombin bound to ATIII, if all thrombin was inhibited by ATIII no FPA would be ever formed.

Above described markers, formed during certain processes are then cleared from circulation only after definite time and thus, depending on their half-life, they represent cumulative, average image of thrombin generation, action or inhibition over a longer period of time, i.e. they do not reflect instant picture of thrombin levels. In addition, prothrombin activation *in vivo* normally increases with age in the healthy population. Therefore, the levels of thrombin production and action need further investigation in order to discriminate between pathological and hemostatic thrombin (Ofosu, 2006).

Although these methods are used as gold standards, they are time-consuming, manually intensive, and not suited for the evaluation of large numbers of clinical samples and give the information about thrombin concentration indirectly.

1.2.4 Free Thrombin as the marker

Thus, as we saw above, routine blood tests show how well fibrin clots and based on this information make qualitative prediction of possible risks of development hypo- or hyper-coagulation states or indicate on already existing disorders due to congenital and acquired reasons. But these tests do not reflect complete hemostatic picture, they do not give quantitative information about instant concentrations of coagulation factors and most importantly of thrombin and hence they do not allow quantitative risk assessment.

Measurement of levels of molecular markers, allows indirect assessment of picture of hemostatic state integrated over larger time based on thrombin generation, activity and inhibition occurred in the past and thus can only indicate already occurred or ongoing disorder.

Thrombin generation assay shows how well the system can react on the trigger of the coagulation and lead to the thrombin generation. By the characteristic parameters of the thrombogram, one can detect the presence of coagulation problems, but it can't register and determine whether there is free thrombin circulating in the blood in the dangerous amounts escaped from the site of the injury.

Hence, a simple clinically useful test indicating coagulability is being increasingly recognized. Despite the challenges associated with low concentration and rapid inactivation by natural inhibitors, direct detection of circulating free thrombin levels, holds great promise to be more reliable test for the prediction of prethrombotic states. As thrombin concentration defines the character of thrombin functions and directly correlates with the different hemostatic states, monitoring dynamic of free thrombin level over time has potential to be powerful marker, more accurately reflecting disease-relevant intermediate phenotypes and thus representing a better basis for diagnostics and prophylaxis, consequently improving patient care and outcomes.

1.2.5 Sensor for free thrombin

Other than drawbacks of existing hemostatic monitoring methods covered above, it should be noted that those methods involve highly complex, costly, and time-consuming procedure that needs to be performed by a laboratory specialist. For some methods (PT, aPPT) diagnostic equipment in hospitals relies on large-scale automated instruments that are geared towards the efficient processing of large batches of prepared samples, whereas other depend on intensive manual manipulation (F1+2, TAT, FPA). Thus, these methods are not adapted for emergency care patient for example with serious conditions as MI or stroke, in which continuous protein measurements are often needed for monitoring anticoagulant or antiplatelet drugs.

Therefore, there is a need for a method that is sufficiently inexpensive, fast, efficient, convenient, durable and reliable to detect marker level (thrombin) at point-of-care by untrained individuals, for example, at medical emergencies or in non-clinical locations (home-testing). For such situations, it is desirable to develop compact and autonomous chips that can measure marker levels in this case thrombin levels within patient blood for the treatment duration of several days. Point-of-care device, moreover, has to be capable of overcoming major challenges of thrombin detection in real conditions, which comprises the variation of thrombin concentration in non-thrombotic and thrombotic states over a broad range (from nM to μM ranges); and the

complexity of the medium (whole blood), where thrombin in complex with factors, numerous species of macromolecules and cells represent interfering factors hindering detection through sedimentation or nonspecific interaction mechanisms.

Recent advancement and achievements in fields of biosensing, nanotechnology and microfluidics offer broad options to tackle those problems. Now it has become possible to treat the complex medium, separate its components and perform detection, in time and cost-effective manner, in one miniaturized device, instead of whole lab. Specificity of detection is guaranteed by special molecules called bio-receptors that through specific interaction called “biorecognition” bind their target (molecule or cell) with high affinity and specificity. Devices employing bio-recognition to detect the target are called biosensors.

Biosensor device comprises at least two or more of the following parts: one, as we’ve said, is the bio-receptor, which could specifically recognize and identify target, and the other is the signal transduction part, which could transform the signal of analyte into some detectable signal. Recognition components, typically enzymes, antibodies or nucleic acids, directly decide the selectivity, sensitivity, stability, as well as application prospects of biosensors. Among them, antibodies were regarded as almost the only choice in protein detection. Recently, a new class of recognition components, aptamer, has attracted tremendous attention and been supposed to be promising alternatives of conventional recognition elements.

Using aptamers as the biosensing element for monitoring free thrombin is regarded to have a great potential. In following sections aptamers and their application for thrombin detection will be discussed in more details.

1.3 Aptamer – as a sensing element for a biosensor

In the past two decades, high-affinity nucleic acid aptamers have been developed for a wide variety of molecules and complex systems such as live cells. Conceptually, aptamers are developed by an evolutionary process, whereby, as selection progresses, sequences with a certain conformation capable of binding to the target of interest emerge and dominate the pool. Aptamers have initially been explored for their importance in molecular medicine, but have enormous potential in other biotechnological fields, especially for analytical application, historically dominated by antibodies. In this section aptamers, their selection process, application in various fields will be discussed.

1.3.1 What are aptamers

Aptamers are artificial receptors, selected through a Darwinian-like evolution method to bind their target with high affinity and specificity. Aptamers are usually short (15-80 nt), single stranded nucleic acid molecules such as RNA or single-stranded DNA (ssDNA) or their unnatural analogues, though double-stranded DNA (dsDNA) and peptide aptamers (Hoppe-Seyler et al., 2004) have also been reported.

Making an historical review, the first examples of *in vitro* selected aptamers were small RNA molecules that bound to either T4 DNA polymerase(Tuerk and Gold, 1990) or organic dyes such as Cibacron Blue and Reactive blue (Ellington and Szostak, 1990), reported independently and almost simultaneously in 1990 [1]. These discoveries, however, were based on the advances in medicinal and molecular biology achieved over the preceding 30 years, out of which work of Sol Spiegelman represented the main breakthrough towards the discovery of aptamers (Joyce, 2007). In the mid-1960s Spiegelman realized that the three fundamental processes of Darwinian evolution – amplification, mutation, and selection – could be elevated to a chemical process and applied to a population of RNA molecules in vitro, thus creating first aptamer, although it was not referred to as such (Mills et al., 1967).

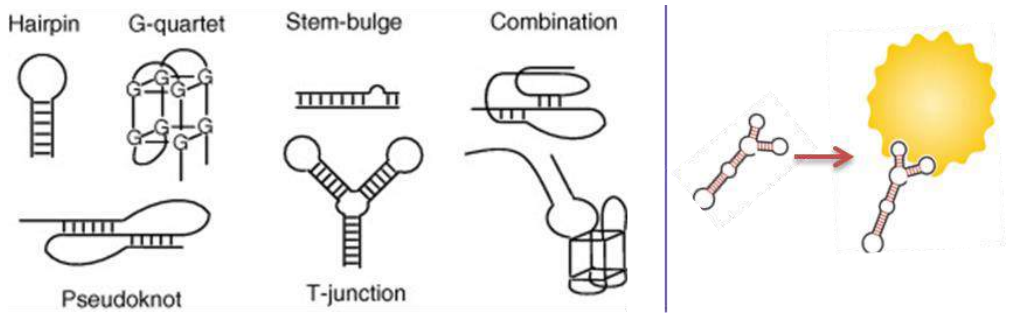

FIGURE 1.10 Schematic illustration of tertiary structures of aptamer, allowing aptamer to adopt specific 3D configuration, necessary for key-lock interaction with target.

[1] Both groups described similar *in vitro* selection process almost simultaneously, Tuerk and Gold coined the term SELEX (Systematic Evolution of Ligands by Exponential Enrichment) for in vitro evolution process of aptamers, whereas Ellington and Szostak gave the name to the aptamers.

The name aptamer, originating from the Latin word "aptus" meaning "to fit" and the Greek word "meros" meaning "part " or "body" (Ellington and Szostak, 1990), references the lock-and-key relationship of aptamers with their targets. In contrast to DNA or RNA sequences, which bind through base-base complementarities, aptamers bind their ligands by folding into well-defined, flexible three-dimensional structures (Fig. 1.10). Three-dimensional shapes of aptamers are characterized by stems, loops, bulges, hairpins, pseudoknots, triplexes, quadruplexes, g-quartets or T-junctions and their combinations (Leontis and Westhof, 2003; Stoltenburg et al., 2007). These conformations allow aptamers to adopt unique interfaces and tightly interact with a wide variety of small and macromolecular targets through dynamic structure compatibility, stacking of aromatic rings, electrostatic and van der Waals interactions, and hydrogen bonding, or from a combination of these effects (Hermann and Patel, 2000; Westhof and Patel, 1997).

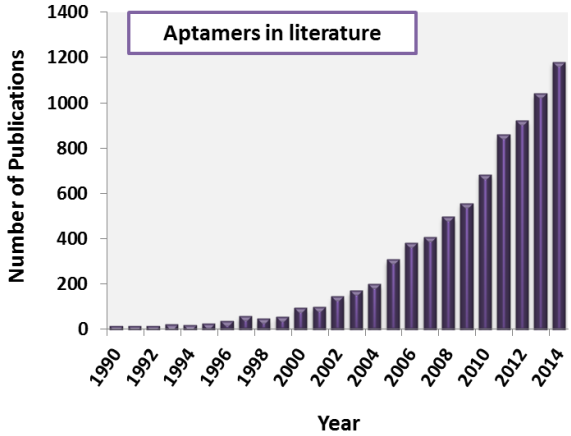

FIGURE 1.11 Aptamers in literature from 1990 to 2014. Results obtained by searching the word "aptamer" in title, abstract or key words of articles indexed by Scopus

Unique structural compatibility, allows aptamers to bind their cognate target with very high affinity and specificity. Having dissociation constants in range from sub-pM to μM, aptamers are comparable with monoclonal antibodies and sometimes even better (Jayasena, 1999). In terms of specificity, aptamers are able to distinguish their target between molecules having the same structure but different functional groups (Jenison et al., 1994), enantiomers (Geiger et al., 1996) closely related macromolecules (Srinivasan et al., 2004) or protein family members (Pagratis et al., 1997).

As a result, since their first appearance, aptamers gained increasing attention evidenced by the expanding number of publications (Fig. 1.11). Consequently aptamers have been selected for wide array of molecular targets (Tombelli et al., 2005) ranging from proteins (Dupont et al., 2011), peptides (Ye et al., 1996), nucleic acids (Noeske et al., 2007), small organic and inorganic molecules (Ellington and Szostak, 1990), antibiotics (Derbyshire et al., 2012), vitamins (Sussman et al., 2000), metal ions (Wrzesinski and Jóźwiakowski, 2008) to even whole cells (Blank et al., 2001; Daniels et al., 2003), viruses (Pan et al., 1995; Wang et al., 2000) or microorganisms (Chang et al., 2013).

1.3.2 Aptamer selection process

Nucleic acid aptamers are screened by a process of *in vitro* selection and evolution referred as SELEX. SELEX, standing for Systematic Evolution of Ligands by EXponential enrichment is combinatorial chemistry technique, developed by Tuerk and Ellington in 1990 (Ellington and Szostak, 1990; Tuerk and Gold, 1990). SELEX enables the selection of ligands from chemically produced oligonucleotide libraries in artificial environment theoretically for any molecular target without the constraints imposed by having to be selected or produced in a living system. With the time, the methodology of SELEX has evolved itself and various formats have been developed beyond the conventional SELEX (Stoltenburg et al., 2007).

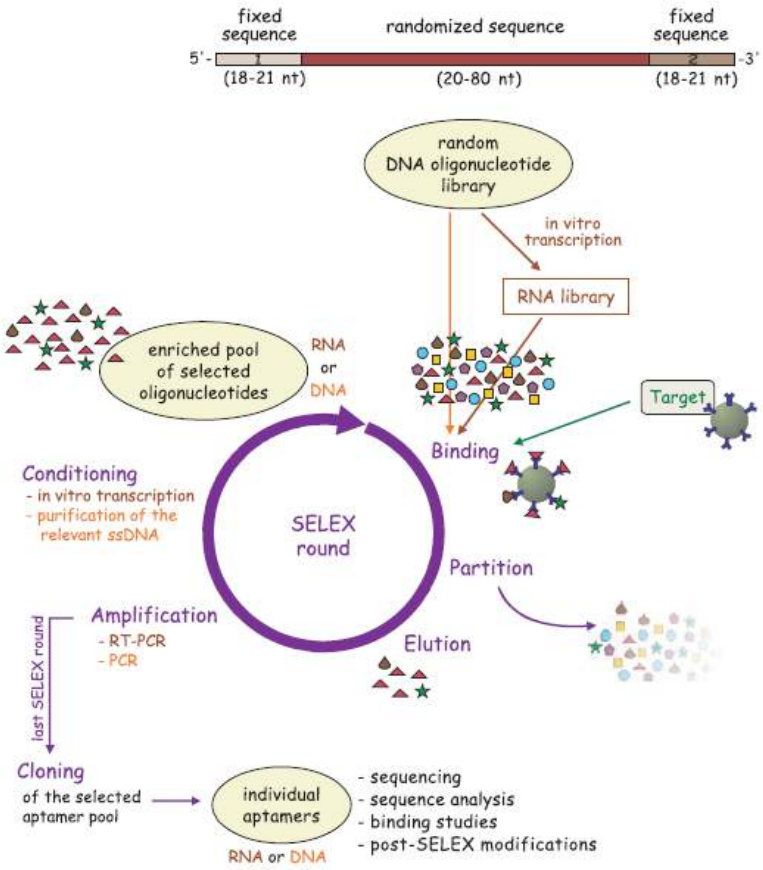

FIGURE 1.12 Scheme of in vitro selection process of aptamers through SELEX . Reprinted from (Strehlitz and Stoltenburg, 2009)

Typically, SELEX process (Fig. 1.12) starts with chemical synthesis of an ssDNA library consisting of about 10^{13} to 10^{15} different oligonucleotides. Each molecule in a library is a liner oligonucleotide with unique sequence, in which central region of randomized 15-60 nt sequence motifs are flanked at both ends by fixed regions containing primer sequences necessary for annealing primers for PCR and/or reverse transcriptase (RT)-PCR amplification. Upon amplification of the randomized pool, RNAs or ssDNAs are generated. This pool is incubated directly with a desired target. The binding complexes are subsequently partitioned from unbound and weakly bound oligonucleotides. Target bound oligonucleotides are eluted and further amplified. The new enriched pool of selected oligonucleotides is used for a binding reaction with the target in the next SELEX round. By iterative cycles (rounds) of selection and amplification under increasingly stringent conditions, the initial random oligonucleotide pool is reduced to relatively few sequence motifs with the highest affinity and specificity for the target. Thus this process drives the selection towards relatively few, but optimized structural motifs able to bind desired targets with high affinity in Darwinian-manner (Göringer et al., 2003). As only the receptor, with dissociation constant in the low nanomolar to high picomolar range is considered as "high affinity", 8 to 15 rounds might be needed until a pool of aptamer candidates for the target is obtained (Marshall and Ellington, 2000).

In order to avoid evolving of non-specific binders to support material (e.g. affinity chromatography column, magnetic beads, nitrocellulose filters etc.), negative selection processes comprising pre-incubation without the target is performed and nonspecifically binding sequences

are excluded (Ellington and Szostak, 1992). Similarly, to avoid cross-reactivity and select aptamers only very specific to the target, a pre-incubation step termed counter-selection is carried out in the presence of potentially interfering molecules (Fitzwater and Polisky, 1996).

Once target-specific oligonucleotide pool is generated, last round of SELEX is stopped just after the amplification step and the PCR products are cloned to get individual aptamer clones from the selected pool. These individual aptamers are sequenced and sequence-analyzed. The identification of common sequences as well as homologous regions in the pool and the comparative analysis of the sequences are conducted to identify consensus motif – the region playing the central role in the specificity of target binding (Hoinka et al., 2012). Selected aptamers are subsequently analyzed by affinity techniques such as SPR, ELONA, fluorescent and radioactive binding assays etc.

SELEX can be conducted virtually for any target; however its success rate has been reported to be at about 50% (Mayer et al., 2010). Target type, size, purity, concentration, charge distribution represent the main constraints of the SELEX. Hence, each target requires unique approach to achieve appropriate selection environment (binding and elution buffers, stringency). Nowadays there are many different modifications of SELEX depending of the specificity of the targets (Stoltenburg et al., 2007). Therefore, selection process might take from weeks to months if completed manually. However, the automated SELEX techniques have been developed and then modified to be applied to the selection of aptamers on a robotic workstation, which allow completing approximately 12 rounds of selection in few days with reduced regents and cost (Cox and Ellington, 2001).

In addition, SELEX has two main limitations: first, is that starting random libraries are always incomplete, given the astronomical number of possible different sequences (4^n different sequences, where n is number of nucleotides in the sequence). Though larger library has higher possibility to contain aptameric sequences, analysis of such system is much more expensive and time consuming (Kim et al., 2007a). Secondly, unfavorable PCR amplification reactions introduce bias towards sequence acquisition, and consequently some sequences, even with the highest affinity, might be neglected and misrepresented (Hamula et al., 2006). One of the main reasons is crosstalk between flanking primer regions with central aptameric sequence.

To overcome limitations of SELEX, the first experimental attempt at non-SELEX selection of nucleic acid aptamers, avoiding PCR amplification step was proposed by Berezovski and Krylov. This method involves repetitive steps of portioning by non-equilibrium capillary electrophoresis of equilibrium mixtures termed NECEEM. This technique allows isolation of high affinity aptamers in fewer rounds (Berezovski et al., 2006). Another method reported recently is DNase-Mediated Single-Cycle Selection enables discovery of DNA Aptamers for proteins blotted on a membrane (Liu et al., 2012).

Computer-assisted library screening methods, on the other hand, offer prediction of potential aptameric sequences allowing synthesis of library with fewer sequences but higher probability. For example, RNA-As-Graph-Pools (RAGPOOLS) web server offers a theoretical tool for RNA in vitro selection and related problems (Kim et al., 2007b); *in silico* selection method for generation RNA library based on RNA secondary and 3D structure and virtual screening of this library was also investigated (Chushak and Stone, 2009).

1.3.3 Aptamer features

Aptamers are attractive receptors for wide range of applications due to their unique combinations of qualities.

Hence, aptamers, characterized by high affinity and selectivity, rival antibodies in all those application fields in which selective recognition is required i.e. in therapeutic, diagnostic and sensing applications (Jayasena, 1999).

Aptamers, being produced through purely chemical process out of nucleic acids enjoy advantages of both chemicals and biological molecules (Tolle and Mayer, 2012). Cost-effective and relatively easy solid phase chemical synthesis of aptamers allows scalable production of aptamers with high reproducibility and purity from commercial sources. Therefore aptamers are less prone to bacterial or viral contamination and batch-to-batch variation. As for selection and production of aptamers, in contrast to antibodies, animal (cellular) host and initiation of immune response are not needed, aptamers can be selected for almost any target in non-physiological even low-immunogenic and toxic.

In contrast to antibodies, nucleic acid aptamers are characterized with remarkable stability; they resist harsh conditions, can undergo reversible chemical or temperature denaturation and show much longer shelf-life. Aptamers often undergo significant conformational changes upon target binding that can be exploited for designing various bio-recognition-based signal transduction formats in biosensing.

Aptamers can function both inside and outside cells, whereas antibodies usually only work outside cells to target secretory proteins or cell surface receptors.

The small size and similarity to endogenous molecules makes aptamers poor antigens, but their half-life in vivo and ex vivo is limited by hydrolytic action of nucleases[1]. However this vulnerability can be easily opposed by chemical modification of the aptamers. Compared to other receptors, the simple chemical structure of aptamer makes it easily amendable to functional modifications which can confer higher stability and nuclease resistance and even improve the overall affinity for the target. Aptamer modification by the introduction of new functional groups brings novel structural/physical/chemical proprieties advantageous for their application in various fields (White et al., 2000). These modifications play important role in aptamer applications and hence, few of them together with the relevant use will be discussed in following paragraph.

[1] Particularly nuclease-sensitive are RNA aptamers, as the hydroxyl group at 2'-position on the ribose promotes phosphodiester bond hydrolysis.

Table 1.2 Aptamers vs. Antibodies

Aptamers	Antibodies
Selection	
SELEX: In vitro Any target (~ 50% success) Any condition Specific site interaction	Cellular immune response in animal host: In vivo Non-toxic, immunogenic target Physiologic conditions Non-defined site of interacting
Production	
Chemical solid phase synthesis: Scalable Cost effective Reproducible No batch-to-batch variation Non-contaminated Easy to add functionalities	Immune response in animal host: Low amount Expensive Batch-to-batch variation Impurities Difficult to add functionalities
Properties	
High affinity High specificity Non-immunogenic Intra and extra cellular action Small size Flexible Functionalities Stability (pH, Temperature) Reversible denaturation Nuclease degradation Long shelf-life	High affinity High specificity Immunogenic Extracellular receptors Large size Non-flexible Sensitive to conditions Irreversible denaturation

1.3.4 Aptamer modifications – dressing up for success

Modifications increase the versatility of aptamer functions and applications. So far, ~100 different modifications can be readily introduced into different parts of aptamers including the nucleosides, the phosphodiester backbone and the 5' and 3' termini *a priori* - within the SELEX process using modified nucleic acid libraries, or *a posteriori* - modifying a selected DNA/RNA aptamer through chemical synthesis or both. In the first case adopted modification has to be compatible with the enzymatic amplification necessary for selection, whereas in the second introduced functional group should be consistent with and non-compromising the aptamer-target recognition. These modifications expand aptamer applications in therapy and diagnostics, detection and as tools in chemical biology (Tolle and Mayer, 2012).

Therapeutic applications: Aptamers possess unique chemical and biochemical characteristics and attractive pharmacokinetic and pharmacodynamic features. The ease and cost-effective synthesis, structural stability across a wide range of temperature and storage conditions, non-immunogenic, non-toxic and degradable character - all these general properties make aptamer interesting tools for therapeutic applications. Aptamers can be used as drugs or as a part of drug-delivery system (Keefe et al., 2010). Since antidotes (complementary DNA), modulating functional performance of aptamers, can easily be designed, aptamers are particularly safe class of therapeutics. Other pharmacokinetic properties such as plasma stability, rate of clearance, uptake and distribution can be further tuned by modifications (Healy et al., 2004).

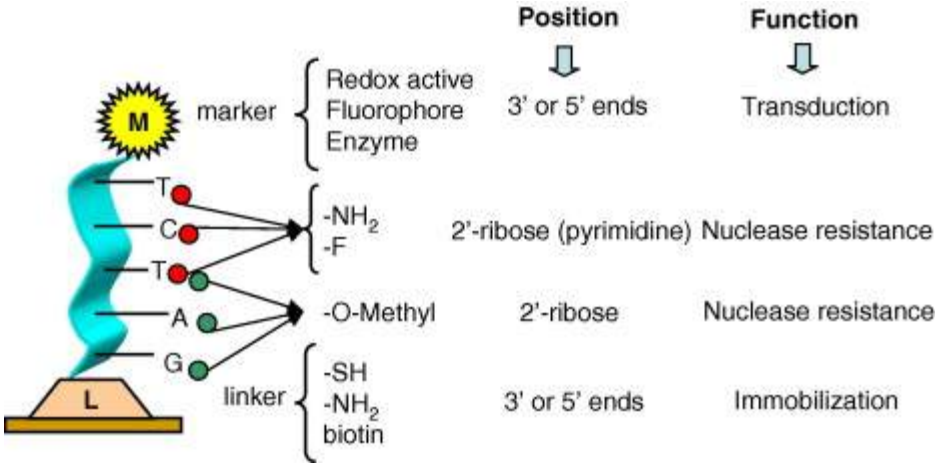

FIGURE 1.13 Schematic illustration of major modifications applied on aptamers to increase stability, append functions and properties. Reprinted from (de-los-Santos-Álvarez et al., 2008)

To address the problem of nuclease resistance for application requiring increased aptamer stability (therapy and in vivo diagnosis) there are several options available: (i) Appending primary amines (2'-NH2) or fluorides (2'-F) to the 2'-position of the pyrimidines or O-methyl groups (2'–OME) to either pyrimidines or purines (Behlke, 2008); (ii) Modification of the phosphodiester backbone with phosphorothioate (thioaptamers); (iii) Locking nucleosides by interlinking 2'-O and 4'-C a methylene group to create Locked Nucleic Acids (LNA) (Petersen and Wengel, 2003); (iv) Circularization or Capping the 3'-termini by various functional groups or inverted thymidine (3'-idT), which creates an additional 5'; (v) Use of chiral (L-aptamers) so-called spiegelmers (Nolte et al., 1996). Single or combinatorial modification of aptamers were shown to not only increase aptamer half-life in serum from several minutes to several days in vivo but also augment their affinity and thermal stability (White et al., 2000).

Circulation half-life, uptake and distribution can be improved by tagging aptamers at the termini. Due to relatively small size (10-15 kDa), aptamers can be easily cleared from human blood through the kidney and liver. Annealing large molecular weight Polyethylene glycol (PEG) or lipid tag extends circulation half-life from few minutes up to one day. Tagging with lipids and cell-penetrating peptides may help tissue uptake of aptamers (Healy et al., 2004).

Aptamers can also be used as delivery vehicles. Aptamers that bind to internalized cell surface receptors can be used for targeted drug and other cargoes delivery into cells. This is very useful for example in cancer chemotherapy, which aims to kill cancer cells with cytotoxic drugs without harming noncancerous cells.

Drug molecules can be directly covalently linked to aptamers (Kanwar et al., 2011). Aptamer combinations with another aptamer, functional biomacromolecule and/or chemical compounds are termed as Chimeras (Burke and Willis, 1998). Aptamers anchored to cargo-bearing liposomes through dialkylglycerol (DAG) or cholesterol functionalities have been used for cargo (Perche and Torchilin, 2013), whereas aptamer-nanoparticle conjugates have found application, for diagnosis, imaging, targeting cancer cells (Huang et al., 2005).

Application in detection: Owning high specificity and affinity in nanomolar (0.1-100 nM) range, and the availability of such a large pool of aptamers makes it possible to develop novel bioassay tools covering areas that include diagnostics, anti-bioterrorism, and environmental and

food analysis. The possibility to conjugate aptamers with functional moieties extends is advantage in many orders. Post selection modification of aptamers at either on 3' or 5' with biotin, thiols, amines, carboxyl, phosphates, and cholesterol not only protects them from exonuclease, but also allows their anchoring and conjugation to enzymes or diverse supports (Tombelli et al., 2005; Zhou et al., 2010, 2011).

Introducing signaling moieties such as fluorophores or chemical reactive (redox) groups provides possibility to combine sensing and signal transduction in one molecule. These qualities offer great flexibility in the design of biosensors (de-los-Santos-Álvarez et al., 2008).

Another type of modification provides cross-linking ability by introducing 5-Br(d)U or 5-I(d)U during SELEX. This type of aptamers are called photoaptamers as under laser irradiation 5-Br(d)U or 5-I(d)U can specifically cross-link with proximal amino acids having aromatic or sulfur groups (Bock et al., 2004).

Especially well-suited for diagnostic purposes seem to be so called SOMAmers - "Slow Off-rate Modified Aptamer". SOMAmers, due to the presence of 5-tryptaminocarbnyl-Ud modifications, contain additional aromatic side chains which enhance hydrophobic and pi-stacking interactions and generate very low-off rates (Gold et al., 2012).

1.3.5 Thrombin aptamers

Thrombin has been one of the most studied targets for aptamer binding and there are various aptamers selected against thrombin.

Following the first reports of isolation of RNA aptamers by SELEX method in 1990 (Ellington and Szostak, 1990; Tuerk and Gold, 1990), Bock and colleagues used thrombin as the first protein target, that normally does not interact with nucleic acids, to select the first single-stranded DNA aptamer (Bock et al., 1992). Since then at least four thrombin-binding aptamers and their various modified versions have been identified. Selection of thrombin aptamers was motivated/guided by the therapeutic application as the anticoagulant and therefore only the aptamers showing the inhibition of fibrinogen clotting have been described and investigated (Macaya et al., 1995). However some thrombin aptamers also become main tools in biosensor development and are widely used as prove of concept. Thrombin aptamers represent about 20% of the 5000 papers published about the use of aptamers for analytical technologies (Deng et al., 2014). Thrombin aptamers will be discussed below.

1.3.5.1 HD1

HD1 aptamer, known also as G15D, HTQ, TBA (Thrombin binding aptamer) or ARC183 (Archemix), is a 15 base long single-stranded DNA aptamer with the sequence 5'-GGTTGGTGTGGTTGG-3'. HD1 was isolated the first in 1992 by Bock et al. as the first ssDNA aptamer against thrombin, the protein with no known nucleic acids binding properties (Bock et al., 1992). Since its discovery, it has been the most investigated aptamer. HD1 was also the first aptamers to be used for aptasensor development.

HD1, shown to inhibit thrombin-catalyzed fibrinogen clotting in vitro and reduce arterial thrombus formation *ex vivo*, binds alpha-thrombin with nanomolar affinity primarily at highly basic anion-binding (fibrinogen-binding) exosite I (Bock et al., 1992; Paborsky et al., 1993), though

there exist some indications of interaction to exosite II as well (Padmanabhan and Tulinsky, 1996). The structure of this aptamer and the mechanism of interaction with thrombin will be in more details discussed in chapter 3.

1.3.5.2 NU172

NU172 with sequence 5'-CGCCTAGGTTGGGTAGGGTGGTGGCG-3' is 26-mer ssDNA aptamer also known an ARC2172 (HUTABARAT, 2010). It was developed as the optimized/alternative form of HD1 (Archemix) for improved therapeutic purposes, which is now under phase II clinical trial (ARCA Biopharma; Mayer et al., 2011). This aptamer is one of the latest thrombin aptamers and is not widely investigated. It is thought to bind exosite I of thrombin with nanomolar affinity, but nothing more is known.

1.3.5.3 HD22

HD22, also known as HTDQ, is the 29-mer ssDNA aptamer with the sequence 5'-AGTCCGTGGTAGGGCAGGTTGGGGTGACT-3' (Tasset et al., 1997). The affinity of HD22 aptamer is slightly better than that of HD1. HD22 recognizes the heparin-binding exosite II of thrombin, inhibiting the activations of FV and FVIII and hence showing moderate effect on fibrinogen regulation, is not considered for therapeutic applications but together with HD1 is often used in sensing. The thrombin-HD22 interaction will be discussed in more details in the chapter 3.

1.3.5.4 Thrombin RNA aptamer

TOG25 or Toggle-25 is a thrombin-binding 25-mer RNA aptamer with sequence of 5'-GGGAACAAAGCUGAAGUACUUACCC-3' contains 2′fluoropyrimidine C and U nucleotides. TOG25 binds to thrombin near exosite II with Kd of about 3 nM, slightly modulating platelet activation but not affecting fibrinogen conversion (White et al., 2001). For this reason, its use as anticoagulant has been abandoned. Although several studies have used RNA aptamer for biosensing application, degradation by nuclease represents main compromising point, rendering this aptamer less attractive (Bompiani et al., 2012).

1.3.5.5 Advantage of multiple binding sites and aptamers

The existence of two anion-binding sites on the surface of thrombin and availability of corresponding aptamers clearly represents the important advantage for biosensor development. Simultaneous targeting of two sites allows increased specificity towards target and flexibility in terms of choosing and developing biosensing strategies. It diversifies also bio-recognition and signal transduction approaches. Indeed in the past decade various aptamer-based approaches for thrombin detection were proposed and some of the most prominent ones will be covered in the next section.

1.4 Aptamer –based detection of thrombin

Aptamers clearly represent very promising biorecognition elements: high affinity and specify assure sensitive and precise biorecognition; small size combined with chemical modifications allows efficient immobilization at high density on the surface of various planar and nanoparticle materials, which is a crucial importance in miniaturized systems such as a bioarrays and biochip; nucleic acid origin grants long shelf-life and chemical and thermal stability, offering advantage of regeneration and reusability; inherent conformational flexibility, ability to form reversible complexes with various molecules together with possibility to conjugate with various dyes, chemical reactive groups and nanomaterials for signal generation and amplification, permit use of aptamers in various biorecognition and signal transductions formats (Jayasena, 1999). Depending on the type of transduction type, the analyte detection could be mainly performed by optical, or electrochemical or mass sensitive techniques.

Thrombin, a protein with two anion-binding sites and with at least two aptamers for each site, opens up a large spectrum of sensing opportunities. Indeed, since the first report of optical aptasensor for thrombin in 1997 (Potyrailo et al., 1998), more than 1000 aptamer-based assays and biosensors coupled with different transduction principles have been described in the literature for thrombin (Deng et al., 2014). However, it should be highlighted, that thrombin was mostly used as a model protein to demonstrate the usefulness of several method and different formats, sometimes for the first time and not all of them aimed to detect thrombin as the real target in real conditions.

1.4.1 Binding assay configuration

Prior to discussing thrombin aptasensors based on various detection methods in more details, it should be noted that sensitivity and transduction of bio-recognition events of those methods depend on the design of the assay. For thrombin, having two distinct binding sites and several aptamers specifically recognizing each of them, there are numerous assay configurations designed. Majority of these designs can be classified into two categories of configuration (Fig. 1.14): (i) single-site binding; and, (ii) dual-site binding (Song et al., 2008).

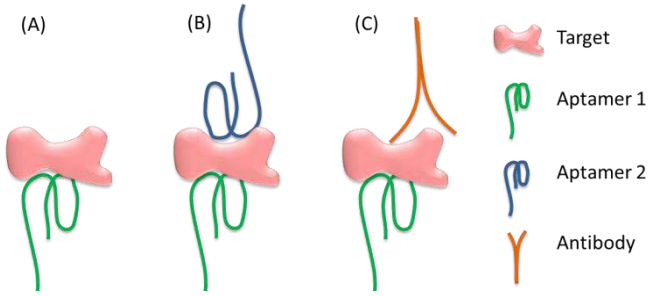

FIGURE 1.14 Aptamer-based detection assay formats for thrombin. (A) Single-site binding ;(B) Dual-site binding involving two aptamers (C)Dual-site binding involving aptamer and antibody.

Single-site binding, although seems to refer simple interaction (Fig. 1.14 (A)), however, contrary to antibodies, chemical composition of aptamers, granting flexibility and ability to form complementary base-pairing and allowing incorporation of signaling moieties, offers wide range of detection opportunities. Apart from single affinity binding to target that can be detected with conventional methods such SPR or QCM, aptamers are also able to give signal output upon bio-

recognition detectible with various optical and electrochemical methods. These methods take advantage of aptamer to take part in molecular beacons, catalytic beacons, enzymatic amplification reactions, interactions with nanomaterials, etc. to generate the signal (Deng et al., 2014).

Double-site binding also known as sandwich assays, is the approach in which the analyte is sandwiched by a pair of receptors, one regarded as capture probe and the other reporter probe (Fig.1.14 (B,C)). Capture probes are often immobilized on the surface of solid supports (e.g., electrodes, glass chips, nanoparticles or micro-particles), while reporter probes are often conjugated with signaling moieties (e.g., fluorophores, enzymes or nanoparticles (NPs)). Double-site binding assay is not only a mean of detection but it assures increased detection specificity as well. As thrombin can bind distinct aptamers on two distinct binding sites without interfering with each other, sandwich assay is one of the most used assay formats. For thrombin the most sandwich format assay use HD1 and HD22 pair (Baldrich et al., 2004; Gill et al., 2006; Ikebukuro et al., 2004), but assays based on HD1 and antibodies (Kang et al., 2008)also have been described. (Ikebukuro et al. 2004, 2005; Osawa et al. 2009) (Kang et al. 2008).

Based on the complexity of the detection, aptamer-based assays might be classified into homogeneous and heterogeneous assays. Homogeneous assays or so-called non separation assays work in a solution phase in "mix and read" format, not demanding immobilization, separation, or washing procedures. Therefore simultaneous target recognition and signal output are two essential requirements for homogeneous assays. Although such assays can potentially deliver simplicity to end users, especially for on-site and resource-limited applications, the disadvantage is lower sensitivity compared to heterogeneous assays. In heterogeneous assays, on the other hand, detection of bound analyte is made after time consuming incubation-washing-separation steps and immobilization might be required (Deng et al., 2014; Sassolas et al., 2011).

1.4.2 Optical detection

Aptamers have been widely used as bio-recognition elements in optical bioassays. Optical approaches include analyte detection either in liquid or at the interface of solid/liquid phase through fluorescence, colorimetry or the alterations the optical properties (surface plasmon resonance (SPR), evanescent wave spectroscopy, etc.)

1.4.2.1 Fluorescence

Fluorescent detection is widely employed due to the easiness of aptamer labeling with fluorescent dyes, the availability of wide array of fluorophores and quenchers, and the consequent ability for real-time detection. Detection is based on a variation in fluorescence properties of a molecular recognition unit that occurs when it interacts with the target. Fluorescence represents the main detection mode described for most homogeneous aptamer-based assays, however it is also used in heterogeneous formats (Sassolas et al., 2011). There are several main strategies developed for reporting biorecognition of thrombin by aptamers using both one-site or sandwich formats (Song et al., 2008).

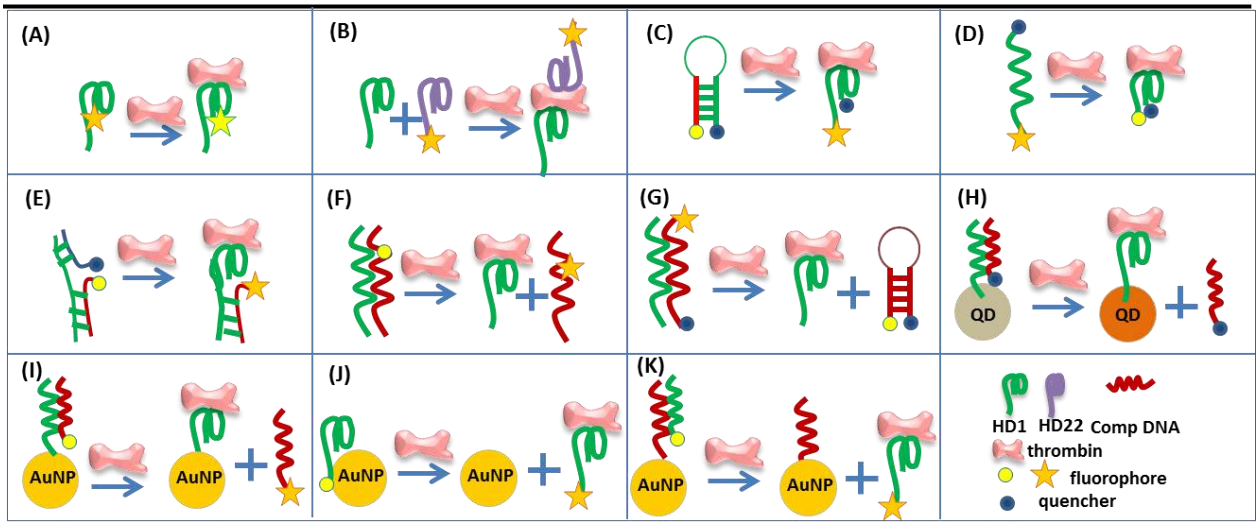

FIGURE 1.15 Aptamer-based fluorescence assays for thrombin detection (A) change of fluorescence anisotropy or intensity upon thrombin binding; (B) ELISA-type detection with fluorescently-labeled secondary aptamer; (C-E, G) FRET turn-on and turn-off formats; (F) Fluorescence turn-on upon thrombin binding; (H) quantum dote or (I-K) gold nanoparticle-mediated turn-on detection of thrombin.

Single-fluorophore-labeled aptamers have been used to report target–aptamer binding by monitoring the changes of fluorescence intensity or anisotropy resulting from the changes of the microenvironment or rotational motion of the fluorophore (Fig. 1.15 (A)). In the very first thrombin aptasensor fluorescently labeled HD1 aptamer was covalently attached to a glass support. Monitoring the evanescent-wave-induced fluorescence anisotropy change upon thrombin addition, they detected sub-nanomolar concentration of thrombin (Potyrailo et al., 1998). Similar approach was used for detection and quantification of thrombin on-chip (McCauley et al., 2003). An interesting assay is based on DNA-tiles containing HD1 aptamer, enabling thrombin detection in sub-nanomolar concentrations (Lin et al., 2006). Aptamers were modified with 3-methylisoxanthopterin (3-MI) fluorophore, in a region undergoing environmental change during thrombin binding and yielding increase in fluorescence signal. First ELISA-like approach for HD1 aptamer and anti-thrombin antibody in direct and competitive experiments enabled sensitive thrombin in low nanomolar range (Baldrich et al., 2004). Later HD22 labeled with fluorescent dye (Edwards and Baeumner, 2010; Meneghello et al., 2012) or quantum dot (Tennico et al., 2010) was used to report the capture of sub-nanomolar concentrations thrombin by surface-immobilized HD1 in sandwich format (Fig. 1.15 (B)).

Taking advantage of the ligand-induced conformational changes of aptamers, a number of assays have been developed based on principle of fluorescence resonance energy transfer (FRET). One of the first attempts included aptabeacon, in which the flourophore-labled 5' termini of HD1 aptamer was extended by a few nucleotides complementary to those at quencher bearing 3'end in order to create stem-loop structure (Hamaguchi et al., 2001). Upon thrombin binding aptamer adopted aptameric confirmation, increasing the distance between the fluorophore and the quencher and therefore reducing the quenching effect and producing fluorescence (Fig. 1.15 (C)). This "turn-on" assay based enabled thrombin detection in range of 10-50 nM concentration. Contrary, fluorescence "turn-off" was used to report the detection of thrombin in sub-nanomolar concentration, by HD1 aptamer bearing fluorophore at one extremity and a quencher on the opposite (Fig. 1.15 (D)), which upon thrombin binding would appear in close proximity to quench the fluorescence (Li et al., 2002). Ingenuous approach to generate fluorescence signal upon

thrombin detection was the use of "structure switching signaling aptamer" (Nutiu and Li, 2003). The construct was composed of duplex made out unlabeled aptamer hybridized with fluorophore-labeled ssDNA and quencher-labeled ssDNA (Fig. 1.15 (E)). Thrombin binding induced release of quencher-bearing ssDNA and enabling fluorescence emission. Further improved strategies were proposed for a simpler competitive molecular beacon that required only the complementary DNA to be modified with fluorescent nucleotide for "turn-on" format (Fig. 1.15 (F)) and fluorophore quencher couple at the extremities for "turn-off" (Fig. 1.15 (G)) option (Li and Ho, 2008).

Other molecular beacons based on above-described strategies were adapted to aptamers conjugated with quantum dots or nanoparticles. For example thrombin aptamer was labeled with quantum QD (Fig. 1.15 (H)), the emission of which was quenched by the quencher embedded in complementary DNA in the absence of thrombin and restored upon competitive DNA displacement by thrombin (Levy et al., 2005). Sub-nanomolar concentrations of thrombin were detected by the essays employing gold nanoparticles (Wang et al., 2008a). Thrombin aptamer was either grafted, hybridized to complementary DNA or just adsorbed on the surface of AuNP, leading to quenching of the fluorescence in the absence of thrombin (Fig. 1.15 (I,J,K)).

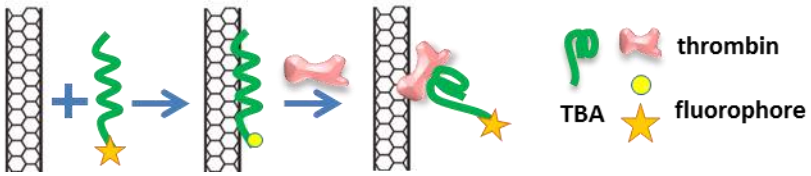

FIGURE 1.16 Fluorescence signal modulation by carbon nanotube. The fluorescence of the labeled aptamer quenches when it is adsorbed on the surface of a carbon nanotube. Once thrombin interacts with the aptamer, the folding of aptamer changes leading to fluorescence signal recovery

Apart for gold nanoparticles various other nanomaterials such as carbon nanotubes (Yang et al., 2008), graphene (Chang et al., 2010), mesoporous carbon microparticles (Zhang et al., 2011b), poly(m-phenylenedi-amine) rods (Zhang and Sun, 2011), and carboxylic carbon nanoparticles (Liu et al., 2011) possess capacity to non-covalently absorb single-stranded DNA and to quench fluorescence with high efficiency (Fig. 1.16). These properties underlay the assays in which the fluorescence of fluorophore- or quantum dot-labeled HD1 is quenched as it is adsorbed on the surface of one of these nanomaterials in the absence of thrombin and fluorescence is restored upon binding the target. (Choi et al., 2006).

1.4.2.2 Colorimetric detection

Colorimetric detection is the second most popular approach homogeneous aptamer-based assays as it offers the simplest sensing mode (Sassolas et al., 2011). Namely, the biorecognition is accompanied with color change, observable in visible spectrum even by necked eye. Assays mostly relay on: (i) aggregation of unmodified or aptamer-modified gold nanoparticles; (ii) aptamer-involving catalytic reactions; (iii) interactions with a cationic polymer.

The popularity of use of **gold nanoparticles for colorimetric detection** relays on the intrinsic property of nanoparticles - the surface plasmon resonance absorption. Due to this phenomenon suspended nanoparticles disperse light in red spectrum, but when particles aggregate absorbance maximum shifts towards blue. Hence, colorimetric assays based on analyte-induced assembly (red-to-blue color change) or disassembly (blue-to-red color change) of unmodified or aptamer-functionalized AuNPs can be distinguished.

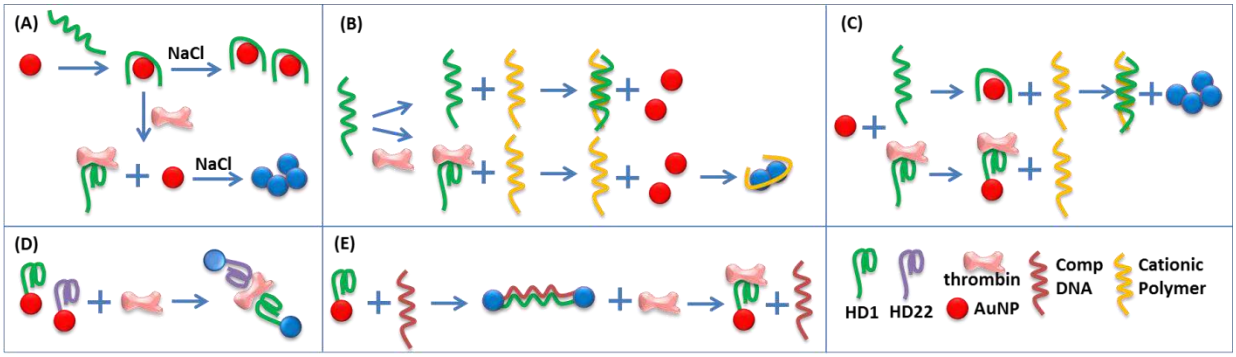

FIGURE 1.17 Colorimetric AuNP–based thrombin aptasensors. Unmodified gold nanoparticles aggregate in the presence (A-B) or in the absence (C) of thrombin. Aptamer-modified gold nanoparticles (D) aggregate when interlinked through thrombin or (E) get stabilized by the presence of thrombin.

A thrombin detection approach based on interaction of unmodified AuNPs and HD22 aptamers in the presence and absence of thrombin was described to detect thrombin concentration in a linear range up to 10 μM with a detection limit of 8.3 x 10^{-10} M (Wei et al., 2007). In the absence of thrombin, due to electrostatic interactions unfolded aptamers adsorbed on the surface of unmodified AuNPs, restricting particle aggregation and stabilizing colloidal solution even in relatively high salt concentration. However following thrombin titration, aptamers changed conformation, salt screened the negative charge and led AuNPs to aggregate, causing a corresponding red-to-blue color change (Fig. 1.17 (A)). Similar approach also with non-modified nanoparticles involved interaction of AuNPs with thrombin-aptamer complex in the presence of salt and cationic conjugated polymer (Xia et al., 2010). Aptamer adsorbed on the surface of AuNP and kept colloidal solution red. Though, when cationic conjugated polymer was added, it removed all unfolded aptamers not paired with thrombin from the surface of AuNP, leading to aggregation of particles (Fig. 1.17 (B)). The more thrombin was titrated the less was the aggregation. Another colorimetric aptasensor based on aggregation of unmodified AuNPs in the presence water-soluble cationic polymer poly(diallyldimethylammonium chloride) (PDDA) allowed thrombin detection down to 1 pM with high selectivity in the presence of other interfering proteins and in human serum sample (Chen et al., 2014). HD1 aptamers adsorbed on the surface of AuNPs stabilized colloidal solution in the presence of PDDA, but following the injection of thrombin aptamers switched the structure and facilitating (PDDA)-induced AuNP aggregation (Fig. 1.17 (C)). Aggregation of HD1-modified AuNPs in the presence of thrombin was first demonstrated by Pavlov (Pavlov et al., 2004). Nanoparticles were cross-linked by thrombin since HD1 interacts not only with exosite I but also with exosite II of thrombin. This approach enabled delectation of thrombin as low as 20 nM concentration. Recently detection sensitivity was improved in similar approach achieving 5 pM detection limit (Peng et al., 2013). Two strategies, one based on aggregation of AuNP modified with two distinct thrombin aptamers (Fig. 1.17 (D)), and another based on disassembly of HD1 aptamer-capped AuNP aggregates interconnected with complementary to HD1 strand (Fig. 1.17 (E)) were investigated in the thesis of Yan (Yan and Zeng, 2010). In the first case thrombin, interacting with both aptamers simultaneously, induced aggregation in sandwich-like manner achieving 10 nM detection limit. Whereas in the second approach, thrombin competed for binding with HD1, displacing complementary strand, and led to disassembly of aggregate. Apart from liquid phase, colorimetric assays for thrombin have been also design for solid phase. For example, a dot-blot assay for

thrombin detection was reported based on thrombin adsorbed nitrocellulose membrane and HD1-AuNPs conjugates (Wang et al., 2008b). Catalytic reduction of silver ions was used for signal amplification allowing thrombin detection at the range of 0.115 to 9.25 pmol in 1% plasma. Xu et al. reported aptamer-AuNPs as probes in aptamer-based dry-reagent strip biosensor for thrombin analysis in sandwich format (Xu et al., 2009). One aptamer was immobilized in test zone and second on the AuNP. In the presence of thrombin, sandwich was assembled on the surface of the test-zone giving color signal. This simple biosensor provided a linear response for thrombin over the concentration range of 5-100 nM, with a detection limit of 2.5 nM.

Wide range **catalytic colorimetric sensors** have been reported for thrombin. Catalytic molecular beacons consisting of thrombin aptamer hairpin and G-quadruplex were developed for colorimetric detection of thrombin oxidation of either 2,20-azinobis(3-ethylbenzthiazoline-6-sulfonic acid) (ABTS) (Li et al., 2008) or 3,30,5,50-tetramethylbenzidine sulfate (TMB) (Zhang et al., 2011a). H_2O_2-mediated oxidation catalyzed by DNAzyme region in the presence, in the first case, and the absence, in another case, hemin groups as cofactor. In the absence of target the G-quadruplex DNAzyme catalyzed the H_2O_2-mediated oxidation of to generate a colorimetric signal, however titration of thrombin induced dissociation of the beacons, causing decrease in catalytic activity and color change. The product can be detected by UV–vis absorption spectrometry. Both assays enabled thrombin detection down to 20 nM concentration. Another approach based on H_2O_2-mediated oxidation of 3,30,5,50-tetramethylbenzidine sulfate involves platinum nanoparticles (PtNPs) in the presence of luminol to catalyze chemiluminescence signal (Gill et al., 2006). Oxidation takes place upon assembly of aptamer/thrombin/aptamer-PtNP sandwich. Further, a peroxidase-mimicking Fe_3O_4 magnetic nanoparticles were used to catalyze the H_2O_2-mediated oxidation of TMB for thrombin detection (Hu et al., 2013). For this purpose, Fe_3O_4 nanoparticles were encapsulated within mesoporous silica and functionalized with aptamer. Without thrombin, H_2O_2 and TMB entered the silica layer and reacted with Fe_3O_4 nanoparticles, giving a strong absorbance signal. However, following the addition of thrombin, formed aptamer-thrombin complex created a block layer outside the nonreactor, making it difficult for substrates to penetrate inside the nanoparticles. Characteristic absorbance signal decreased with increase of thrombin concentration achieving detection limit of 0.19 nM. Another aptamer-based colorimetric platform thrombin detection was developed, taking advantage of aptamer-functionalized magnetic particles (MPs) for target capture, concentration and separation, and aptamer-conjugated gold nanoparticle (AuNP)-catalyzed color bleaching reaction of methyl orange (MO) to generate the colorimetric signals. This essay allowed detection of human thrombin with a detection limit of approximately 320 pM for naked eye observation, 30 pM with the help of a UV-vis instrument (Li et al., 2013).

Metal complex [Ru(phen)2(dppz)]2+ was used in **displacement assays** for the detection proteins including thrombin in sub-nanomolar range within buffer and serum (Jiang et al., 2004). This assay took advantage of the luminescence signal decrease due to the release of rutherium from thrombin RNA aptamer-bound state upon protein/aptamer binding. Easy and universally applicable colorimetric approach was described by using a cationic water-soluble polymer polythiophene (Ho and Leclerc, 2004). In the absence the cationic polymer binds to the negatively charged backbone of the aptamer. When thrombin aptamer folds into G-quadruplex

conformation upon thrombin binding, the polymer prefers wrapping around it, inducing colorimetric response, color change from red to orange, enabling detection as low as 2 x 10^{-15} mol of human thrombin.

1.4.2.3 Other solid-phase optical methods

Methods based on Surface Plasmon Resonance (SPR), Surface Enhances Resonance Scattering (SERS), wave guide resonators, enable thrombin detection through target interaction with surface-immobilized aptamer in one site or sandwich type format. These methods can be incorporated in fluidic systems for lab-on-chip applications.

Surface plasmon resonance (SPR) spectroscopy, in combination with one-step direct binding, competition, and sandwiched formats, was applied to study thrombin binding to HD1 and HD22 aptamers and showed linear increase in signal in the range 5-250 nM of thrombin (Tang et al., 2007). Surface plasmonic fiber devices using immobilized HD1 aptamer were demonstrated to detect thrombin from sub-pM to high nanomolar concentrations in one-site binding format (Allsop et al., 2010). Sensitivity of SPR might be further enhanced by introducing long-period fiber gratings (LPG) (Coelho et al., 2014). Another technique recently employed for the detection of protein on aptamer microarrays is Surface Plasmon Resonance Imaging, which has an advantage of SPR combined with micro arrays and optical detection allowing detection simultaneously several analytes through one site-binding or sandwich enzymatic amplification assay. As low as 0.5 pM thrombin was detected with RNA aptamers (Li et al., 2007).

SERS aptasensors for thrombin detection relay on another interesting property of gold nanoparticles - Surface Enhanced Raman Scattering. HD1-AuNPs have been used in SERS for thrombin detection. Wang et al. developed a SERS sensor for thrombin recognition using Au NPs labeled with aptamer and Raman reporters (rhodamine 6G) (Wang et al., 2007). Biorecognition of as low as 0.5 nM thrombin concentration was achieved by assembly of gold substrate-HD1/thrombin/HD22-AuNPs sandwich construct, which gave enhanced signal in the presence of silver particles. Recently, Cho et al. reported a surface enhanced resonance Raman scattering (SERRS) sensing mechanism based on thrombin induced displacement of Raman probe (methylene blue) modified HD1 from Au NPs (Cho et al., 2008a). The SERS signal decreased with increasing thrombin concentration over the range of 0.1 nM to 1 μM, with an LOD of 0.1 nM. In addition, the sensor allowed detection of 1 nM thrombin in the presence of 10% fetal calf serum.

An optical microsphere resonator biosensor using immobilized HD1 aptamer to capture thrombin enabled detection of thrombin in one-site binding assay from 10 nM up to 5 μM concentration (Zhu et al., 2006). Recently micro ring resonator was shown to detect the capture of 0.5 nM thrombin by surface immobilized HD1 aptamer (Byeon and Bailey, 2011). Thrombin in the concentration range of 0.5–75 nM was detected using resonant mirror method (IAsys instrument (Neosensors Ltd., UK)) (Strehlitz et al., 2008). Thrombin sensing was realized in one-site binding assay by HD1 aptamer bound to the surface of the cuvette.

1.4.3 Electrochemical detection

Electrochemical detection is of particular interest as it is simple, highly sensitive, compatible with novel microfabrication technologies and relatively low-cost. Electrochemical

detection concerns the recognition of a binding complex on conductive surfaces that induces to variations in the current, potential, resistance or capacitance of the solution-electrode interface, due to chemical reactions or redox indicators. These methods, including (volt)amperometric, impedimetric, potentiometric transducers or a combination require aptamer immobilization on

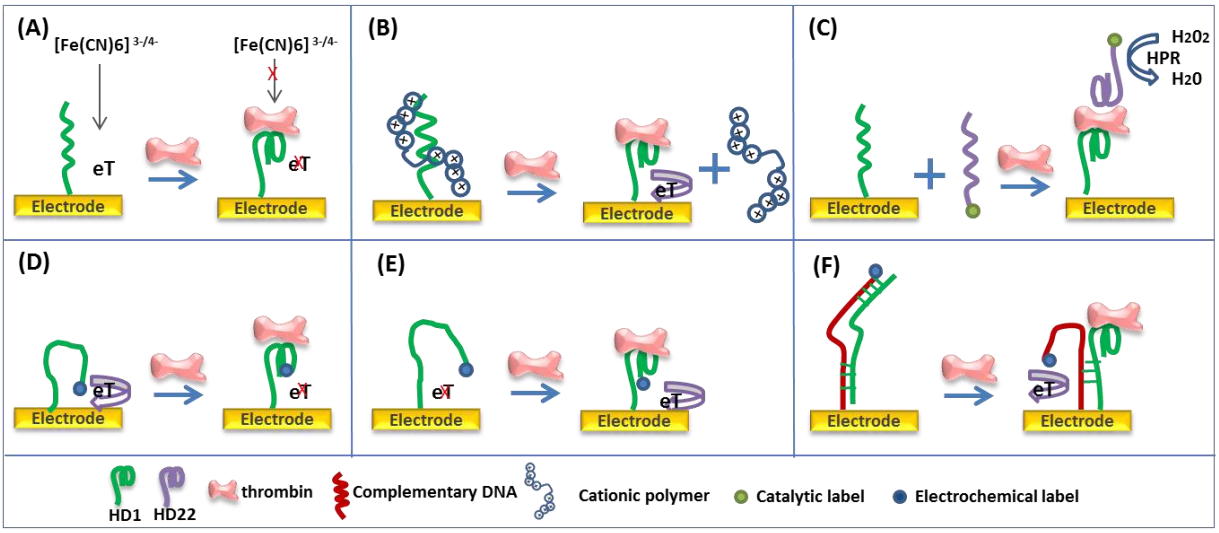

FIGURE 1.18 Aptamer-based electrochemical assays for thrombin detection. The presence of thrombin sterically (A) shields or (B) enables electron transfer to electrode; (C) Secondary reporting aptamer, upon binding to captured thrombin in the sandwich format, catalyzes the chemical reaction; Thrombin binding turns (D) off or (E-F) on the electron transfer from the aptamer-bound electrochemical label.

the surface and in some approaches conjugation with enzymes, redox moieties or nanoparticles (Deng et al., 2014; Song et al., 2008). In general aptamers are immobilized on gold electrodes but the use of various nanomaterials and conductive films such as nanotubes (Porfireva et al., 2010), MWCNTs (Kara et al., 2010), Graphene-nanoparticles (Jiang et al., 2012), PAMAM dendrimers (Zhang et al., 2009), pyrolized surfaces (Lee et al., 2008), nano-Au/thionine multilayer film (Yuan et al., 2010) enhance the sensitivity of electrochemical detection for 2-3 orders, enabling sensing of thrombin in several pM concentration. Electrochemical signals are typically generated through three main mechanisms: (i) label-free (ii) with conjugated catalytic labels and (iii) altering the proximity of electrochemical labels to the electrodes (Song et al., 2008).

For **label-free** detection, impedance is one of the most commonly reported transduction techniques for electrochemical aptasensors, as detection can be achieved simply following target binding, which changes the impedance. The transduction principle is mainly based on monitoring the electron-transfer of the electrochemical redox marker [Fe(CN)6]3-/4- , whose access to the surface and therefore electron transfer is impeded or enhanced, depending on the specific experimental set-up (Fig. 1.18 (A)). Detection of low nanomolar concentration of thrombin were reported in various studies (Cai et al., 2006; Castillo et al., 2012; Radi et al., 2005). The sensitivity of this format can be further enhanced for example by denaturing captured thrombin upon addition of guanidine hydrochloride that causes and increases blocking effect against electron transfer, achieving detection limit of 10 fM (Xu et al., 2006). Similar detection limit was achieved using neutralizer displacement strategy (Das et al., 2012). A thrombin aptamer was tethered to the surface of an electrode and was hybridized with a neutralizer, composed of peptide DNA (PNA) and cationic amino acids. Upon binding to thrombin, the aptamer changed its structure and released the neutralizer, turning on the electrochemical signal (Fig. 1.18 (B)).

The use of **catalytic labels**, including redox enzymes and nanoparticles, for thrombin detection, often requires a sandwich assay format to produce thrombin-specific signals. The first example of an electrochemical aptasensor was reported by Ikebukuro et al. who reported used a sandwich format to detect thrombin by chronoamperometry (Ikebukuro et al., 2004, 2005). HD1 aptamer was immobilized a gold electrode to capture thrombin to which further HD29 aptamer bearing either enzyme–glucose dehydrogenase (GDHPc) or pyrroquinoline quinone glucose dehydrogenase ((PQQ)GDH) was bound. Electrical current change upon addition and consequent degradation of glucose correlated to the captured thrombin concentration, achieving a detection limit of 1 μM for GDHPc and 10 nM in the case of (PQQ)GDH. Similar approach, again sandwich format, employed HD22 aptamer now linked to horseradish peroxidase (HRP) as a catalytic label. The HRP catalyzed the relay-mediated reduction of H_2O_2 (Fig. 1.18 (C)) , measured by amperometric signal allowed detection of thrombin of 80 nM (Mir et al., 2006). Recently, 0.1 nM detection limit was achieved through DPV monitoring of enzymatic ascorbic acid oxidation by alkaline phosphatase, conjugated to HD22 reported aptamer via streptavidin-biotin linkage (Xu et al., 2013). Other option to improve the sensitivity is use of various nanomaterials have as more efficient catalytic labels. For example, use of PtNPs instead of enzymes to catalyze H_2O_2, allowed amplified detection of thrombin with detection limit of 1 nM (Polsky et al., 2006). Application of AuNPs, QDs and graphene oxides for amplified signals of voltammetric and impedimetric aptasensors achieving thrombin detection at sub-pM levels have been also described (Bai et al., 2012; Deng et al., 2009; He et al., 2007; Numnuam et al., 2008).

Another type of electrochemical approaches takes advantage of aptamer flexibility and justified conformational changes that aptamers undergo upon binding to thrombin and involve signal transduction through alteration of electrochemical label positions. Electrochemical labels, such as ferrocene, methylene blue (MB) or methylene green (MG) are either attached at the end of the aptameric sequences or electrostatically confined to the aptamers backbone in various one-site binding homogeneous assay formats (Evtugyn et al., 2008; Hianik et al., 2005; Radi and O'Sullivan, 2006). For example, a "switch-off" thrombin aptasensor was constructed by immobilizing a methylene blue labeled HD22 aptamer (Xiao et al., 2005a). In the absence of thrombin, the flexible conformation of the aptamer chain allowed electrical communication between MB and the electrode, generating a voltammetric response. But, upon binding to thrombin, aptamer assembled into a G-quadruplex structure, distancing and shielding methylene blue from electron-transfer communication with the electrode (Fig. 1.18 (D)). This assay enabled thrombin detection with limit of 20 nM. Another assay now in "switch-on" format was reported (Sánchez et al., 2006). Thrombin aptamer folding into a G-quadruplex structure upon thrombin binding was exploited to bring in the proximity of the electrode ferrocene label, which was located too far from the electrode to facilitate the electron transfer in the absence of target (Fig. 1.18 (E)). This assay allowed specific thrombin detection in the range of 1-30 nM. Similar "switch-on" mechanism with LOD of 11 nM, was reported by Bang, who used a thrombin aptabeacon immobilized over the electrode surface with MB indicator, which was released upon binding with thrombin when the stem loop was opened, leading change position of redox label from the surface (Bang et al., 2005). Another "signal-on" mechanism with detection limit of 3 nM was achieved by electrode-immobilized HD1 that was hybridized with complementary probe labeled

with MB at the extremity (Xiao et al., 2005b). Upon thrombin injection aptamer dehybridized its complementary strand, granting flexibility to it and enabling interaction with methylene blue label and the electrode (Fig. 1.18 (F)). Based on the principle that molecular conductivity of DNA double helices depend on their conformational state, Huang and co-workers (Huang et al., 2008) developed an aptasensor for thrombin by incorporating a thrombin aptamer into a double-helical conduction path, formed by introducing three-way junction. Ferrocene electrochemical label was conjugated to the strand encompassing an aptamer sequence. The three-way junction structure prevented conduction between ferrocene and the electrode in the absence of thrombin, whereas after titration of thrombin altered conformation of junction, switched on conductivity and led to increased signal, allowing detection of picomolar concentration of thrombin in various samples, including diluted serum.

1.4.4 Mass sensitive detection of thrombin

Mass sensitive detection methods offer label-free detection of the target measuring mass change on the sensor surface. The main mass-sensitive aptasensors include acoustic wave-based sensors such as quartz crystal microbalance and Love-wave devices. These methods allow real-time and flow through measurements, however the detection sensitivity is not as high as for above-described optical and electrochemical methods.

The quartz crystal microbalance (QCM)-based piezoelectric biosensors register the changes in frequency of a quartz crystal resonator as a result variation of mass per unit area due to bioselective adsorption. In the first experiment with QCM method the capture of thrombin by immobilized HD1 aptamer, allowed detection of thrombin in the re range of 1-150 nM with nM sensitivity (Hianik et al., 2005). The sensitivity in the similar range was achieved with HD1 immobilized piezoelectric sensor also for serum samples spiked with thrombin (Bini et al., 2007). The sensitivity of QCM for the detection of thrombin by HD1 aptamer was further improved using homogeneous sandwich approach with the same aptamer-conjugated gold nanoparticles (Pavlov et al., 2004). Due to the larger mass of the gold nanoparticles, the change in oscillation frequency was significantly larger than in previous case. Similar approach, but now with heterogeneous sandwich format, in which gold-nanoparticle bound HD22 was allowed to interact with thrombin-HD1 complex on the surface of the crystal microbalance with dissipation monitoring (QCM-D). Conjugated nanoparticles enhanced not only the frequency change but also dissipation signals allowing thrombin detection in range of 10-150 nM (Chen et al., 2010).

Love-wave sensors is a type of surface acoustic wave (SAW) sensor in which mechanically generated shear horizontal acoustic wave is guided in a layer on the surface of the sensor. Love-wave sensors exhibit the highest sensitivity in mass sensitive methods working in aqueous solution. Microfluidic Love-sensor chips coated with HD1 aptamer (Schlensog et al., 2004) or thrombin RNA aptamer (Gronewold et al., 2005) enabled thrombin detection in the range of 0.05-5 μM, which shows comparable sensitivity to QCM, however further improvements in sensitivity are still necessary to compete with other label-free techniques. Sandwich format with use of nanoparticle-conjugated secondary aptamer could be used to enhance the sensitivity.

1.4.5 Thrombin detection in real samples

Here, we highlight two heterogeneous thrombin-detection approaches that could be used for thrombin detection as the clinical marker within serum.

The first strategy is enzymatic electrochemical assay using sandwich approach to capture the target (Centi et al., 2007). Thrombin was first captured by HD1-coated magnetic beads, allowing magnetic separation for removing supernatant and washing steps. Thrombin-bound beads were then incubated with biotin-labeled HD22 solution, to assemble the ternary (HD1-throbin-HD22) complex. Now this complex was allowed to conjugate with streptavidin-alkaline phosphatase through biotin label of HD22. After washing and re-suspension beads were transferred onto the surface of the screen-printed strip electrode. The localization of the beads was assured by the magnetic block placed on the bottom of the working electrode. Upon addition of enzymatic substrate (α-naphthyl phosphate) DPV signal was measured, allowing thrombin detection in concentration range of 0.1-100 nM.

The second approach enabled thrombin detection directly blood sample via enzymatic cleavage of thrombin fluorogenic substrate (Müller et al., 2011). Blood sample was collected in tubes with anticoagulant citrate buffer and reversible thrombin active-site inhibitor argatroban to avoid coagulation and undesired inhibition of thrombin by endogenous inhibitors. Blood sample was transferred in microtiter modules containing immobilized HD1-HD22 dimer aptamer. After capturing thrombin by aptamer dimer wells were washed to remove plasma remains and reversibly bound argatroban. Subsequently, a thrombin-specific peptide substrate bearing a fluorogenic probe (H-D-CHA-Ala-Arg-AMC, 4) was added for quantitative determination of the captured active thrombin. This method achieved 1 pM detection limit. This approach is the first and only commercial aptamer-based thrombin quantification assay existing on the market (Oligobind, Sekiui Diagnostics).

Despite their ingenious designs, both strategies, described in this section, require incubation, washing steps, and time for enzymatic reaction are therefore time-consuming and incompatible with real-time, continuous monitoring of thrombin concentration.

1.4.6 Conclusions

Thrombin-aptamer couple is mostly used as a model to demonstrate achievement in bio - detection and sensing technology in general. Diversity and achieved detection range of the aptamer-base strategies for thrombin quantification is indeed fascinating, demonstrating that thrombin aptamers coupled with various materials and techniques are readily able to detect thrombin from low pM to several μM concentration. However mostly these assays use thrombin as a model for the proof of principle and neglect selectivity, specificity, sensitivity and accuracy of assay in real samples - parameters extremely important for using devise in clinical applications. Some assays are incompatibles with miniaturization, require laborious involvement of trained lab workers or time-consuming. Thus, the aim of developing the real-time aptasensor for detection of free circulating thrombin has not been yet achieved.

1.5 Objectives of the thesis

As demonstrated, on one hand, there is a medical problem - the need of real-time monitoring of free circulating thrombin for improving patient care, avoiding development thromboembolic and hemorrhagic complications; and, on the other hand, there is a aptamer-based nano(bio)technological field, that could respond to the above medical challenge. However, the fact that till now, despite such a vivid interest towards development of thrombin aptasensors, the goal of continuous free thrombin detection has not been yet achieved, indicates the complexity of the problem - thrombin detection in real conditions. To make technology meet these challenges and deliver the suitable product, together with the complicated sensor integration-related questions, some basic points, namely specificity and affinity of thrombin aptamers in real conditions, have to be made clear and considered when designing an aptasensor.

Thus, the aim of this thesis is to investigate different solutions for the integration of thrombin-binding aptamers in point-of-care devices for continuous monitoring of thrombin in real-like environment. Namely we intend to take advantage of possibility to target two different binding sites of thrombin by HD1 or NU172 and HD22 and to explore the ways of their implementation in optical detection of thrombin.

The likelihood of success in designing such sensor depends on how well the thrombin-aptamer interaction is understood. On one hand, an assay design and consequently time needed for single measurement and sensitivity depend largely on kinetic parameters of thrombin-aptamer binding reactions. On the other hand, sensor specificity depends of aptamer selectivity in real-like biological condition. For this reason, as the first objective we decided to evaluate thrombin aptamers by investigating aptamer interaction with thrombin and possible interfering species in simplified and complex mediums. Characterization of the thrombin-aptamer interaction by SPR method is described in the third chapter.

Aptamer immobilization, as the necessary part of most sensors, especially reusable ones, represents as well one of the main challenges, since immobilization strategy strongly influences sensitivity, specificity, functionality and therefore reproducibility of the sensor. In addition sensitivity and detection regime is strongly influenced by the grafting density of the sensing element. The question regarding the optimal choice of aptamer immobilization strategy on the planar and nanomaterial surfaces is addressed in the fourth chapter. Aptamer-grafting strategies are evaluated according to complexity of immobilization and characterization procedures, aptamer grafting density and functionality. The fifth chapter concerns the controlled arrangement of aptamer-modified gold nanoparticles on the surface for the multi-optional sensing and signal transduction applications.

The sixth chapter concerns the aggregation of aptamer-modified gold NP-s, as the approach for thrombin sensing and characterizing of aptamer functionality.

Finally, the seventh chapter describes our intention of providing an efficient homogeneous sensing approach for improved thrombin detection in complex matrixes, by simultaneously increasing specificity, selectivity and affinity, and decreasing non-specific interactions. This format could be implemented for reusable thrombin detection in liquid phase or at the interface of the solid support.

1.6 References

Allsop, T., Nagel, D., Neal, R., Davies, E.M., Mou, C., Bond, P., Rehman, S., Kalli, K., Webb, D.J., Calverhouse, P., et al. (2010). Aptamer-based surface plasmon fibre sensor for thrombin detection. p. 77151C – 77151C – 6.

Anderson, F.A., and Spencer, F.A. (2003). Risk Factors for Venous Thromboembolism. Circulation *107*, I – 9 – I – 16.

ARCA Biopharma Study of NU172 as Anticoagulation in Patients Undergoing Off-pump CABG Surgery - Full Text View - ClinicalTrials.gov.

Archemix The Aptamer Therapeutics Company : Archemix.

Baglin, T. (2005). The measurement and application of thrombin generation. Br. J. Haematol. *130*, 653–661.

Bai, L., Yuan, R., Chai, Y., Yuan, Y., Wang, Y., and Xie, S. (2012). Direct electrochemistry and electrocatalysis of a glucose oxidase-functionalized bioconjugate as a trace label for ultrasensitive detection of thrombin. Chem. Commun. *48*, 10972–10974.

Baldrich, E., Restrepo, A., and O'Sullivan, C.K. (2004). Aptasensor development: elucidation of critical parameters for optimal aptamer performance. Anal. Chem. *76*, 7053–7063.

Bang, G.S., Cho, S., and Kim, B.-G. (2005). A novel electrochemical detection method for aptamer biosensors. Biosens. Bioelectron. *21*, 863–870.

Bauer, K.A. (1993). Laboratory markers of coagulation activation. Arch. Pathol. Lab. Med. *117*, 71–77.

Becker, R.C., and Spencer, F.A. (1998). Thrombin: Structure, Biochemistry, Measurement, and Status in Clinical Medicine. J. Thromb. Thrombolysis *5*, 215–229.

Behlke, M.A. (2008). Chemical modification of siRNAs for in vivo use. Oligonucleotides *18*, 305–319.

Berezovski, M., Musheev, M., Drabovich, A., and Krylov, S.N. (2006). Non-SELEX Selection of Aptamers. J. Am. Chem. Soc. *128*, 1410–1411.

Berntorp, E., and Salvagno, G.L. (2008). Standardization and clinical utility of thrombin-generation assays. Semin. Thromb. Hemost. *34*, 670–682.

Bick, R.L., and Haas, S. (2003). Thromboprophylaxis and thrombosis in medical, surgical, trauma, and obstetric/gynecologic patients. Hematol. Oncol. Clin. North Am. *17*, 217–258.

Bick, R.L., and Kaplan, H. (1998). SYNDROMES OF THROMBOSIS AND HYPERCOAGULABILITY: Congenital and Acquired Causes of Thrombosis. Med. Clin. North Am. *82*, 409–458.

Bini, A., Minunni, M., Tombelli, S., Centi, S., and Mascini, M. (2007). Analytical Performances of Aptamer-Based Sensing for Thrombin Detection. Anal. Chem. *79*, 3016–3019.

Blank, M., Weinschenk, T., Priemer, M., and Schluesener, H. (2001). Systematic Evolution of a DNA Aptamer Binding to Rat Brain Tumor Microvessels SELECTIVE TARGETING OF ENDOTHELIAL REGULATORY PROTEIN PIGPEN. J. Biol. Chem. *276*, 16464–16468.

Blann, A.D., Fitzmaurice, D.A., and Lip, G.Y.H. (2003). Anticoagulation in hospitals and general practice. BMJ *326*, 153–156.

Bock, C., Coleman, M., Collins, B., Davis, J., Foulds, G., Gold, L., Greef, C., Heil, J., Heilig, J.S., Hicke, B., et al. (2004). Photoaptamer arrays applied to multiplexed proteomic analysis. PROTEOMICS *4*, 609–618.

Bock, L.C., Griffin, L.C., Latham, J.A., Vermaas, E.H., and Toole, J.J. (1992). Selection of single-stranded DNA molecules that bind and inhibit human thrombin. Nature *355*, 564–566.

Bode, W. (2006). The structure of thrombin: a janus-headed proteinase. Semin. Thromb. Hemost. *32 Suppl 1*, 16–31.

Bompiani, K.M., Monroe, D.M., Church, F.C., and Sullenger, B.A. (2012). A high affinity, antidote-controllable prothrombin and thrombin-binding RNA aptamer inhibits thrombin generation and thrombin activity. J. Thromb. Haemost. *10*, 870–880.

Borissoff, J.I., Spronk, H.M.H., Heeneman, S., and ten Cate, H. (2009). Is thrombin a key player in the "coagulation-atherogenesis" maze? Cardiovasc. Res. *82*, 392–403.

Brummel, K.E., Paradis, S.G., Butenas, S., and Mann, K.G. (2002). Thrombin functions during tissue factor-induced blood coagulation. Blood *100*, 148–152.

Burke, D.H., and Willis, J.H. (1998). Recombination, RNA evolution, and bifunctional RNA molecules isolated through chimeric SELEX. RNA N. Y. N *4*, 1165–1175.

Byeon, J.-Y., and Bailey, R.C. (2011). Multiplexed Evaluation of Capture Agent Binding Kinetics Using Arrays of Silicon Photonic Microring Resonators. The Analyst *136*, 3430–3433.

Cai, H., Lee, T.M.-H., and Hsing, I.-M. (2006). Label-free protein recognition using an aptamer-based impedance measurement assay. Sens. Actuators B Chem. *114*, 433–437.

Castillo, G., Trnkova, L., Hrdy, R., and Hianik, T. (2012). Impedimetric Aptasensor for Thrombin Recognition Based on CD Support. Electroanalysis *24*, 1079–1087.

Castoldi, E., and Rosing, J. (2011). Thrombin generation tests. Thromb. Res. *127, Supplement 3*, S21–S25.

Centi, S., Tombelli, S., Minunni, M., and Mascini, M. (2007). Aptamer-Based Detection of Plasma Proteins by an Electrochemical Assay Coupled to Magnetic Beads. Anal. Chem. *79*, 1466–1473.

Di Cera, E. (2007). Thrombin as procoagulant and anticoagulant. J. Thromb. Haemost. JTH *5 Suppl 1*, 196–202.

Chang, H., Tang, L., Wang, Y., Jiang, J., and Li, J. (2010). Graphene Fluorescence Resonance Energy Transfer Aptasensor for the Thrombin Detection. Anal. Chem. *82*, 2341–2346.

Chen, Q., Tang, W., Wang, D., Wu, X., Li, N., and Liu, F. (2010). Amplified QCM-D biosensor for protein based on aptamer-functionalized gold nanoparticles. Biosens. Bioelectron. *26*, 575–579.

Chen, Z., Tan, Y., Zhang, C., Yin, L., Ma, H., Ye, N., Qiang, H., and Lin, Y. (2014). A colorimetric aptamer biosensor based on cationic polymer and gold nanoparticles for the ultrasensitive detection of thrombin. Biosens. Bioelectron. *56*, 46–50.

Cho, H., Baker, B.R., Wachsmann-Hogiu, S., Pagba, C.V., Laurence, T.A., Lane, S.M., Lee, L.P., and Tok, J.B.-H. (2008a). Aptamer-Based SERRS Sensor for Thrombin Detection. Nano Lett. *8*, 4386–4390.

Cho, J., Furie, B.C., Coughlin, S.R., and Furie, B. (2008b). A critical role for extracellular protein disulfide isomerase during thrombus formation in mice. J. Clin. Invest.

Choi, J.H., Chen, K.H., and Strano, M.S. (2006). Aptamer-Capped Nanocrystal Quantum Dots: A New Method for Label-Free Protein Detection. J. Am. Chem. Soc. *128*, 15584–15585.

Chung, I., and Lip, G.Y.H. (2003). Virchow's triad revisited: blood constituents. Pathophysiol. Haemost. Thromb. *33*, 449–454.

Chushak, Y., and Stone, M.O. (2009). In silico selection of RNA aptamers. Nucleic Acids Res. *37*, e87.

CoaguChek® XS system CoaguChek® XS system.

Coelho, L., Queirós, R.B., Santos, J.L., Martins, M.C.L., Viegas, D., and Jorge, P.A.S. (2014). DNA-Aptamer optical biosensors based on a LPG-SPR optical fiber platform for point-of-care diagnostic. p. 89570K – 89570K – 7.

Cox, J.C., and Ellington, A.D. (2001). Automated selection of anti-protein aptamers. Bioorg. Med. Chem. *9*, 2525–2531.

Cuthbert, R.J.G. (1999). Monitoring Antithrombotic Therapy. In Antithrombotics, A.C.G.U. M.D, and K.P. Gallagher, eds. (Springer Berlin Heidelberg), pp. 129–155.

Dahlbäck, B. (2000). Blood coagulation. Lancet *355*, 1627–1632.

Dang, O.D., Vindigni, A., and Di Cera, E. (1995). An allosteric switch controls the procoagulant and anticoagulant activities of thrombin. Proc. Natl. Acad. Sci. U. S. A. *92*, 5977–5981.

Daniels, D.A., Chen, H., Hicke, B.J., Swiderek, K.M., and Gold, L. (2003). A tenascin-C aptamer identified by tumor cell SELEX: Systematic evolution of ligands by exponential enrichment. Proc. Natl. Acad. Sci. *100*, 15416–15421.

Das, J., Cederquist, K.B., Zaragoza, A.A., Lee, P.E., Sargent, E.H., and Kelley, S.O. (2012). An ultrasensitive universal detector based on neutralizer displacement. Nat. Chem. *4*, 642–648.

Davie, E.W., and Ratnoff, O.D. (1964). WATERFALL SEQUENCE FOR INTRINSIC BLOOD CLOTTING. Science *145*, 1310–1312.

Deb, P., Sharma, S., and Hassan, K.M. (2010). Pathophysiologic mechanisms of acute ischemic stroke: An overview with emphasis on therapeutic significance beyond thrombolysis. Pathophysiology *17*, 197–218.

Deng, B., Lin, Y., Wang, C., Li, F., Wang, Z., Zhang, H., Li, X.-F., and Le, X.C. (2014). Aptamer binding assays for proteins: The thrombin example—A review. Anal. Chim. Acta *837*, 1–15.

Deng, C., Chen, J., Nie, Z., Wang, M., Chu, X., Chen, X., Xiao, X., Lei, C., and Yao, S. (2009). Impedimetric Aptasensor with Femtomolar Sensitivity Based on the Enlargement of Surface-Charged Gold Nanoparticles. Anal. Chem. *81*, 739–745.

Derbyshire, N., White, S.J., Bunka, D.H.J., Song, L., Stead, S., Tarbin, J., Sharman, M., Zhou, D., and Stockley, P.G. (2012). Toggled RNA aptamers against aminoglycosides allowing facile detection of antibiotics using gold nanoparticle assays. Anal. Chem. *84*, 6595–6602.

Al Dieri, R., de Laat, B., and Hemker, H.C. (2012). Thrombin generation: What have we learned? Blood Rev. *26*, 197–203.

Dupont, D.M., Andersen, L.M., Botkjaer, K.A., and Andreasen, P.A. (2011). Nucleic acid aptamers against proteases. Curr. Med. Chem. *18*, 4139–4151.

Dupuy, E., Habib, A., Lebret, M., Yang, R., Levy-Toledano, S., and Tobelem, G. (2003). Thrombin induces angiogenesis and vascular endothelial growth factor expression in human endothelial cells: possible relevance to HIF-1α. J. Thromb. Haemost. *1*, 1096–1102.

Edwards, K.A., and Baeumner, A.J. (2010). Aptamer sandwich assays: label-free and fluorescence investigations of heterogeneous binding events. Anal. Bioanal. Chem. *398*, 2635–2644.

Ehrlich, H.J., Gebbink, R.K., Preissner, K.T., Keijer, J., Esmon, N.L., Mertens, K., and Pannekoek, H. (1991). Thrombin neutralizes plasminogen activator inhibitor 1 (PAI-1) that is complexed with vitronectin in the endothelial cell matrix. J. Cell Biol. *115*, 1773–1781.

Eisenberg, P.R., Sherman, L.A., Schectman, K., Perez, J., Sobel, B.E., and Jaffe, A.S. (1985). Fibrinopeptide A: a marker of acute coronary thrombosis. Circulation *71*, 912–918.

Ellington, A.D., and Szostak, J.W. (1990). In vitro selection of RNA molecules that bind specific ligands. Nature *346*, 818–822.

Ellington, A.D., and Szostak, J.W. (1992). Selection in vitro of single-stranded DNA molecules that fold into specific ligand-binding structures. Nature *355*, 850–852.

Esmon, C.T. (2000). Regulation of blood coagulation. Biochim. Biophys. Acta BBA - Protein Struct. Mol. Enzymol. *1477*, 349–360.

Evtugyn, G.A., Porfireva, A.V., Hianik, T., Cheburova, M.S., and Budnikov, H.C. (2008). Potentiometric DNA Sensor Based on Electropolymerized Phenothiazines for Protein Detection. Electroanalysis *20*, 1300–1308.

Fenton, J., Ofosu, F., Brezniak, D., and Hassouna, H. (1998). Thrombin and Antithrombotics. Semin. Thromb. Hemost. *24*, 87–91.

Fitzwater, T., and Polisky, B. (1996). A SELEX primer. Methods Enzymol. *267*, 275–301.

Frenkel, E.P., Shen, Y.-M., and Haley, B.B. (2005). The direct thrombin inhibitors: their role and use for rational anticoagulation. Hematol. Oncol. Clin. North Am. *19*, 119–145, vi – vii.

Furie, B., and Furie, B.C. (2008). Mechanisms of Thrombus Formation. N. Engl. J. Med. *359*, 938–949.

Gailani, D., and Broze, G.J. (1991). Factor XI activation in a revised model of blood coagulation. Science *253*, 909–912.

Galdal, K.S., Lyberg, T., Evensen, S.A., Nilsen, E., and Prydz, H. (1985). Thrombin induces thromboplastin synthesis in cultured vascular endothelial cells. Thromb. Haemost. *54*, 373–376.

Garcia, J.G.N., Siflinger-Birnboim, A., Bizios, R., Del Vecchio, P.J., Fenton, J.W., and Malik, A.B. (1986). Thrombin-induced increase in albumin permeability across the endothelium. J. Cell. Physiol. *128*, 96–104.

Gawaz, M. (2004). Role of platelets in coronary thrombosis and reperfusion of ischemic myocardium. Cardiovasc. Res. *61*, 498–511.

Gill, R., Polsky, R., and Willner, I. (2006). Pt Nanoparticles Functionalized with Nucleic Acid Act as Catalytic Labels for the Chemiluminescent Detection of DNA and Proteins. Small *2*, 1037–1041.

Gold, L., Walker, J.J., Wilcox, S.K., and Williams, S. (2012). Advances in human proteomics at high scale with the SOMAscan proteomics platform. New Biotechnol. *29*, 543–549.

Göringer, H.U., Homann, M., and Lorger, M. (2003). In vitro selection of high-affinity nucleic acid ligands to parasite target molecules. Int. J. Parasitol. *33*, 1309–1317.

Griffin, J.H. (1995). Blood coagulation. The thrombin paradox. Nature *378*, 337–338.

Gronewold, T.M.A., Glass, S., Quandt, E., and Famulok, M. (2005). Monitoring complex formation in the blood-coagulation cascade using aptamer-coated SAW sensors. Biosens. Bioelectron. *20*, 2044–2052.

Hamaguchi, N., Ellington, A., and Stanton, M. (2001). Aptamer Beacons for the Direct Detection of Proteins. Anal. Biochem. *294*, 126–131.

Hamula, C.L.A., Guthrie, J.W., Zhang, H., Li, X.-F., and Le, X.C. (2006). Selection and analytical applications of aptamers. TrAC Trends Anal. Chem. *25*, 681–691.

He, P., Shen, L., Cao, Y., and Li, D. (2007). Ultrasensitive Electrochemical Detection of Proteins by Amplification of Aptamer–Nanoparticle Bio Bar Codes. Anal. Chem. *79*, 8024–8029.

Healy, J.M., Lewis, S.D., Kurz, M., Boomer, R.M., Thompson, K.M., Wilson, C., and McCauley, T.G. (2004). Pharmacokinetics and biodistribution of novel aptamer compositions. Pharm. Res. *21*, 2234–2246.

Hemker, H.C., and Beguin, S. (1995). Thrombin generation in plasma: lts assessment via the Endogenous thrombin Potential. Thromb. Haemost. *1*, 134–138.

Hemker, H.C., Giesen, P., AlDieri, R., Regnault, V., de Smed, E., Wagenvoord, R., Lecompte, T., and Béguin, S. (2002). The calibrated automated thrombogram (CAT): a universal routine test for hyper- and hypocoagulability. Pathophysiol. Haemost. Thromb. *32*, 249–253.

Hemker, H.C., Al Dieri, R., and Béguin, S. (2004). Thrombin generation assays: accruing clinical relevance. Curr. Opin. Hematol. *11*, 170–175.

Hemker, H.C., Al Dieri, R., De Smedt, E., and Béguin, S. (2006). Thrombin generation, a function test of the haemostatic-thrombotic system. Thromb. Haemost. *96*, 553–561.

Heneghan, C., Ward, A., Perera, R., Self-Monitoring Trialist Collaboration, Bankhead, C., Fuller, A., Stevens, R., Bradford, K., Tyndel, S., Alonso-Coello, P., et al. (2012). Self-monitoring of oral anticoagulation: systematic review and meta-analysis of individual patient data. Lancet *379*, 322–334.

Hermann, T., and Patel, D.J. (2000). Adaptive recognition by nucleic acid aptamers. Science *287*, 820–825.

Hianik, T., Ostatná, V., Zajacová, Z., Stoikova, E., and Evtugyn, G. (2005). Detection of aptamer–protein interactions using QCM and electrochemical indicator methods. Bioorg. Med. Chem. Lett. *15*, 291–295.

Ho, H.-A., and Leclerc, M. (2004). Optical Sensors Based on Hybrid Aptamer/Conjugated Polymer Complexes. J. Am. Chem. Soc. *126*, 1384–1387.

Hoffman, M., and Monroe, D.M. (2001). A cell-based model of hemostasis. Thromb. Haemost. *85*, 958–965.

Hoffman, M., and Monroe, D.M. (2007). Coagulation 2006: a modern view of hemostasis. Hematol. Oncol. Clin. North Am. *21*, 1–11.

Hoinka, J., Zotenko, E., Friedman, A., Sauna, Z.E., and Przytycka, T.M. (2012). Identification of sequence–structure RNA binding motifs for SELEX-derived aptamers. Bioinformatics *28*, i215–i223.

Hoppe-Seyler, F., Crnkovic-Mertens, I., Tomai, E., and Butz, K. (2004). Peptide aptamers: specific inhibitors of protein function. Curr. Mol. Med. *4*, 529–538.

Hu, P., Han, L., Zhu, C., and Dong, S.J. (2013). Nanoreactors: a novel biosensing platform for protein assay. Chem. Commun. *49*, 1705–1707.

Huang, C.-C., Huang, Y.-F., Cao, Z., Tan, W., and Chang, H.-T. (2005). Aptamer-Modified Gold Nanoparticles for Colorimetric Determination of Platelet-Derived Growth Factors and Their Receptors. Anal. Chem. *77*, 5735–5741.

Huang, Y.C., Ge, B., Sen, D., and Yu, H.-Z. (2008). Immobilized DNA Switches as Electronic Sensors for Picomolar Detection of Plasma Proteins. J. Am. Chem. Soc. *130*, 8023–8029.

HUTABARAT, R. (2010). Anti-Thrombin aptamer formulations and methods for use.

Ikebukuro, K., Kiyohara, C., and Sode, K. (2004). Electrochemical Detection of Protein Using a Double Aptamer Sandwich. Anal. Lett. *37*, 2901–2909.

Ikebukuro, K., Kiyohara, C., and Sode, K. (2005). Novel electrochemical sensor system for protein using the aptamers in sandwich manner. Biosens. Bioelectron. *20*, 2168–2172.

Jayasena, S.D. (1999). Aptamers: an emerging class of molecules that rival antibodies in diagnostics. Clin. Chem. *45*, 1628–1650.

Jenison, R.D., Gill, S.C., Pardi, A., and Polisky, B. (1994). High-resolution molecular discrimination by RNA. Science *263*, 1425–1429.

Jiang, L., Yuan, R., Chai, Y., Yuan, Y., Bai, L., and Wang, Y. (2012). Aptamer-based highly sensitive electrochemical detection of thrombin via the amplification of graphene. The Analyst *137*, 2415–2420.

Jiang, Y., Fang, X., and Bai, C. (2004). Signaling Aptamer/Protein Binding by a Molecular Light Switch Complex. Anal. Chem. *76*, 5230–5235.

Joyce, G.F. (2007). Forty Years of In Vitro Evolution. Angew. Chem. Int. Ed. *46*, 6420–6436.

Kang, Y., Feng, K.-J., Chen, J.-W., Jiang, J.-H., Shen, G.-L., and Yu, R.-Q. (2008). Electrochemical detection of thrombin by sandwich approach using antibody and aptamer. Bioelectrochemistry Amst. Neth. *73*, 76–81.

Kanwar, J.R., Roy, K., and Kanwar, R.K. (2011). Chimeric aptamers in cancer cell-targeted drug delivery. Crit. Rev. Biochem. Mol. Biol. *46*, 459–477.

Kappelle, L.J. (2011). Preventing Deep Vein Thrombosis After Stroke: Strategies and Recommendations. Curr. Treat. Options Neurol. *13*, 629–635.

Kara, P., de la Escosura-Muñiz, A., Maltez-da Costa, M., Guix, M., Ozsoz, M., and Merkoçi, A. (2010). Aptamers based electrochemical biosensor for protein detection using carbon nanotubes platforms. Biosens. Bioelectron. *26*, 1715–1718.

Keefe, A.D., Pai, S., and Ellington, A. (2010). Aptamers as therapeutics. Nat. Rev. Drug Discov. *9*, 537–550.

Kessels, H., Béguin, S., Andree, H., and Hemker, H.C. (1994). Measurement of thrombin generation in whole blood--the effect of heparin and aspirin. Thromb. Haemost. *72*, 78–83.

Kim, N., Gan, H.H., and Schlick, T. (2007a). A computational proposal for designing structured RNA pools for in vitro selection of RNAs. RNA *13*, 478–492.

Kim, N., Shin, J.S., Elmetwaly, S., Gan, H.H., and Schlick, T. (2007b). RagPools: RNA-As-Graph-Pools--a web server for assisting the design of structured RNA pools for in vitro selection. Bioinforma. Oxf. Engl. *23*, 2959–2960.

Kitchen, S., and Preston, F.E. (1999). Standardization of prothrombin time for laboratory control of oral anticoagulant therapy. Semin. Thromb. Hemost. *25*, 17–25.

Koch, K., Berkel, S.S. van, Wal, M.M.E.B. van de, Nieuwland, P.J., Hest, J.C.M. van, and Rutjes, F.P.J.T. (2009). Thrombin generation test in microfluidic systems. J. Appl. Phys. *105*, 102012.

Korte, W., Clarke, S., and Lefkowitz, J.B. (2000). Short Activated Partial Thromboplastin Times Are Related to Increased Thrombin Generation and an Increased Risk for Thromboembolism. Am. J. Clin. Pathol. *113*, 123–127.

Lee, J.A., Hwang, S., Kwak, J., Park, S.I., Lee, S.S., and Lee, K.-C. (2008). An electrochemical impedance biosensor with aptamer-modified pyrolyzed carbon electrode for label-free protein detection. Sens. Actuators B Chem. *129*, 372–379.

Leontis, N.B., and Westhof, E. (2003). Analysis of RNA motifs. Curr. Opin. Struct. Biol. *13*, 300–308.

Levine, M.N., Raskob, G., Beyth, R.J., Kearon, C., and Schulman, S. (2004). Hemorrhagic complications of anticoagulant treatment: the Seventh ACCP Conference on Antithrombotic and Thrombolytic Therapy. Chest *126*, 287S – 310S.

Levy, M., Cater, S.F., and Ellington, A.D. (2005). Quantum-Dot Aptamer Beacons for the Detection of Proteins. ChemBioChem *6*, 2163–2166.

Li, N., and Ho, C.-M. (2008). Aptamer-Based Optical Probes with Separated Molecular Recognition and Signal Transduction Modules. J. Am. Chem. Soc. *130*, 2380–2381.

Li, J.J., Fang, X., and Tan, W. (2002). Molecular Aptamer Beacons for Real-Time Protein Recognition. Biochem. Biophys. Res. Commun. *292*, 31–40.

Li, T., Wang, E., and Dong, S. (2008). G-quadruplex-based DNAzyme for facile colorimetric detection of thrombin. Chem. Commun. 3654–3656.

Li, W., Li, J., Qiang, W., Xu, J., and Xu, D. (2013). Enzyme-free colorimetric bioassay based on gold nanoparticle-catalyzed dye decolorization. The Analyst *138*, 760–766.

Li, Y., Lee, H.J., and Corn, R.M. (2007). Detection of Protein Biomarkers using RNA Aptamer Microarrays and Enzymatically Amplified SPR Imaging. Anal. Chem. *79*, 1082–1088.

Lin, C., Katilius, E., Liu, Y., Zhang, J., and Yan, H. (2006). Self-Assembled Signaling Aptamer DNA Arrays for Protein Detection. Angew. Chem. Int. Ed. *45*, 5296–5301.

Liu, J., Li, J., Jiang, Y., Yang, S., Tan, W., and Yang, R. (2011). Combination of π–π stacking and electrostatic repulsion between carboxylic carbon nanoparticles and fluorescent oligonucleotides for rapid and sensitive detection of thrombin. Chem. Commun. *47*, 11321–11323.

Liu, Y., Wang, C., Li, F., Shen, S., Tyrrell, D.L.J., Le, X.C., and Li, X.-F. (2012). DNase-Mediated Single-Cycle Selection of Aptamers for Proteins Blotted on a Membrane. Anal. Chem. *84*, 7603–7606.

López, J.A., and Chen, J. (2009). Pathophysiology of venous thrombosis. Thromb. Res. *123, Supplement 4*, S30–S34.

López, Y., Paloma, M.J., Rifón, J., Cuesta, B., and Páramo, J.A. (1999). Measurement of prethrombotic markers in the assessment of acquired hypercoagulable states. Thromb. Res. *93*, 71–78.

de-los-Santos-Álvarez, N., Lobo-Castañón, M.J., Miranda-Ordieres, A.J., and Tuñón-Blanco, P. (2008). Aptamers as recognition elements for label-free analytical devices. TrAC Trends Anal. Chem. *27*, 437–446.

Macaya, R.F., Waldron, J.A., Beutel, B.A., Gao, H., Joesten, M.E., Yang, M., Patel, R., Bertelsen, A.H., and Cook, A.F. (1995). Structural and Functional Characterization of Potent Antithrombotic Oligonucleotides Possessing Both Quadruplex and Duplex Motifs. Biochemistry (Mosc.) *34*, 4478–4492.

Macfarlane, R.G. (1964). An Enzyme Cascade in the Blood Clotting Mechanism, and its Function as a Biochemical Amplifier. Nature *202*, 498–499.

Makris, M., Van Veen, J.J., Tait, C.R., Mumford, A.D., Laffan, M., and The British Committee for Standards in Haematology (2013). Guideline on the management of bleeding in patients on antithrombotic agents. Br. J. Haematol. *160*, 35–46.

Mann, K.G. (2003a). Thrombin formation. Chest *124*, 4S – 10S.

Mann, K.G. (2003b). Thrombin*: Can't live without it; probably die from it. Chest *124*, 1S – 3S.

Mann, K.G., Jenny, R.J., and Krishnaswamy, S. (1988). Cofactor Proteins in the Assembly and Expression of Blood Clotting Enzyme Complexes. Annu. Rev. Biochem. *57*, 915–956.

Mann, K.G., Butenas, S., and Brummel, K. (2003). The dynamics of thrombin formation. Arterioscler. Thromb. Vasc. Biol. *23*, 17–25.

Maragoudakis, M.E., Tsopanoglou, N.E., and Andriopoulou, P. (2002). Mechanism of thrombin-induced angiogenesis. Biochem. Soc. Trans. *30*, 173–177.

Marieb, E.N., and Hoehn, K. (2012). Human Anatomy & Physiology, Books a la Carte Edition (Boston: Pearson).

Marshall, K.A., and Ellington, A.D. (2000). In vitro selection of RNA aptamers. Methods Enzymol. *318*, 193–214.

Martinelli, I., Bucciarelli, P., and Mannucci, P.M. (2010). Thrombotic risk factors: basic pathophysiology. Crit. Care Med. *38*, S3–S9.

Mayer, G., Ahmed, M.-S.L., Dolf, A., Endl, E., Knolle, P.A., and Famulok, M. (2010). Fluorescence-activated cell sorting for aptamer SELEX with cell mixtures. Nat. Protoc. *5*, 1993–2004.

Mayer, G., Rohrbach, F., Pötzsch, B., and Müller, J. (2011). Aptamer-based modulation of blood coagulation. Hämostaseologie *31*, 258–263.

McCauley, T.G., Hamaguchi, N., and Stanton, M. (2003). Aptamer-based biosensor arrays for detection and quantification of biological macromolecules. Anal. Biochem. *319*, 244–250.

Meijer, M. van, Smilde, A., Tans, G., Nesheim, M.E., Pannekoek, H., and Horrevoets, A.J.G. (1997). The Suicide Substrate Reaction Between Plasminogen Activator Inhibitor 1 and Thrombin Is Regulated by the Cofactors Vitronectin and Heparin. Blood *90*, 1874–1882.

Meneghello, A., Sosic, A., Antognoli, A., Cretaio, E., and Gatto, B. (2012). Development and Optimization of a Thrombin Sandwich Aptamer Microarray. Microarrays *1*, 95–106.

Mills, D.R., Peterson, R.L., and Spiegelman, S. (1967). An extracellular Darwinian experiment with a self-duplicating nucleic acid molecule. Proc. Natl. Acad. Sci. U. S. A. *58*, 217–224.

Mir, M., Vreeke, M., and Katakis, I. (2006). Different strategies to develop an electrochemical thrombin aptasensor. Electrochem. Commun. *8*, 505–511.

Müller, J., Becher, T., Braunstein, J., Berdel, P., Gravius, S., Rohrbach, F., Oldenburg, J., Mayer, G., and Pötzsch, B. (2011). Profiling of Active Thrombin in Human Blood by Supramolecular Complexes. Angew. Chem. Int. Ed. *50*, 6075–6078.

Narayanan, S. (1999). Multifunctional roles of thrombin. Ann. Clin. Lab. Sci. *29*, 275–280.

Nilsson, I.M., Ljungner, H., and Tengborn, L. (1985). Two different mechanisms in patients with venous thrombosis and defective fibrinolysis: low concentration of plasminogen activator or increased concentration of plasminogen activator inhibitor. Br. Med. J. Clin. Res. Ed *290*, 1453–1456.

Noeske, J., Schwalbe, H., and Wöhnert, J. (2007). Metal-ion binding and metal-ion induced folding of the adenine-sensing riboswitch aptamer domain. Nucleic Acids Res. *35*, 5262–5273.

Nolte, A., Klussmann, S., Bald, R., Erdmann, V.A., and Fürste, J.P. (1996). Mirror-design of L-oligonucleotide ligands binding to L-arginine. Nat. Biotechnol. *14*, 1116–1119.

Nossel, H.L., Yudelman, I., Canfield, R.E., Butler, V.P., Spanondis, K., Wilner, G.D., and Qureshi, G.D. (1974). Measurement of Fibrinopeptide A in Human Blood. J. Clin. Invest. *54*, 43–53.

Numnuam, A., Chumbimuni-Torres, K.Y., Xiang, Y., Bash, R., Thavarungkul, P., Kanatharana, P., Pretsch, E., Wang, J., and Bakker, E. (2008). Aptamer-Based Potentiometric Measurements of Proteins Using Ion-Selective Microelectrodes. Anal. Chem. *80*, 707–712.

Nutiu, R., and Li, Y. (2003). Structure-Switching Signaling Aptamers. J. Am. Chem. Soc. *125*, 4771–4778.

Ofosu, F.A. (2006). Review: Laboratory markers quantifying prothrombin activation and actions of thrombin in venous and arterial thrombosis do not accurately assess disease severity or the effectiveness of treatment. Thromb. Haemost. *96*, 568–577.

Oligobind, and Sekiui Diagnostics OLIGOBIND® Thrombin activity assay - Product – Sekisui Diagnostics.

Omar, M.N., and Mann, K.G. (1987). Inactivation of factor Va by plasmin. J. Biol. Chem. *262*, 9750–9755.

Osterud, B., and Rapaport, S.I. (1977). Activation of factor IX by the reaction product of tissue factor and factor VII: additional pathway for initiating blood coagulation. Proc. Natl. Acad. Sci. U. S. A. *74*, 5260–5264.

Ouriel, K. (2001). Peripheral arterial disease. The Lancet *358*, 1257–1264.

Paborsky, L.R., McCurdy, S.N., Griffin, L.C., Toole, J.J., and Leung, L.L. (1993). The single-stranded DNA aptamer-binding site of human thrombin. J. Biol. Chem. *268*, 20808–20811.

Padmanabhan, K., and Tulinsky, A. (1996). An Ambiguous Structure of a DNA 15-mer Thrombin Complex. Acta Crystallogr. D Biol. Crystallogr. *52*, 272–282.

Pagratis, N.C., Bell, C., Chang, Y.F., Jennings, S., Fitzwater, T., Jellinek, D., and Dang, C. (1997). Potent 2'-amino-, and 2'-fluoro-2'-deoxyribonucleotide RNA inhibitors of keratinocyte growth factor. Nat. Biotechnol. *15*, 68–73.

Pan, W., Craven, R.C., Qiu, Q., Wilson, C.B., Wills, J.W., Golovine, S., and Wang, J.F. (1995). Isolation of virus-neutralizing RNAs from a large pool of random sequences. Proc. Natl. Acad. Sci. *92*, 11509–11513.

Pavlov, V., Xiao, Y., Shlyahovsky, B., and Willner, I. (2004). Aptamer-Functionalized Au Nanoparticles for the Amplified Optical Detection of Thrombin. J. Am. Chem. Soc. *126*, 11768–11769.

Pelzer, H., Schwarz, A., and Heimburger, N. (1988). Determination of human thrombin-antithrombin III complex in plasma with an enzyme-linked immunosorbent assay. Thromb. Haemost. *59*, 101–106.

Pelzer, H., Schwarz, A., and Stüber, W. (1991). Determination of human prothrombin activation fragment 1 + 2 in plasma with an antibody against a synthetic peptide. Thromb. Haemost. *65*, 153–159.

Peng, Y., Li, L., Mu, X., and Guo, L. (2013). Aptamer-gold nanoparticle-based colorimetric assay for the sensitive detection of thrombin. Sens. Actuators B Chem. *177*, 818–825.

Perche, F., and Torchilin, V.P. (2013). Recent Trends in Multifunctional Liposomal Nanocarriers for Enhanced Tumor Targeting. J. Drug Deliv. *2013*, e705265.

Petersen, M., and Wengel, J. (2003). LNA: a versatile tool for therapeutics and genomics. Trends Biotechnol. *21*, 74–81.

Polsky, R., Gill, R., Kaganovsky, L., and Willner, I. (2006). Nucleic Acid-Functionalized Pt Nanoparticles: Catalytic Labels for the Amplified Electrochemical Detection of Biomolecules. Anal. Chem. *78*, 2268–2271.

Porfireva, A.V., Evtugyn, G.A., Ivanov, A.N., and Hianik, T. (2010). Impedimetric Aptasensors Based on Carbon Nanotubes – Poly(methylene blue) Composite. Electroanalysis *22*, 2187–2195.

Potyrailo, R.A., Conrad, R.C., Ellington, A.D., and Hieftje, G.M. (1998). Adapting Selected Nucleic Acid Ligands (Aptamers) to Biosensors. Anal. Chem. *70*, 3419–3425.

Quinn, C., Hill, J., and Hassouna, H. (2000). A guide for diagnosis of patients with arterial and venous thrombosis. Clin. Lab. Sci. J. Am. Soc. Med. Technol. *13*, 229–238.

Radi, A.-E., and O'Sullivan, C.K. (2006). Aptamer conformational switch as sensitive electrochemical biosensor for potassium ion recognition. Chem. Commun. 3432–3434.

Radi, A.-E., Acero Sánchez, J.L., Baldrich, E., and O'Sullivan, C.K. (2005). Reusable Impedimetric Aptasensor. Anal. Chem. *77*, 6320–6323.

Rahman, A., Anwar, K.N., Uddin, S., Xu, N., Ye, R.D., Platanias, L.C., and Malik, A.B. (2001). Protein kinase C-delta regulates thrombin-induced ICAM-1 gene expression in endothelial cells via activation of p38 mitogen-activated protein kinase. Mol. Cell. Biol. *21*, 5554–5565.

Ramakrishnan, V., Reeves, P.S., DeGuzman, F., Deshpande, U., Ministri-Madrid, K., DuBridge, R.B., and Phillips, D.R. (1999). Increased thrombin responsiveness in platelets from mice lacking glycoprotein V. Proc. Natl. Acad. Sci. U. S. A. *96*, 13336–13341.

Ramakrishnan, V., DeGuzman, F., Bao, M., Hall, S.W., Leung, L.L., and Phillips, D.R. (2001). A thrombin receptor function for platelet glycoprotein Ib-IX unmasked by cleavage of glycoprotein V. Proc. Natl. Acad. Sci. U. S. A. *98*, 1823–1828.

Rickles, F.R., Patierno, S., and Fernandez, P.M. (2003). TIssue factor, thrombin, and cancer*. Chest *124*, 58S – 68S.

Roderique, E.M., and Wynands, J.E. (1967). Blood coagulation and haemostasis: a review. Can. Anaesth. Soc. J. *14*, 129–151.

Sánchez, J.L.A., Baldrich, E., Radi, A.E.-G., Dondapati, S., Sánchez, P.L., Katakis, I., and O'Sullivan, C.K. (2006). Electronic "Off-On" Molecular Switch for Rapid Detection of Thrombin. Electroanalysis *18*, 1957–1962.

Sassolas, A., Blum, L.J., and Leca-Bouvier, B.D. (2011). Homogeneous assays using aptamers. The Analyst *136*, 257–274.

Schlensog, M.D., Gronewold, T.M.A., Tewes, M., Famulok, M., and Quandt, E. (2004). A Love-wave biosensor using nucleic acids as ligands. Sens. Actuators B Chem. *101*, 308–315.

Schulman, S., Beyth, R.J., Kearon, C., Levine, M.N., and American College of Chest Physicians (2008). Hemorrhagic complications of anticoagulant and thrombolytic treatment: American College of Chest Physicians Evidence-Based Clinical Practice Guidelines (8th Edition). Chest *133*, 257S – 298S.

Siller-Matula, J.M., Schwameis, M., Blann, A., Mannhalter, C., and Jilma, B. (2011). Thrombin as a multi-functional enzyme. Focus on in vitro and in vivo effects. Thromb. Haemost. *106*, 1020–1033.

Smith, S.A. (2009). The cell-based model of coagulation. J. Vet. Emerg. Crit. Care *19*, 3–10.

Sobieszczyk, P., Fishbein, M.C., and Goldhaber, S.Z. (2002). Acute Pulmonary Embolism Don't Ignore the Platelet. Circulation *106*, 1748–1749.

Song, S., Wang, L., Li, J., Fan, C., and Zhao, J. (2008). Aptamer-based biosensors. TrAC Trends Anal. Chem. *27*, 108–117.

Sonne, O. (1988). The specific binding of thrombin to human polymorphonuclear leucocytes. Scand. J. Clin. Lab. Invest. *48*, 831–838.

Srinivasan, J., Cload, S.T., Hamaguchi, N., Kurz, J., Keene, S., Kurz, M., Boomer, R.M., Blanchard, J., Epstein, D., Wilson, C., et al. (2004). ADP-Specific Sensors Enable Universal Assay of Protein Kinase Activity. Chem. Biol. *11*, 499–508.

Stoltenburg, R., Reinemann, C., and Strehlitz, B. (2007). SELEX—A (r)evolutionary method to generate high-affinity nucleic acid ligands. Biomol. Eng. *24*, 381–403.

Strehlitz, B., Nikolaus, N., and Stoltenburg, R. (2008). Protein Detection with Aptamer Biosensors. Sensors *8*, 4296–4307.

Sussman, D., Nix, J.C., and Wilson, C. (2000). The structural basis for molecular recognition by the vitamin B 12 RNA aptamer. Nat. Struct. Biol. *7*, 53–57.

Tang, Q., Su, X., and Loh, K.P. (2007). Surface plasmon resonance spectroscopy study of interfacial binding of thrombin to antithrombin DNA aptamers. J. Colloid Interface Sci. *315*, 99–106.

Tappenden, K.A., Gallimore, M.J., Evans, G., Mackie, I.J., and Jones, D.W. (2007). Thrombin generation: a comparison of assays using platelet-poor and -rich plasma and whole blood samples from healthy controls and patients with a history of venous thromboembolism. Br. J. Haematol. *139*, 106–112.

Tasset, D.M., Kubik, M.F., and Steiner, W. (1997). Oligonucleotide inhibitors of human thrombin that bind distinct epitopes. J. Mol. Biol. *272*, 688–698.

Tennico, Y.H., Hutanu, D., Koesdjojo, M.T., Bartel, C.M., and Remcho, V.T. (2010). On-Chip Aptamer-Based Sandwich Assay for Thrombin Detection Employing Magnetic Beads and Quantum Dots. Anal. Chem. *82*, 5591–5597.

Tilburg, N.H. van, Rosendaal, F.R., and Bertina, R.M. (2000). Thrombin activatable fibrinolysis inhibitor and the risk for deep vein thrombosis. Blood *95*, 2855–2859.

Tolle, F., and Mayer, G. (2012). Dressed for success – applying chemistry to modulate aptamer functionality. Chem. Sci. *4*, 60–67.

Tombelli, S., Minunni, M., and Mascini, M. (2005). Analytical applications of aptamers. Biosens. Bioelectron. *20*, 2424–2434.

Triplett, D.A. (2000). Coagulation and Bleeding Disorders: Review and Update. Clin. Chem. *46*, 1260–1269.

Tripodi, A. (2008). The history of phenotypic testing in thrombosis and hemostasis. Semin. Thromb. Hemost. *34*, 585–592.

Tuerk, C., and Gold, L. (1990). Systematic evolution of ligands by exponential enrichment: RNA ligands to bacteriophage T4 DNA polymerase. Science *249*, 505–510.

Van Veen, J.J., Gatt, A., and Makris, M. (2008). Thrombin generation testing in routine clinical practice: are we there yet? Br. J. Haematol. *142*, 889–903.

Villamediana, L.M., Rondeau, E., He, C.J., Medcalf, R.L., Peraldi, M.N., Lacave, R., Delarue, F., and Sraer, J.D. (1990). Thrombin regulates components of the fibrinolytic system in human mesangial cells. Kidney Int. *38*, 956–961.

Vu, T.K., Wheaton, V.I., Hung, D.T., Charo, I., and Coughlin, S.R. (1991). Domains specifying thrombin-receptor interaction. Nature *353*, 674–677.

Wang, J., Jiang, H., and Liu, F. (2000). In vitro selection of novel RNA ligands that bind human cytomegalovirus and block viral infection. RNA *6*, 571–583.

Wang, W., Chen, C., Qian, M., and Zhao, X.S. (2008a). Aptamer biosensor for protein detection using gold nanoparticles. Anal. Biochem. *373*, 213–219.

Wang, Y., Wei, H., Li, B., Ren, W., Guo, S., Dong, S., and Wang, E. (2007). SERS opens a new way in aptasensor for protein recognition with high sensitivity and selectivity. Chem. Commun. 5220–5222.

Wang, Y., Li, D., Ren, W., Liu, Z., Dong, S., and Wang, E. (2008b). Ultrasensitive colorimetric detection of protein by aptamer–Au nanoparticles conjugates based on a dot-blot assay. Chem. Commun. 2520–2522.

Wei, H., Li, B., Li, J., Wang, E., and Dong, S. (2007). Simple and sensitive aptamer-based colorimetric sensing of protein using unmodified gold nanoparticle probes. Chem. Commun. 3735–3737.

Westhof, E., and Patel, D.J. (1997). Nucleic acids from self-assembly to induced-fit recognition. Curr. Opin. Struct. Biol. *7*, 305–309.

White, R., Rusconi, C., Scardino, E., Wolberg, A., Lawson, J., Hoffman, M., and Sullenger, B. (2001). Generation of species cross-reactive aptamers using "toggle" SELEX. Mol. Ther. J. Am. Soc. Gene Ther. *4*, 567–573.

White, R.R., Sullenger, B.A., and Rusconi, C.P. (2000). Developing aptamers into therapeutics. J. Clin. Invest. *106*, 929–934.

Wrzesinski, J., and Jóźwiakowski, S.K. (2008). Structural basis for recognition of Co2+ by RNA aptamers. FEBS J. *275*, 1651–1662.

Xia, F., Zuo, X., Yang, R., Xiao, Y., Kang, D., Vallée-Bélisle, A., Gong, X., Yuen, J.D., Hsu, B.B.Y., Heeger, A.J., et al. (2010). Colorimetric detection of DNA, small molecules, proteins, and ions using unmodified gold nanoparticles and conjugated polyelectrolytes. Proc. Natl. Acad. Sci. *107*, 10837–10841.

Xiao, Y., Lubin, A.A., Heeger, A.J., and Plaxco, K.W. (2005a). Label-Free Electronic Detection of Thrombin in Blood Serum by Using an Aptamer-Based Sensor. Angew. Chem. Int. Ed. *44*, 5456–5459.

Xiao, Y., Piorek, B.D., Plaxco, K.W., and Heeger, A.J. (2005b). A Reagentless Signal-On Architecture for Electronic, Aptamer-Based Sensors via Target-Induced Strand Displacement. J. Am. Chem. Soc. *127*, 17990–17991.

Xu, F., Hua, M., Luo, L., Du, H., and Yang, Y. (2013). Electrochemical aptamer sensor for thrombin detection based on Au nanoneedle and enzymatic ascorbic acid oxidization. J. Nanosci. Nanotechnol. *13*, 558–563.

Xu, H., Mao, X., Zeng, Q., Wang, S., Kawde, A.-N., and Liu, G. (2009). Aptamer-Functionalized Gold Nanoparticles as Probes in a Dry-Reagent Strip Biosensor for Protein Analysis. Anal. Chem. *81*, 669–675.

Xu, Y., Yang, L., Ye, X., He, P., and Fang, Y. (2006). An Aptamer-Based Protein Biosensor by Detecting the Amplified Impedance Signal. Electroanalysis *18*, 1449–1456.

Yan, Y., and Zeng, H. (2010). Synthesis and structure investigation of stabilized aromatic oligoamides and their interaction with G-quadruplex structures. National university of Singapore.

Yang, R., Tang, Z., Yan, J., Kang, H., Kim, Y., Zhu, Z., and Tan, W. (2008). Noncovalent Assembly of Carbon Nanotubes and Single-Stranded DNA: An Effective Sensing Platform for Probing Biomolecular Interactions. Anal. Chem. *80*, 7408–7413.

Ye, X., Gorin, A., Ellington, A.D., and Patel, D.J. (1996). Deep penetration of an α-helix into a widened RNA major groove in the HIV-1 rev peptide–RNA aptamer complex. Nat. Struct. Mol. Biol. *3*, 1026–1033.

Yuan, Y., Yuan, R., Chai, Y., Zhuo, Y., Liu, Z., Mao, L., Guan, S., and Qian, X. (2010). A novel label-free electrochemical aptasensor for thrombin based on the {nano-Au/thionine}n multilayer films as redox probes. Anal. Chim. Acta *668*, 171–176.

Zhang, Y., and Sun, X. (2011). A novel fluorescent aptasensor for thrombin detection: using poly(m-phenylenediamine) rods as an effective sensing platform. Chem. Commun. *47*, 3927–3929.

Zhang, L., Zhu, J., Li, T., and Wang, E. (2011a). Bifunctional colorimetric oligonucleotide probe based on a G-quadruplex DNAzyme molecular beacon. Anal. Chem. *83*, 8871–8876.

Zhang, Y., Liu, S., and Sun, X. (2011b). Mesoporous carbon microparticles as a novel fluorescent sensing platform for thrombin detection. Biosens. Bioelectron. *26*, 3876–3880.

Zhang, Z., Yang, W., Wang, J., Yang, C., Yang, F., and Yang, X. (2009). A sensitive impedimetric thrombin aptasensor based on polyamidoamine dendrimer. Talanta *78*, 1240–1245.

Zhou, J., Battig, M.R., and Wang, Y. (2010). Aptamer-based molecular recognition for biosensor development. Anal. Bioanal. Chem. *398*, 2471–2480.

Zhou, L., Wang, M.-H., Wang, J.-P., and Ye, Z.-Z. (2011). Application of Biosensor Surface Immobilization Methods for Aptamer. Chin. J. Anal. Chem. *39*, 432–438.

Zhu, H., Suter, J.D., White, I.M., and Fan, X. (2006). Aptamer Based Microsphere Biosensor for Thrombin Detection. Sensors *6*, 785–795.

CHAPTER 2. MATERIALS AND METHODS

In this chapter are listed all the chemicals, reagents, computational methods and instruments used for the research described in the following chapters of this thesis. The theoretical background of the main experimental techniques employed in these studies is covered as well.

2.1 Reagents and chemicals

2.1.1 Chemicals

NaCl, KCl, KH_2PO_4, K_2HPO_4, Na_2HPO_4, NaH_2PO_4, $MgCl_2$, $CaCl_2$, , Tris, HEPES, TEMED, DTT, EDAC, NHS, Gly, MES, Tween 20, Triton X-100, SDS, Ethanol, DMSO, HCl, H_2SO_4, HF, acetic acid, H_2O_2, Bromphenol blue all molecular biology grade, were purchased from Sigma-Aldrich (France).

2.1.2 Proteins:

Purified human α-Thrombin (MW 36000 g/mol) (1500-3500 NIH units/mg), Heparin Cofactor II (MW 65600 g/mol) and α2-Macroglobulin (725000 g/mol) from human plasma were obtained from Sigma-Aldrich (Schelldorf, Germany). Prothrombin (MW 72000 g/mol), Antithrombin III (58,200 g/mol), FXa (44000g/mol) and were from STAGO (France). Molecular biology grade BSA (66500 g/mol) was purchased from New England BioLabs (USA). Unstained protein ladder for SDS PAGE with broad range standards (MW 6,500–200,000 g/mol) was obtained from BioRad (France). All lyophilized proteins were reconstituted in deionized ultrapure water following manufacturer's instructions. Stock solutions were stored in small aliquots in freezer at temperature of -20 °C. For the experiment the aliquot was thawed at ambient temperature, ultrasonicated for few seconds and kept on ice to maintain their activity. The concentration of Thrombin and Antithombin III was determined by UV absorbance at 280 nm using molar extinction coefficients of 67000 L mol-1 cm-1 (Fenton et al., 1977) and 38000 L mol-1 cm-1 respectively (Nordenman et al., 1977).

Murine plasma was generously provided by Sanofi-Aventis R&D department Toulouse, France (Dr. Laurence Millet).

2.1.3 Substrates and inhibitors:

Reversible direct thrombin inhibitor Argatroban monohydrate (MW 508,635 g/mol) was obtained from Sigma. Direct FXa inhibitor Rivaroxaban (MW 435.882 g/mol) was supplied by Bayer Healthcare (Wuppertal, Germany). Thrombin chromogenic substrate S-2238 (H-D-Phe-Pip-Arg-pNA-2HCl) (MW 625.6 g/mol) was purchased from Chromogenix (Milan, Italy). Highly concentrated stock solutions (1 mM) were prepared by dissolving Thrombin and FXa inhibitors and

chromogenic substrate in 10% DMSO and distilled water mixture. Stock solutions were stored at +4°C up to 6 month.

2.1.4 Single stranded DNA:

All single-stranded DNA sequences given in Table 2.1 were custom-synthetized by Eurogentec (Belgium). All sequences bearing biotin, thiol or amine groups at the 5' terminus between the functional group and aptameric sequence 20 thymine spacer for flexibility was included. DNA samples were received in dry format. 0.5 mM concentration stock solutions in water were prepared and kept in aliquots at – 20 °C.

2.1.5 Nanoparticles

Carboxyl modified fluorescent beads of 100 nm diameter, with fluorescence maximum at 532 nm wavelength were obtained from Banglabs. Colloidal solutions of gold nanoparticles 20 and 80 nm size were obtained from BBInternational (United Kingdom).

Table 2.1 ssDNA sequences

Name	**Sequence**	**Application**
HD1ref	**5'-biotion-20xT-GTT-TGT-TGT-TTG-TTG-3'**	**SPR**
HD1	**5'-biotion-20xT-GGT-TGG-TGT-GGT-TGG-3'**	
HD2ref	**5'-biotion-20xT-GAC-TGC-GTT-GCA-GGA-CGG-TTG-TTT-GAG-TC-3'**	
HD2	**5'-biotion-20xT-AGT-CCG-TGG-TAG-GGC-AGG-TTG-GGG-TGA-CT-3'**	
NU172ref	**5'-biotion-20xT-CGC-CAA-GGA-AGT-GAA-GAG-AGG-AGG-CG**	
NU172	**5'-biotion-20xT-CGC-CTA-GGT-TGG-GTA-GGG-TGG-TGG-CG**	
HD1thiol	**5'-SH-20xT-GGT-TGG-TGT-GGT-TGG-3'**	**Gold surface and AuNPs**
HD1'thiol	**5'-SH-20xT-CCA-ACC-ACA-CCA-ACC-3'**	
HD2 thiol	**5'-SH-20xT-AGT-CCG-TGG-TAG-GGC-AGG-TTG-GGG-TGA-CT-3'**	
Nu172 thiol	**5'-SH-20xT-CGC-CTA-GGT-TGG-GTA-GGG-TGG-TGG-CG-3'**	
cssHD1	**5'-CCA-ACC-ACA-CCA-ACC-3'**	
HD1 Alex532	**5'- SH-20xT-GGT-TGG-TGT-GGT-TGG-Alex532-3'**	
HD1 rhodG6	**5'-GGT-TGG-TGT-GGT-TGG-rhodG6-3'**	
HD1 amine	**5'-NH3-20xT-GGT-TGG-TGT-GGT-TGG-3'**	**Polymer surface and particles**
HD22 Amine	**5'-NH3-20xT-AGT-CCG-TGG-TAG-GGC-AGG-TTG-GGG-TGA-CT-3'**	
A amine	**5'-NH3-20xT-GAC-TAC-TAC-TGA-CTA-CTG-3'**	
B amine	**5'-NH3-20xT-CAG-TAG-TCA-GTA-GTA-GTC-3'**	
S1	**5'–GGTTGGTGTGGTTGG-TTTT*T*ATTCGCGAAGAA*T*AAATTTT-AGTCCGTGGTAGGGCAGGTTGGGGTGACT -3'**	**Aptadimer**
S2	**5'- GGTTGGTGTGGTTGG -TTTTTTTTCA*T*AAGATTTTTTTTTTTTTTTC*T*TATGTTTTTTTT-AGTCCGTGGTAGGGCAGGTTGGGGTGACT-3'**	

2.1.6 Buffers

All the reagents for buffers were of analytical grade and obtained from Sigma. After preparation buffers were kept at +4 °C up to 1 month. Prior to use, all buffers were filtered in 0.22 µM filter and degased first by ultra-sonication and then by incubation under vacuum for 10 mins.

The following buffers and solutions were used for different experiments:

SPR experiment:

- Immobilization buffer for biotinylated aptamers: HBS-EP from GE-Healthcare containing 10 mM HEPES pH 7.4, 150 mM NaCl, 3.4 mM EDTA, 0.005% Surfactant P2;
- Running buffer: phosphate buffered saline (PBS) pH 7.4 containing 10mM Phosphate, 145 mM NaCl, 5 mM KCl , 1 mM $MgCl_2$ and 1 mM $CaCl_2$ as running buffer; NSBr – nonspecific binding reducer- from GE Healthcare was added to running buffet for reduction nonspecific binding in some experiments with plasma;
- Surface regeneration solutions: 2 M KCl and/or 1 M NaCl with 50 mM NaOH.

SDS PAGE separation:

- Loading buffer containing 2% w/v SDS, 2 mM DTT, 4% glycerol, 40 mM Tris-HCl, pH 6.8, 0.01% w/v Bromophenolblue;
- Running buffer composed of 25 mM Tris-HCl, 200 mM Glycine, 0.1% w/v SDS;
- Stacking gel with 0.125 M Tris-HCl pH 6.8, 0.1% w/v SDS, 3% w/v acrylamide,0.025% TEMED and AP;
- Separating gel containing 0.375 M Tris-HCl pH 8.8, 0.1% w/v SDS, 10% w/v acrylamide, 0.025% TEMED and AP;
- Staining solution composed of 0.1% Coomassie Brilliant Blue R-250 in 40% alcohol, 10% acetic acid;
- Destaining water solution of 50% alcohol and 10% acetic acid.

Chromogenic substrate cleavage assay:

- Activation buffer: PBS-BSA of pH7.5 containing 10 mM Phosphate, 145 mM NaCl, 5 mM KCl , 1 mM $MgCl_2$, 1 mM $CaCl_2$ and 0.1% BSA.

Functionalization of Gold surface:

- Thiol deprotection solution: 0.18 nM PB at pH 7.4 with 0.1 M DTT;
- Grafting buffer: 0.01 nM PB at pH 7.4, 0.7 M NaCl and only for AuNPs 0.1% Tween 20;
- Aggregation assay buffer: PBS pH 7.4 containing 10 mM Phosphate, 145 mM NaCl, 5 mM KCl , 1 mM $MgCl_2$ and 1 mM $CaCl_2$.

Functionalization of PS nanoparticles:

- Particle washing buffer: 50 mM MES buffer of pH 4.5;
- Coupling buffer: 500 µL 50 mM MES buffer of pH 6.2, containing 10 mM EDAC and 100 mM NHS;
- Capping buffer: 10 mM glycine buffer of pH 6;
- Storing and aggregation buffer: PBS pH 7.4 containing 10 mM Phosphate, 145 mM NaCl, 5 mM KCl , 1 mM $MgCl_2$ and 1 mM $CaCl_2$.

Aptadimer Fluorescence: PBS pH 7.4 containing 10 mM Phosphate, 145 mM NaCl, 5 mM KCl , 1 mM $MgCl_2$ and 1 mM $CaCl_2$ as running buffer.

2.2 Computational resources

2.2.1 Molecular structures

Molecular models of aptamers and proteins were reconstructed form crystallographic and NMR data obtained from Protein Data Bank (www.RSCB.org). We used following molecular structures:

Table 2.2 Molecular structures used to build the molecular models

Molecule	Structure name	Source
Thrombin	**3U69**	**(Figueiredo et al., 2012)**
Thrombin HD1	**4DII**	**(Russo Krauss et al., 2012)**
Thrombin HD22	**4I7Y**	**(Russo Krauss et al., 2013)**
Thrombin-HCII	**1JMO**	**(Baglin et al., 2002)**
Thrombin-ATIII	**1TB6**	**(Li et al., 2004)**
Alpha-2-macroglobulin	**4ACQ**	**(Marrero et al., 2012)**
Prothrombin fragment1	**2PF2**	**(Soriano-Garcia et al., 1991)**
Prethrombin2	**1HAG**	**(Vijayalakshmi et al., 1994)**
Meizothrombin desF1	**1AOH**	**(Martin et al., 1997)**

2.2.2 Visualization softwares

For visualization molecular models in 3D and measuring the intermolecular distances we used PyMole molecular graphics system software (www.pymole.org, Schrodinger).

For prediction of secondary structure of ssDNA, calculation melting temperatures, molecular weight, extinction coefficients online resources of Mfold (http://mfold.rna.albany.edu/) and oligoanalyzer (https://eu.idtdna.com/calc/analyzer) were used.

For image analysis Image J software was used (http://imagej.nih.gov/).

2.3 Experimental methods and instruments

2.3.1 Surface plasmon resonance

Surface plasmon resonance method is the bio-analytical technique that relies on an optical phenomenon of resonance of surface plasmons on the interface of the two optical mediums. It occurs when p-polarized light at a certain wavelength and angle is reflected off a thin metal film (a thin gold film coated on the sensor chip) under the condition of total internal reflection (TIR). The light excites surface plasmons in the metal at a certain incident angle, called resonance angle. Plasmons generate an evanescent wave in the metal film that extends hundreds of nanometers from the surface into the medium above. The excited surface plasmons are very sensitive to the refractive index change at the surface of the thin metal film. Thus when the refractive index of the surface changes the angle of incident light at which the resonance occurs also changes.

In SPR biosensors, this refractive index change is brought about by binding of analyte in solution to ligand immobilized on the sensor surface. Tracking the change in the incident angle required for SPR allows one to monitor biomolecular interactions in real-time. Recent reviews (Daghestani and Day, 2010; Pattnaik, 2005) and dedicated webpage (Marquart and SPR-Pages, 2014) offer an broader overview of SPR theory and different SPR configurations.

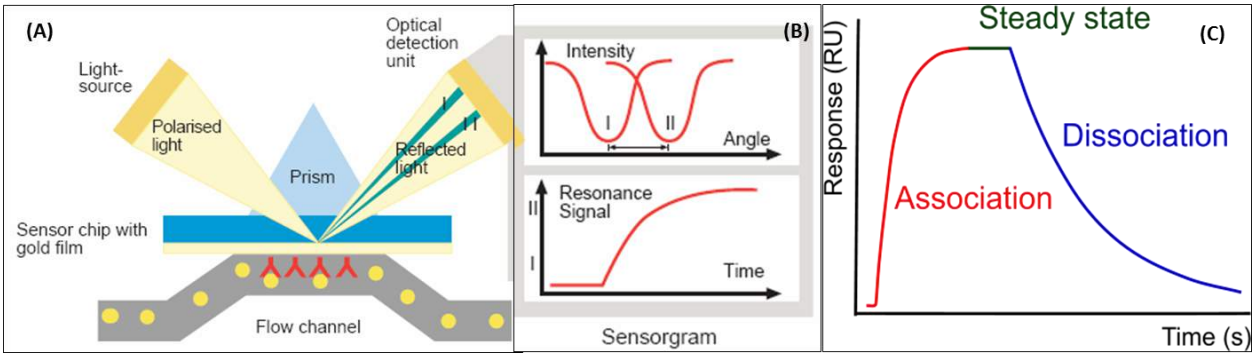

FIGURE 2.1 (A) The principle of the SPR sensor: binding of the analyte to the immobilized ligand induces changes in intensity of the light, reflected form the surface. (B) The change between resonance angles represents the response to analyte binding called sensogram. (C) Response of sensogram increases during analyte-ligand association is constant at steady state and decreases in during complex dissociation.

The change of the incident angle required for SPR is defined as SPR signal in the unit of response unit (RU). Plotting the SPR signal over time during the interaction between an analyte and a ligand, results in a sensorgram - a visual representation of the interaction over time (Fig. 2.1 (B)). When analyte is flowed over the sensor chip and starts association with the immobilized ligand SPR response increases until binding equilibrium is established and sensogram reaches plateau (Fig. 2.1 (A)). As soon as the analyte solution is replaced with buffer, formed analyte-ligand complex dissociates and then the SPR response decreases (Fig. 2.1 (C)). Fitting the sensorgram data to a binding model allows for the calculation of the association (*ka*) and dissociation (*kd*) rate constants and determination of the binding affinity. Thus, SPR can provide a wide variety of important information on biomolecular interactions such as the specificity, affinity, qualitative ranking, kinetics, and thermodynamics of binding. In more details, the

calculation of kinetic constants with homogeneous and heterogeneous analyte models is discussed in chapter 3.

In our studies ***SPR measurements*** were performed to characterize interaction between the thrombin aptamers and thrombin; and to investigate behavior of thrombin aptamers in the presence of nonspecific proteins. Measurements were carried out mostly on Biacore 3000 and Biacore T200 (GE Healthcare) machines using streptavidin-coated SA sensor chip for respective instruments (GE-Healthcare). The response signal provided by the SPR instrument is a direct measure of resonant angle. 1000 RU corresponds approximately to a surface concentration of 1 ng/mm2 for an average protein ligand.

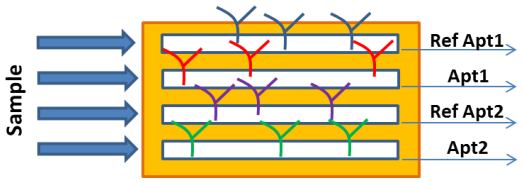

FIGURE 2.2 Flow cells on the SPR sensor chip functionalized with reference and aptameric sequences

The microfluidic pathways of both Biacore instruments contain a single sensor surface overlaid by four flow cells (Fig. 2.2) that allows using one or two flow cells functionalized with reference sequences as a true reference during a single sample injection (Biacore Handbook).

2.3.2 Dynamic light scattering

Dynamic light scattering (DLS) also referred as Quasi-Elastic Light Scattering (QELS) is a non-invasive, well-established technique for measuring the size and size distribution of molecules, micelles and particles typically in the submicron region dispersed in liquid.

When the monochromatic laser light hits the particles or molecules in the suspension, due to their Brownian motion light gets scattered at different intensities. This scattered light then undergoes either constructive or destructive interference by the surrounding particles, and within this intensity fluctuation information about the time scale of movement of the scatterers is contained. The dynamic intensity data is then collected using an autocorrelator to determine the size distribution of particles or molecules in a sample. Autocorrelation analyzes the degree of similarity of signal intensity over a period of time. The rate of decay for the correlation function occurs in milliseconds and depends on the particle size. Smaller particles move more quickly through solution than larger particles. This means that the intensity signal for smaller particles should fluctuate more rapidly than for larger particles and as a result the correlation decreases at a faster rate as seen in the figure 2.3 (A,B).

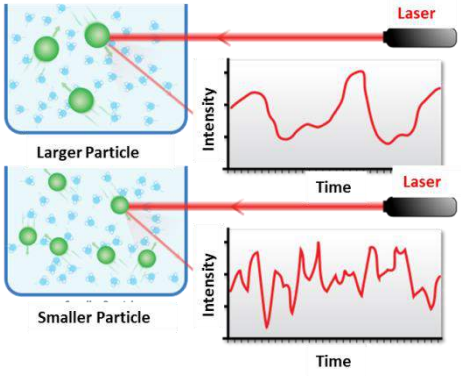

(A)

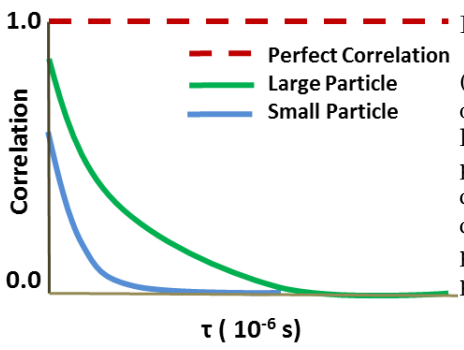

(B)

FIGURE 2.3 (A) Intensity fluctuations of light scattered from larger and smaller particles. (B) Decay of correlation functions in case of small and large particles is compared to perfect correlation.

For a monodisperse particle system experiencing Brownian motion the correlation function *G(t)* decays exponentially with decay constant Γ:

$$G(t) = e^{-\Gamma t} \quad (2.1)$$

The exponential decay is related to the velocity of Brownian motion of the particles, specifically to the diffusion coefficient *D*.

$$\Gamma = q^2 D \quad (2.2)$$

Where q is the wave vector which depends on the λ wave length of the incident laser light, n_0 the optical index and θ the angle between the detector and the sample cell.

$$q = \frac{4\pi n_0}{\lambda} \sin\frac{\theta}{2} \quad (2.3)$$

Hence the particle size can be calculated using the Stokes-Einstein relationship.

$$D = \frac{kT}{6r\pi\eta} \quad (2.4)$$

Where k is Boltzmann constant, T is absolute temperature, η is the viscosity of the solution and *r* is the hydrodynamic radius of the particle.

In our study, DLS method was used to investigate the size of nanoparticles before and after DNA-functionalization steps. With periodical DLS measurement the hydrodynamic radius of the particles was monitored to observe the kinetics of the particle aggregation. DLS measurements were performed on Zetasizer Nano (Malvern Instruments). Samples placed in 100 µL volume disposable plastic cuvettes were illuminated with 4mW HeNe laser (632 nm) and the scattered light was monitored with a detector positioned at the scattering angle of 173°. Instrument also allowed controlling the temperature of the sample through temperature-controlled jacket for cuvette. The same instrument allowed measurement of the Zeta potential of the nanoparticles.

2.3.3 Zeta potential

Zeta potential is a measure of the magnitude of the electrostatic or charge repulsion or attraction between particles, and is one of the fundamental parameters known to affect stability. In solution the presence of the net charge on the surface of a particle affects the distribution of surrounding ions, causing accumulation of the counter-ions (Fig. 2.4). The region over which this influence extends is called the electrical double-layer, composed of two separate areas. The area where ions attach strongly to the particle is called the Stern layer which is followed by the outer diffusive layer. When the particle starts moving under the influence of gravity or applied voltage, ions within the Stern layer and for some extent from diffusive layer will move with the particle. That "boundary" surface beyond which ions from diffusive layer do not move with particles is

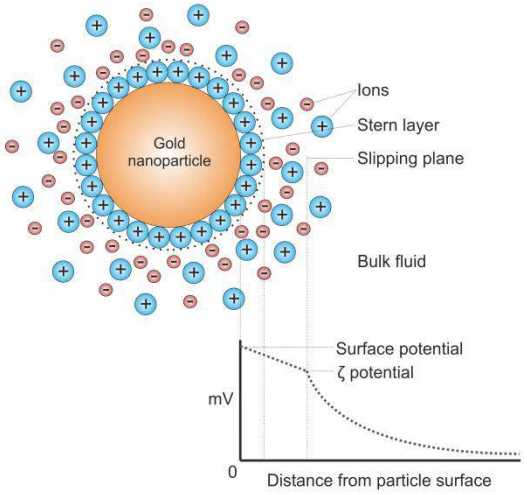

FIGURE 2.4 Schematic representation of the distribution of ions around a charged particle in solution.

called hydrodynamic shear of the slipping plane. The electrostatic potential that exists on the slipping surface is the zeta potential. When zeta potential of particles has large negative or positive values (40-60 mV), then particles repel each other and the suspension will be stable.

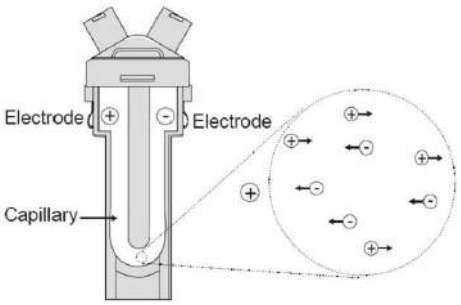

FIGURE 2.5 Cuvette with electrodes for measuring Zeta potential.

To measure the zeta potential, typically electric field is applied to suspension (Fig. 2.5). Charged particles are attracted to the oppositely charged electrodes. From electrophoretic mobility (U_E) of the particles, zeta potential (Z) can be determined through Henry equation:

$$U_E = 2\varepsilon Z f(Ka)/3\eta \qquad (2.5)$$

Where ε is a dielectric constant of medium, η is viscosity and $f(Ka)$ is Henry's function, with Ka being the ratio of particle radius to the double layer thickness (the Debye length). For systems with particles larger than 200 nm into high ionic strength solution, the zeta potential is calculated according to the Smoluchowski model, where and $f(Ka) = 1.5$. For smaller particles with non-polar media Huckel approximation is used with $f(Ka) = 1$.

In our study zeta potential measurements were performed on Zetasizer Nano in order characterize gold and polymer particle stability in water and buffer and the surface charge difference before and after functionalization steps.

2.3.4 UV-Vis spectroscopy

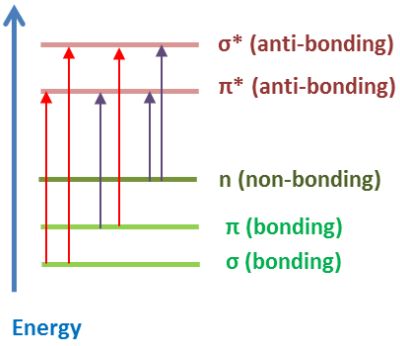

FIGURE 2.6 Possible electron jumps upon light absorption. Black arrows show energetically possible electron transitions by light in UV-Visible range. Red arrow show transitions requiring larger energy than UV-Visible light can provide.

Ultraviolet–visible or just UV-Vis spectroscopy[1] refers to **absorption spectroscopy** or **reflectance spectroscopy** that uses light the in the visible and adjacent, near-UV or near-infrared ranges. In UV-Vis region of the electromagnetic spectrum, molecules undergo electronic transitions from the ground state to the excited state. UV-Vis absorption spectroscopy observes transition of π-electrons or non-bonding electrons from the ground state to higher anti-bonding molecular orbitals (Fig. 2.6). The absorption or reflectance in the visible range directly affects the perceived color of the chemicals involved.

Out of various applications UV-Vis spectroscopy is routinely used in analytical chemistry for the quantitative determination of different analytes in solution. *Beer-Lambert Law* establishes the connection between the absorbance (A_λ) of a chromophore at a given wavelength (λ) and its concentration (c): the higher the concentration of the molecule, the greater its absorbance.

[1] Spectroscopy is general is the study of the interaction between matter and radiated energy. Spectroscopic data is represented as a plot of the response of interest as a function of wavelength or frequency, called a spectrum.

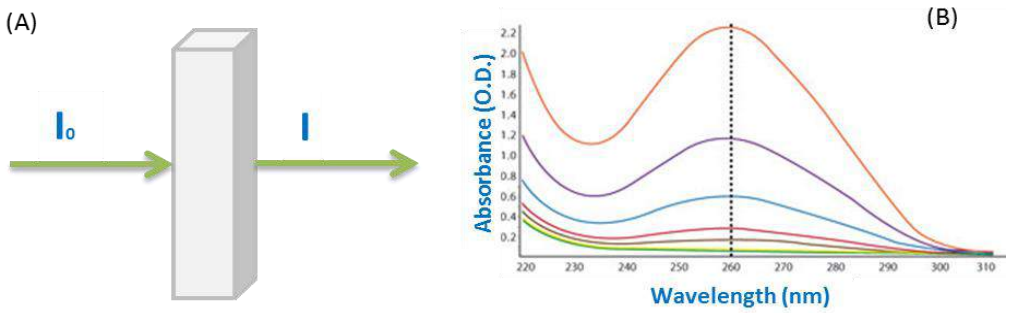

FIGURE 2.7 (A) When light passing through the sample gets absorbed, transmitted intensity is lower than the that of incident light. (B) Absorbance of increasing concentration of the DNA. Absorbance maximum is observed at 260 nm wavelength. The larger the concentration of the DNA in the sample the higher is absorbance

$$A_\lambda = log_{10}\left(\frac{I_0}{I}\right) = \varepsilon_\lambda cL \qquad (2.6)$$

I_0 is the intensity of the incident light at a given wavelength, I is the transmitted intensity, L is the path length through the sample, and ε_λ is molar absorptivity or extinction coefficient of chemical species, representing fundamental molecular property in a given wavelength, solvent, at a particular temperature and pressure. To determine the concentration, ideally, wavelength corresponding to maximum absorbance is selected (Fig. 2.7).

$$c = \frac{A_{\lambda max}}{\varepsilon_{\lambda max} L} \qquad (2.7)$$

For example the concentration of peptides and proteins is determined by measuring absorbance at the wavelength of 280 nm, whereas characteristic absorbance maximum for DNA is at 260 nm (Fig. 2.7 (B)).

We used to UV-Vis absorption spectroscopy not only to measure the concentration but also to evaluate the size of gold nanoparticles in solution, since the maximum of the absorption depends on the size of the colloidal particles.

By time-dependent measurements of UV-Vis absorption, we monitored the kinetics of the chromogenic substrate cleavage by thrombin.

UV absorbance measurements in our case were performed with: (i) Nanodrop 2000C (Thermo Scientific), enabling measurement absorbance of a single sample both in cuvette and as µL volume drop (Fig.2.8 (A)); and (ii) Tecan Infinite® 200 PRO (Tecan, Switzerland), enabling reading absorbance of 96-well plates over time with regulated temperature (Fig. 2.8 (B)).

(A)

(B)

FIGURE 2.8 UV-Vis Spectrophotometer (A)Nanodrop 2000C and (B) Tecan 200 PRO

2.3.5 Fluorescence spectroscopy

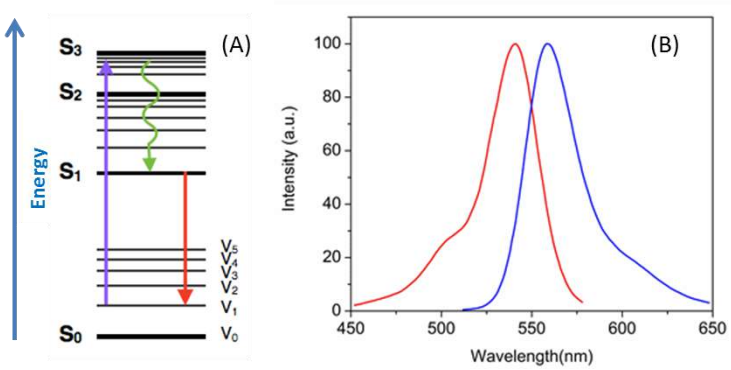

FIGURE 2.9 (A) Jablonski diagram of electronic levels. Purple arrow shows the transition from ground to excited state, green arrow demonstrates internal conversion and red arrow shows fluorescence emission. (B) Absorption (red) and emission (blue) spectrum of a fluorophore Alexa 532 .

Fluorescence spectroscopy also known as spectrofluorometry is a type of electromagnetic spectroscopy which analyzes fluorescence i.e. the emission of the light from a substance that has absorbed light. Similar to UV-Vis absorption, fluorescence is based on the transition of outer electrons upon irradiation with ultraviolet and visible light. While absorption measures transitions from the ground state to the excited state, fluorescence deals with transitions from the excited state to the ground state. Thus the fluorophore is first excited, by absorbing a photon, from its ground electronic state to one of the various vibrational states in the excited electronic state, and then it relaxes to its ground state by emitting a photon (Fig.2.9 (A)). In most cases, the emitted light has a longer wavelength, and therefore lower energy, than the absorbed radiation (Fig. 2.9 (B)).

Most fluorimeters have dual monochromators and a continuous excitation light source to record both an excitation spectrum and a fluorescence spectrum. In order to avoid interference with transmitted excitation light the fluorescence is mostly measured at a 90° angle relative to the excitation light. When measuring fluorescence spectra, the wavelength of the excitation light is kept constant, preferably at a wavelength of high absorption, and the emission monochromator scans the spectrum. For measuring excitation spectra, the wavelength passing though the emission filter or monochromator is kept constant and the excitation monochromator is scanning.

The excitation spectrum generally is identical to the absorption spectrum as the fluorescence intensity is proportional to the absorption. But, unlike to UV/visible spectroscopy, attained fluorescence spectra are not “standard”, they depend on the device, i.e. there is inter-device variation in the fluorescence intensity.

For fluorescence measurements in our case were used: (i) Xenius XC (Safas, Monaco) and (ii) thermal cycler MyCycler (Biorad) allowing simultaneous measurement of several samples in multi-well plastic plate; and (iii) custom-maid fluorimeter from the imaging platform of IPBS-CNRS and (iv) FLS980 fluorimeter (Edinburgh instruments) for the single sample measurement in quartz cuvette with high sensitivity.

2.3.6 FRET

Fluorescence or Förster energy transfer (FRET) is a non-radiative mechanism of energy transfer between a donor fluorophore and acceptor molecule. The acceptor can be another fluorophore or a non-fluorescent molecule (Didenko, 2001). Through long–range dipole-dipole interactions an energetically excited donor, induces the raise of the energy state of the electron to higher vibrational levels in a nearby acceptor. As a result of resonant coupling, fluorescence of the donor decreases or quenches (Fig.2.10). Transferred energy can be emitted as red-shifted fluorescence if the acceptor is a fluorophore or as heat. Requirement for FRET pair is that the fluorescence emission spectrum of the donor must overlap the absorption spectrum of the acceptor.

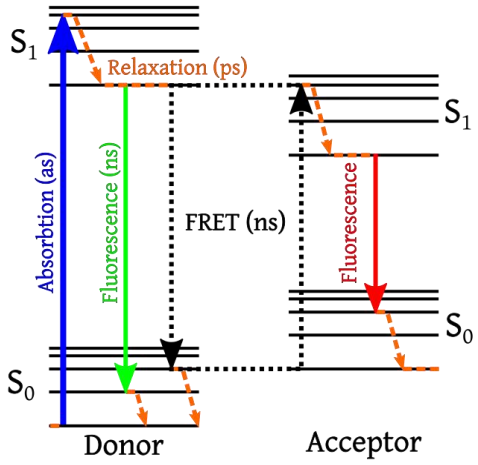

FIGURE 2.10 Jablonski diagram of FRET

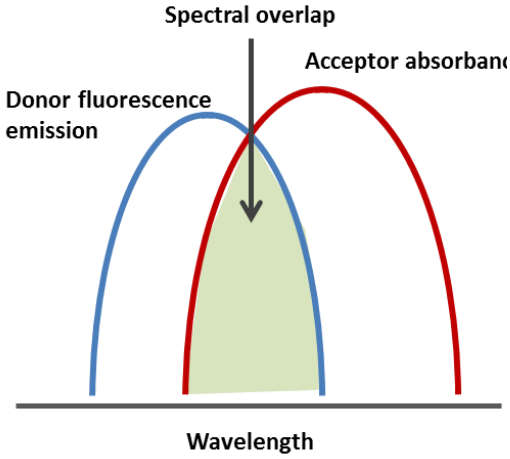

FIGURE 2.11 Spectral overlap of donor fluorescence spectra and acceptor absorbance spectra

The effective energy transfer is dependent on the distance between the donor and the acceptor molecules R and the Förster Radius R_o.

$$E = \frac{R_o^6}{(R_o^6 + R^6)} \qquad \text{Eq. 2.8}$$

R_o describes the distance between the donor and acceptor at which 50% of the excited state energy is transferred from the donor to the acceptor. Förster Radius depends on the quantum yield of the donor in the absence of the acceptor (Q_0), the refractive index of a liquid medium (n), the relative orientation of the transition dipoles (k^2), and the spectral overlap integral (J) (Fig. 2.11).

$$R_o^6 = 8.8 \times 10^{-28} \times (k^2 n^{-4} Q_0 J) \qquad \text{Eq. 2.9}$$

How to calculate the R_o for particular donor-acceptor couple is described here (Linnet, 2012). Typically R_o is between 40 Å to 70 Å. The most sensitive range of the distance between the fluorophores R is 0.7–1.4 Ro, corresponding to 90–10% FRET efficiency.

Dependency of FRET efficiency on orientation and distance of the donor/acceptor couple can be exploited for the design of biosensors. FRET biosensors have been engineered to detect a broad range of molecular events such as, conformational changes upon protein - binding interactions.

2.3.7 The setup of convective assembly

Experiments of convective assembly of nanoparticle were performed on the platform, developed at LAAS by Mike Genevieve during his PhD work. The setup is schematically shown on figure 2.12 and more detailed description is available in the thesis (Geneviève, 2009).

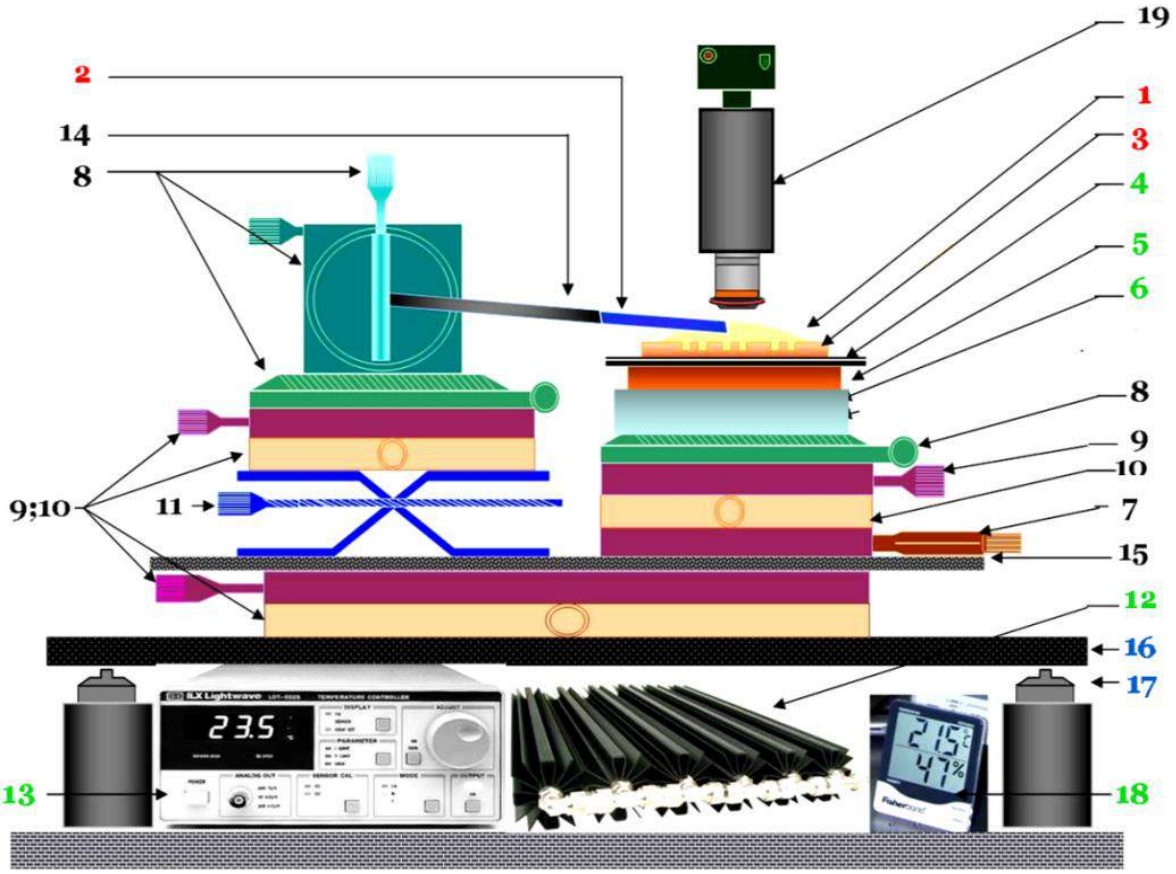

FIGURE 2.12 Experimental platform for convective assembly. Drop of colloid (1), glass slide (2), solid support (3), copper platform (4), Peltier element (5), cooler (6), motorized stage (7), adjustment handles (8,9) positioning platforms (10,11), radiator (12), temperature regulator (13), glass slide holder(14), platform (15), anti-vibration table (16), pneumonic feet (17) Thermometer and hygrometer (18), optical microscope coupled with CCD camera (19)

The central part of the instrument is the motorized translation stage (7) on top which a beforehand cleansed and treated solid substrate (3) is fixed. Drop (1) of colloidal solution (50 uL) is between moving substrate and a glass slide fixed (2) above at a distance of 0.5-1 mm from the surface. Moving of solid support with optimal velocity induces dragging of the meniscus, formed on the interface of air/liquid, and thus spreads colloid solution over the surface as a thin film.

In order to control the evaporation rate, a solid substrate is fixed on top of the copper plate (4) under which a Peltier element (5) is located. The Peltier is regulated with the circulating liquid (6) passing through the radiator (12), the temperature of which is adjusted with manual regulator (13). It gives possibility to set an experimental temperature from +5 °C to 55 °C with accuracy of ±0.002 °C and stability of ±0.004 °C.

The entire setup of sample holder with temperature controller is mounted on motorized stage (7). Various adjustable handles (screws) (8,9,19) allow precise positioning of sample

platform. Movement of the stage is controlled with software, allowing displacement with velocities in a range of 0.1-1000 um/s. The second stage (stationary) is responsible for fine-tuning the glass slide and its holder (14) at desired distance and angle from substrate surface

To avoid and exclude the influence of external vibrations and noise on the experiment, the instrument is placed on the special anti-vibration table for optics (16), standing on pneumatic feet (17).

An optical microscope coupled with CCD camera (19) is set on top of the sample to provide direct observation of the assembly process. Humidity and room temperature (18) are measured in the course of the deposition as the external and important parameters of the experiment.

2.3.8 Measurement of Contact angle

We accessed the surface tension of a liquid by measuring the contact angle between a liquid and a surface with Digidrop.

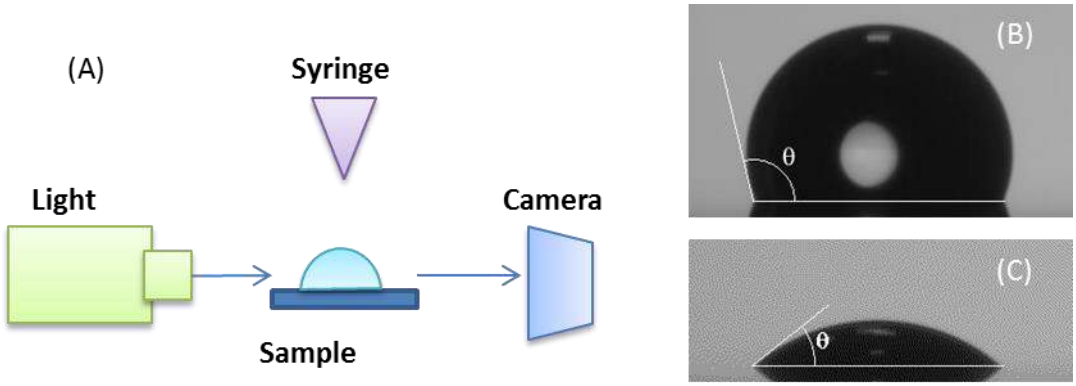

FIGURE 2.13 (A) schematic illustration of the setup for contact angle measurements. Images of the water drop on hydrophobic (B) and hydrophilic surfaces (C).

We used an optical instrument based on reflected microscopy with computer-assisted shape recognition. A drop of liquid deposited on a desired support, is detected by CCD camera and the treated by software (Fig. 2.13 (A)). If the angle is large then the surface is hydrophobic (Fig. 2.13 (B)), if the angel is small then the surface is hydrophilic (Fig. 2.13 (C)). This method allows measuring a contact angle with accuracy of 0.1°.

2.3.9 Scanning Electron Microscopy

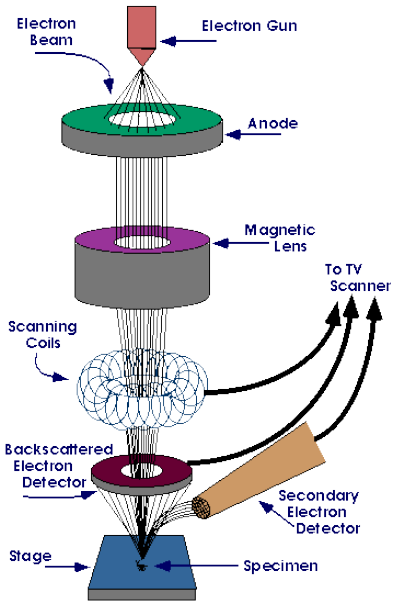

FIGURE 2.14 Illustration of the SEM instrument

A scanning electron microscope (SEM) is a type of electron microscope that gives the information about surface topography and composition of the sample by scanning the sample with the focused beam of electrons. Specific detectors record backscattered electrons, secondary electrons and X-rays reemitted upon electron-matter interaction. The backscattered electrons reveal the topography of the sample surface with the resolution 1 to 20 nm, the secondary electrons give the chemical contrast, whereas X-rays bear the information about the chemical composition. Magnification in a SEM can be controlled over a range of up to 6 orders of magnitude from about 10 to 500,000 times.

In a typical SEM, an electron beam is thermionically emitted from an electron gun fitted with a tungsten filament cathode. Electrons are accelerated with electric field to energy level of 0.1-30 keV and focused by passing through magnetic lenses, before they interact with a sample to be studied (Fig. 2.14). Samples generally are mounted rigidly on a specimen holder called inside a vacuum chamber. For the most instruments, specimens must be electrically conductive, at least at the surface, and electrically grounded to prevent the accumulation of electrostatic charge at the surface (AMMRF).

In our studies all SEM imaging of convectively assembled particles were performed with the field Emission Scanning Electron Microscope Hitachi-S4800. This instrument with maximal resolution of 1nm equipped with both secondary electron and backscattering electron detectors. The samples were on silicon wafer, which represents a conducting surface.

2.4 References

AMMRF Background information - What is scanning electron microscopy? | MyScope.

Baglin, T.P., Carrell, R.W., Church, F.C., Esmon, C.T., and Huntington, J.A. (2002). Crystal structures of native and thrombin-complexed heparin cofactor II reveal a multistep allosteric mechanism. Proc. Natl. Acad. Sci. *99*, 11079–11084.

Daghestani, H.N., and Day, B.W. (2010). Theory and Applications of Surface Plasmon Resonance, Resonant Mirror, Resonant Waveguide Grating, and Dual Polarization Interferometry Biosensors. Sensors *10*, 9630–9646.

Didenko, V.V. (2001). DNA Probes Using Fluorescence Resonance Energy Transfer (FRET): Designs and Applications. BioTechniques *31*, 1106–1121.

Fenton, J.W., Fasco, M.J., and Stackrow, A.B. (1977). Human thrombins. Production, evaluation, and properties of alpha-thrombin. J. Biol. Chem. *252*, 3587–3598.

Figueiredo, A.C., Clement, C.C., Zakia, S., Gingold, J., Philipp, M., and Pereira, P.J.B. (2012). Rational Design and Characterization of D-Phe-Pro-D-Arg-Derived Direct Thrombin Inhibitors. PLoS ONE *7*, e34354.

Geneviève, M. (2009). Assemblage dirigé d'objets à partir de solutions colloïdales.

Li, W., Johnson, D.J.D., Esmon, C.T., and Huntington, J.A. (2004). Structure of the antithrombin–thrombin–heparin ternary complex reveals the antithrombotic mechanism of heparin. Nat. Struct. Mol. Biol. *11*, 857–862.

Linnet, T. (2012). Forster distance calculator - PyMOLWiki.

Marquart, A., and SPR-Pages (2014). SPR Overview.

Marrero, A., Duquerroy, S., Trapani, S., Goulas, T., Guevara, T., Andersen, G.R., Navaza, J., Sottrup-Jensen, L., and Gomis-Rüth, F.X. (2012). The Crystal Structure of Human α2-Macroglobulin Reveals a Unique Molecular Cage. Angew. Chem. Int. Ed. *51*, 3340–3344.

Martin, P.D., Malkowski, M.G., Box, J., Esmon, C.T., and Edwards, B.F. (1997). New insights into the regulation of the blood clotting cascade derived from the X-ray crystal structure of bovine meizothrombin des F1 in complex with PPACK. Struct. Lond. Engl. 1993 5, 1681–1693.

Nordenman, B., NYSTRöm, C., and BJörk, I. (1977). The Size and Shape of Human and Bovine Antithrombin III. Eur. J. Biochem. *78*, 195–203.

Pattnaik, P. (2005). Surface plasmon resonance: applications in understanding receptor-ligand interaction. Appl. Biochem. Biotechnol. *126*, 79–92.

Russo Krauss, I., Merlino, A., Randazzo, A., Novellino, E., Mazzarella, L., and Sica, F. (2012). High-resolution structures of two complexes between thrombin and thrombin-binding aptamer shed light on the role of cations in the aptamer inhibitory activity. Nucleic Acids Res. *40*, 8119–8128.

Russo Krauss, I., Pica, A., Merlino, A., Mazzarella, L., and Sica, F. (2013). Duplex–quadruplex motifs in a peculiar structural organization cooperatively contribute to thrombin binding of a DNA aptamer. Acta Crystallogr. D Biol. Crystallogr. *69*, 2403–2411.

Soriano-Garcia, M., Padmanabhan, K., de Vos, A.M., and Tulinsky, A. (1991). The Ca2+ ion and membrane binding structure of the Gla domain of Ca-prothrombin fragment 1. Biochemistry (Mosc.) *31*, 2554–2566.

Vijayalakshmi, J., Padmanabhan, K.P., Mann, K.G., and Tulinsky, A. (1994). The isomorphous structures of prethrombin2, hirugen-, and PPACK-thrombin: changes accompanying activation and exosite binding to thrombin. Protein Sci *3*, 2254–2271.

CHAPTER 3. THROMBIN INTERACTION WITH APTAMERS

3.1 Introduction

Biomolecular recognition is central to biosensing (Chambers et al., 2008), since it governs specificity, sensitivity and time of analyte detection. These three parameters represent the most important requirements of biosensor (Foulds and Lowe, 1985). Therefore during sensor development the first and the most important step is to understand well the process and mechanism how the sensing element, in our case aptamer, recognizes and interacts with its molecular target - thrombin.

Indeed thrombin aptamers HD1 and HD22 have been the most studied aptamers as they not only satisfy aptameric requirements (affinity and specificity) but also show their effect on modulation of coagulation process (Bock et al., 1992; Kretz et al., 2006; Tasset et al., 1997). These qualities make them interesting candidates both as the anticoagulant for therapeutic applications, and as sensing elements, in affinity biosensing. Truly, over the past two decades, significant research effort has explored the properties and emerging applications of these aptamer resulting in more than 1000 publications (Deng et al., 2014). However, thrombin-aptamer couple is mostly used as a model system to demonstrate achievement in bio -detection and sensing technology in general. Such approaches do not require comprehension the problematics of thrombin detection in reality and consequently they do not push the existing boundaries of understanding thrombin –aptamer interactions. The complexity of thrombin detection in real environment remains underestimated and therefore under-investigated Hence when it comes to an actual problem of developing aptamer–based sensor for substantial purposes i.e. thrombin detection in real-like conditions, we are still confronted with unanswered questions of feasibility of such sensor.

In this chapter we desire to identify the key points of the thrombin-aptamer interactions, which are essential for sensor development but remain still untacked, and to try finding exhaustive answers about specificity and sensitivity of thrombin detection in real-like environment.

To understand the complexity of the problem, first, let us have an overview what is known about the molecular structure of thrombin, its activation and interactions with substrates and aptamers.

3.1.1 Activation of prothrombin into thrombin

Thrombin in is the activated form of zymogen prothrombin. Mature prothrombin is glycoprotein with 579 amino acids and arranged in four domains: Gla domain, two adjacent Kringle domains and catalytic domain with A and B chains (Fig. 3.1). Prothrombin is proteolytically activated to by factor Xa or by the prothrombinase complex consisting of factor Xa and Va. Prothrombin is cleaved, first at R320 (located between the A and B chains) to generate meizothrombin and then at R271 (located between the A chain and Kringle 2) to generate thrombin and fragment F1+2. Although kinetically less favored, an alternative activation pathway is also possible (Lane et al., 2005).

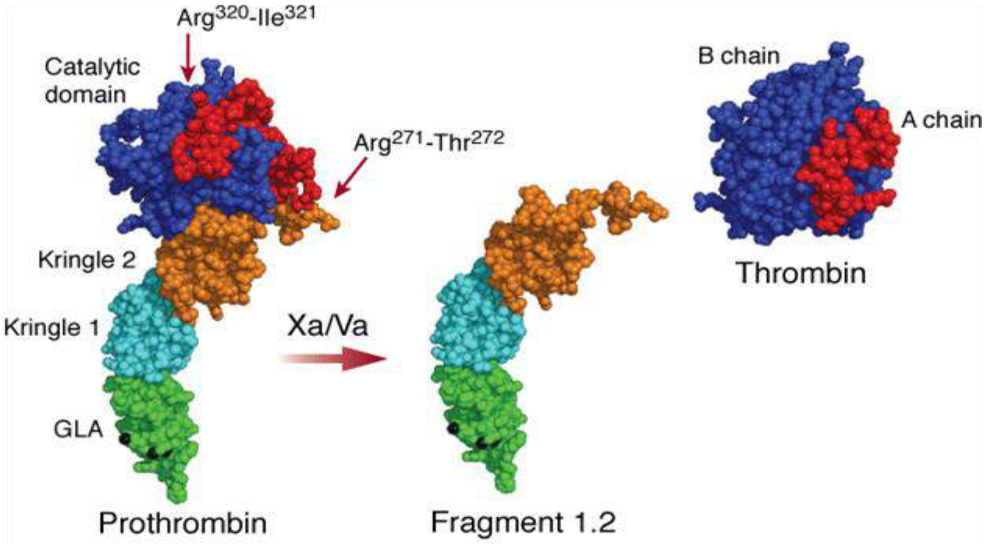

FIGURE 3.1. Activation of prothrombin. Molecular model reconstructed by superposition of crystal structures of prothrombin fragment1 (2PF2), prethrombin2 (1HAG), Meizothrombin desF1(1AOH). Upon prothrombin cleavage at Arg271 prothrombin Fragment 1.2 is realized and cleavage at Arg320 creates mature thrombin.

As a result of activation α-thrombin represents only the half of the prothrombin molecule (36 kDa and 72 kDa respectively) since it lost the domains important for initial recognition interactions and was left with two polypeptide chains A and B. This loss permits exposure of cryptic functional regions, which were well hidden within prothrombin and now play crucial role for extending the range and specificity of thrombin's actions (Crawley et al., 2007).

3.1.2 Thrombin structure and interactions

As we showed in the first chapter thrombin is involved in more than dozen paradoxically opposite reactions. These multiple interactions, in which thrombin participates, raise the question of how it knows which substrate it should interact with and cleave. The question how thrombin realizes recognition and interaction with these multiple biomolecules, can be addressed only by considering how the activity of thrombin is controlled by its structure.

Thus, thrombin is composed of two polypeptide chains A and B. The light chain A consisting of 36 residues is linked by a single disulfide bond to the heavy chain B with 259 residues that contains three intra-chain disulfide bonds (Siller-Matula et al., 2011). The B chain is

shaped like a sponge, with deep crevices and large protuberances on its water-accessible surface, hosting the entrance to the active site and all functional epitopes of the enzyme. The active-site, containing serine residue S195 involved in the nucleophilic attack of the target peptide bond, is located in a deep canyon formed by the flanking hydrophobic 60-insertion and hydrophilic γ-loops (Di Cera, 2003).

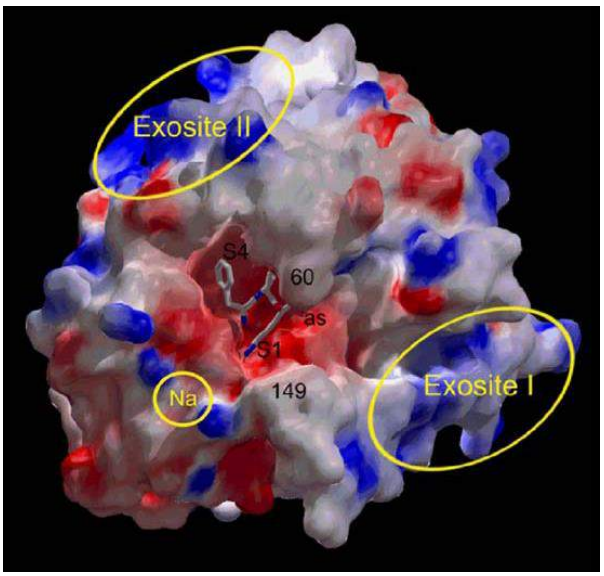

FIGURE 3.2 Solid Connolly surface representation of human α-thrombin in covalent complex with PPACK. Thrombin is colored according to the electrostatic surface potential (red:negative; blue: positive). Reprinted from (Bode, 2006).

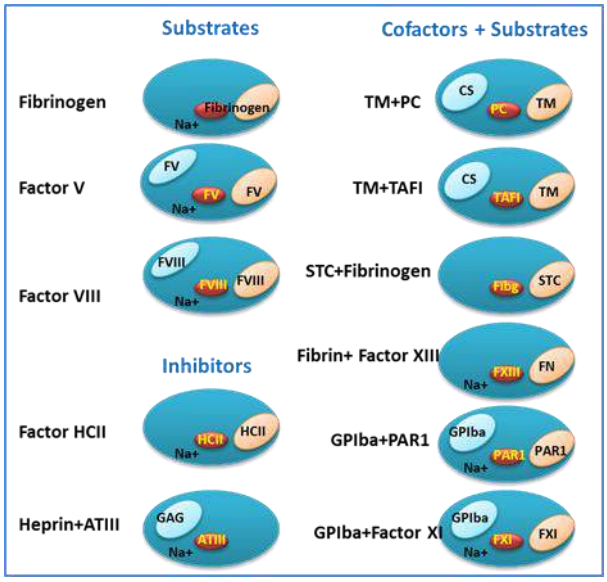

FIGURE 3.3 Schematic interaction of thrombin (represented as large ellipsoid) and its different surface regions binding substrates, inhibitors, carbohydrates and cofactors. Adapted from (Bode, 2006).

The wealth of thrombin interactions depends on a rich repertoire of mechanisms underlying substrate recognition (Di Cera, 2003). For establishing these interactions thrombin also has two anion-binding exosites (I and II), made up of clusters of surface- exposed basic residues. These charged patches interact with negatively-charged regions of thrombin cofactors and substrates. Occupancy of exosites I and II may induce allosteric changes to the active site to promote catalysis (Bode, 2006).

Exosite I is located "east" of the active site (Fig 3.2). It contains hydrophobic patches and charged residues K36, H71, R73, R75, Y76, R77a, and K109/110 and acts as steering for active site substrates such as fibrinogen, fibrin, PAR-1, PAR-3, PAR-4, thrombomodulin, heparin cofactor II, factors V, VIII, XI and XIII (Fig. 3.3).

Exosite II is positioned "west" of the active site (Fig 3.2). It is also centered on charged residues R93, K236, K240, R101, and R233, but unlike exosite I, exosite II has no hydrophobic patches on its surface. Exosite II is the local for docking antithrombin III, PAR-1, factors V, VIII and XI, protein C and TAFI (Fig. 3.3) through interaction with polyanionic ligands glycosaminoglycan cofactors and carbohydrates such as heparin, GpIbα and chondroitin sulphate (CS) (Bode, 2006).

Another important loop contains a site for Na+ binding The binding of a sodium ion modulates thrombin allosterically and regulates procoagulant and anticoagulant activities (Di Cera, 2003).

3.1.3 Binding of thrombin aptamers to thrombin

3.1.3.1 Molecular structure ofHD1

HD1 aptamer is known to interact with exosite I of thrombin. Despite ambiguities in previous X-ray and NMR models (Macaya et al., 1995; Padmanabhan and Tulinsky, 1996 of HD1, recent study finally confirmed that HD1 folds into a stable unimolecular antiparallel quadruplex structure containing two G-quartets spaced by two TT loops and a TGT referred as chair-like structure(Russo Krauss et al., 2012). In the structure of HD1, G1, G6, G10 and G15 form the top layer of G-tetrad; G2, G5, G11 and G14 form the second layer. Potassium ion fits the cavity between the two G-tetrad planes of HD1 properly and coordinately interacts with eight oxygen atoms in G-quadruplex. K+ cations stabilize quadruplex conformation of HD1 and improve the thermal stability (Kankia and Marky, 2001).

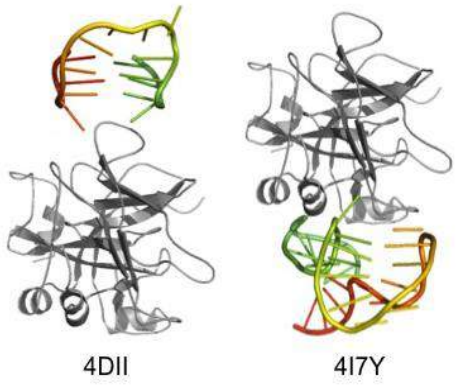

FIGURE 3.4 Molecular structures of thrombin complex with HD1 (4DII) and HD22 (4I7Y)

HD1 interacts with thrombin exosite I through TT loops acting as a pincer-like system (Fig. 3.4). T4 and T13 are mainly involved in polar interactions whereas T3 and T12 form hydrophobic contacts. The amino residues His71, Arg75, Tyr76, Arg77, Asn78, Ile79, Tyr117 in the exosite I of thrombin are involved in the interaction with HD1. Since the aptamer sequence is palindromic, two almost identical binding regimes where observed, they differ from each other by 180° rotation with respect to thrombin, the only significant difference is confined to the orientation of the TGT loop Russo Krauss et al., 2012).

In addition, there is also an evidence that TGT loop might interact with certain amino residues of exosite II (Padmanabhan and Tulinsky, 1996; Pagano et al., 2008; Russo Krauss et al., 2011)

3.1.3.2 Molecular structure of HD22

The structure of aptamer HD22 was solved only recently with a 2.4 Å resolution (Russo Krauss et al., 2013). Unlike HD1, HD22 has a duplex/G-quadruplex mixed structure (Fig. 3.4). The nucleotides 1-3 and 25-27 with an additional C4-G23 form a duplex motif, and the sequence ranging from G5 to G20 folds into a G-quadruplex structure with four connection loops: T9-A10, T18-T19, G13-C14-A15 and an one-nucleotide loop (T6). In G-quadruplex motif, two G-tetrad planes are formed by G5-G7-G12-G16 and G8-G11-G17-G20. There is a 90-degree turn between the G-quadruplex and duplex motifs (Russo Krauss et al., 2013).

HD22 interacts with the exosite II of thrombin via the nucleotides G23, T24, G25, A26, C27 in the duplex and T9, T18, T19, G20 in G-quadruplex. On thrombin side, the residues Tyr89, His91, Pro92, Arg93, Tyr94, Asn95, Trp96, Arg97, Arg126, Leu130, Arg165, Lys169, His230, Arg233, Trp237, Val241 and Phe245 take part in the interaction. Since the exosite II is positively charged, motifs of exosite II create ion pairs with the HD22 backbone, mostly in the duplex region. Formed complex is stabilized by hydrophobic interactions observed in the G-quadruplex region (T9, T18 and T10).

3.1.4 Kinetic parameters of thrombin-aptamer interactions

Several fundamental studies were carried out to get an answer about the affinity of aptamers to thrombin with different surface and volume-based techniques such as SPR, QCM summarized it the table 3.1 and 3.2 respectively for HD1 and HD22.The variation between reported values is significant not only for inter methods but also intra. Obviously, it is difficult to say which of these values are true for that particular conditions in which we would like to work.

Table 3.1 Reaction and affinity constants of HD1 aptamer interaction with thrombin known from the literature determined with various methods

Complex	Method	k_{on} $10^6 M^{-1}s^{-1}$	k_{off} $10^{-3} s^{-1}$	K_d $10^{-9} M$	Source
HD1-Thrombin exosite 1	**SPR**	1.3	1.80	1.38	(Davis, 1994)
		0.290	1.80	6.2	(Davis 1994)
		0.19	3.83	20.2	(Hasegawa et al., 2008)
		0.66	4.7	7.1	(Müller et al., 2008)
		0.52	89	171	(Lin et al., 2011)
		0.023	9.54	421	(Pinto, 2012)
		-	-	102.6	(Pasternak et al., 2011)
	RIfS	0.075	3.38	45.4	(Goji and Matsui, 2011)
	IAsys	-	-	11.06	(Strehlitz et al., 2008)
	labeling	-	-	10-25	(Macaya et al. 1995)
	fluorescence	-	-	34	(Kretz et al., 2006)

Table 3.2 Reaction and affinity constants of HD22 aptamer interaction with thrombin known from the literature determined with various methods

Complex	Method	k_{on} $10^6 M^{-1}s^{-1}$	k_{off} $10^{-3} s^{-1}$	K_d $10^{-9} M$	Source
HD22-thrombin exosite2	**SPR**	0.44	1.54	3.5	(Hasegawa et al., 2008)
		0.35	0.82	2.4	(Müller et al., 2008)
		0.58	2.86	4.91	(Pinto, 2012)
		0.84	92	110	(Lin et al., 2011)
	QCM	97	86000	88	(Hianik et al., 2007)
	ITC	-	-	94	(Nallagatla et al., 2009)
	fluorescence	-	-	29	(Kretz et al., 2006)

3.1.5 "Million-dollar questions"

Based on what is known, below are listed the key questions, on our opinion, requiring to be answered, before considering construction of aptamer-based thrombin sensor.

3.1.5.1 Sensitivity

Sensitivity of detection depends great deal on the properties of molecular interaction between thrombin and aptamer. Namely it depends not only on affinity, but also on rate contents, characterizing how quickly complex is formed and how strong is the interaction. As we saw in previous paragraph, only the range of the thrombin-aptamer affinity constant is known. But what are the rate-constants in the experimental conditions that we intend to use? Even more interesting, is to know interaction character of aptamers with thrombin not only in simplified condition, but also in real-like environment.

3.1.5.2 Specificity

On one hand, sensing elements, aptamers, when selected by SELEX, are the most specific and affine of all the other nucleotide strands in the library, meaning that they bind their target the best. Therefore they should guarantee selective and sensitive detection of the target. However in real conditions like a plasma or blood, in the presence of my many other biomolecules, initial target may not be the only fitting partner for aptamer and in this case specificity of detection is compromised. Cross-reactivity with other targets might often be one of the biggest drawbacks. Thus the behavior of the aptamers in the real-like conditions, need to be investigated.

On the other hand, target, depending of the function, might be interacting with wide array of molecules that can also complicate accurate detection. In this respect, thrombin is indeed a very tricky target. Thrombin is the multidomain protease, generated by proteolyctical activation of coenzyme prothrombin, to which it bares structural similarities. Thrombin is actively involved in diverse physiological processes and therefore it recognizes and interacts with multiple substrates (Di Cera, 2003). Therefore specify of the detection is highly depended on behavior of aptamers.

The first most important question concerns interaction of aptamers with prothrombin, the precursor of thrombin that is present in the blood with micromolar concentration. It is known, to be recognized by HD1, and interaction is characterized with affinity comparable to thrombin (Kretz et al., 2006; Müller et al., 2008). But only little is known for prothrombin interaction with HD22. Even more, it is interesting whether there is the difference in the signatures of thrombin and prothrombin binding to HD1.

Thrombin, regulating numerous reactions is on its own regulated by inhibitors, hence when considering real environment we have to take in account that thrombin might be in complex with the regulated or regulating molecules. Therefore the second question concerns the ability of aptamers to discriminate between free and thrombin complexes. Of particular interests are thrombin complexes with its natural inhibitors ATIII, HCII and A2M, since ultimately all thrombin gets irreversibly inhibited and cleared form the circulation by them (Siller-Matula et al., 2011).

3.1.6 Objectives of this study

Thus, in this work we want to address these above-mentioned questions and answer them with surface plasmon resonance method. SPR method is not only sensitive method, which gives us possibility to simultaneously measure association and dissociation rate constants and thus access the affinity, but it also represents an example of the surface based affinity sensors, that can give us insight of strong and weak points of using such method when designing a sensor.

The aim is to start with the simple conditions, i.e. to perform kinetic experiments of thrombin and prothrombin interactions with aptamers; then characterize interaction of aptamers with thrombin-inhibitor complexes and nonspecific proteins; and finally go towards more complex case where thrombin instead of buffer will be in diluted plasma. This approach is expected to elucidate which reactions and at which step could be limiting thrombin detection by the aptamers.

We also want to investigate aptamer NU172, that, similarly to HD1 is known to interact with the exosite I with nanomolar affinity (Mayer et al., 2011), however characterization of association and dissociation rate constants neither for thrombin nor prothrombin hasn't been reported.

3.2 Experimental

3.2.1 SPR experiments

3.2.1.1 Immobilization of thrombin-binding aptamers on the surface of SPR sensor chip

For the aptamer immobilization, a single step attachment approach was chosen. For this reason aptamers had biotin-modified 5' end and sensor chip SA was functionalized with streptavidin. To avoid steric hindrances, aptamers contained a 20-Thymine spacer between the biotinylated end and the aptameric sequences.

The sensor chip allowed working with four flow-cells, i.e. we could use four patches for aptamer immobilization. On the first two patches we immobilized one of the aptamers and corresponding scrambled aptamer sequence[1]. Another aptamer and its scrambled sequence were immobilized on the remaining patches. Each DNA was immobilized at a separate step. It should be noted, that in all measurements HD1 and HD22 where examined together on the same sensor chip, whereas for NU172 similar experiments were performed on the separate sensor surface, having also HD22 immobilized to ensure the similarity between the experiments

Before immobilization of biotinylated aptamers on SA senor chip, the surface of the chip was primed with HBS-EP buffer and rinsed by 3 consecutive 1 minute-long injections of 1 M NaCl and 50 mM NaOH solution at rate of 30 µl/min.

For kinetic analysis low surface density of a ligand has crucial importance. In general, for kinetic measurements, when the analyte is injected, a total analyte response of maximal 100 RU is desired. The amount of ligand (in response units) to be immobilized, corresponding to desired maximal response, can be calculated by following relationship:

$$R_{ligand} = \frac{R_{max} \times Mr_{ligand}}{Mr_{analyte} \times Valency_{ligand}} \ (R.U.) \tag{3.1}$$

Of course, there is the linear relation between response and amount of ligand immobilized to the sensor surface and the theoretical number of ligand sites after immobilization can be calculated with following equation:

$$ligand_{sites} = \frac{R_{ligand}}{Mr_{ligand} \times Valency_{ligand}} \ (pmol \times mm^2) \tag{3.2}$$

Thus, for the kinetic experiments, over the clean sensor chip surface solution of 10 nM aptamer in HBS-EP buffer was flown at a rate of 30 µl/min. A 12 sec long ligand injection was sufficient to obtain immobilization level of 40±5 RU.

In the case of interaction analysis, where the obtained result has more qualitative (yes/no) character, higher surface density of ligand is better. For this reason, aptamer solution was injected longer (about 2 minutes) until 500±50 RU response was achieved.

[1] Scrambled aptamers were used as the reference for nonspecific interactions, the impact of which was then subtracted from the response of the corresponding aptamers. Scrambled aptamers have the same length as the corresponding aptamers but their sequence is highly altered. (See chapter 2 for the sequences).

3.2.1.2 Protein interaction with aptamers

In typical SPR experiments proteins (thrombin, prothrombin, BSA, and 100 fold diluted plasma) in PBS running buffer were injected into the system allowing interaction with surface-immobilized aptamers for 3 minutes at a constant flow rate of 30 µl/min and constant temperature of 25 °C. Association phase was followed with running buffer injection for 120-180 seconds to allow complex dissociation. After each injection, surface was regenerated with 30 sec pulse of 2 M KCl and let stabilize for 120 seconds. Kinetic experiments were made in duplicate.

In order to get insight into the **kinetics of thrombin interaction with the aptamers** set of physiologically relevant concentrations of proteins ranging from 0.78 nM to 50 nM was used. In the case of prothrombin, two kinetic experiments in the same concentration range as for thrombin were performed in the presence and absence of argatroban - thrombin active site blocking agent. As argatroban is a reversible thrombin inhibitor, final concentration of 50 µM was used to keep the active site of thrombin continuously blocked.

Whether or not the presence of **thrombin** can be detected **in abundance of prothrombin**, was investigated by injecting mixture of various proportions of thrombin and prothrombin keeping total protein concentration equal to 50 nM (50 nM thrombin, 40/10 thrombin/prothrombin, 30/20 thrombin/prothrombin, 20/30 thrombin/prothrombin, 10/40 thrombin/prothrombin, 50 nM prothrombin).

To verify **aptamer specificity** kinetic experiments were also performed with 12.5 nM- 3.2 µM BSA, the most abundant plasma protein, and thrombin complexes with its natural inhibitors ATIII, HCII and A2M in various stoichiometric ratios (thrombin concentration 12.5 nM, inhibitor concentration 12.5, 50, 200, 800 nM).

Behavior of thrombin natural inhibitors ATIII and HCII in the presence of aptamer bound thrombin was studied by injecting (coinject mode) increasing (12,5; 50; 200; 800; 1500 nM) concentrations of inhibitors right after association phase of thrombin in mass transport limited conditions, (with high surface density of aptamers 500±50 RU)

Aptamer specificity towards thrombin **in real-like conditions** was investigated by injecting thrombin concentrations in 100 and 10 times diluted murine plasma. Murine plasma prior to use was centrifuged at 14000 rpm for 5 minutes; supernatant was collected and filtered in 0.22 µM filter. Plasma then was diluted either 10 or 100 times in PBS containing 0, 1 or 10 mg/mL nonspecific binding reducer (NSBr).

3.2.2 SDS PAGE separation

In order to elucidate the composition of prothrombin sample, sodium dodecyl sulfate-polyacrylamide gel electrophoresis (SDS-PAGE) was carried out according to the method of Laemmli (Laemmli, 1970). Briefly, in assembled glass cassette for electrophoresis freshly prepared separating gel was poured and let to reticulate for 20-30 minutes. Over the separating gel well-forming comb was placed and fresh stacking gel was injected. Stacking gel was allowed to gelate for 30 minutes. Meanwhile, 20 µL prothrombin of 8 µM concentration was mixed with loading buffer and incubated for 5 minutes in boiling water bath to facilitate protein denaturation. Protein sample was loaded into solidified acrylamide wells. Molecular weight size marker of known molecular weight was placed in a separate lane in the gel. Acrylamide cassette was placed in electrode chamber with and all together in the tank with Tris running buffer. 100 V of 20 mA constant current was applied to separate proteins for 2 hours until bromophenol blue marker reached bottom of the gel. After the completion of the electrophoresis, the gel was fixed with 10% trichloroacetic acid for 5 minutes. For visualization of the separated proteins gel was incubated with staining solution of CBB till the appearance of clear bands on the gel (1 hour). Gel was diffusion-destained by repeated washing in destaining solution. Intensity of SDS bands was analyzed with image J software.

3.2.3 Chromogenic substrate cleavage assay

The presence of thrombin and its activity can be monitored by hydrolysis of chromogenic substrate that upon cleavage starts to absorb the light. In all of our experiments kinetics of cleavage of 83 µM concentration chromogenic substrate S2238 was monitored by measuring absorbance at 405 nm. Samples of 100 µL final volumes were prepared in duplicates and placed in 96 plates for absorbance measurement. Thrombin and FXa where pipetted the last in order to avoid missing the begging of the activation. All assays were performed with PBS-BSA activation buffer at 20° C, cleavage kinetics was recorded up to 1 hour.

We compared kinetics of chromogenic substrate hydrolysis of samples with various thrombin concentrations (1.3, 4.5, 13, 45, 130 nM) with the 200 nM prothrombin sample in order to verify the presence of thrombin in prothrombin sample.

In order to follow prothrombin activation into thrombin by FXa and to evaluate effect of aptamer the presence on prothrombin activation as well, we let 2.5, 5, 25 and 50 nM FXa to interact with 100 nM prothrombin in the presence and absence of 0.5, 1 and 2 µM HD1 or HD22.

To observe the inhibition of prothrombin activation by of FXa at different time points 1 µM of direct FXa inhibitor rivaroxaben was added after each 5 minutes to the samples containing 100 nM prothrombin and 50 nM FXa.

3.3 Data analysis of SPR kinetic experiments:

Before analysis of a kinetic data, signals from the reference flow cells and blank sample were subtracted from the signal of sample cell, to remove impact of all the nonspecific interactions.

In order to access affinity and reaction contacts of thrombin or prothrombin interaction with aptamers, date were globally fitted with nonlinear least square method with floating parameters (R_{max}, k_a, k_d) using integrated rate equations either for one-to-one interaction or more complex, heterogeneous analyte models derived below.

3.3.1 One-to-one binding

The most commonly used and the simplest model for description interaction of immobilized ligand and injected analyte is the Langmuir model (3.3), applicable in the vast majority of cases. It assumes that one monovalent and homogenous analyte (A) interacts with homogenous ligand (L) and that all binding events are independent. Formed complex (LA) follows pseudo-first order kinetics, assuming that reaction is not mass transport limited. (o'shannessy 1993).

$$A + L \underset{k_d}{\overset{k_a}{\rightleftarrows}} AL \tag{3.3}$$

The association constant k_a represents the rate of the complex formation, while dissociation constant k_d is the rate of complex decay. The rate equation describing AL complex formation at time t, may be written as:

$$\frac{d[AL]}{dt} = k_a[A][L] - k_d[AL] \tag{3.4}$$

Taking in account that ligand concentration is solution stays constant, $[A]_t = constant$ and with reaction time ligand concentration changes$[L]_t = [L]_{max} - [AL]_t$, then

$$\frac{d[AL]}{dt} = k_a[A]([L]_{max} - [AL]_t) - k_d[AL] \tag{3.5}$$

Term $[L]_{max}$ corresponds to maximum concentration of the ligand. The observed SPR signal R is proportional to formed complex, and the maximum signal R_{max} will be proportional to the maximum ligand concentration of the surface. Therefore eqution (3.5) becomes:

$$\frac{dR}{dt} = k_a[A]([R]_{max} - R) - k_dR \tag{3.6}$$

It is convenient to analyze date in terms of integrated form of rate equation (3.6, since it directly derives k_a and k_d

$$R_t = \frac{[A]R_{max}k_a}{[A]k_a + k_d}\left(1 - \frac{1}{e^{([A]k_a + k_d)t}}\right) \tag{3.7}$$

This equation assumes that $R_{t=o}$= o, however if the baseline is not zero baseline correction can be achieved either by subtracting the response before the injection of the analyte, or by adding additional fitting parameter R_i that is equivalent value of the signal at the point of analyte injection. R_i also accounts also for any change in response due to the refractive index change upon

binding of analyte. Equation (3.7) gives advantage to derive k_a and k_d from single binding experiment.

When the analyte solution has traversed the flow cell and the buffer is injected instead, equations (3.6) and (3.7) will have following expressions:

$$\frac{dR}{dt} = -k_d R \tag{3.8}$$

$$R_t = R_a e^{-k_d t} \tag{3.9}$$

The integrated rate equation of the dissociation process shows that rate of complex dissociation follows simple exponential decay. Ra is the signal level at the end of association phase. If even after complete dissociation of the complex the response is not equal to zero, correction of the baseline might be achieved by adding again new fitting parameter R ($t \to \infty$), representing response after infinite time

3.3.2 Heterogeneous analyte model

This model describes more complex interaction, when the immobilized ligand is interacting with bivalent or several species of analytes and the binding events are independent.

In the case of bivalent analyte, assuming that binding sites are not equivalent and have distinct association and dissociation rate constants and that only one site of the analyte interacts with the ligand at a time, integrated rate equations of association dissociation phases can be expressed by the equations (3.8) and (3.9):

$$R_t = \frac{[A]R_{max1}k_{a1}}{[A]k_{a1} + k_{d1}}\left(1 - \frac{1}{e^{([A]k_{a1}+k_{d1})t}}\right) + \frac{[A]R_{max2}k_{a2}}{[A]k_{a2} + k_{d2}}\left(1 - \frac{1}{e^{([A]k_{a2}+k_{d2})t}}\right) \tag{3.10}$$

$$R_t = R_{a1}e^{-k_{d1}t} + R_{a2}e^{-k_{d2}t} \tag{3.11}$$

Where k_{a1} and k_{d1} are reaction constants describing interaction of site of the analyte and the ligand with the maximal response of R_{max1} and k_{a2} and k_{d2} are describing interaction of the second site with maximal response of R_{max2}. R_{a1} and R_{a2} represent corresponding amplitudes of dissociation. Concentration of the analyte $[A]$ is the same for both sites.

When the system of the analyte contains two different species of various concentrations $[A1]$ and $[A2]$, in this case integrated rate equation for association and dissociation phases will look like equations (3.12) and (3.11) respectively.

$$R_t = \frac{[A1]R_{max1}k_{a1}}{[A1]k_{a1} + k_{d1}}\left(1 - \frac{1}{e^{([A1]k_{a1}+k_{d1})t}}\right) + \frac{[A2]R_{max2}k_{a2}}{[A2]k_{a2} + k_{d2}}\left(1 - \frac{1}{e^{([A2]k_{a2}+k_{d2})t}}\right) \tag{3.12}$$

3.4 Results: Interaction of HD1, HD22 and NU172 aptamers with thrombin and prothrombin

Aptamers are selected for their high affinity towards desired targets. However, the affinity constant represents the ratio of association rate constant k_a and dissociation rate constant k_d, thus similar affinities can be a result of different kinetics. For sensor development along with the high affinity it is also extremely important to know kinetic parameters that reveal valuable information how rapidly a complex is formed and how rapidly it falls apart. Knowledge of underlying kinetic parameters is therefore relevant for better understanding of the molecular basis of complex formation and stability. Surface plasmon resonance enables to follow binding interactions in real time and determine kinetic parameters. We performed kinetic experiments of HD1, HD22 and NU 172 aptamer interaction both with thrombin and its precursor protein prothrombin.

3.4.1 Flow rate optimization for non-mass transport limited kinetics

In order to determine kinetic constants of reaction precisely, all the factors affecting their determination should be limited and therefore proper experimental design is critical. In all surface-based analysis methods one of the most important phenomenon influencing apparent constants of binding reaction of analyte to surface-bound ligand is the mass transport. Mass transport limitation emerges when the transport of an analyte molecule from bulk solution to the sensor surface, where it binds an immobilized ligand, is much slower than the association of ligand and analyte itself. This effect leads to partial or no kinetic information in the binding data. Under laminar flow conditions used in Biacore, the rate of transport of the analyte to the surface is proportional to the cube root of the flow rate, and is also influenced by the dimensions of the flow cell, the diffusion properties of the analyte and the ligand density on surface.

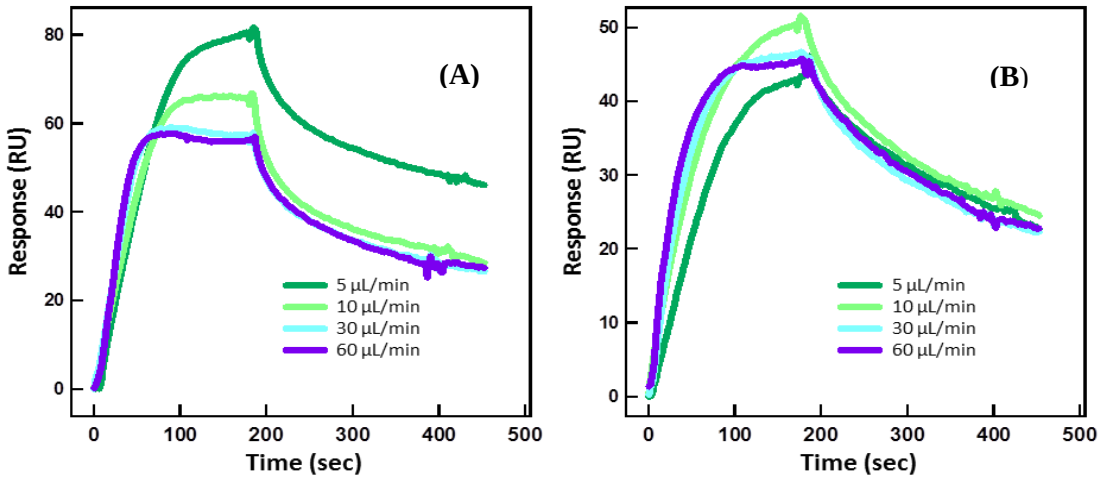

FIGURE 3.5 Determination an optimal flow rate for kinetic experiments. 12.5 nM thrombin was flown over HD1 (A) and HD22 (B) aptamers at 5 ,10, 30 and 60 µL/min injection rates

In order to diminish mass transport effect, only two experimental conditions can be adjusted. First, during the ligand immobilization the surface density has to be low and, second, during the kinetic experiment the flow rate of analyte solution has to be high enough. In all our kinetic experiments the level of the ligand immobilization was equal to about 40 RU, which

taking in account molecular weights of ligand and analyte, represents sufficiently low density required for precise measurements (eq. 3.1 and 3.2). For the purpose of selection of an appropriate flow rate, it was necessary to perform injection of fixed concentration of thrombin with different flow rate. For this reason 12,5 nM thrombin was injected over the surface functionalized with HD1 and HD22 for 3 minutes with 5, 10, 30 and 60µL/min flow rates (Fig. 3.5FIGURE 3.5).

The response of thrombin interaction with aptamers differed significantly at low flow rates of 5 µL/min and 10 µL/min, meaning, that at this rates association kinetics was influenced by mass transport. With increase of the injection rate, interaction response stabilized and didn't show significant change between 30 and 60 µL/min. We assumed that already at 30 µL/min flow rate thrombin-aptamer interaction is not mass transport limited and thereafter all experiments where performed at this rate.

3.4.2 Kinetics of thrombin interaction with HD1, HD22 and NU172

To observe binding kinetics of α-thrombin and immobilized HD1, HD22, NU172 aptamers and determine governing reaction constants, various concentrations of thrombin ranging from 0.78 nM to 50 nM were injected for 180 seconds with the flow rate of 30 um/min. Following suggestions of SPR instrument manufacturer, thrombin concentrations were obtained by 2 fold serial dilutions of the highest concentration of 50 nM, so that a concentration range of about 0.1-10 times expected KD was covered.

Significant response signal was observed even at thrombin concentration as low as 0.78 nM (Fig. 3.6). The highest response was observed for thrombin interaction with HD1 aptamer, then for HD22 and the smallest for the NU172[1].

In order to calculate reaction constants, sensograms of thrombin binding to aptamers were initially described with the simplest 1:1 interaction model (eq. 3.7), assuming that HD1 and NU172 interact with exosite 1 and HD22 binds to exosite2 of Thrombin.

For HD22 1:1 interaction model described the association and dissociation reactions pretty well (Fig. 3.7 (C)) and corresponding reactions constants k_a and k_d and consequently K_d were deduced easily (Table 3.3).

However in the case of HD1 and NU172 aptamers (Fig. 3.7 (A) and (B) respective), known to recognize fibrinogen binding exosite I of thrombin, fitting one-to-one binding model failed to describe entire kinetics (mostly dissociation part), indicating that thrombin interaction with these aptamers has more complicated character than it is assumed widely.

[1]We should note that the kinetics for NU172 was performed as the separate experiment with different type of SA sensor chip having HD22 immobilized as the control. The response of the control kinetic experiment of thrombin interaction with HD22 (not shown here) was similar to the experiment shown here but with smaller Rmax up to 5-6 RU. Namely, the maximal response for the 25 nM Thrombin in one case was 40 RU and in another was 34 RU. This small difference could be explained with inter experimental and inter surface variation. Nevertheless maximal response for NU172 was smaller than corresponding response for HD22.

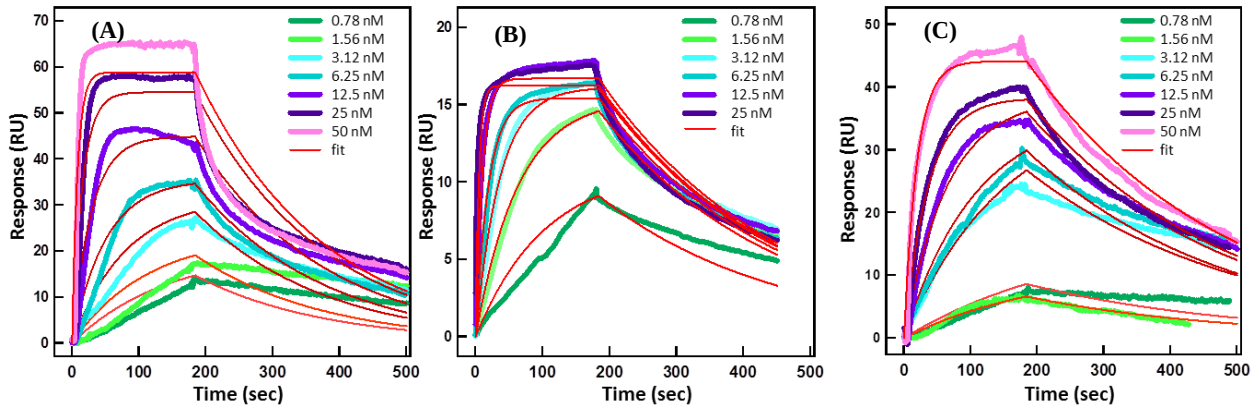

FIGURE 3.6 Determination of dissociation constants by surface plasmon resonance. Interaction kinetics of the DNA aptamer HD1 (A), NU172 (B) and HD22 (C) with increasing concentrations from 0.78 to 50 nM of α-Thrombin. Red lines represent the fitting of 1:1 binding model.

Complexity of this interaction might be hidden in the ability of these aptamers to recognize not only exosite I but also heparin binding exosite II. This hypothesis in the case of HD1 has solid arguments. Some of the very first NMR and X-ray studies suggested that one molecule of HD1 aptamer could simultaneously bind two different molecules of thrombin with distinct manner (Padmanabhan and Tulinsky, 1996). Indeed this was confirmed with the most recent NMR study showed that HD1 binds thrombin exosite I with pincer-like conformation of TT-loops[1], in addition, TGT loop being exposed towards solvent can interact with heparin-binding site of another Thrombin (Russo Krauss et al., 2011, 2012). This means that apart from binding exosite I, HD1 might have some affinity towards thrombin exosite II, which could be reflected in the sensogram.

As for the aptamer NU172, nothing is known about its structure and mechanism of binding to thrombin apart, that it interacts with exosite I, since with this binding, it inhibits generation of fibrin and modulates coagulation(Mayer et al., 2011). However, for both aptamers HD1 and NU172 there is the further evidence of interaction with more than one sites of thrombin. Namely, thrombin-induced aggregation gold nanoparticles (results chapter 6) functionalized either with HD1 or NU172, suggests that one thrombin molecule is capable of interacting simultaneously with two aptamers of the same type. Notably, no aggregation is observed for HD22-functionlized gold nanoparticles. Thus, this gives us right to consider thrombin as a bivalent analyte for HD1 or NU172.

Assuming bivalent character of the thrombin towards HD1 and NU172 and supposing that one thrombin molecule can interact only with one site of aptamer at a time i.e. binding events are independent (one thrombin cannot be captured by two aptamers simultaneously), heterogeneous analyte binding model (Eq. 3.9 and 3.10) was fitted to kinetic data (Fig. 3.7). This model seems to describe interaction much better than the initial 1:1 model. We obtained reaction and affinity constants for two sites (Table 3.5).

[1] (Russo Krauss et al. 2012) also showed that due to the symmetry with the helix axis there are two binding modes of TT-loops differing only by a 180 rotation about the helix axis when compared with thrombin exosite I. These modes are practically equivalent, the only difference is the orientation of the TGT loop. We don't consider existence of these two modes in SPR data analysis.

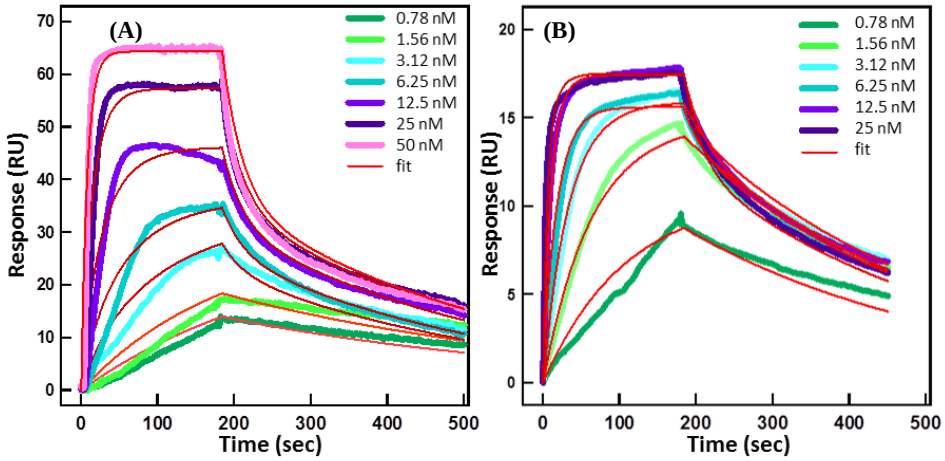

FIGURE 3.7 Determination of dissociation constants by surface plasmon resonance. Interaction kinetics of the DNA aptamer HD1 (A) and NU172 (B) with increasing concentrations from 0.78 to 50 nM of α-Thrombin. Date was fitted with heterogeneous analyte model

Table 3.3 Reaction and affinity constants of thrombin interaction with HD1, NU172 and HD22 aptamers.

aptamer	Fitting model	Binding site	k_a 10^6 $M^{-1}s^{-1}$	k_d 10^{-3} s^{-1}	K_d 10^{-9} M	Residence time s
HD1	**1:1**	**Exosite1**	2.36±0.12	5.03±0.28	2.14±0.23	137.8
	Heterogeneous analyte	**Exosite1**	2.12±0.10	2.52 ±.0.28	1.19±0.15	277.2
		Exosite2	1.91±0.31	32.60±4.90	17.4±3.60	21.3
NU172	**1:1**	**Exosite1**	7.75±0.08	3.86±0.16	0.50±0.02	179
	Heterogeneous analyte	**Exosite1**	8.12±0.10	3.06±0.11	0.38±0.02	225.3
		Exosite2	1.10±0.06	51.7±5.10	46.9±6.50	13.4
HD22	**1:1**	**Exosite2**	1.02±0.10	3.20±0.13	3.16±0.34	216.6

Data analysis revealed that aptamer NU172 has several fold higher affinity towards exosite I (0.4 nM) than HD1 (1.2 nM), due to the higher association constant (7.8 x 10^6 $M^{-1}s^{-1}$ and 2.1 x 10^6 $M^{-1}s^{-1}$ respectively for NU172 and HD1) even though the half-life of thrombin-aptamer complex is slightly larger for HD1 (277 sec) than for NU172 (225 sec).

As for the affinity for the exosite II [1], as expected, HD22 has the best and the highest affinity (3.2 nM), followed by the HD1 (17.4 nM) and NU172 (47 nM). Interestingly, association constants for all of these three aptamers are very close (1.9 x 10^6 $M^{-1}s^{-1}$, 1.1 x 10^6 $M^{-1}s^{-1}$ and 1.1 x 10^6 $M^{-1}s^{-1}$ respectively for HD1, NU172 and HD22), but the main difference is in the stability of the complexes, HD1 and NU172 dissociate very rapidly compared to HD22. This proves our hypothesis that HD1 and NU172 interact with exosite II, but this binding is weaker than interactions of HD22 with exosite II and HD1 and NU172 with exosite I. Nevertheless, we shouldn't forget that, by definition, aptamers may have affinities as low as low-micromolar, thus giving to HD1 and NU172 full authority to be called - "aptamers for both binding sites of thrombin".

[1]Based on the experimental results of gold nanoparticle aggregation, presented in chapter 6, we can confidently tell that HD1 and NU172 bind to two (not more) distinct sites of thrombin: one is exosite I and the second site is exosite II.

3.4.3 Kinetics of prothrombin interaction with HD1 and HD22

Prothrombin is the precursor zymogen of thrombin. Activation of prothrombin into thrombin occurs in two-step, through cleavage at Arg271 and Arg320 (Wood et al., 2011). After cleavages Gla and Kringle domains of Prothrombin are removed and remaining A and B chains form the activated thrombin (Fig. 3.1) that represents only the half of the prothrombin molecule (36 kDa and 72 kDa respectively). On the prothrombin molecule active cleft and anion-binding sites are either premature or hidden. The anion-binding exosite I is located on the surface of prothrombin and accessible for interaction, but it is characterized with low affinity to the ligands and is therefore called proexositeI. Only after proteolytic cleavage and thrombin formation affinity for its ligands increases, meaning that during activation exosite I undergoes allosteric changes (Bukys et al., 2006). On the other hand anion-binding exosite II is well hidden inside prothrombin and becomes well-exposed only after cleavage of Arg271 on the surface of thrombin or prethrombin2 (Kretz et al., 2006). Studies showed clear evidence that HD1 is interacting with exosite1 (Kretz et al., 2006) with comparable to thrombin affinity (Müller et al., 2008) but yet, whether kinetic parameter of binding reaction are the same and whether there is the mean to distinguish thrombin from prothrombin upon binding that remains unanswered.

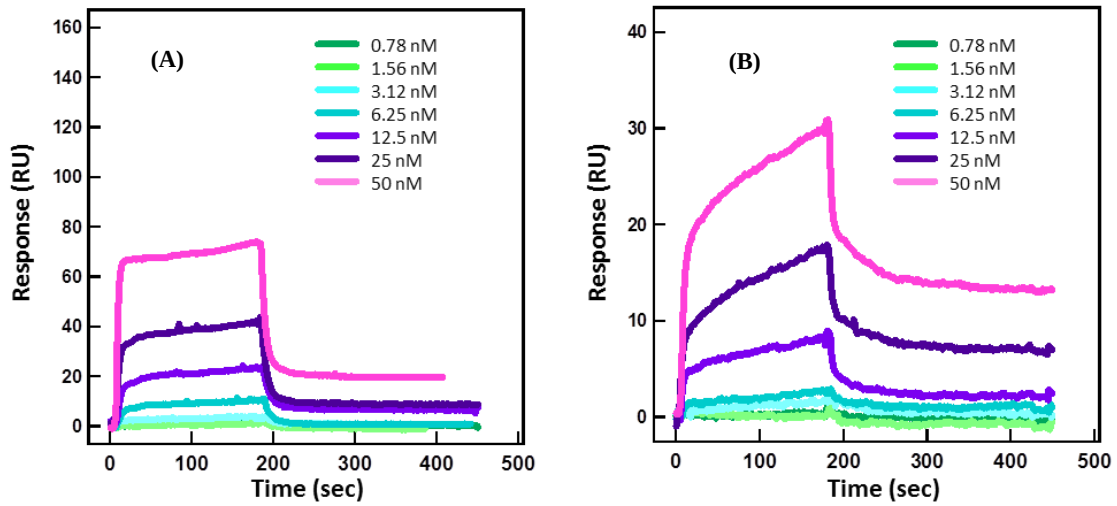

FIGURE 3.8 Sensograms of HD1 (A) and HD22 (B) aptamer interaction with increasing concentrations of prothrombin, ranging from 0.78 to 50 nM.

First, we tried to answer this question by performing the similar kinetic analysis for prothrombin to what was done in the case of thrombin, by injecting prothrombin concentrations from 0.78 nM to 50 nM over HD1 and HD22 aptamer-covered surface. The results turned out to be surprising (Fig. 3.8). We let prothrombin to interact with both HD1 and HD22 aptamers, expecting binding only with HD1, however signal of interaction with HD22 was unexpectedly very high (Fig, 3.8 (B)). Yet it couldn't be attributed to nonspecific interactions. In addition, observed signal for both aptamers was different from the response seen for just thrombin, characterized with fast association and dissociation. The only explanation for this effect was the presence of thrombin and/or other intermediate species between thrombin and prothrombin bearing exosite II exposed for specific interactions (Fig. 3.9).

3.4.4 Investigation of integrity and purity of prothrombin

To verify purity of the sample, we carried out **SDS PAGE separation** of prothrombin sample. Moreover to see whether there was thrombin in stock solution, **chromogenic substrate activation assay** was performed with several known concentrations of thrombin and 200 nM prothrombin.

Indeed, SDS PAGE separation results (Fig.3.9) confirmed that in prothrombin sample apart from prothrombin were also present other intermediate species, such as meizothrombin, prethorombin1 and/or[1] meizothrombin desF1 (52 kDa), α-thrombin and/or prethrombin 2 (36 kDa) and prothrombin fragment F1.2 (31 kDa). The main components of the sample were prothrombin 60% followed with about 30% of prethrombin and/or meizothrombin.

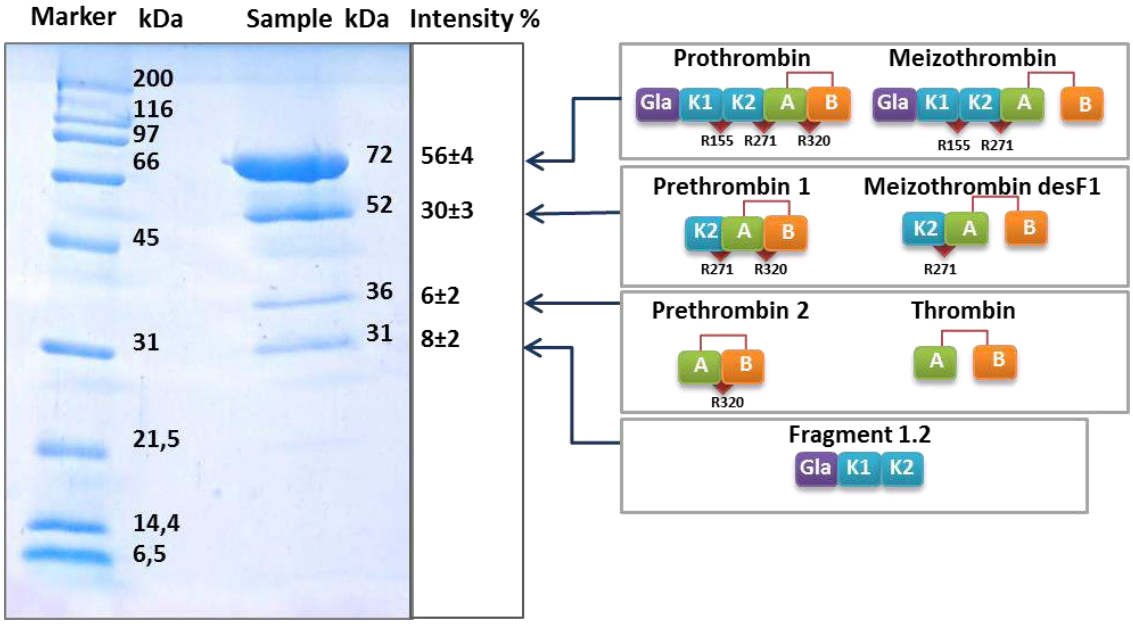

FIGURE 3.9 SDS PAGE separation of prothrombin sample showing that sample along with the prothrombin contains species of three different molecular weights that might correspond to prothrombin cleavage products such as meizothrombin, prethorombin1 and/or meizothrombin desF1, α-thrombin and/or prethrombin 2 and prothrombin fragment F1.2.

Chromogenic substrate cleavage assay, on the other hand, showed that in prothrombin stock solution there was only minute concentration (much less than 1 nM) of thrombin that induced insignificant cleavage of chromogenic substrate compared to 1 nM thrombin (Fig. 3.10). Since the prothrombin was of good quality in stock solution, it means that **degradation occurred during the sample preparation or in the course of the experiment.** From the literature it known that if there is some minute concentration of thrombin, it can initiate cleavage of prothrombin and thus autocatalyze its own production. Meizothormbin or meizothrombin desF1 and thrombin are capable of cutting Arg155 and thus transforming prothrombin into prethrombin1, meizothormbin into meizothrombin desF1, α-thrombin is further able to cut Arg288 to produce β- and γ- thrombins (Fischer et al., 1996).

[1] The difference between prethrombin and meizothrombin, prethrombin1 and meizothrombin desF1 as well as prethrombin2 and thrombin couples is only in absence of the cleavage at Arg320 in first of them. Since by SDS PAGE we now can distinguish molecules only by molecular weight, but we are not able to say which conformations are present is the investigated sample.

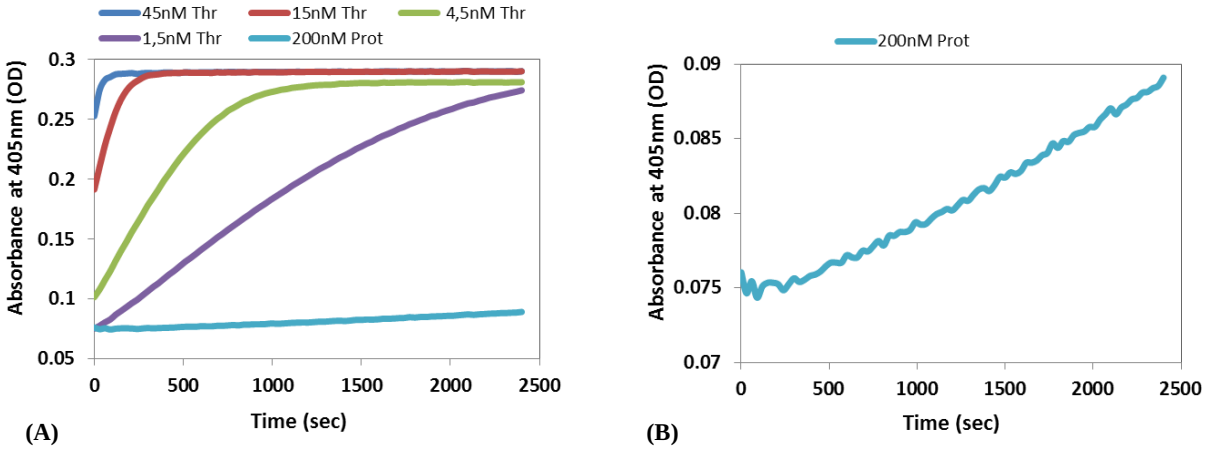

FIGURE 3.10 Kinetics of cleavage of chromogenic substrate S2238 by 1.5, 4.5, 15 and 45 nM thrombin (A)and 200 nM prothrombin (A-B)

3.4.5 Kinetics of prothrombin interaction with aptamers in the presence of Argatrobane

Knowing about the instability of prothrombin in the presence of thrombin, we decided to add high concentration (50 μM) argatroban, the small molecule reversibly inhibiting thrombin active site, directly to the running buffer. The presence of high concentration argatroban guaranteed that thrombin would have been almost always inhibited from interaction with non-activated prothrombin.

New set of experiments were performed with the same concentrations of prothrombin but in the excess of the argatroban for HD1, HD22 and NU172. In such conditions binding of prothrombin was exclusively observed with HD1, NU172. From Fig. 3.11 It is clear that signal for HD1 and NU172 is neither artefact nor effect of local refractive index change, since if it was the case, we would have had the same bulk effect for HD22 as well. But as we see the injection of similar sample did not induce any change in refractive index in the case of HD22. Thus our supposition on effect of autoactivation was confirmed.

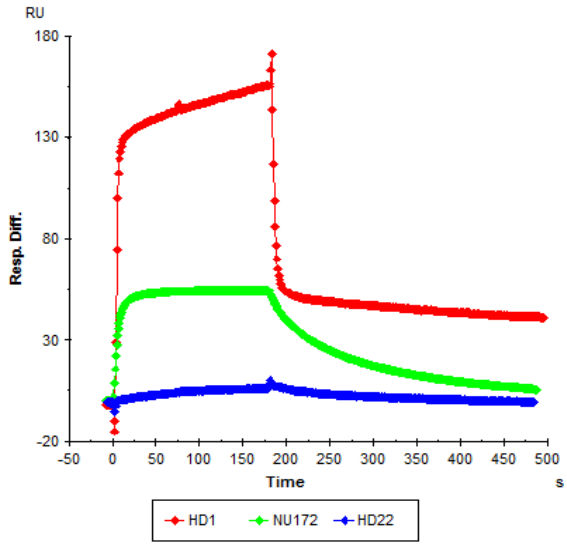

FIGURE 3.11 Overlaid sensograms of aptamer HD1, NU172 and HD22 interaction with 50 nM Prothrombin incubated with 1μM argatroban

Kinetics of interaction of prothrombin with HD1 was different than that with thrombin. The response intensity was much higher (more than twice) for prothrombin than for the same concentration thrombin. Before going into quantitative analysis, the observation of sensogram (Fig.3.11) of HD1 interaction with prothrombin shows very fast association dynamics that never reaches equilibrium. The dissociation phase has also very stiff descend but is not reaching zero. This suggests that observed signal represents the sum of two or several interactions, one part of which is characterized with very high on- and off- rate (reaching the limit of the instrument sensitivity) and another with comparably lower on- and off- rate.

Meaning that, despite of inactivation of thrombin active site, prothrombin sample still contained some other species. Since binding of thrombin to aptamer HD1, as shown above, is not characterized, with such an aggressive signature, these extremely fast on and off rates can be attributed to prothrombin (and other intermediate species). Overall, by the shape of the sensogram, it can be attributed to the class of difficult-to-interpret interactions (Rich and Myszka, 2008).

For NU172 as well, the signal of interaction with prothrombin was different from the response of binding to thrombin. The intensity of the response was several times higher than in the case of thrombin. However association and dissociation phases were slower and less combative than for HD1. During the association phase stable equilibrium was reached and by dissociation phase signal tended to return to initial baseline.

Fitting the kinetic data, at first, was performed manually with **1:1 interaction model**, assuming that sample contained only prothrombin. In the case of HD1 we neglected the absence of equilibrium signal and added bulk effect for dissociation phase in order to compensate the signal of slow dissociation which followed the drastic complex decay (Fig. 3.12 (A)). For NU172 only the effect of bulk was added.

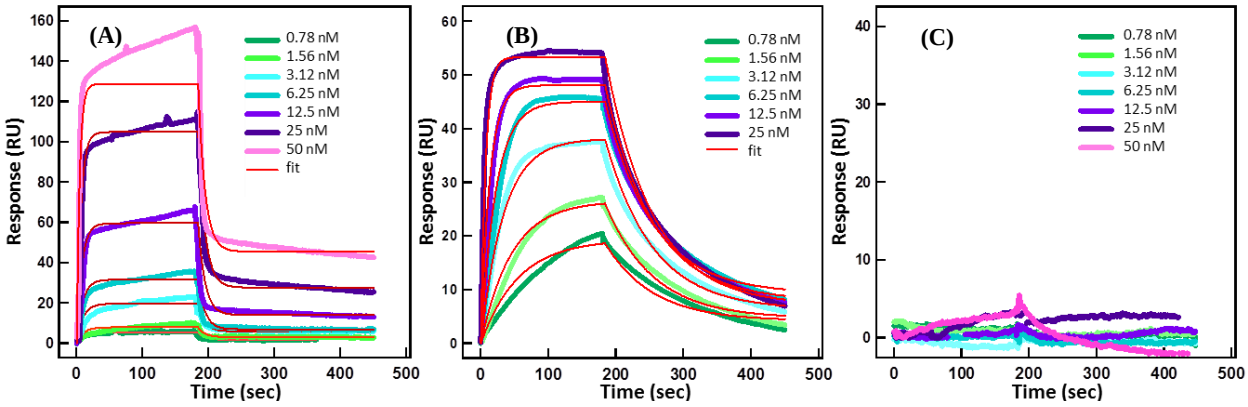

FIGURE 3.12 Sensograms of HD1(A), NU172 (B) and HD22 (C) aptamer interaction with increasing concentrations of prothrombin incubated with 1 μM argatroban. Red line represents fitting of the 1:1 binding model

As we see from the Fig.3.12 (A) obtained fitting curve for HD1 doesn't comprise slow association segment, which in the 1:1 binding case should have been flat, describing signal saturation at equilibrium. For NU172 fit is much better (Fig. 3.12 (B)). Calculated reaction constants are given in the table 3.4.

Despite of very quick association (k_a=2.6x10^6 $M^{-1}s^{-1}$), dissociation rate is also very elevated for HD1 leading to very short half-life of HD1-prothrombin complex (10 s) and dissociation constant of 37 nM. In the case of NU172 association is also pretty fast (k_a=4.6x10^6 $M^{-1}s^{-1}$) but dissociation is slower than for HD1, so it comes out to have better complex stability (47 sec) and one order of magnitude improved affinity (3.3 nM) towards prothrombin. Again it has to be brought to attention that experiments for HD1 and NU172 were performed separately on different surfaces and the quality/density of the immobilized aptamers is thus different, giving distinct Rmax values, which influences the shape of the sensogram.

Table 3.4 Reaction and affinity constants of prothrombin interaction with HD1, NU172 and HD22 aptamers.

Aptamer	Fitting model	Binding molecule	k_a 10^6 $M^{-1}s^{-1}$	k_d 10^{-3} s^{-1}	K_d 10^{-9} M	Residence time s
HD1	**1:1**	**Prothrombin**	2.61±0.12	96.8±8.61	37.2±3.26	9.6
	Two analytes	**Prothrombin**	2.44±0.06	115±10.02	47.2±3.51	6
		Prethrombin1	0.11±0.03	0.51±0.05	4.85±0.41	1351
NU172	**1:1**	**Prothrombin**	4.56±0.47	14.9±0.27	3.26±0.33	46.4
HD22	**1:1**	**prothrombin**	-	-	-	-

Obviously, the complex character of prothrombin interaction with HD1 cannot be described adequately by the 1:1 binding model; however it gives an idea about the range of the governing reaction constants. Furthermore use of more sophisticated models doesn't guarantee finding the exact one, correctly representing the case.

Indeed, we performed additional **data fitting with BIAevaluation** software for sensograms only representing interaction of 6.25 nM and 50 nM prothrombin with HD1. We used several built-in models like "interaction with drifting baseline", "mass transport" (fitting not shown here) with adjustment of different parameters, but none of them gave neither good fit nor sane parameters. At last, the satisfying fit was achieved once we used **heterogeneous analyte model**, where we assumed that prothrombin sample had similar composition as shown on the SDS-page results. Namely, it was composed of 40% protein with molecular weight 52 kDa (prethrombin/meizothormbin desF1) and 60% protein with M.W. 72 kDa (prothrombin). Obtained fitting curves described both the fast and slow association and dissociation. By the results of the model, the larger molecule, prothrombin, has to be the one which associates with high on-rate (k_a=2.44 x 10^6 $M^{-1}s^{-1}$) and dissociates super rapidly, staying in complex with HD1 only for 6 seconds. On the other hand, molecule with 52 kDa molecular weight (either prethrombin1 or meizothrombin desF1), is the one, involved in slower interactions with relatively low on-rate k_a=1.1 x 10^5 $M^{-1}s^{-1}$ but with extremely long residence time (1350 sec) resulting in 4.6 nM affinity. If we compare results obtained using one-to-one and heterogeneous analyte model for prothrombin we get very similar association rate constants and range of affinity. Interestingly, fitting similar model and conditions didn't give realistic results for NU172.

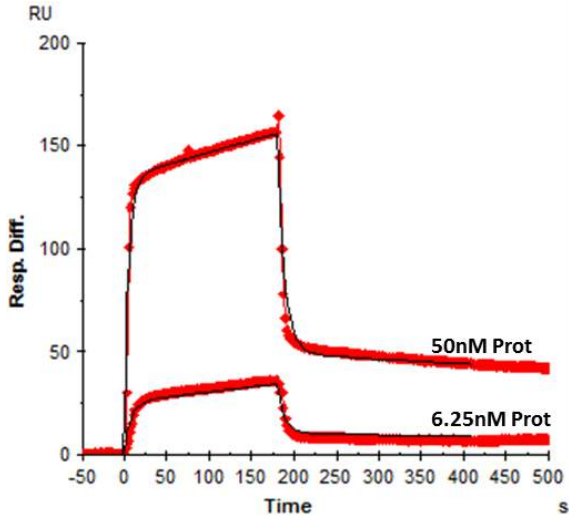

FIGURE 3.13.Sensograms of interaction of 6.25 nM and 50 nM prothrombin interaction with HD1. Black line represents the fitting of the heterogeneous analyte model assuming that sample is composed of 60% 72 kDa protein and 40% 52 kDa protein. Fitting was made by BIAevaluation software

3.4.6 Following prothrombin activation with aptamers

As we saw above the character of interaction of aptamers is different for thrombin and prothrombin. However in real plasma samples concentration of prothrombin is usually up to 0.1 mg/mL (1.4 µM) (Butenas et al., 1999) that is much higher (with order of 10^3) than the concentration of possible circulating free thrombin ((Mann et al., 2003)). It is interesting and, even more, necessary to know whether we can be able to **distinguish the contribution of thrombin from prothrombin** when they are present simultaneously in the sample for **example during thrombin generation** process.

In the blood, thrombin is generated from the zymogen prothrombin by the prothrombinase complex, composed of the trypsin-like protease factor Xa, the cofactor factor Va, phospholipid membranes and Ca2+(Davie et al., 1991). FXa on its own is also able to cleave prothrombin but with 100 fold lower rate than prothrombinase. In the lab, we can follow the thrombin generation, catalyzed by prothrombinase complex or only by FXa, through monitoring hydrolysis of chromogenic or fluorogenic substrate. Upon activation of thrombin more and more substrate gets cleaved inducing characteristic absorption or/and fluorescence. We are interested to know whether we can follow similar process with surface based affinity sensor, in general, and by SPR, in this particular case.

3.4.6.1 Optimal FXa concentration

Before observing thrombin generation SPR we need to understand the process of thrombin generation and adjust parameters for consequent experimental design. For this reason we performed several thrombin generation assays by FXa and monitored it with cleavage of chromogenic substrate S2238.

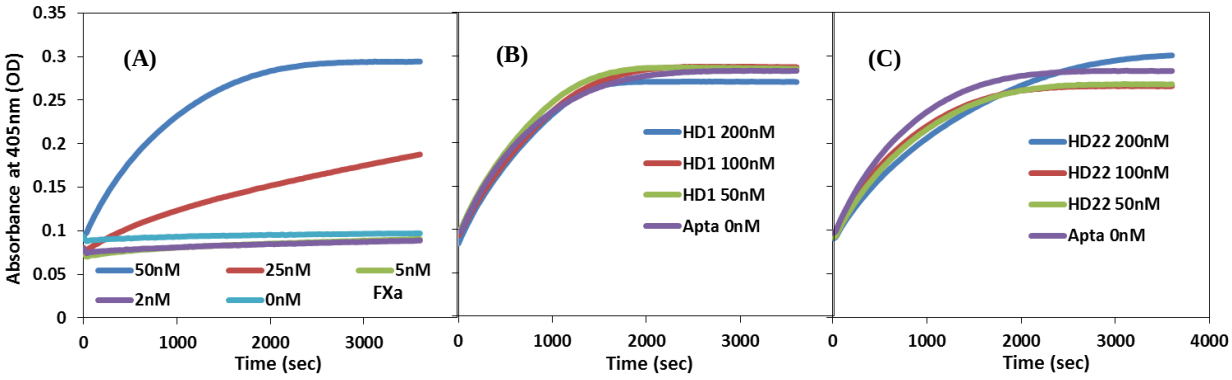

FIGURE 3.14 kinetics of chromogenic substrate cleavage by thrombin activated form100 nM prothrombin in the presence 2, 5, 25 and 50 nM FXa.(A), or 50 nM FXa and 50, 100, 200 nM HD1 (B) or HD22(C)

The first experiment was performed to see how much time it takes to activate 100nM Prothrombin by different concentrations of FXa (2, 5, 10, 50 nM). We wanted select an optimal concentration of FXa to carry out further experiments, so that they would be slow enough to observe all the stages of thrombin activation but on the same time wouldn't take more than 1 hour, to avoid degradation of the sample (Fig. 3.14 (A)). We observed that 50 nM FXa takes up to 30 minutes to fully activate all the thrombin, which was optimal for our further experiments, whereas lower concentrations took much longer time.

3.4.6.2 Effect of aptamer presence on prothrombin activation with FXa

Very important is as well to evaluate whether the presence of aptamers can alter the cleavage of the prothrombin by FXa. For this reason during the thrombin generation experiment various concentrations (50, 100 and 200 nM) of aptamer HD1 and HD22 were carried out. As we see form the Fig. 3.14 (B) and (C), the curves of the chromogenic substrate cleavage in the presence of aptamers were almost identical to the one without aptamers. Meaning that, the presence of HD1 and HD22 in these concentrations doesn't influence neither the interaction of prothrombin with FXa nor the interaction between thrombin and S2238.

3.4.6.3 Designing thrombin generation experiment for SPR

Once we found the optimal concentration of FXa and clarified that aptamers do not affect thrombin generation, we can start designing SPR experiment for real-time monitoring thrombin generation process. Of course when we say "to follow the prothrombin conversion process with SPR", we think of injecting aliquots of the same sample at different time points to see the change between characteristic sensograms rather than observing single long sensogram. To obtain instant picture of the process we need to hold the activation process, i.e. stop the activity of FXa at desired time points. This can be achieved by adding to the system high concentration (1 μM) of FXa inhibitor rivaroxaban at appropriate moment (Fig. 3.15).

To visualize our idea, i.e. show the effect of FXa inhibition at different time points, we again performed classical thrombin generation assay. We pipetted same sample containing prothrombin and S2238 in 8 different wells. FXa was injected into all wells, except the first well, where along with FXa we put also rivaroxaban at the same time, and started absorbance acquisition. After five minutes rivaroxaben was injected in the second well continuing recording of absorbance, after next 5 minutes rivaroxaben was injected in the third well and so on, we injected FXa inhibitor in following wells one buy one after each 5 minutes delay. The last well we kept uninhibited by rivaroxaben.

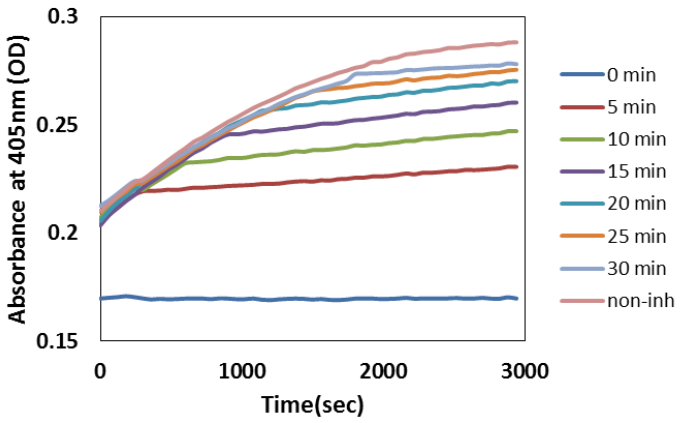

FIGURE 3.15 Kinetics of chromogenic substrate cleavage by thrombin activated from 100 nM Prothrombin with 50 nM FXa. Activity of FXa was inhibited by rivaroxaben each 5 minutes.

Fig.3.14. illustrates the outcome of this experiment. As we see (as it was expected) the rate of thrombin generation is the highest at the begging of experiment, where the concentration of prothrombin is the highest as well, and drops with the increase of the thrombin concentration (Fig. 3.16 (A)). Meaning that concentration of thrombin is not directly proportional to the time passed and when we perform SPR experiment we don't know the exact composition of sample (thrombin/prothrombin ratio) unless we carry out additional calculations to determine actual concentration of thrombin.

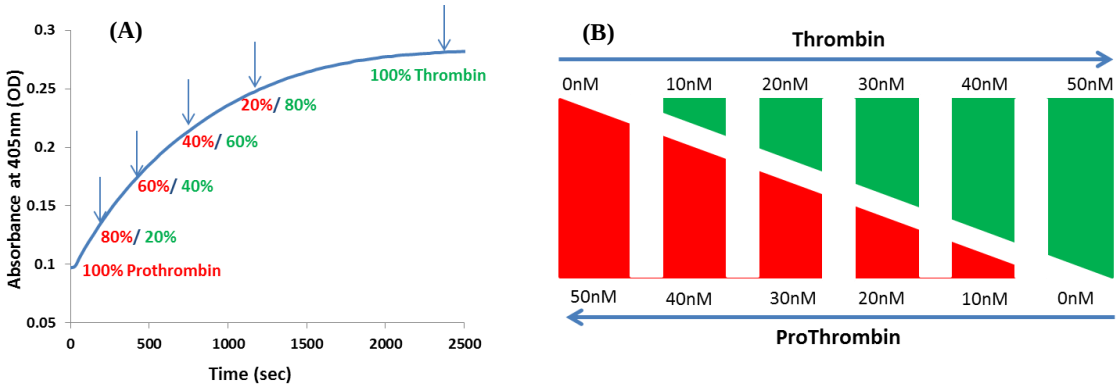

FIGURE 3.16 Schematic illustration of sample composition during thrombin generation assay (A) and in the samples used to perform SPR experiment with thrombin and prothrombin mixture (B)

Thus, instead of stopping prothrombin activation after each 5 minutes or at the times where the calculated ratio of thrombin and prothrombin is desired and , it is much easier and convenient to **make a sample with predefined composition of thrombin and prothrombin** (Fig.3.16 (B)). This approach allows performing SPR experiment avoiding the presence of FXa and rivaroxaben, compounds that could complicate the system.

3.4.6.4 SPR experiment of thrombin-binding-aptamer interaction with the mixture of prothrombin and thrombin

To mimic real activation process, samples of different prothrombin/ thrombin composition were made, so that the total concentration of protein was fixed to be. We started with 100% prothrombin and gradually decreased content by 20 percent increasing at the same the concentration of thrombin (Fig. 3.16 (B)). These samples were used to carry out kinetic experiments on SPR for HD1, HD22 and NU172 (Fig. 3.17).

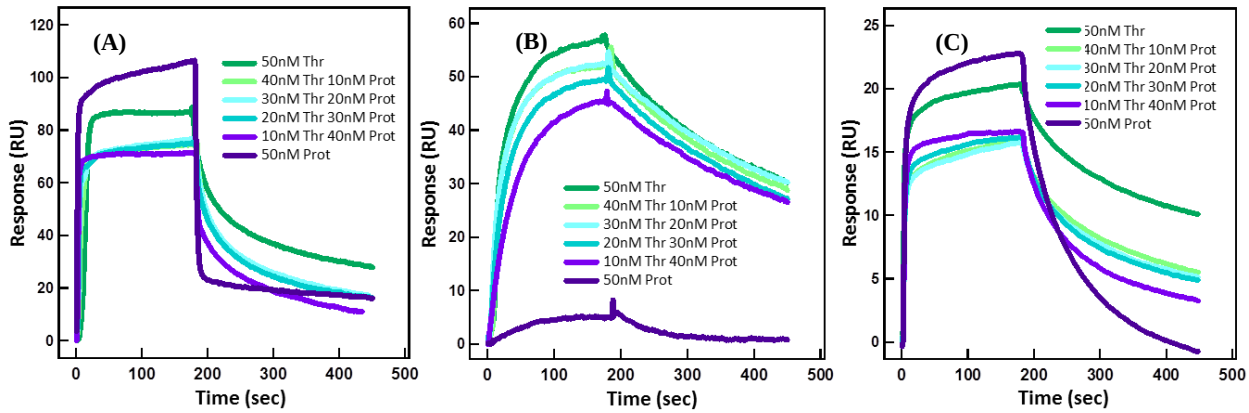

FIGURE 3.17 Sensograms of HD1 (A), HD22 (B) and NU172 (C) aptamer interaction with samples of various thrombin and prothrombin composition

For HD1 and NU 172 the highest signal was observed for the sample with 100% prothrombin and then with 100% thrombin. The difference between these two samples was evident: remarkably quick association and dissociation was observed for prothrombin sample compared to only thrombin (Fig. 3.17 (A) and (C)).

In the case of HD22, the signal from 100% prothrombin was the least observed. The intensity of the signal increased with the augmentation of thrombin percentage in the sample. For

HD1 and NU172 all the rest of samples gave almost the same signature, making it impossible to guess the composition of the sample only by looking at sensograms.

Since an observed SPR signal represents integrated response of analyte binding, by differentiating the signal by time we can obtain the rate or binding at every time point. This action is called derivative method. Derivative methods have been widely used in analytical spectroscopy as qualitative fingerprinting technique to accentuate small structural differences between nearly identical spectra and to enhance the resolution of overlapping spectral bands. We applied this approach to try to interpret overlapping sensograms of HD1. Since in affinity biosensors the most important part of interaction is signature of association, we took closer look to the beginning (first 30 seconds) of sensogram derivatives.

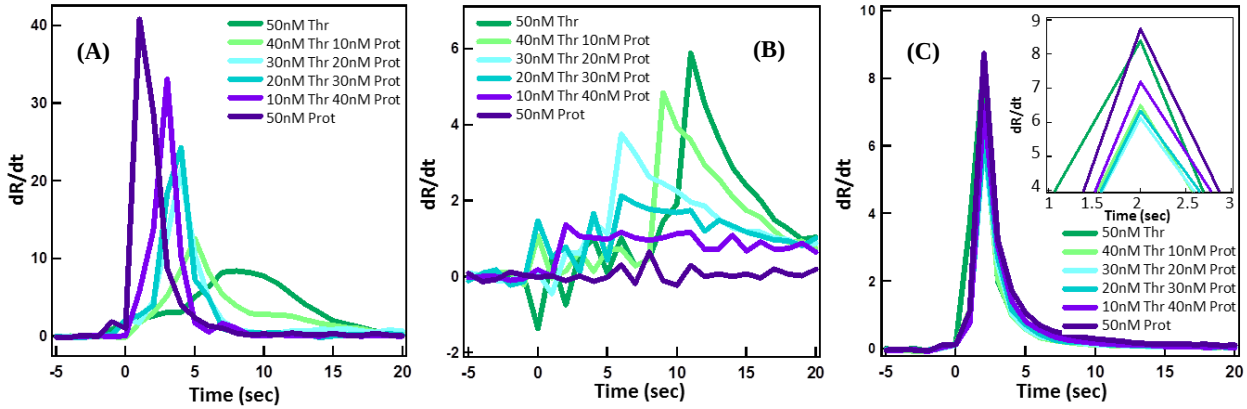

FIGURE 3.18 The first derivatives of SPR response during association phase for various composition thrombin/prothrombin mixtures to HD1 (A), HD22 (B) and NU172 (C) aptamers.

Figure 3.18 illustrates results of differentiation of the SPR response by time. In the case of HD1 there is clear difference between thrombin and prothrombin derivatives. Prothrombin associates to HD1 quicker than thrombin and that's why we can see the higher peak of the derivative emerging the soonest for the prothrombin (Fig. 3.18 (A)). With decrease of the percentage of prothrombin composition in the sample peak becomes lower, wider and smaller.

For HD22 due to the absence of the interaction with prothrombin, the highest peak is observed for the 50 nM thrombin (Fig. 3.18 (B)). Intensity of characteristic peak decreases with diminution of thrombin content in the sample.

Interaction of aptamer NU172 has very similar association patterns with both thrombin and prothrombin and therefore it is difficult to see clear difference in the derivatives during the association phase (Fig. 3.18 (C)).

This simplified experiment showed that if we have tried to follow thrombin generation from prothrombin point by point, yes, we would indeed be able to see a transformation of the SPR signal following the thrombin activation but only in the case of HD1 and HD22. For HD1 the maximum (equilibrium state) response would decrease with augmentation of the activated thrombin, and in the case of HD22 the maximum of the signal would increase with the thrombin generation. Of course, HD22 is the best option for this purpose.

3.4.7 Conclusions for thrombin and prothrombin interaction with aptamers

With SPR method we studied interaction of HD1, HD22 and NU172 aptamers with both thrombin and prothrombin to understand interaction kinetics between target and the proteins and performed interesting experiment with thrombin and prothrombin mixture to simulate prothrombin conversion into thrombin. We showed that all three aptamers have very high affinity in low nanomolar range for thrombin and suggested that HD1 and NU172 apart from binding to exosite I may also bind to exosite II with slightly less but nanomolar affinity. Only HD22 is selective between thrombin and prothrombin, whereas HD1 and NU172 interact with prothrombin with affinity one order of magnitude lower than for thrombin. Interaction of HD1 has very specific signature that makes possible to distinguish interaction of thrombin binding form prothrombin.

From point of view of therapeutic application, where the main interest is the effect of inhibition of binding different molecules to thrombin binding sites, of course, obtained results once again show that high affinity of aptamers towards thrombin makes them very good candidate as modulators of coagulation. Whereas from the point of view of application of aptamers as sensing elements in biosensor development, where the specificity (selectivity) is as important as sensitivity (affinity), HD1 and NU172 arise more questions concerning specificity. Namely, if they interact with two distinct epitopes of thrombin with such high affinities, will they be able to discriminate thrombin between other serine proteases (coagulation factors) in coagulation cascade, since they bare structural similarities? In general, will these aptamers be specific at all in plasma? Some of these questions will be discussed below.

3.5 Results of aptamer interaction with Thrombin-inhibitor complexes

Thrombin as the key protease in coagulation is regulating various reactions, but on its own it is also tightly regulated. The regulation of thrombin is mainly achieved with stoichiometric and irreversible inhibition of the thrombin active site by natural plasma inhibitors Antithrombin III, Heparin cofactor II and Alpha-2-macroglobulin. Inhibited thrombin complexes are then cleared from the blood circulation system in liver. Whether aptamers can interact with inhibitor-thrombin complex or affect complex formation was examined with SPR method.

3.5.1 Antihrombin III

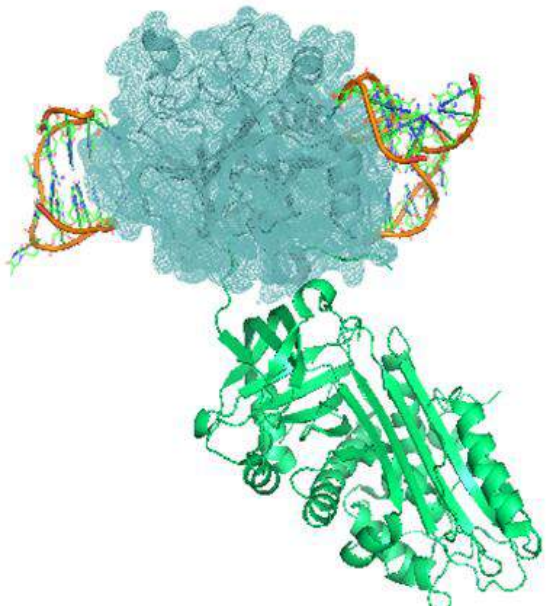

FIGURE 3.19 Molecular model of Interaction of HD1 and HD22 aptamers with thrombin-ATIII complex. The model is constructed with the program PyMol by superposing structures of Thrombin-ATIII (1TB6) complex and HD1 (4DII) and HD22 (4I7Y) aptamers

ATIII is the major natural inhibitor of thrombin present in blood plasma at the concentration of 2.5 μM. (Conard et al., 1983). It is shown to accounts for 60% of plasma anticoagulant activity (Walker and Royston, 2002). ATIII forms 1-to-1 complex with thrombin inhibiting active site with k_{on}=1.23x10^4 M^{-1}s^{-1}. Inhibition of thrombin increases 10000 fold in the presence of glycosaminoglycans, for example in the presence of heparin k_{on}=1.19x10^8 M^{-1}s^{-1} (Myles et al., 1998). As it is shown Fig. 3.19and known form literature (Li et al., 2004; Myles et al., 1998), in the absence of glycosaminoglycans, ATIII doesn't require contact with neither of anion binding sites for binding to thrombin active site (Fig. 3.19) (Gronewold et al., 2005). However, whether thrombin-ATIII complex can bind to aptamers, hasn't been studied.

3.5.1.1 Interaction of Thrombin-ATIII complex with immobilized HD1 and HD22 aptamers

In order to investigate interaction of thrombin aptamers with thrombin-ATIII complex, thrombin (12.5 nM) incubated for 30 minutes at room temperature with various concentrations (12.5, 50, 200, 800 nM) of ATIII was flowed over the immobilized aptamers HD1, HD22 and Nu172 (Fig. 3.20).

At the stoichiometric concentration of ATIII, SPR response comparable to 12.5 nM thrombin was observed, suggesting that either ATIII-thrombin complex interacts with the aptamers the same way as with just thrombin or, at low concentration such as 12.5 nM, ATIII cannot inhibit all the thrombin in 30 minutes due to the low $k_{on,}$ and therefore the signal represents the interaction of uninhibited thrombin with aptamers (Fig. 3.20 green curves). If we take in account the value of k_{on} and perform numerical simulations (Fig. 3.21 (A)), we obtain curves of thrombin-ATIII complex formation over time. Figure 3.21 (B) shows that when

incubated for 30 minutes less the 20% of thrombin is inhibited by 12.5 nM ATIII, with increase of the concentration of ATIII, percentage of inhibited thrombin increases. That's why, injections of thrombin with higher ATIII concentration, led to drastic diminution of the signal for all aptamers (Fig. 3.20).

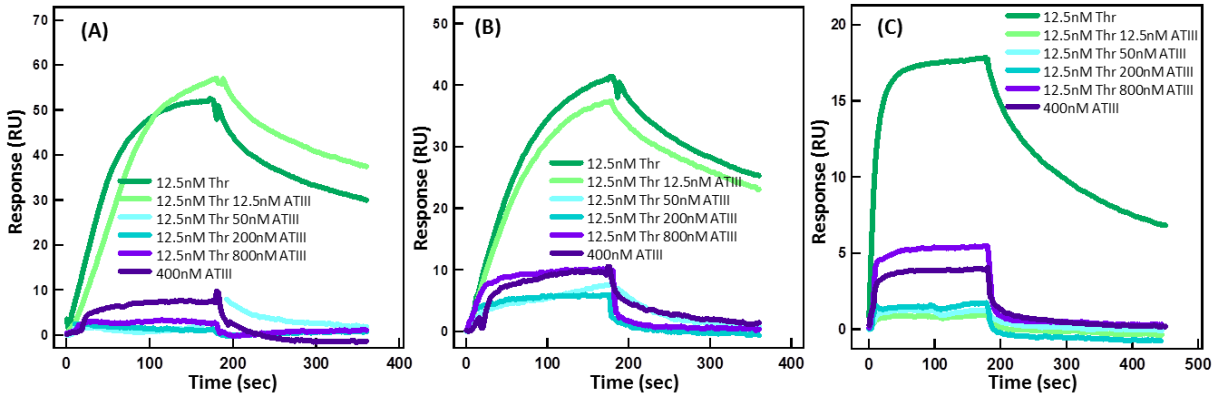

FIGURE 3.20 Sensograms of interaction of immobilized aptamers HD1 (A), HD22 (B) and NU172 (C) with 12.5 nM thrombin incubated for 30 minutes with various concentrations of ATIII from 12..5 to 800 nM.

This shows that at higher concentration of ATIII all the thrombin in complex with the inhibitor and such complex doesn't interact with either of aptamers. The result is surprising, since, as shown on the molecular model (Fig. 3.19), the binding of the ATIII shouldn't sterically be an obstacle for aptamer binding. It can be supposed that binding of ATIII has an allosteric effect on thrombin, distorting the topography of exosites for aptamer binding (Parekh et al., 2008). Indeed, several studies revealed communication between active site and exosites inducing allosteric effects.(Fredenburgh et al., 1997; Petrera et al., 2009)

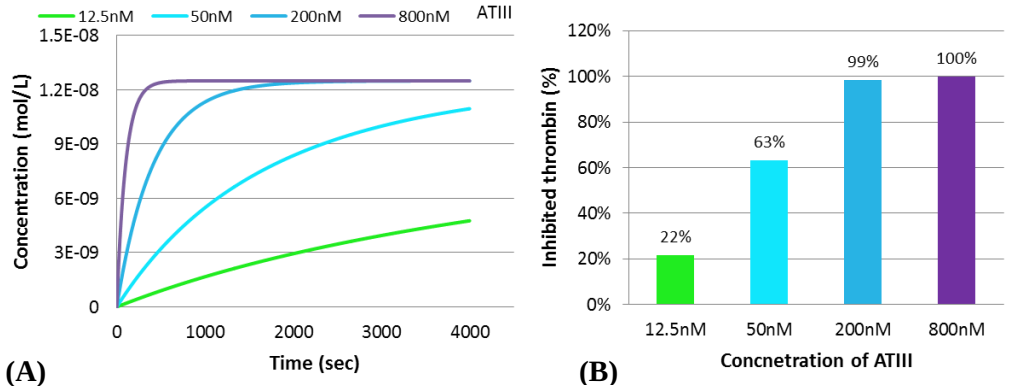

FIGURE 3.21 Inhibition of thrombin by 12.5, 50, 200 and 800 nM ATIII. (A) Numerical simulation of 12.5 nM thrombin inhibition by various concentrations of ATIII. (B) Concentration of inhibited thrombin after 30 minutes of incubation with different concentrations of ATIII, predicted by numerical simulation.

With increasing concentrations of ATIII, slight increment of the signal was observed for HD22 and NU172, resembling nonspecific interactions with the surface. The injection of 400nM ATIII without thrombin was performed as the control to verify if non-specific interactions between ATIII and aptamers take place. Control experiment revealed the the presence of lightweight non-specific interactions with both aptamers, characterized by fast off rate.

3.5.1.2 Interaction of ATIII with aptamer-bound thrombin

On the other hand, it is also important to evaluate thrombin-ATIII complex formation, in the case where thrombin is already bound to an aptamer. For this purpose increasing concentrations of ATIII (12.5, 50, 200, 800, 1500 nM) was flowed over preformed thrombin-aptamer (HD1 and HD22) complex. This experiment was performed at mass transport limited mode with high surface density of aptamers (ligand immobilization level corresponding to 500 RU), in order to keep as much thrombin at surface as possible. At such conditions, bound thrombin, as soon as it dissociates from one ligand, rebinds another and therefore instead of dissociation, steady signal is observed.

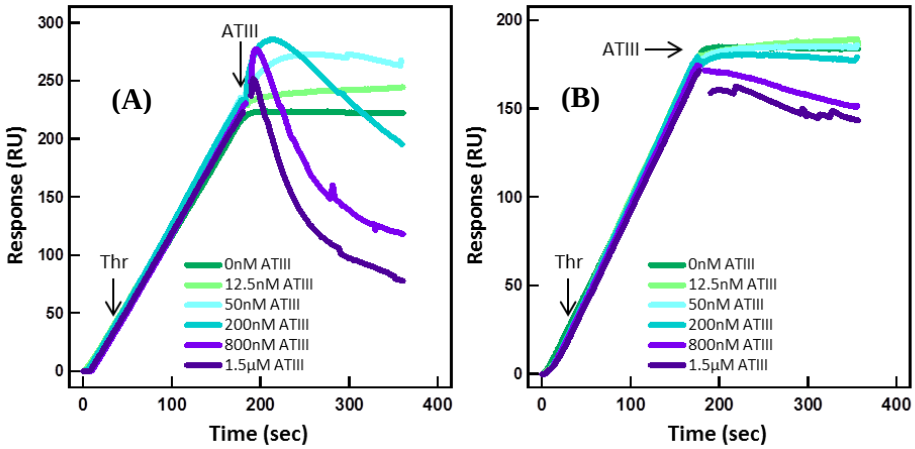

FIGURE 3.22 Sensograms of interaction of various concentrations of ATIII with 12.5 nM thrombin bound to immobilized HD1(A) and HD22 (B) aptamers. First 12.5 nM thrombin was flown over the densely immobilized aptamers for 3 minutes and then right away increasing concentrations of ATIII were injected.

As shown on FIGURE 3.22 (A), injection of increasing concentrations ATIII, promotes dissociation of thrombin from HD1. At low concentration (12.5 and 50 nM) of ATIII, following the injection of the inhibitor, slight increase of the signal compared to only thrombin is observed. This effect could be interpreted as the formation of ternary complexes of HD1-thrombin-ATIII, though this complex shouldn't be very stable, thrombin-ATIII form so-called loose complex. Furthermore, it can be seen at the beginning of the injection of higher concentrations (200-1500 nM) of ATIII how the signal increases for few seconds and then drops corresponding to binding of inhibitor to thrombin and consequent removal of formed complex form the aptamer HD1. This result suggests that binding HD1 to exosite 1, doesn't alter the recognition of thrombin active cleft by ATIII (Holland et al., 2000), but once the firm (irreversible) complex between ATIII and thrombin is formed (Stone and Hermans, 1995) HD1 cannot rebind dissociated thrombin in thrombin-ATIII complex, due to the conformational changes. This interpretation is consistent with the results by published by Parekh (Parekh et al., 2008).

As for HD22 (Fig. 3.22 (B)), no significant interaction (neither association nor dissociation) with aptamer-bound thrombin is observed for ATIII concentrations from 12.5 to 200 nM. Starting from 800 nM ATIII, minute dissociation of thrombin occurs. We can suppose that for ATIII binding to thrombin active site, exosite II has to be accessible. At the same time, ATIII cannot displace HD22 aptamer easily. Once the thrombin–HD22 complex is disassociates, only then it is possible for ATIII to capture liberated thrombin. However, at lower concentrations of ATIII, time needed to diffuse and form the complex with thrombin is longer than needed for thrombin

rebinding from one aptamer to another. At higher concentrations, more ATIII is available to inhibit thrombin as soon as it dissociates from the HD22 aptamer.

To summarize, above-described studies show that ATIII-thrombin complex cannot be detected by either of aptamers, but ATIII might have slight nonspecific interactions with all (HD1, H22 and NU172) aptamers. HD22 interacting with heparin binding site of thrombin disturbs docking of ATIII, Whereas HD1- thrombin dissociates when ATIII binds thrombin.

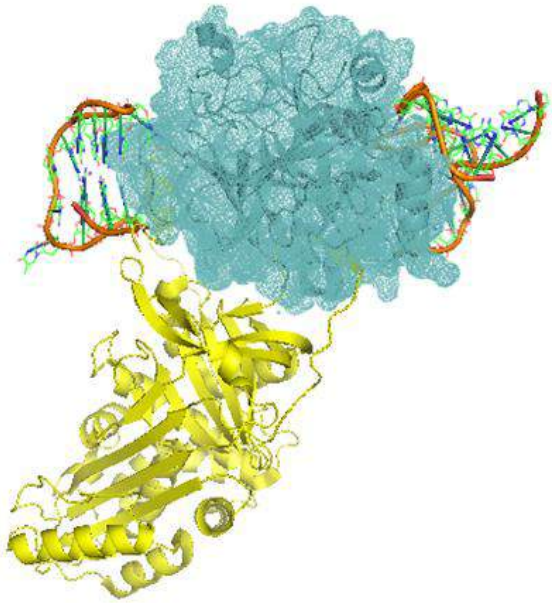

FIGURE 3.23 Interaction of HD1 and HD22 aptamers with thrombin-HCII complex. Superposed structures of Thrombin-HCII complex (1JMO) and thrombin aptamersHD1 (4DII) in the left and HD22 (4I7Y) in the right

3.5.2 Heparin cofactor II

HCII, likewise to ATIII, is the member of the serine protease inhibitor superfamily (Potempa et al., 1994), responsible for 30% anticoagulant activity in plasma. HCII irreversibly inhibits active site of thrombin with the k_{on}=1.11x10^3 M^{-1}s^{-1} (Myles et al., 1998). From the crystal structure of HCII-thrombin complex shown on Figure 3.23 , it is visible that, HCII uses exosite I for docking when binding thrombin (Baglin et al., 2002).

3.5.2.1 Interaction of HCII-thrombin complex with HD1 and HD22

Interaction of HCII-thrombin complex with immobilized thrombin binding aptamers HD1, HD22 and NU172 was investigated by injection thrombin-HCII complexes with different stoichiometric ratio of the inhibitor over aptamer functionalized surface (Fig. 3.4).

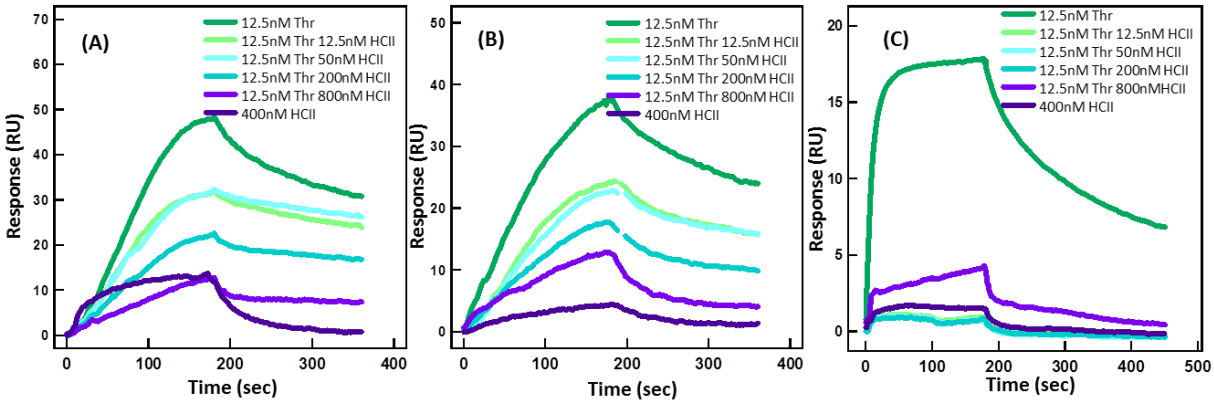

FIGURE 3.24 Sensograms of interaction of immobilized aptamers HD1 (A), HD22 (B) and NU172 (C) with 12.5 nM thrombin incubated for 30 minutes with various concentrations of HCII from 12.5 to 800 nM

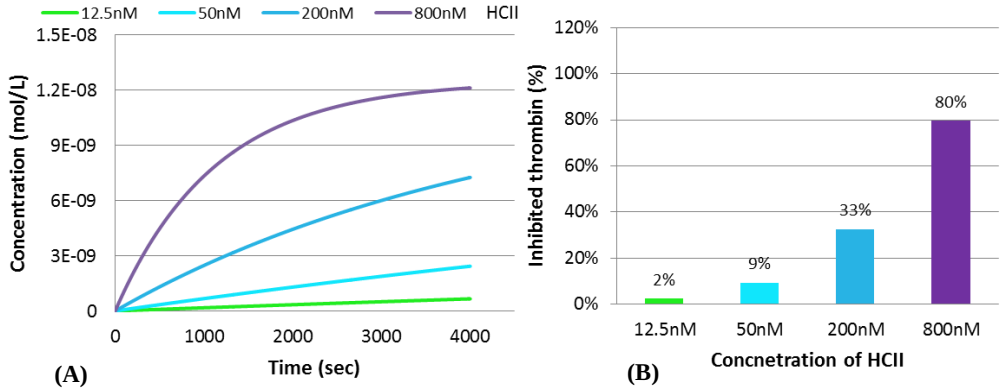

FIGURE 3.25 Inhibition of thrombin by 12.5, 50, 200 and 800 nM HCII. (A) Numerical simulation of 12.5 nM thrombin inhibition by various concentrations of HCII. (B) Concentration of inhibited thrombin after 30 minutes of incubation with different concentrations of HCII, predicted by numerical simulation.

HD1 and HD22 aptamers showed similar trend of gradual diminution of the signal with the increase of the HCII concentration (Fig. 3.24 (A) and (B)). Numerical simulation of irreversible inhibition of thrombin by heparin cofactor II shown on figure 3.25 (B) indicates that 30 minutes of incubation with HCII are not enough to completely inhibit all the thrombin. Therefore decrease of response with increase of HCII concentrations means, that signal is due to uninhibited thrombin, and once thrombin forms complex with HCII such complex doesn't interact with neither of aptamers. In the case of NU172 we let HCII to incubate longer than 30 minutes with thrombin and therefore more thrombin was inhibited and thrombin-HCII complex didn't interact with NU172. We deduce that thrombin-HCII complex, once formed, is invisible to all thrombin aptamers and especially if glycosaminoglycans (GAGs) are present. GAGs would facilitate thrombin inhibition occupying heparin binding exosite II and prevent binding of aptamers even more.

What we can detect, though, is the nonspecific interaction of HCII with the aptamer HD1 and NU172. Interaction of 400 nM HCII with aptamers yielded the signal equal to 30 % of signal of only 12.5 nM thrombin. In real sample of non-coagulating plasma, where concentration of HCII is 1.4 μM (Tollefsen et al., 1982), the signal might be comparable to thrombin signal.

3.5.2.2 Interaction of HCII with aptamer-bound thrombin.

Similarly to ATIII, interaction of aptamer-bound thrombin with HCII was investigated by coinjection of increasing concentrations of inhibitor just after injection of 12.5 nM thrombin over densely immobilized aptamer surface.

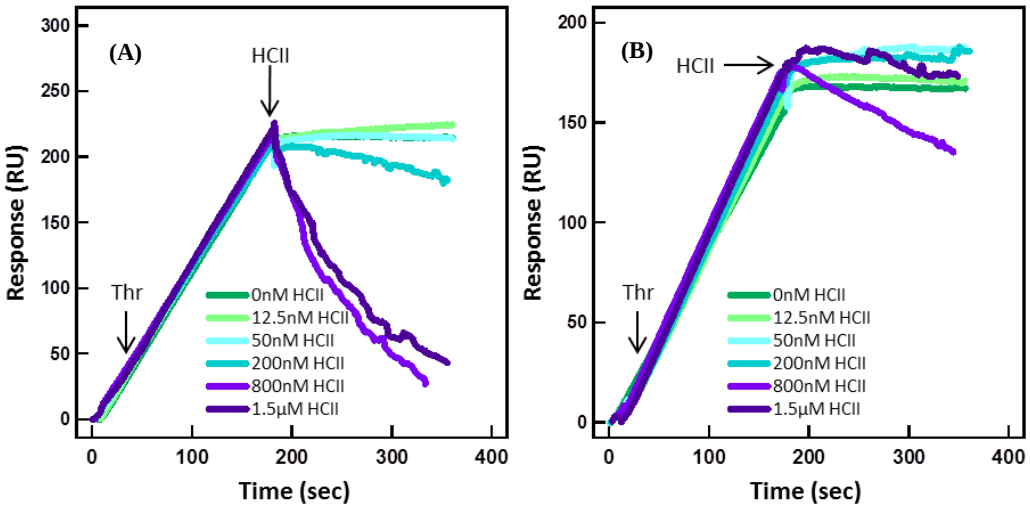

FIGURE 3.26 Sensograms of interaction of various concentrations of HCII with 12.5 nM thrombin -bound to immobilized HD1 (A) and HD22 (B) aptamers. First 12.5 nM thrombin was flown over the densely immobilized aptamers for 3 minutes and then right away increasing concentrations of HCII were injected

Figure 3.26 (A) shows that high concentration of HCII starting from 200nM associate with HD1 aptamer-bound thrombin and the complex is rapidly dissociated from the aptamer. This effect is expected from the geometry of HCII binding to thrombin exosite I, (Fig. 3.23) that is main binding site for HD1 as well. I.e. HCII competes with HD1 and wins binding for thrombin exosite I. However it should be noted, the fact that more than 200 nM HCII was required for the successful outcome of this challenge, indicates that HD1 binding modulates HCII interaction with thrombin exosite I (Holland et al., 2000).

In the case of HD22 aptamer –bound thrombin no significant effect of HCII presence was observed. It is important to acknowledge that HCII didn't attack thrombin-HD22 complex, that can be explained by the fact that exosite II of thrombin, recognized by HD22, doesn't come interact with HCII during the complex formation in the absence of GAG. However, no increase of signal indicates that binding of HD22 to thrombin induces changes in thrombin structure that HCII is not able to interact with the well exposed exosite I. Again we see the trace of the allosteric linkages between the exosites.

To sum up, HCII-thrombin complex is not interacting with none of the aptamers, most probably due to the allosteric inactivation of exosite II following the irreversible inhibition of exosite I. HCII shows very low affinity towards HD22-thombin complex. HCII competes for HD1 aptamer-bound thrombin, removing it from the aptamer.

3.5.3 Alpha-2 macroglobulin

Alpha-2 macroglobulin is a serum protein functioning as the broad range irreversible proteinase inhibitor. A2M is a large molecule with a molecular weight of 720 KDa (Arakawa et al., 1989). It is composed of four identical subunits forming large central cavity where proteases are trapped as prey. Proteinases remain active but prevented from further contact with high molecular weight substrates. Interaction of thrombin and A2M is described with association rate constant k_{on}=2.5x10^{3}M^{-1}s^{-1}. (Feinman et al., 1985). The structure of A2M-thrombin complex is not available. FIGURE 3.27 represents structures of A2M and thrombin molecules separately (Marrero et al., 2012); This image allows to appreciate how large A2M is compared to thrombin and to imagine how thrombin can be wrapped and encapsulated in the scaffold of A2M. It was shown that small fluorogenic peptides cans still access active cleft of A2M-entrapped thrombin (Hemker et al., 2002). However there is no evidence about A2M-thrombin complex interaction with thrombin aptamers.

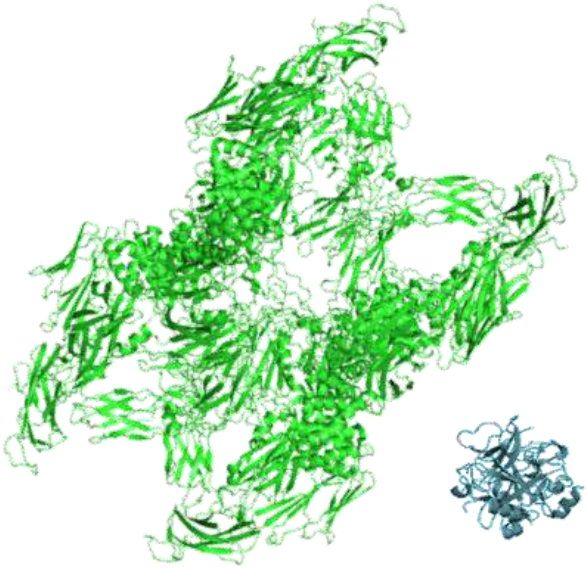

FIGURE 3.27 Structures of alpha-2-Macroglobulin (4ACQ) and thrombin (3U69)

To answer the question whether surface-immobilized aptamers HD1, HD22 and Nu172 can interact with A2M-thrombin complex, similarly to previous experiments with ATIII and HCII, thrombin incubated with increasing concentrations of A2M was flowed over sensor surface (Fig. 3.28).

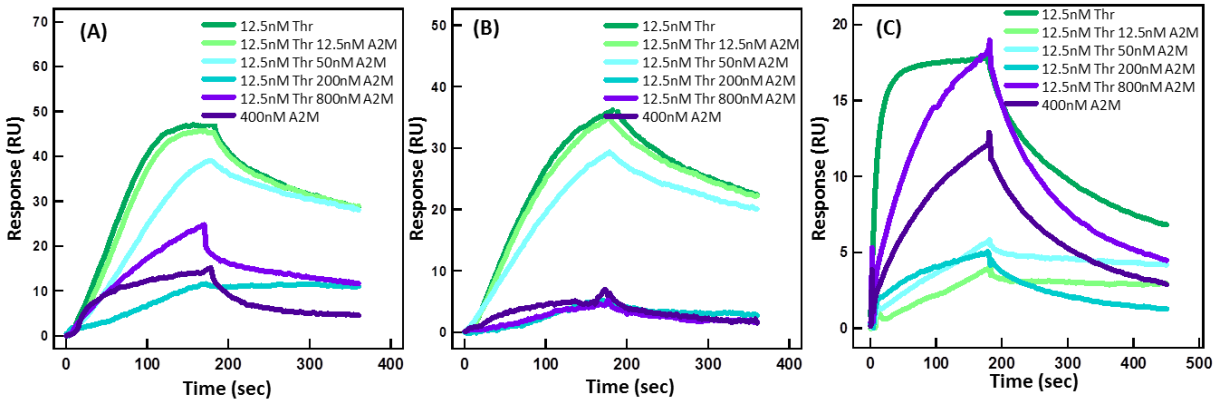

FIGURE 3.28 Sensograms of interaction of immobilized aptamers HD1 (A), HD22 (B) and NU172 (C) with 12.5 nM thrombin incubated for 30 minutes with various concentrations of A2M from 12.5 to 800 nM.

According to numerical simulations (Fig. 3.29 (B)), after 30 minutes of incubation with 12.5 and 50nM A2M, 12.5nM thrombin is only partially inhibited. The signal of interaction of with these samples decreases with decrease of free thrombin, suggesting that the response was solely from interaction with thrombin and not thrombin-inhibitor complex. We can explain this result

by two hypotheses: either the entrapped thrombin is completely wrapped in A2M and aptamers cannot squeeze inside the A2M scaffold to bind thrombin; or, alternatively, thrombin might have been accessed by aptamers only if they weren't attached to the surface due to steric repulsion. Since there is no structure available for thrombin–A2M complex, it is difficult to say what is true.

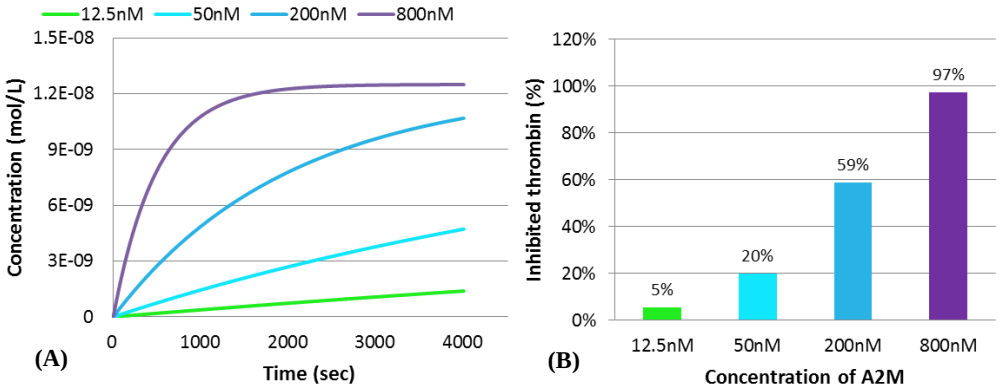

FIGURE 3.29 Inhibition of thrombin by 12.5, 50, 200 and 800 nM A2M. (A) Numerical simulation of 12.5 nM thrombin inhibition by various concentrations of A2M. (B) Concentration of inhibited thrombin after 30 min of incubation with different concentrations of A2M, predicted by numerical simulation.

At higher concentrations of A2M thrombin inhibition occurs faster and therefore SPR signal should go down to zero. But in the case HD1 and NU172 aptamerss at inhibitor concentrations higher than 200 nM, response started to increase again. Injection of 400nM A2M revealed that both HD1 and NU172 are engaged in nonspecific interactions with A2M, and with increase of concentration response becomes stronger. The conclusion of this set of experiments is that, surface bound aptamers do not interact with thrombin entrapped by A2M. But A2M on its own shows significant nonspecific interactions with HD1 and NU172 surface.

3.5.4 Conclusions

Above studies on interaction of immobilized thrombin aptamers with thrombin-natural inhibitor complexes showed that, none of the aptamers are able to interact with complex of thrombin with ATIII, HCII or A2M either due to inhibition of binding site, inaccessibility of thrombin or inhibitor-induced allosteric changes. For ATIII and HCII binding to thrombin induces allosteric changes on thrombin binding sites, since despite of absence of geometric constraints for binding aptamers on exposed exosites, no interaction with either of aptamers is observed. And in the case of A2M surface-bound aptamers cannot penetrate the scaffold of the A2M either because of the size or due to the fact that they are attached to the surface.

NU172 revealed nonspecific interactions with A2M. In the case of HD1, it tends to interact nonspecifically with ATIII, HCII and A2M with several micromolar affinities. Considering the normal concentrations of these inhibitors in real samples of blood or plasma, we should expect that the signal of HD1 due to these nonspecific interactions will be comparable and even exceed the signal from thrombin.

We conclude that HD22 is the most relevant for real sample characterization.

3.6 Results of aptamer specificity in native-like environment

Results obtained from kinetic experiments of thrombin interaction with aptamers inform us that aptamers possess low nanomolar range affinity to thrombin. But on the same time we saw that ambiguous interactions with aptamers might take place as well. As the ultimate aim of building biosensor for thrombin sensing is to be able to detect target protein in its real environment, such as plasma or blood, it is important to know how aptamers will behave in such complex medium. We need to be sure that sensing elements, and namely aptamers, are specific enough to discriminate between thrombin and nonspecific compounds of blood. Unfortunately, SPR instrument has its limitation for working in such complex mediums as blood or whole plasma, but aptamer specificity was still possible to verify with BSA and diluted plasma.

3.6.1 Interaction with bovine serum albumin

Before performing SPR experiments with plasma, interaction of aptamers with the most abundant plasma protein serum albumin was investigated (Adkins et al., 2002). Serum albumin is present in the concentration of 500-700 μM concentrations in plasma and it possesses multifunctional binding properties. One of the main roles of serum albumin is to transport fatty acids, hormones, nutrients, drugs etc. Serum albumin is also prone to have nonspecific interactions. The presence in high concentration and ability to interact with wide array of molecules makes serum albumin a susceptible candidate for nonspecific interactions also with aptamers.

Specificity of aptamers HD1, HD22 and NU172 was verified by injecting various concentrations (12.5 nM – 3.2 μM) of bovine serum albumin. The sensograms of interaction of immobilized HD1, HD22 and NU172 with BSA are shown on figure 3.30

At low concentrations (12.5-200 nM) of BSA, none of the aptamers showed any nonspecific

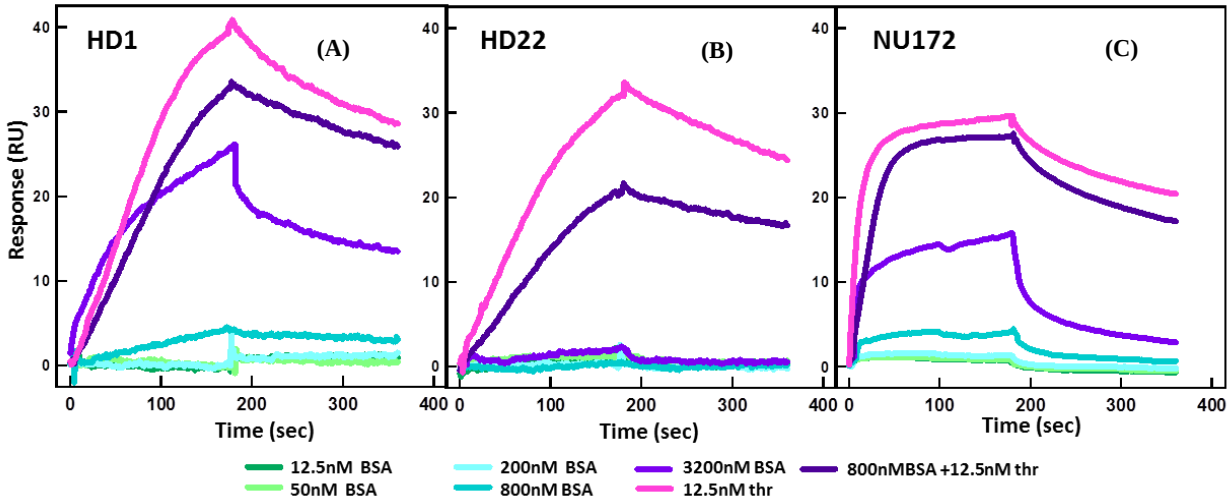

FIGURE 3.30 Sensograms of immobilized HD1 (A) , HD22 (B) and NU172 (C) aptamer the interaction with increasing concentrations of BSA from12.5 nM to 3.2 μM and 800 nM BSA spiked with 12.5 nM Thrombin

interactions with BSA. Starting from 800 nM, HD1 and NU172 aptamers, unlike to HD22, revealed

nonspecific binding to BSA (Fig. 3.30 (A) and (C)). Nonspecific signal became significant for 3.2 μM concentration, suggesting that affinity of BSA to HD1 and NU172 is in micromolar range.

Since bovine serum albumin and human serum albumin are homologous proteins and bear structural similarities, we may assume that the effect observed with BSA might also be true for HSA. If we take in account the real concentration of serum albumin in plasma, we can deduce that in the observed signal for HD1 and NU172 interaction with real plasma sample, the main contribution will be due to the nonspecific interaction with serum albumin. Nonspecific signal for serum albumin interaction should be much higher than the signal from thrombin itself.

The presence of BSA also showed to have slight interfering effect on thrombin association with aptamers. Thrombin of 12.5 nM concentration, injected with 800 nM BSA, showed lowered response compared to the same concentration of pure thrombin for all aptamers. But this effect was more prominent for HD22 (Fig. 3.30 (B)), with the difference in the signals of about 40%.

3.6.2 Interaction with plasma

Plasma represents a complex medium, containing 60-80 mg/ml of proteins in addition to various small molecules such as salts, lipids, amino acids, and sugars (Adkins et al. 2002). It is estimated that up to 10,000 proteins might be commonly present in serum, with varying concentrations, the lowest reaching 10 orders of magnitude less than concentration of albumin separately (Anderson and Anderson, 2002). Performing SPR measurement within such a rich environment, represents limitation for the instrument, therefore experiments were performed with diluted plasma.

3.6.2.1 HD1 and HD22 aptamer interaction with 100-fold diluted plasma

To investigate behavior of aptamers HD1 and HD22 in real like condition we used murine plasma. Murine plasma, centrifuged and filtered prior to experiment, was first diluted 100 times in PBS running buffer and then injected over the surface modified with HD1 and HD22. Interaction results are shown on Fig 3.31.

Injection of 100-fold diluted plasma in PBS buffer gave significant response, especially for HD1. The response of HD1 interaction with plasma was about 4 times higher compared to the signal of the same aptamer interaction with 12.5 nM thrombin. The signal of aptamer HD22 interaction with diluted plasma was slightly higher than that of binding to 12.5 nM thrombin. The same diluted plasma spiked with 12.5 and 50 nM thrombin induced response much less than only plasma sample or only thrombin, due to the irreversible saturation of the surface. Quality of obtained responses didn't allow calibration. Therefore it is impossible to give any quantitative interpretation. Nevertheless, it is important to point out, that the signals shown on figure 3.31 represent the differences between responses from the flow cells with aptamer and reference sequences. This means that aptameric sequences compared to their references had affinity towards some proteins in plasma, and notably thrombin.

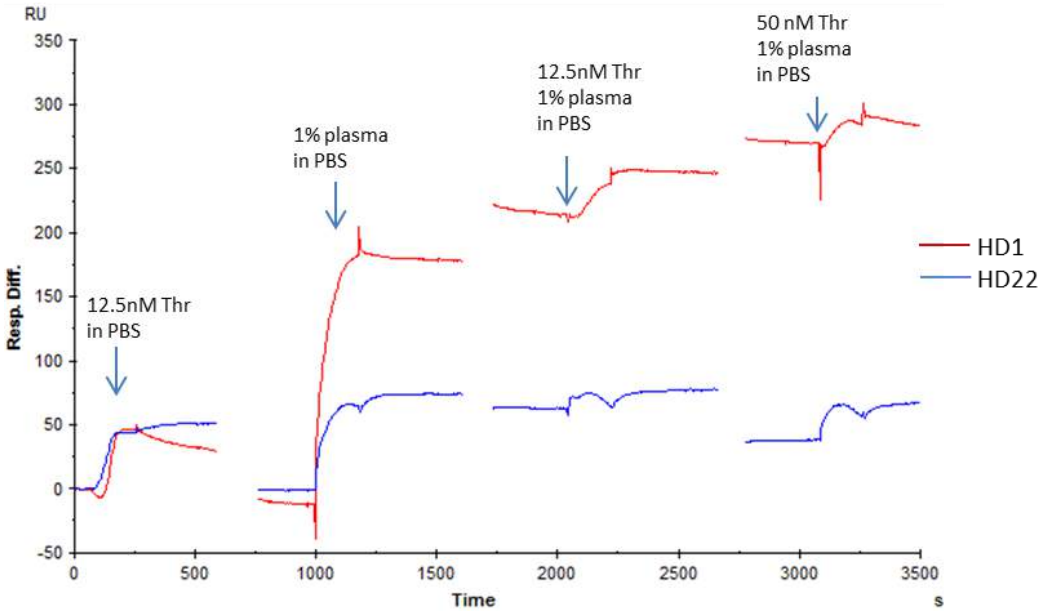

FIGURE 3.31 Sensograms of immobilized HD1 and HD22 aptamer interaction with plasma diluted 100 fold in PBS.

For both aptamers after interaction with plasma sample, it was impossible to regenerate the sensing surface and return to the preinjection baseline. With injection of thrombin spiked plasma, baseline of HD1, shifted even more, whereas baseline of HD22 remained the same. We suppose that the significant response from plasma sample and shift in baseline are due to several factors, the main of which are: (i) specific and non-specific interactions of aptamers (notably HD1) with plasma proteins such as endogenous thrombin, prothrombin, serum albumin etc. (the last two shown above to interact with HD1) and (ii) non-specific interactions of the surface with plasma content.

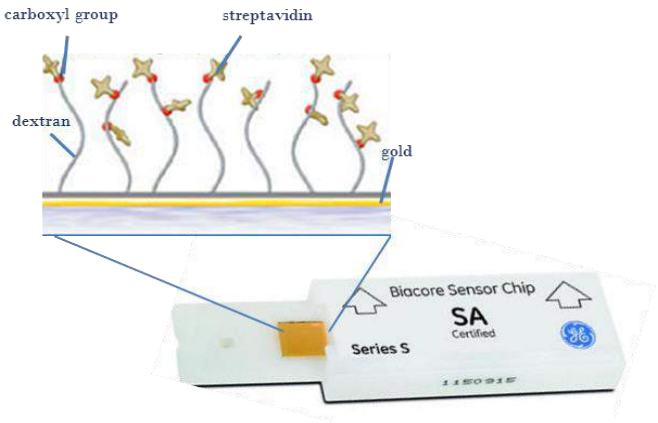

FIGURE 3.32 Surface of the Biacore SA sensor chip. Gold surface of the chip is functionalized with dextran molecules bearing streptavidin molecules bound with carboxyl functional groups.

The non-specific interactions with the surface are the common limitation of methods based on affinity adsorption. The more complex is the surface coverage the more is the chance of having non-specific interactions. Presented experiments were performed on the SA sensor chip (FIGURE 3.32), the surface of which presents gold layers covered with a dense forest of dextran molecules bearing streptavidin molecules covalently bound with carboxyl groups for capturing biotinylated ligand. Dextran molecules tend to attach non-specifically and irreversibly various biomolecules from plasma, complicating the analysis of specific binding interactions and rendering surface unfit for further experiments.

3.6.2.2 Interaction of HD1 and HD22 aptamers with plasma in the presence of NSB-reducer

In order to reduce nonspecific binding with surface, for next set of experiments in plasma, nonspecific binding reducer (NSBr) buffer was added as suggested by the Biacore manufacturer. Carboxymethyl dextran is the main component of NSBr. It has a similar structure to the dextran matrix on the sensor surface, thereby reducing non-specific binding of complex sample components to the surface via a competition effect.

Initially, plasma was diluted in 10 mg/ml NSB reducer buffer. 1000 times dilution of plasma, induced response of HD1 comparable to the signal of only 12.5 nM thrombin. HD22 showed only insignificant interaction. Surface regeneration was successful and baseline shift wasn't observed (Fig. 3.33).

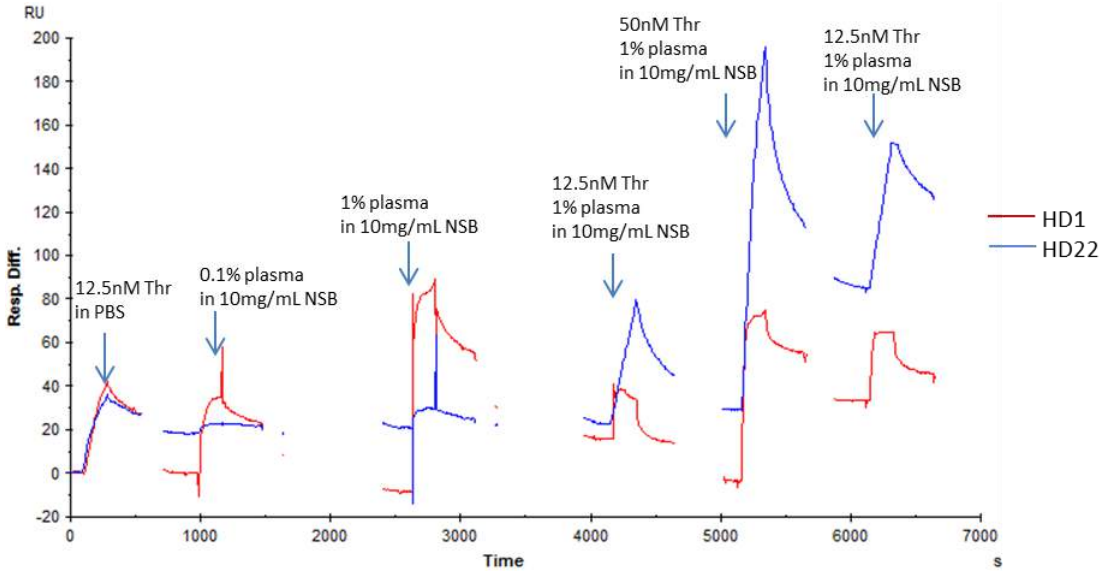

FIGURE 3.33 Sensograms of immobilized HD1 and HD22 aptamer interaction with plasma diluted 1000 or 100 times in 10 mg/mL NSB reducer and spiked with 50 nM and duplicate of 12.5 nM thrombin.

Thereafter plasma was diluted 100 times in 10 mg/ml NSB reducing solution. Response signal increased for both aptamers, with HD1 still showing higher interaction than HD22. Injection of plasma samples spiked with 12.5, 50 and again 12.5 nM thrombin gave well distinct signals between lower and higher concentrations (Fig. 3.34). Although the signals for duplicates

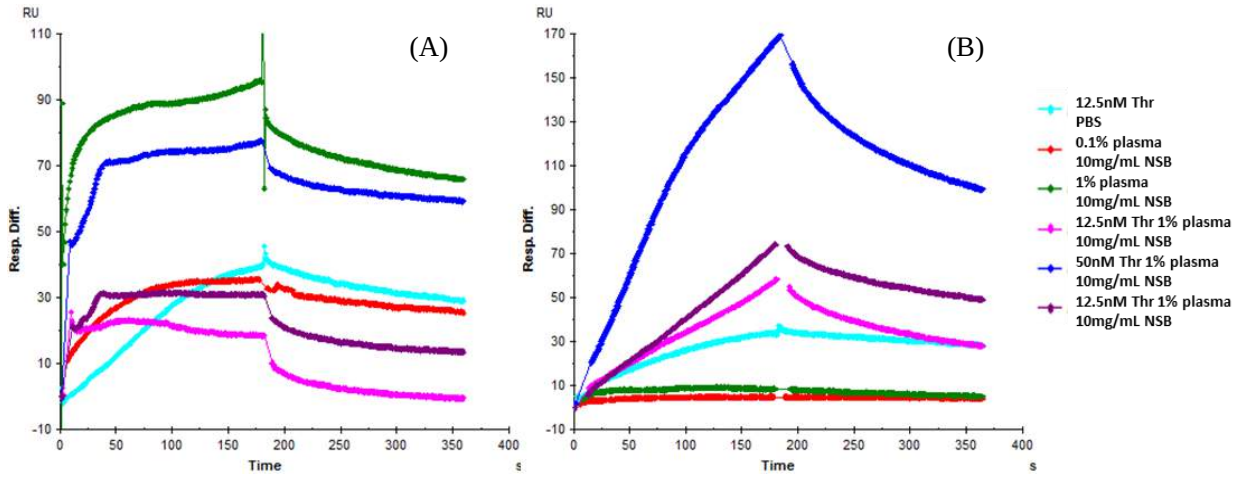

FIGURE 3.34 Overlaid sensograms of immobilized HD1 (A) and HD22 (B) aptamer interaction with plasma diluted 100 times in 10 mg/mL NSB reducer and spiked with 50 nM and duplicate of 12.5 nM thrombin.

weren't completely identical, aptamers and in particular HD22 (Fig. 3.34 (B)), showed to perform well and identify thrombin in these experimental conditions (1% plasma in 10 mg/mL NSB reducer).

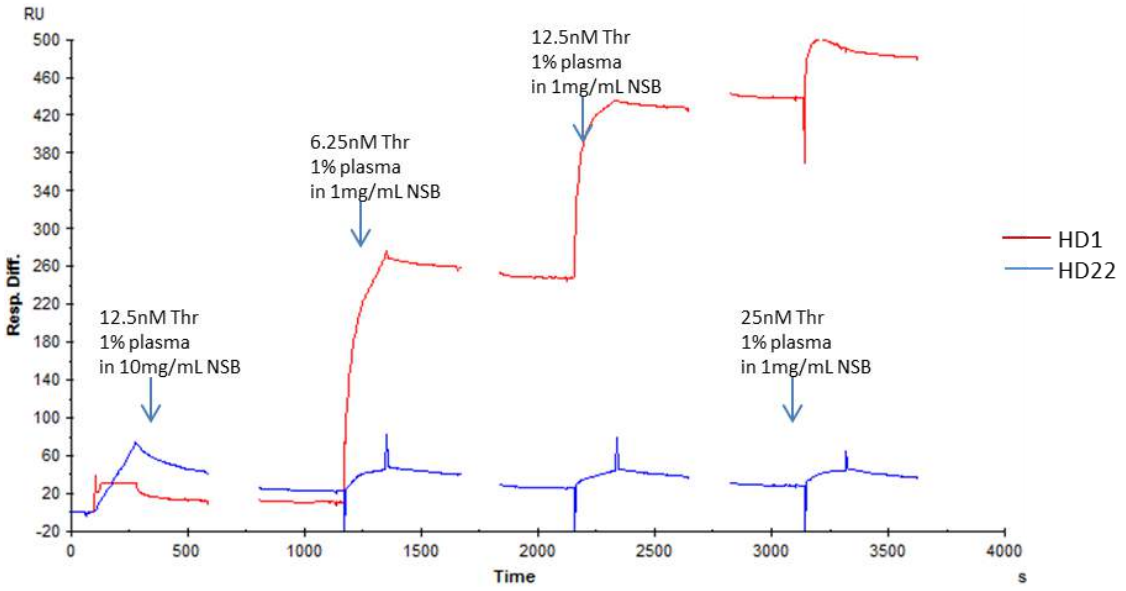

FIGURE 3.35 Sensograms of immobilized HD1 and HD22 aptamer interaction with 100 times diluted plasma in 1 mg/mL NSB reducer spiked with 6.25, 12.5 and 25 nM thrombin.

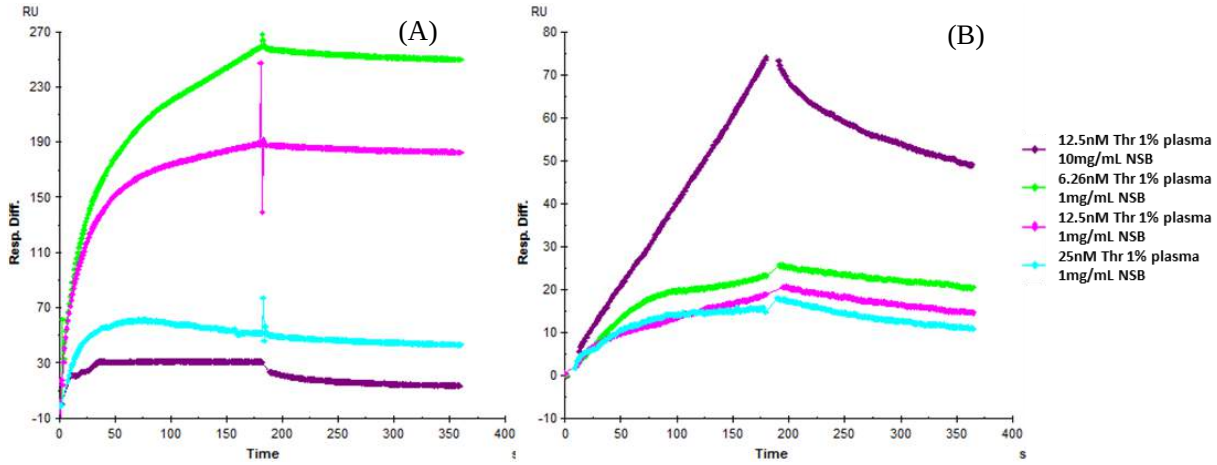

FIGURE 3.36 Overlaid sensograms of immobilized HD1 (A) and HD22 (B) aptamer interaction with 100 times diluted plasma in 1 mg/mL NSB reducer spiked with 6.25, 12.5 and 25 nM thrombin.

When the concentration of the NSB reducer was decreased to 1mg/mL, that is the concentration suggested by the manufacturer, nonspecific interaction of plasma with the surface became again significant (Fig. 3.35). Both aptamers failed again to show meaningful responses for plasma samples spiked with 6.25, 12.5 and 25 nM thrombin. HD1 aptamer instead of giving higher response with increase of the thrombin content gave less and less signal (Fig. 3.36 (A)). With each injection of sample it was evident how nonspecific interactions both with aptamer HD1 and the surface saturated the surface capacity and it became completely impossible to return to initial baseline (Fig. 3.35 red curves). In the case of HD22 the shift of the baseline wasn't observed (Fig. 3.35 blue curves), but capacity of the surface to bind the thrombin obviously diminished so that it could not reflect the increase of the thrombin concentration with each sample (Fig. 3.36 (B)). We

can suppose that this effect was due to the simultaneous and comparable saturation of HD22 and HD22 reference surfaces by nonspecific bindings.

Overlaid sensograms represented on FIGURE 3.33 and 3.36 show behavior of aptamers in 1% plasma in 10 mg/mL and 1 mg/mL NSB reducer. Comparison of these results gives us two main results very important for aptamer-based thrombin sensor development: Firstly, in overall HD22 showed much better performance towards specificity to thrombin than HD1. One of the most important factors why HD1 is getting so much interactions could be the ability of HD1 to interact with prothrombin which is abundant is the plasma. We can clearly see the advantage of using as a recognition element aptamers interacting only with the exosite II[1]. Secondly, these experiments in slightly different environmental conditions highlight how much non-specific interactions affect thrombin recognition by aptamers: Environment together with the surface chemistry have immense effect on performance of target detection.

Possible solutions to the encountered problems could be introduction of more competing agents or surfactants (SDS) in the sample and selecting optimal surface such as bare gold instead of dextran matrix.

As we see the main limitation of the SPR method in the case of plasma is that we are not able to distinguish what gets adsorbed to the surface, is this specific or nonspecific interaction, since whatever sticks to the surface changes the refraction index and induces SPR response. This shows that in all label free sensing methods (QCM, ring resonator), if optimal chemistry for surface modification and environmental conditions aren't selected, there is a big chance to observe nonspecific attachment of the molecules from plasma, saturating the surface and obstructing binding of specific target.

3.6.3 *Conclusions*

We studied the behavior of aptamers in the presence of nonspecific but abundant plasma protein BSA, which induced nonspecific response in the cases of HD1 and NU172 aptamers. Further experiments with diluted plasma showed that nonspecific interaction of plasma proteins even in the case of 100 fold dilution is sufficient to irreversibly block the surface of the sensor rendering it useless for further experiments. In the presence of nonspecific binding reducer, the share of nonspecific interactions with the sensor surface was diminished, and we could make the evaluation about the performance of the aptamer HD1 and HD22 in plasma.

[1] Although we haven't performed experiments in diluted plasma for NU172 but as it also binds exosite 1 of thrombin, we can predict to have similar signal as for HD1 in the plasma, due to the undesired interactions with prothrombin.

3.7 Conclusions

This study was the first step-by-step investigation of thrombin-aptamer interaction to design a functional sensor in plasma.

Surface plasmon resonance technique was used as the main tool to investigate interaction of thrombin binding aptamers with thrombin, prothrombin, thrombin-inhibitor (ATIII, HCII and A2M) complexes, nonspecific targets and diluted plasma.

Binding kinetics of thrombin and prothrombin elucidated complex character of interaction with HD1 and NU172, suggesting that both aptamers interact with thrombin not with one but two sites with low nanomolar affinities. In the case of prothrombin, HD1 and NU172 aptamers revealed one order of magnitude less affinity than for thrombin. Aptamer HD22 didn't show any interaction with prothrombin, however inactivation of residual thrombin by argatroban was needed to avoid prothrombin auto activation phenomenon.

We showed that thrombin-inhibitor complexes were completely incapable of binding to either of the aptamers, due to possible allosteric changes even though binding sites were still exposed for interaction in the case of inhibition by ATIII and HCII. However HD1 and NU172 are susceptible in the nonspecific interactions with molecules of ATIII, HCII, A2M and BSA

HD1 has very characteristic signature of interaction with prothrombin making it distinguishable from the binding with thrombin. But in the presence of diluted plasma, where there is also endogenous prothrombin and thrombin, it was impossible to say what was contributing to the response from HD1. Clearly, interaction with all above seen molecules (ATIII, HCII, A2M and BSA) and prothrombin and other plasma molecules resulted in very high nonspecific signal for HD1. HD22, on the other hand, proved to be specific enough to deserve being used as the sensing element for thrombin detection.

Interaction with plasma samples highlighted the importance of the careful selection of surface, aptamer grafting methods and buffers. Although complex character of plasma medium is overwhelming, HD22 with 10 mg/mL NSBr solution allows for thrombin detection at 10 nM range in 100-fold diluted plasma.

3.8 References

Adkins, J.N., Varnum, S.M., Auberry, K.J., Moore, R.J., Angell, N.H., Smith, R.D., Springer, D.L., and Pounds, J.G. (2002). Toward a Human Blood Serum Proteome Analysis By Multidimensional Separation Coupled With Mass Spectrometry. Mol. Cell. Proteomics *1*, 947–955.

Anderson, N.L., and Anderson, N.G. (2002). The human plasma proteome: history, character, and diagnostic prospects. Mol. Cell. Proteomics MCP *1*, 845–867.

Arakawa, H., Nishigai, M., and Ikai, A. (1989). alpha 2-macroglobulin traps a proteinase in the midregion of its arms. An immunoelectron microscopic study. J. Biol. Chem. *264*, 2350–2356.

Baglin, T.P., Carrell, R.W., Church, F.C., Esmon, C.T., and Huntington, J.A. (2002). Crystal structures of native and thrombin-complexed heparin cofactor II reveal a multistep allosteric mechanism. Proc. Natl. Acad. Sci. *99*, 11079–11084.

Bock, L.C., Griffin, L.C., Latham, J.A., Vermaas, E.H., and Toole, J.J. (1992). Selection of single-stranded DNA molecules that bind and inhibit human thrombin. Nature *355*, 564–566.

Bode, W. (2006). Structure and interaction modes of thrombin. Blood Cells. Mol. Dis. *36*, 122–130.

Bukys, M.A., Orban, T., Kim, P.Y., Beck, D.O., Nesheim, M.E., and Kalafatis, M. (2006). The Structural Integrity of Anion Binding Exosite I of Thrombin Is Required and Sufficient for Timely Cleavage and Activation of Factor V and Factor VIII. J. Biol. Chem. *281*, 18569–18580.

Butenas, S., Veer, C. van't, and Mann, K.G. (1999). "Normal" Thrombin Generation Presented in part at the XVIth Congress of the International Society on Thrombosis and Haemostasis, June 6-12, 1997, Florence, Italy (abstr PS-1653), at the 15th International Congress on Thrombosis, October 16-21, 1998, Antalya, Turkey (abstr 234), and at the 40th Annual Meeting of the American Society of Hematology, December 4-8, 1998, Miami Beach, FL (abstr 151). Blood *94*, 2169–2178.

Di Cera, E. (2003). THrombin interactions*. CHEST J. *124*, 11S – 17S.

Chambers, J.P., Arulanandam, B.P., Matta, L.L., Weis, A., and Valdes, J.J. (2008). Biosensor recognition elements. Curr. Issues Mol. Biol. *10*, 1–12.

Conard, J., Brosstad, F., Lie Larsen, M., Samama, M., and Abildgaard, U. (1983). Molar antithrombin concentration in normal human plasma. Haemostasis *13*, 363–368.

Crawley, J.T.B., Zanardelli, S., Chion, C.K.N.K., and Lane, D.A. (2007). The central role of thrombin in hemostasis. J. Thromb. Haemost. *5*, 95–101.

Davie, E.W., Fujikawa, K., and Kisiel, W. (1991). The coagulation cascade: initiation, maintenance, and regulation. Biochemistry (Mosc.) *30*, 10363–10370.

Davis, S. (1994). Kinetic Characterization of Thrombin-Aptamer Interactions. Biajournal *1*, 29.

Deng, B., Lin, Y., Wang, C., Li, F., Wang, Z., Zhang, H., Li, X.-F., and Le, X.C. (2014). Aptamer binding assays for proteins: The thrombin example—A review. Anal. Chim. Acta *837*, 1–15.

Feinman, R.D., Yuan, A.I., Windwer, S.R., and Wang, D. (1985). Kinetics of the reaction of thrombin and alpha 2-macroglobulin. Biochem. J. *231*, 417–423.

Fischer, B.E., Schlokat, U., Mitterer, A., Grillberger, L., Reiter, M., Mundt, W., Dorner, F., and Eibl, J. (1996). Differentiation between proteolytic activation and autocatalytic conversion of human prothrombin. Activation of recombinant human prothrombin and recombinant D419N-prothrombin by snake venoms from Echis carinatus and Oxyuranus scutellatus. Protein Eng. *9*, 921–926.

Foulds, N.C., and Lowe, C.R. (1985). What's new: Biosensors: Current applications and future potential. BioEssays *3*, 129–132.

Fredenburgh, J.C., Stafford, A.R., and Weitz, J.I. (1997). Evidence for allosteric linkage between exosites 1 and 2 of thrombin. J. Biol. Chem. *272*, 25493–25499.

Goji, S., and Matsui, J. (2011). Direct Detection of Thrombin Binding to 8-Bromodeoxyguanosine-Modified Aptamer: Effects of Modification on Affinity and Kinetics. J. Nucleic Acids *2011*.

Gronewold, T.M.A., Glass, S., Quandt, E., and Famulok, M. (2005). Monitoring complex formation in the blood-coagulation cascade using aptamer-coated SAW sensors. Biosens. Bioelectron. *20*, 2044–2052.

Hasegawa, H., Taira, K., Sode, K., and Ikebukuro, K. (2008). Improvement of Aptamer Affinity by Dimerization. Sensors *8*, 1090–1098.

Hemker, H.C., Giesen, P., AlDieri, R., Regnault, V., de Smed, E., Wagenvoord, R., Lecompte, T., and Béguin, S. (2002). The calibrated automated thrombogram (CAT): a universal routine test for hyper- and hypocoagulability. Pathophysiol. Haemost. Thromb. *32*, 249–253.

Hianik, T., Ostatná, V., Sonlajtnerova, M., and Grman, I. (2007). Influence of ionic strength, pH and aptamer configuration for binding affinity to thrombin. Bioelectrochemistry Amst. Neth. *70*, 127–133.

Holland, C.A., Henry, A.T., Whinna, H.C., and Church, F.C. (2000). Effect of oligodeoxynucleotide thrombin aptamer on thrombin inhibition by heparin cofactor II and antithrombin. FEBS Lett. *484*, 87–91.

Kankia, B.I., and Marky, L.A. (2001). Folding of the thrombin aptamer into a G-quadruplex with Sr(2+): stability, heat, and hydration. J. Am. Chem. Soc. *123*, 10799–10804.

Kretz, C.A., Stafford, A.R., Fredenburgh, J.C., and Weitz, J.I. (2006). HD1, a thrombin-directed aptamer, binds exosite 1 on prothrombin with high affinity and inhibits its activation by prothrombinase. J. Biol. Chem. *281*, 37477–37485.

Lane, D.A., Philippou, H., and Huntington, J.A. (2005). Directing thrombin. Blood *106*, 2605–2612.

Li, W., Johnson, D.J.D., Esmon, C.T., and Huntington, J.A. (2004). Structure of the antithrombin–thrombin–heparin ternary complex reveals the antithrombotic mechanism of heparin. Nat. Struct. Mol. Biol. *11*, 857–862.

Lin, P.-H., Chen, R.-H., Lee, C.-H., Chang, Y., Chen, C.-S., and Chen, W.-Y. (2011). Studies of the binding mechanism between aptamers and thrombin by circular dichroism, surface plasmon resonance and isothermal titration calorimetry. Colloids Surf. B Biointerfaces *88*, 552–558.

Mann, K.G., Butenas, S., and Brummel, K. (2003). The dynamics of thrombin formation. Arterioscler. Thromb. Vasc. Biol. *23*, 17–25.

Marrero, A., Duquerroy, S., Trapani, S., Goulas, T., Guevara, T., Andersen, G.R., Navaza, J., Sottrup-Jensen, L., and Gomis-Rüth, F.X. (2012). The Crystal Structure of Human α2-Macroglobulin Reveals a Unique Molecular Cage. Angew. Chem. Int. Ed. *51*, 3340–3344.

Mayer, G., Rohrbach, F., Pötzsch, B., and Müller, J. (2011). Aptamer-based modulation of blood coagulation. Hämostaseologie *31*, 258–263.

Müller, J., Freitag, D., Mayer, G., and Pötzsch, B. (2008). Anticoagulant characteristics of HD1-22, a bivalent aptamer that specifically inhibits thrombin and prothrombinase. J. Thromb. Haemost. JTH *6*, 2105–2112.

Myles, T., Church, F.C., Whinna, H.C., Monard, D., and Stone, S.R. (1998). Role of Thrombin Anion-binding Exosite-I in the Formation of Thrombin-Serpin Complexes. J. Biol. Chem. *273*, 31203–31208.

Nallagatla, S.R., Heuberger, B., Haque, A., and Switzer, C. (2009). Combinatorial Synthesis of Thrombin-Binding Aptamers Containing iso-Guanine. J. Comb. Chem. *11*, 364–369.

Padmanabhan, K., and Tulinsky, A. (1996). An Ambiguous Structure of a DNA 15-mer Thrombin Complex. Acta Crystallogr. D Biol. Crystallogr. *52*, 272–282.

Pagano, B., Martino, L., Randazzo, A., and Giancola, C. (2008). Stability and Binding Properties of a Modified Thrombin Binding Aptamer. Biophys. J. *94*, 562–569.

Parekh, P., Martin, J., Chen, Y., Colon, D., Wang, H., and Tan, W. (2008). Using Aptamers to Study Protein–Protein Interactions. In Protein – Protein Interaction, M. Werther, and H. Seitz, eds. (Springer Berlin Heidelberg), pp. 177–194.

Pasternak, A., Hernandez, F.J., Rasmussen, L.M., Vester, B., and Wengel, J. (2011). Improved thrombin binding aptamer by incorporation of a single unlocked nucleic acid monomer. Nucleic Acids Res. *39*, 1155–1164.

Petrera, N.S., Stafford, A.R., Leslie, B.A., Kretz, C.A., Fredenburgh, J.C., and Weitz, J.I. (2009). Long Range Communication between Exosites 1 and 2 Modulates Thrombin Function. J. Biol. Chem. *284*, 25620–25629.

Pinto, A. (2012). Real-time aptapcr: a novel approach exploiting nucleic acid aptamers for ultrasensitive detection of analytes for clinical diagnostic and in food analysis. Rovira I Virgili.

Potempa, J., Korzus, E., and Travis, J. (1994). The serpin superfamily of proteinase inhibitors: structure, function, and regulation. J. Biol. Chem. *269*, 15957–15960.

Rich, R.L., and Myszka, D.G. (2008). Survey of the year 2007 commercial optical biosensor literature. J. Mol. Recognit. *21*, 355–400.

Russo Krauss, I., Merlino, A., Giancola, C., Randazzo, A., Mazzarella, L., and Sica, F. (2011). Thrombin-aptamer recognition: a revealed ambiguity. Nucleic Acids Res. *39*, 7858–7867.

Russo Krauss, I., Merlino, A., Randazzo, A., Novellino, E., Mazzarella, L., and Sica, F. (2012). High-resolution structures of two complexes between thrombin and thrombin-binding aptamer shed light on the role of cations in the aptamer inhibitory activity. Nucleic Acids Res. *40*, 8119–8128.

Russo Krauss, I., Pica, A., Merlino, A., Mazzarella, L., and Sica, F. (2013). Duplex–quadruplex motifs in a peculiar structural organization cooperatively contribute to thrombin binding of a DNA aptamer. Acta Crystallogr. D Biol. Crystallogr. *69*, 2403–2411.

Stone, S.R., and Hermans, J.M. (1995). Inhibitory mechanism of serpins. Interaction of thrombin with antithrombin and protease nexin 1. Biochemistry (Mosc.) *34*, 5164–5172.

Strehlitz, B., Nikolaus, N., and Stoltenburg, R. (2008). Protein Detection with Aptamer Biosensors. Sensors *8*, 4296–4307.

Tasset, D.M., Kubik, M.F., and Steiner, W. (1997). Oligonucleotide inhibitors of human thrombin that bind distinct epitopes. J. Mol. Biol. *272*, 688–698.

Tollefsen, D.M., Majerus, D.W., and Blank, M.K. (1982). Heparin cofactor II. Purification and properties of a heparin-dependent inhibitor of thrombin in human plasma. J. Biol. Chem. *257*, 2162–2169.

Walker, C.P.R., and Royston, D. (2002). Thrombin generation and its inhibition: a review of the scientific basis and mechanism of action of anticoagulant therapies. Br. J. Anaesth. *88*, 848–863.

Wood, J.P., Silveira, J.R., Maille, N.M., Haynes, L.M., and Tracy, P.B. (2011). Prothrombin activation on the activated platelet surface optimizes expression of procoagulant activity. Blood *117*, 1710–1718.

CHAPTER 4. IMMOBILIZATION OF APTAMERS ON SURFACE

4.1 Introduction

Surface functionalization is important in many areas, but particularly in chemical and biological solid-phase (surface-based) sensors, because of the central role played by the interface between sensor and sample. Chemical modification of sensor surfaces is used in two major ways: **first, to attach selective biorecognition element** for recognition of target species in the sample and, **second, to increase the selectivity** of a sensor by reduction of interferences arising from non-specific interactions (Taylor and Schultz, 1996). In addition immobilization density of sensing element determines regime and time required for biorecognition (Esteban Fernández de Ávila et al., 2013). Hence, as the detection of an analyte with biosensors is dramatically influenced by the preparation of the biosensing surface including choice of sensing layers and coupling methods, from point of view of biosensor development, immobilization of biorecognition element on surfaces is one of the most important steps that has to be optimized at an early stage, in order to maximize the performance of detection.

The expectation from surface functionalization, first of all, is to obtain an ordered and oriented layer of sensing elements, enabling bio-recognition. However main challenge upon functionalization is also to ensure unaffected affinity, high grafting density and flexibility of bio-receptor and, at the same time, low nonspecific adsorption, low noise to signal ratio (Dugas et al., 2010). In addition, for reusable sensors, crucial parameter is the stability of the functionalized recognition element after regeneration steps. Out of these parameters only flexibility and associated degree of freedom can be fine-tuned by incorporating flexible spacers attached close to the surface that can lift sensing elements in a ”solution-like” environment, avoid steric hindrances and allow optimum binding.

The other above-mentioned parameters depend on choice of functionalization procedure. The choices of surface functionalization strategies depend, on one hand, on available types of terminal functional groups linked to sensing elements; and, on the other hand, on choice of solid substrate. These determine the type of chemistry that can be used for conjugation (Fig. 4.1).

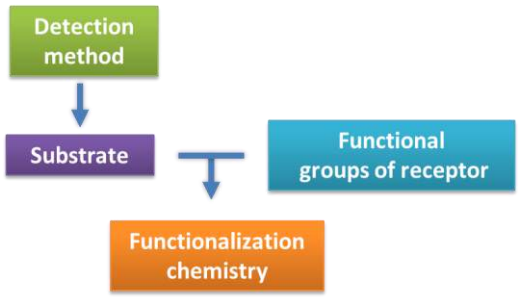

FIGURE 4.1 Scheme of decision making for functionalization chemistry

For aptamers, adding various functional groups doesn’t represent a difficulty, but most commonly used termini modifications are amine, thiol, carboxyl, phosphate or biotin functionalities (Tolle and Mayer, 2012).

The choice of substrate is predicated predominately by the readout format of the molecular association or application area, such as SPR, QCM, electrochemical, fluorescence, methods atomic force microscopy, capillary electrophoresis, affinity chromatography etc.

Thus, different analytical methods require various materials, including, but not limited to, gold, glass, silica and silicon surfaces, carbon nanotubes, quantum dots, carbohydrates, polymer and bioorganic substrates for probe immobilization (Balamurugan et al., 2008). These substrates can be used as a planar support or as nanoparticles to produce monomolecular layer or multilayers of controlled thickness (Dugas et al., 2010).

In this chapter, we explore different surfaces and methods of aptamer immobilization techniques.

4.1.1 Methods of immobilization of aptamers

Aptamers being oligonucleotides are immobilized with chemical methods previously developed for DNA sensors (Wittmann and Marquette, 2006). The most common method for DNA attachment to a surface or affinity reactions are physical adsorption, chemisorption, covalent linking, bio-coating (Balamurugan et al., 2008; Nimse et al., 2014; Zhou et al., 2011).

4.1.2 Physical adsorption

Physical adsorption is the easiest method for attaching nucleic acids to surface as no reagents or modifications are required and where no chemical bonds are formed. Electrostatic attraction between opposite charges of DNA phosphate backbone and surface is the most common mechanism. But adsorption yields a layer of sparsely bound molecules that do not resist thorough washing steps that are required to regenerate the surface. Moreover most of the immobilized probe lies in a position that is not favorable to interactions (Banica, 2012).

Despite these inconveniences, aptamer adsorption-desorption has been used in biosensors with bare carbon, composite carbon (Banica, 2012), graphene oxide (Song et al., 2014; Wu et al., 2011), carbon nanotubes (Li et al., 2014) or titanium dioxide (Zhang et al., 2014) surfaces. Typically adsorbed aptamer is fluorescently-labeled, but fluorescence is quenched due to close proximity with the surface possessing quenching properties. Fluorescence or chemilluminescense signal is reemitted following aptamer desorption from the sensor surface and consequently upon interaction with target.

Although, adsorption is considered as a promising immobilization method for mass-production of disposable screen-printed sensors, for reusable affinity sensors stability of the attached aptamer layer is important during binding and regeneration phase. Thus methods of immobilization based on physical adsorption of DNA by means of electrostatic interactions are not exactly suitable for affinity sensor development.

4.1.3 Chemisorption

Chemisorption is a kind of adsorption, which involves, in contrast with physical adsorption, a chemical reaction between the surface and the adsorbate, creating new chemical bonds on the surface. After chemisorption, compared to physisorption, much less molecules are laying on a surface and more are accessible for interaction. In addition, regeneration doesn't induces desorption of grafted molecules (Lalauze, 2012; Nimse et al., 2014).

A famous example of chemisorption is interaction of gold surface and sulfur functional groups of ligand to form a strong S-Au bond. Sulfur-gold interaction enables a single-point attachment of the probe that gives it conformational mobility that in turn results in a relatively high reactivity (Bain et al., 1989). This method is widely used to graft thiol-labeled aptamers on the gold surface due to its simplicity and because gold layers are often used in various types of chemical and biological sensors (electrochemistry, SPR, QCM, gold nanoparticles etc.).

4.1.4 Covalent attachment

In the covalent approaches a chemical bond is made between the surface and the attached species, which is the irreversible process (Dugas et al., 2010). The nature of this bond and the types of modification which can be carried out depend on the particular surface and the chemical functional groups present on the surface. Therefore it is often required to form suitable functional groups on the support surface prior to crosslinking with the probe. Through covalent attachment aptamers can be immobilized on various substrates such as glass, silicon, carbon, gold, polymers etc. The three most common groups employed for surface attachment of nucleic acids are hydroxyl, amine, and carboxyl (Mascini, 2009).

Hydroxylated surfaces are first modified with carbonyldiimidazole (CDI) to form a reactive intermediate, which forms a stable carbamate bond to an amino-terminated aptamer group.

Amine-terminated surfaces provide several options for aptamer attachment: A surface amine group can be modified with glutaraldehyde, which forms an imine bond leaving the other aldehyde free for repeating this chemistry with an amino-terminated aptamer group; Symmetrical diisothiocyanates have been used as bifunctional linkers for attachment of amine-functionalized surfaces to either thiol-terminated or amine-terminated aptamers.

Carboxyl-terminated surfaces can be coupled to with amino modified-aptamers with EDC/NHS coupling chemistry.

Even though, coupling of probes to a solid support may be time consuming, costly and less successfully achieved than non-covalent attachment, but it results in a rugged recognition layer that is suitable for multiple uses (Banica, 2012).

4.1.5 Bio coatings

Bio coating of surface such as avidin or one of its derivatives, have been shown to be highly successful for immobilizing biotin-tethered aptamers on various surfaces (e.g., gold, silicates, polymers) (Balamurugan et al., 2008). This method is operationally easy, and mainly requires incubation of the biotin-tethered aptamer with the avidin-coated substrate at room temperature in a buffer solution to give efficient immobilization of biotin to avidin (Mascini, 2009). In turn avidin and neutravidin are usually linked chemically to the organic layer formed by 3,3-dithiopropionic acid di(N -succinimidyl ester). Neutravidin is very convenient because it can be chemisorbed directly on gold and glass and does not require additional chemical modification of the surface (Mascini, 2009).

4.1.6 Aim of this study

As we have seen above various surface and aptamer modifications require specific chemical protocols. Some of them are easy to perform but some of them are requiring good hand-one experience. The quality of obtained layers also differs in terms of grafting density, functionality, nonspecific adsorption. Characterization of the immobilized aptamers represents also important point.

The aim of the study discussed in this chapter is to explore aptamer- grafting techniques on various surfaces and to evaluate their application for bio-sensing. Supports for functionalization were selected from based on their properties as sensing platforms. We intended to investigate functionalization of gold and polycarbonate planar substrates and gold and polystyrene nanoparticles.

Gold surface was selected as it is the most utilized surface due to its advantageous properties. Gold is air-stable and doesn't oxidize. It is commercially easily available as a film or as nanoparticles. Gold film can be deposited on various substrates which diversifies its application and utility. Discontinuous gold films, evaporated on transparent substrates with standard microfabrication technologies, show localized surface plasmon extinction in the visible-to-NIR range that is highly sensitive to changes in the dielectric properties of the contacting medium, thus enabling to monitor the binding of molecular layers to the Au film with high sensitivity (Karakouz et al., 2008). Surface plasmon resonance, total internal reflection fluorescence spectroscopy, Surface enhanced resonance Raman and resonance Raman scattering methods are all based on the optical properties of gold (Anker et al., 2008; McNay et al., 2011) In addition gold is good electric conductor and it can be used as the electrode in electrochemical sensors.

The most prevalent property of gold is the ease of immobilization of thiol-bearing molecules, through gold-sulfur bond formation. Formed layer represents monolayer with highly ordered nature (Bain et al., 1989). Considering the fact that gold nanoparticles have larger specific surface than planar surface, we decided to investigate both surfaces.

Polycarbonate represents also very interesting material for sensor development especially for disposable point-of-care sensors, since it is widely available and cheaper than glass (Ahn et al., 2004). It offers advantages of optical transparency for spectroscopic signal recovery and do not quench fluorescence signals as is the case for gold (or other metal) substrates. On the other hand it has improved optical and mechanical properties than many types of glasses, is resistant to chemical, temperature and high impact and what's the most important - it is moldable. In contrast to gold surface, grafting chemistry is a bit complicated, since first functional groups on the surface have to be activated and only then covalent coupling reaction with amino-labeled DNA can be performed.

Polystyrene particles where selected due to their fluorescent properties. Commercially they can be synthetized with various colors and surface functionalities. Compared to gold nanoparticles their density is about 20 times smaller and therefore sedimentation problem doesn't exist even for several μm size particles.

4.2 Experimental

4.2.1 Immobilization of aptamers on gold

In order to immobilize aptamers on gold we used DNA strands with thiol functional group added at the 5' end (Bain et al., 1989). To increase flexibility of the aptamer we added linker composed of 20 thymines between aptameric sequence and thiol group. Sulfur, present in the thiol functional group is known to form moderately stable quasi-covalent (chemoadsorption) bond with gold (126-146 kJ/mol)(Nuzzo et al., 1987). This bond is widely used to attach biological linkers, functional groups and other molecules to gold surfaces. We functionalized both gold films and gold nanoparticles. DNA sample preparation is similar for both cases.

4.2.1.1 Preparation of the thiol-modified DNA for grafting

The terminal sulfur atoms of thiolated DNA form dimers in solution, especially in the presence of oxygen. Dimerization greatly lowers the efficiency of subsequent coupling reactions such as DNA immobilization on gold. Common way to reduce disulfide bonds is to mix thiolated molecule with dithiothreitol (DTT) (Cleland, 1964).

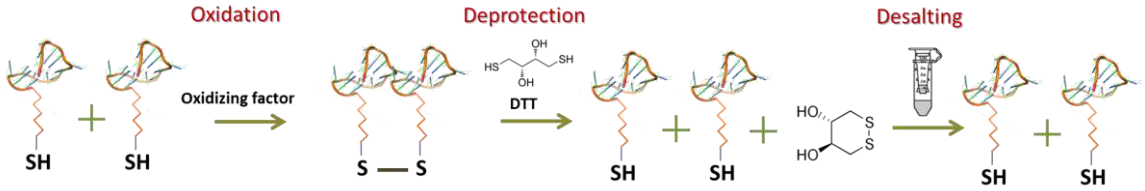

FIGURE 4.2 Schematic representation of oxidation, deprotection and desalting stages of thiolated DNA

In our experiments thiolated ends of aptamer (4 μM) were activated by cleavage of the disulfide bolds using 0.1 M of freshly prepared DTT dissolved in 0.2 mM phosphate buffer over an hour period of incubation at room temperature. DTT was then removed by passing DNA–DTT mixture through the size-exclusion chromatographic column (NAP-5) that can treat up to 50 μL solution retaining small molecules like salt and DTT, but letting larger molecules of DNA to flow through. This procedure is called desalting (Fig. 4.2). During desalting initial concentration of DNA is expected to be reduced with 10%.

4.2.1.2 Functionalization of planar gold surface with thiolated DNA

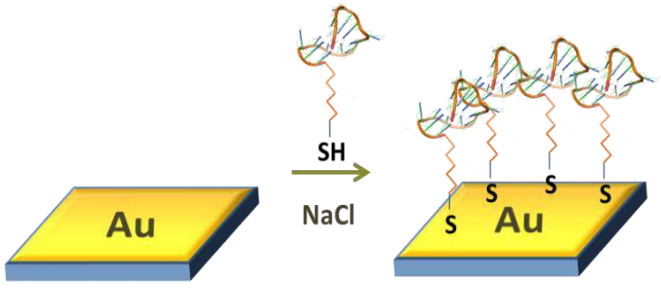

FIGURE 4.3 Schematic illustration of planar gold surface functionalization with thiolated DNA

Gold coated silicon wafer (with 5 nm titanium as adhesion layer, between silicon and 100 nm gold film) was cut in 2x2cm chips. Gold-covered chips were cleaned with freshly prepared Piranha solution for 10 min on a rocker to remove any impurities. The wafer was then rinsed copious amount of double distilled water and dried with N2.

Sample of freshly desalted ssDNA

was mixed with NaCl and PB to obtain solution with final concentration of 0.7 M and 10 mM, respectively. DNA mixture was poured over the gold surface (Fig. 4.3). Treatment with piranha renders gold surface hydrophilic, thus DNA solution spread over the surface and covered it completely. Surface was left to incubate overnight at room temperature in covered Petri dish in the bottom of which was wet tissue paper, in order to maintain high humidity and reduce evaporation of liquids from the sample. After the incubation, the wafer was rinsed with plenty of water and dried under nitrogen flux.

4.2.1.3 Functionalization of gold nanoparticles with thiolated DNA

We used the protocol developed by Mirkin (Mirkin et al., 1996) and further optimized (Hurst et al., 2006; Liu and Lu, 2006) for DNA grafting on gold nanoparticles.

Prior to functionalization, commercial gold nanoparticles, of 20 and 80 nm diameter, were sonicated for 2 minutes to resuspend sedimented and aggregated particles. To ensure that colloid hasn't aggregated and to adjust colloid concentration, the next step was to measure the UV absorbance of the sample. Since gold nanoparticles possess strong plasmon field, they absorb light and, with increasing the size, the characteristic maximum of absorbance increases. So by measuring the absorbance of gold colloid, on one hand it is possible to make a quality check - If particles have aggregated irreversibly, the color of colloid solution will be more bluish and the absorbance maximum will be shifted; and on the other hand, determine the concentration of suspended particles using simply Beer-Lambert law (eq. 2.7).

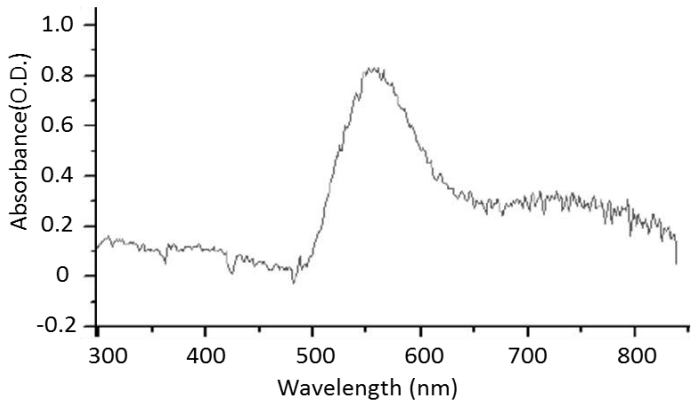

FIGURE 4.4 UV absorbance spectra of 80 nm diameter spherical gold nanoparticles

Absorbance maximum for 20 nm diameter NPs is at 520 nm with extinction coefficient ε =8.78 × 10^8 L/(mol*cm). For 80 nm diameter particles the maximum absorbance is at 550 nm (Fig. 4.4) and corresponding extinction coefficient is ε=6.85 × 10^{10} (Haiss et al., 2007; Liu et al., 2007). For functionalization we adjusted concentration of particles to be to 1 O.D. that corresponds to 7 x 10^{11} and 1.1 x 10^{11} particles respectively for 20 and 80 nm diameter (BBInterntional solutions 2014).

50 µL freshly deprotected thiolated aptamers were added to 950 µL of 1 O.D. NPs and the concentration of phosphates was adjusted to 10 mM by incorporating Phosphate buffer (NaH_2PO_4/K_2HPO) of pH7.4. To avoid aggregation of the gold nanoparticles Tween 20 with final 0.01% concentration was also injected. To facilitate aptamer grafting on the gold surface, the charge at the surface has to be destabilized by addition of NaCl. But sudden increase of salt concentration induces unwanted aggregation of particles. Therefore salt was titrated in small

portions every 20 minutes, so that with each step, increment of salt concentration was 0.1 M, until final concentration of NaCl became 0.7 M. This procedure is called salt aging (Fig. 4.5). After each titration of NaCl, appropriate amount of PB and tween were also added, to maintain constant concentration of PB and surfactant, and sample was sonicated for 1 min. This solution was left overnight on a microtube-rotator to prevent sedimentation.

After overnight incubation, to remove excess DNA, samples were centrifuged at 14000 rpm for 20 and 5 minutes respectively for 20 and 80 nm nanoparticles. The dark pellet of the particles appeared on the bottom of the tube and solution lost purple color. Supernatant was discarded and the pallet was suspended in double distilled water after 1 minute sonication. After three-four centrifugation and re-suspension step, water suspension of DNA-functionalized gold particles was stored at 4°C.

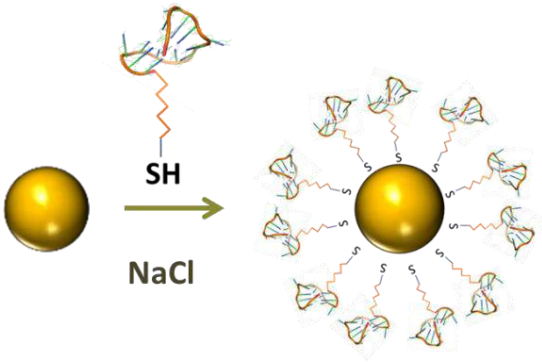

FIGURE 4.5 Schematic illustration of gold NP functionalization of with thiolated DNA

Average size of the gold particles was measured before and after functionalization with DLS method. Observed change of about 15 nm indicated successful functionalization step.

4.2.2 Immobilization of aptamers on the carboxyl-modified polystyrene beads

To functionalize carboxyl modified polystyrene beads (surface titration value of carboxyl is 288 µmoles COOH groups/gram beads) we used ssDNA bearing amino group with C6 linker at 5' extremity. As, for all the cases, here also between aptameric sequence and functional group spacer of 20 thymines was included. For linking the surface and DNA covalently, we used carbodiimide coupling chemistry following the protocol form the manufacturer (TechNote 205 Banglabs).

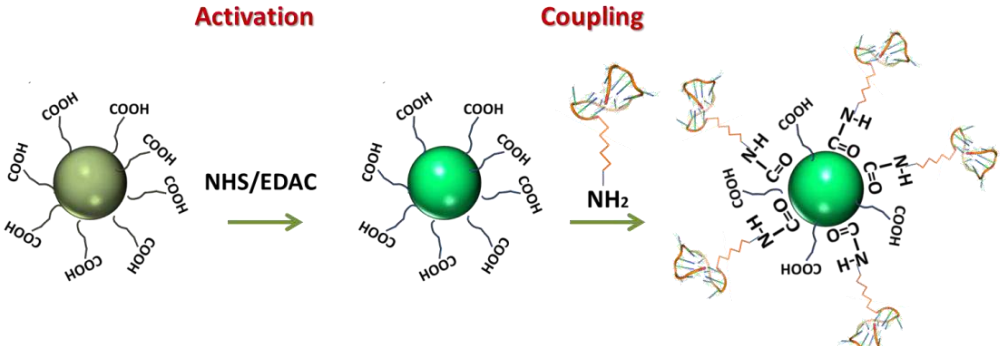

FIGURE 4.6 Schematic illustration of functionalization of carboxyl-modified latex nanoparticles with amino-modified DNA

100 µL of 0.1 µM carboxylate modified fluorescent polystyrene beads of 20 mg/mL concentration were diluted in 900 µL 50 mM MES buffer of pH 4.5. After vortexing for few seconds samples were centrifuged for 30 min at 14000 rpm. Supernatant was discarded and pellet was resuspended in 1mL 50 mM MES buffer. This step was repeated 2 times in order to wash the beads. After last centrifugation, pellet was reconstituted in 500 µL 50 mM MES buffer of pH 6.2, containing 10 mM EDAC and 100 mM NHS and let to incubate for 20 minutes mixing (Fig. 4,6). DNA was added an incubated for 2-3 hours at room temperature in a microtube rotator.

Subsequently mixture was centrifuged for 30 min at 14000 rpm to sediment the particles. The supernatant was removed and 250 µL double-distilled water was added, the mixture was vortexed and sonicated and again centrifuged for 30 minutes. This step was performed twice for water, twice in 10 mM glycine buffer of pH 6, twice with finally particles were resuspended in PBS buffer of pH 7.4 and stored in the fridge at 4 °C.

4.2.3 Immobilization of aptamers on polycarbonate surface

One cm thick polycarbonate sheet was cut into 1x2 cm size rectangular chips. Polycarbonate chips were rinsed with ethanol and dried. To activate i.e. to form polar functionalities and mostly reactive COOH (carboxyl) on the surface of polycarbonate, substrate was introduced inside PVA Tepla microwave Plasma system for O2 Plasma treatment at power of 200 W for 30 seconds.

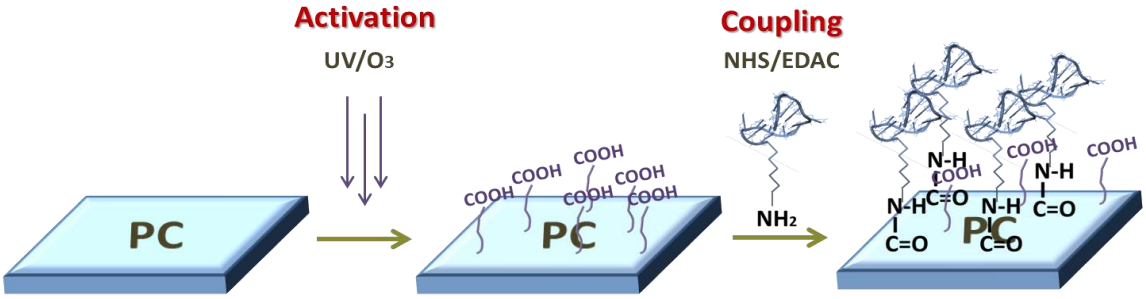

FIGURE 4.7 Schematic illustration of functionalization of polycarbonate surface with amino-modified DNA

Over the activated surface 200µL amino-modified DNA sample was immediately poured. DNA sample contained 1 µM oligonucleotides mixed with 50 mM MES buffer at pH4.5, 10 mM 1-Ethyl-3-(3-Dimethylaminopropyl)carbodiimide (EDAC) and 100 mM N-Hydroxysuccinimide (NHS). Polycarbonate substrate with DNA sample was incubated overnight in the covered petri dish with the wet tissue paper on the bottom to maintain high humidity level. After incubation surface was rinsed with distilled water and dried under nitrogen flux. (Tamarit-López et al., 2011)

4.2.4 Characterization of grafted aptamer functionality by np aggregation

Aggregation experiments were performed with Zetasizer Nano S (Malvern technologies, the principle of the method is described in Chapter 2), that allowed to measure average hydrodynamic radius of the aggregate in time-dependent manner. Aptamer- functionalized nanoparticles were diluted in PBS buffer to obtain final concentration of particles of 0.1 O.D. This concentration of gold nanoparticles corresponds to 1.9 nM aptamers. First the initial size of the NP was measured as the control assuring that there was no aggregation without thrombin, and only then the protein was introduced. Experiments were performed at room temperature in disposable plastic cuvettes for small volume samples.

Verification of aptamers specificity towards nonspecific protein: Specificity of the aptamers towards thrombin was verified by injecting Bovine Serum Albumin of final concentration of 100 nM instead of Thrombin.

4.2.5 Characterization of aptamer grafting density on the surface of gold NPs

4.2.5.1 Determination of surface density of gold nanoparticle-bound-aptamers

In order to determine the density of aptamer grafting, we need to know number of particles in the sample and the amount of DNA in the sample (Demers et al., 2000; Hurst et al., 2006).

For this reason 80 nm gold nanoparticles were functionalized with thiolated HD1 aptamer labeled with fluorescent dye Rhodamine G6. After last step of cleaning, pellet of gold nanoparticles was resuspended in 200 µL solution containing 0.5 M DTT and 0.2 M PB buffer of pH7.4. DTT disrupts gold-sulfur bond and displaces DNA from the particles (Thaxton et al., 2005).

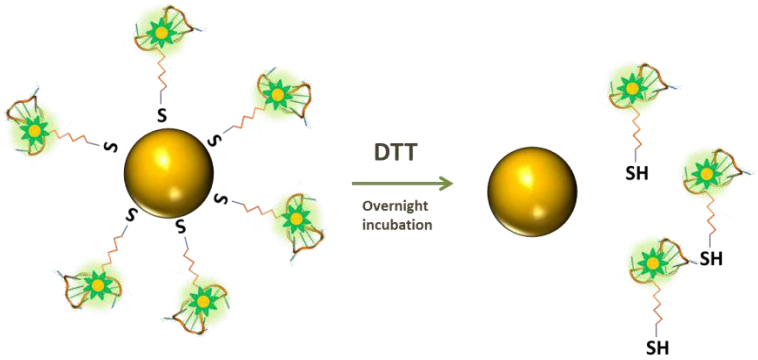

FIGURE 4.8 Illustration of thiolated fluorescent ssDNA displacement after incubation with DTT

Before letting the sample to incubate overnight in the microtube rotator, UV-visible spectroscopy measurement was performed to determine the concentration of gold nanoparticles in the sample (eq. 2.7).

After the overnight incubation oligonucleotides were released into solution (Fig. 4.8). After centrifugation gold precipitate was removed and fluorescence of the sample was measured. To determine oligonucleotide concentration, 80 µL of supernatant was placed in a 96-well plate and the fluorescence was compared to a standard curve prepared by 2 fold serial dilution of 200 nM the same Rhodamine G6 –labeled fluorescent DNA. Because the Rhodamine G6 fluorophore is sensitive to pH, the oligonucleotide samples for the standard curve were prepared with the same 0.5 M DTT and 0.2 M PB buffer solution. During the fluorescence measurement, the fluorophore was excited at 550 nm and the emission was collected at 580 nm, close to the characteristic absorbance and emission maximums of Rhodamine G6. The fluorescence signal was compared to the signals obtained from standard curve and concentration of the fluorescent DNA in the sample was determined.

4.2.5.2 Determination of surface density of functional aptamer

Not all the DNA after functionalization step will be bound to the surface specifically (will be lying on the surface via bonding of the nitrogen lone pairs of the nucleotide bases) or will be accessible for interaction. It is important to know what is the functional aptamer density that are able for interaction with protein or with complementary strand (Demers et al., 2000).

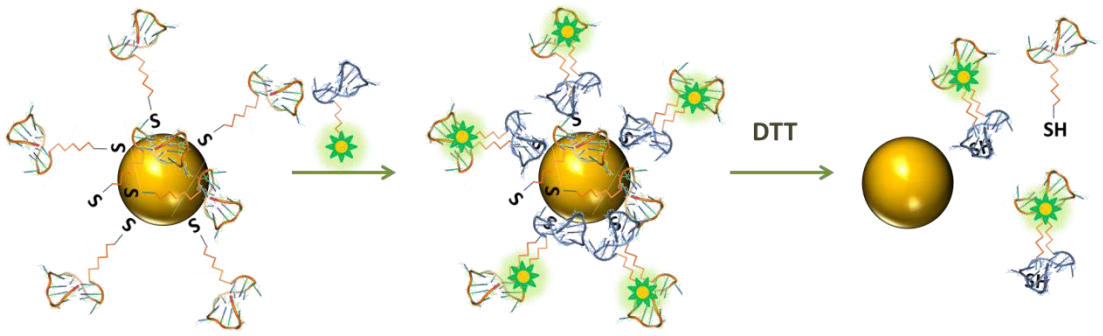

FIGURE 4.9 Illustration of displacement fluorescent dsDNA after incubation with DTT. First AuNP-bound ssDNA was incubated with complementary florescent strand and then both of them were displaced by DTT.

In order to determine how much of grafted DNA is in conformation to bind the target we performed similar experiment as for determination just DNA density with exception that the pellet of 80 nm gold particles functionalized with non-labeled HD1 aptamer, were resuspended in 100 µL PBS solution of pH7.4 containing 500 nM complementary to HD1 ssDNA labeled with Alexa532 fluorophore. To achieve hybridization, sample was incubated for 2 hours at room temperature (Fig. 4.9). After hybridization, it was necessary to remove unbound fluorescent DNA. For this reason sample was centrifuged and supernatant was discarded. Pellet was reconstituted in 200 µL solution of 0.2 M PB and 0.5 M DTT and let to incubate overnight. After incubation, UV absorbance measurement and subsequent centrifugation supernatant was collected and fluorescence was compared with fluorescence of the standard curve of 20 to 100 nM concentration samples. During the fluorescence measurement, the fluorophore was excited at 530 nm and the emission was collected at 560 nm.

4.3 Validation algorithm

Here we have to mention that we did not intend to carry out in-depth characterization of surface with sophisticated methods nor developed new ways or methods for aptamer grafting on the surface, but we tried to evaluate what we should expect from the different simple grafting methods on important and widely used material surfaces. Using only optical microscopy, dynamic light scattering (DLS), Zeta potential, UV-vis and fluorescence spectroscopy we followed the **validation criteria** to characterize aptamer grafting.

4.3.1 Validation Criteria:

Qualitative criteria:

- Show that **surface is DNA functionalize**d observing with microscopy or Zetapotential/DLS;
- Verify whether **grafted aptamers are functioning** to recognize specific targets

Quantitative criteria:

- Characterize (if possible) **surface density of grafted aptamers** and their **functional efficiency**.

To assume that aptamer immobilization was successful qualitative criterion needs to be fulfilled unconditionally.

Under verifying functional capabilities of immobilized aptamers we mean indeed examining interactions of surface-bound aptamers with thrombin. For nanoparticles this can be achieved by mixing aptamer-bound nanoparticles with thrombin and observing the change of average diameter by DLS method. But mixing particles with different aptamers recognizing distinct epitopes of thrombin in the presence of thrombin, should lead to the interlinking particles and lead to aggregation. If functionalization is not successful or thrombin is not accessible, no aggregation should be observed.

4.4 Results of aptamer immobilization on planar support

Immobilization of aptamers on the planar support has crucial importance for reusable, solid-phase affinity sensors. We decided to investigate aptamer immobilization on two distinct planar surfaces; polycarbonate and gold, with different optical and chemical properties and requiring distinct chemical procedures, but both of them have very high potential to be used as a support for immobilization of sensing element. However we highlight, that the characterization used for planar supports is minimal compared to nanoparticles.

4.4.1 Polycarbonate substrate

Thus first candidate for the functionalization was polycarbonate substrate. We functionalized by O2 plasma activation and subsequently formed carboxyl groups were coupled with carbodiimide chemistry to amino-modified DNA. In order to visualize the presence of DNA on the surface, we grafted on the surface fluorescently labeled amino-modified DNA bearing Alexa 532 fluorophore.

We tried to observe fluorescence intensity difference between non-functionalized and DNA-functionalized PC surface by means of fluorescence microscopy. We were surprised to see that both modified and non-modified surface, when illuminated with green light for excitation Alexa532, were fluorescent. In fact, whole thickness of the polycarbonate sample was fluorescent. This was an effect of autofluoresence. Studies (Hawkins and Yager, 2003; Piruska et al., 2005) show that due to some additives or impurities introduced during the manufacturing, PC might exhibit strong absorbance and certain level of autofluoresence, that may fade out to a lower intensity with the time (several hours) of light exposure, but it can be still limiting factor for high-sensitivity optical fluorescence detection.

Different studies have shown successful application of the polycarbonate surface (Ahn et al., 2004; Tamarit-López et al., 2011), but it is worth mentioning that quality of the PC varies with the differences in processes of manufacturing that will manifest themselves as differences in fluorescence. Also important is that the post-production age and handling of material from the same vendor can vary.

Thus, failing the very first validation criteria and learning that PC surface is not always the best choice for application in sensing, we didn't continue any further experiments with polycarbonate surface.

4.4.2 Gold surface

Next we investigated aptamer immobilization on gold surface, deposited over the surface of silicon wafer. For immobilization we used thiol-terminated aptamers and followed well established protocol. In order to verify aptamer grafting through microscope, aptamers where fluorescently labeled with Rhodamine G6 dye. (Fig. 4.10)

The difference in fluorescence intensity between functionalized and non-functionalized surface was significant. We saw clear brightness of the Rhodamine G6 modified gold specimen compared to control gold surface. This result gives us possibility to get the qualitative information, that functionalization step was successful, but for characterization whether immobilization is due to physisorption or chemisorption and how functional are grafted aptamers require further experiments.

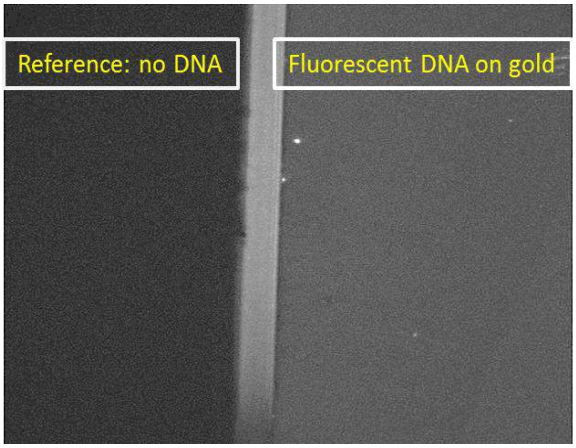

FIGURE 4.10 Grafting of the DNA on planar gold surface. On the left is the non-modified gold surface. On the right, thiolated DNA labeled with Rhodamine G6 fluorophore is grafted on the gold surface.

Methods that have been used for surface analysis of structure and composition of the aptamer monolayers include X-ray photoelectron spectroscopy (XPS) and infrared spectroscopy methods (Opdahl et al., 2007), contact angle measurements, quartz crystal microbalance, and electrochemical methods (Castelino et al., 2005; Herne and Tarlov, 1997). However these methods require special instruments and expertise. We decided to simplify characterization problem by using gold nanoparticles, that are easier to be handled than planar surface, but general properties of grafting would be the same.

4.5 Results of aptamer immobilization on nanoparticles

On one hand nanoparticle represent nano-scale surfaces, that are easier to handle but, on other hand, nanoparticles on their own are important objects with properties unique to nano-objects (Anker et al., 2008). In addition, nanoparticles offer the advantage of high surface to volume ratios and the possibility of combining with bulk characterization techniques. Thus, investigating their functionalization for application in bio-sensing is also very interesting subject.

4.5.1 Gold nanoparticles

First, gold nanoparticles were functionalized to answer the open question from the functionalization of planar gold surface. Since they possess unique properties such as colorimetric, conductivity, nonlinear optical properties, easy functionalization with biological recognition elements, gold nanoparticles also hold great promise for biosensing together with biological and medicinal applications.

We functionalized gold nanoparticles of 20 or 80 nm size through chemisorption of thiolated ssDNA strands. To verify that the particle were well functionalized we performed measurement of the average hydrodynamic diameter by dynamic light scattering before and after functionalization procedure. Average change in size with 20-25 nm for 20 nm diameter and 15-20 nm for 80 nm diameter particles confirmed successful grafting of the DNA on the surface of the particles. Fig. 4.11 shows the overlaid distributions of size of particles before and after functionalization step.

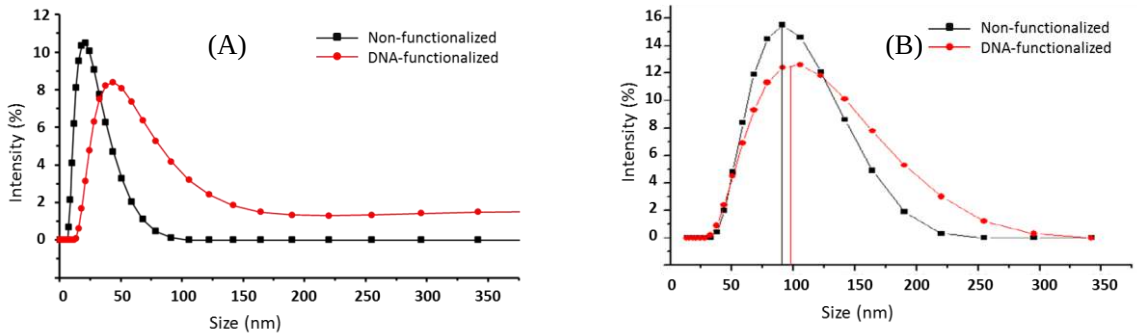

FIGURE 4.11 Size distribution of non-functionalized and aptamer-functionalized (A) 20 nm and (B) 80 nm size gold nanoparticles measured with DLS

The onset in hydrodynamic radius is related to the fact that aptamers are polymers with intra-chain hydrodynamic interactions (Zimm model), which increases the overall hydrodynamic drag of NP plus aptamers. Effect is larger on smaller particles, therefor average change in size after functionalization for 20 nm gold nanoparticles is larger than in the case of 80 nm size NPs (Diallo et al., 2009; Zimm and Bragg, 1959).

Measuring Zeta potential of the particles, the effective surface potential at the hydrodynamic "shear surface" close to the solid-liquid interface, showed how surface charge of gold particles changed after functionalization step. It is assumed that for bear metal particles without an oxide layer, surface shouldn't have inherent change but the negative zeta potential is due to preferential adsorption of negative ions to the surface. For coated particles zeta potential

describes the region at the boundary between the solvent and the coating. (Dougherty et al., 2008) The initial zeta potential for bear AuNP measured in water was -39 ± 1 mV, after functionalization step zeta potential of aptamer-functionalized gold particles became -27± 1 mV, this significant change also confirms the successful functionalization.

After having confirmed that functionalization step was successful, we wanted to verify whether the surface-grafted aptamers survived grafting procedure and still maintained their aptameric character of binding target.

4.5.2 Aggregation of aptamer-functionalized Nanoparticles

To show that aptamers where functioning well we decided induce the aggregation of the aptamer-functionalized particles. Since HD1 and HD22 can simultaneously interact with two distinct exosites of the same thrombin molecule, thrombin can act as the linker or bridge between two NPs functionalized one with HD1 (HD1-AuNP) and the second with HD22 (HD22-AuNP) (Fig. 4.12).

Aggregation of particles functionalized with complementary strands, or with strands interacting with the common target, has been previously shown in many studies including for thrombin and its aptamers (Lin et al., 2009; Mirkin et al., 1996; Pavlov et al., 2004; Zhao et al., 2008). In most studies aggregation kinetics is followed by eye or UV absorbance technique, where they observe the change of characteristic absorbance spectrum (shift of the colloid color form Bordeaux to purple and blue with increase of the size) upon aggregation. We instead followed course of aggregation with DLS, measuring the instant average size of aggregate with defined time intervals.

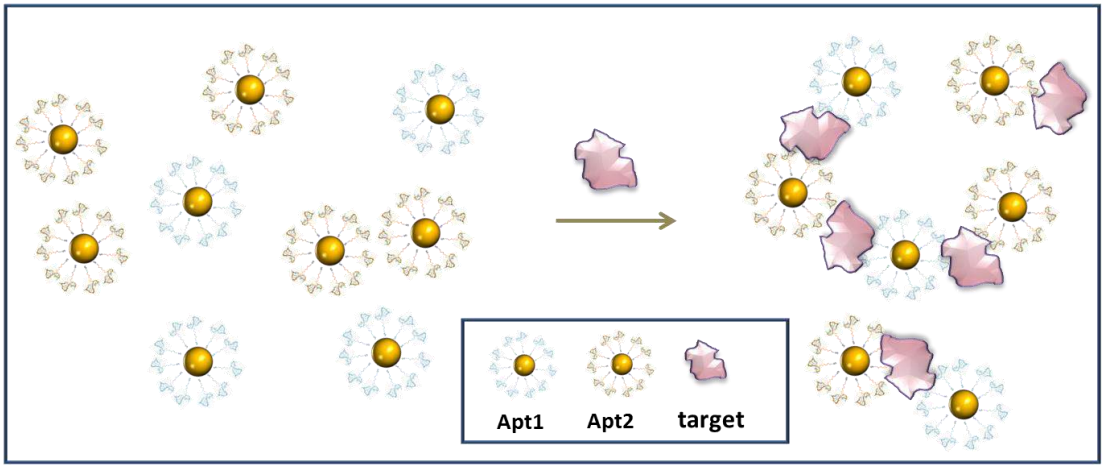

FIGURE 4.12 Schematic illustration of thrombin-assisted aggregation of nanoparticles functionalized with aptamers interacting either with one or another exosite of thrombin.

We performed aggregation experiment with the mixture of 20 nm size HD1-AuNP and HD22-AuNP in the presence of 30 nM thrombin. As we see on the Fig.4.13 (A), the particle aggregation induced by thrombin started immediately and aggregate size reached up to 800 nm in following 40 minutes. Thus we endorsed the activity of the grafted aptamers.

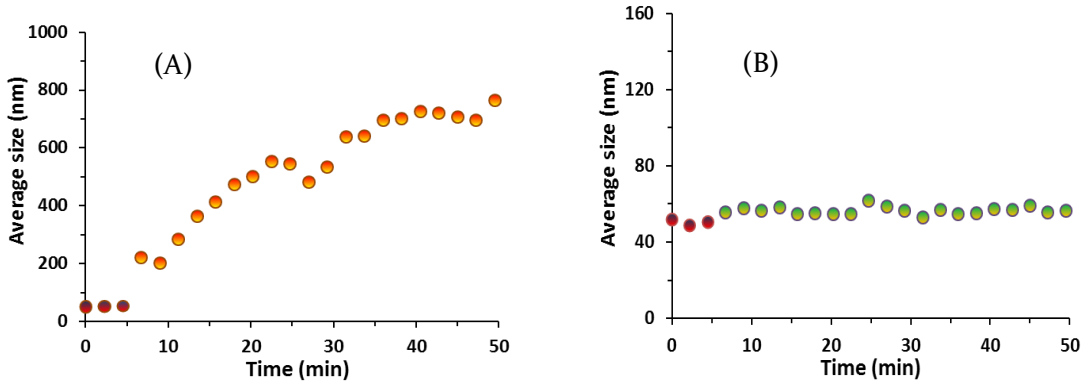

FIGURE 4.13 Aggregation kinetics of 20 nm size AuNP functionalized with HD1 or HD22 aptamers in the presence of (A) 30 nM Thrombin and (B) 100 nM BSA. First three points represent the average size of AuNP before aggregation in the absence of a protein.

In order to make sure that this aggregation didn't occur due to perturbation of the balance of colloid system in the presence of any protein leading to aggregation, we decided to perform similar aggregation experiment with BSA, the protein that is non-specific to aptamers and is present in plasma in high amount. Fig. 4.13 (B) shows that the titration of BSA in the mixture of 20 nm size HD1-AuNP and HD22-AuNP induced only marginal increase (3-5 nm) of average size of the particles and no further increase in averages size, indicating aggregation, was observed. This result shows that aggregation in the presence of thrombin indeed happened due to specific and simultaneous interaction of HD1- and HD22- modified NPs with appropriate binding sites of thrombin.

In addition, a significant result is that, we can argue that in the case of BSA observed slight augmentation of the average size was due to nonspecific interaction with one of the aptamers but since there was no simultaneous interaction with both aptamers no aggregation was observed and, basically, with this example we demonstrate how targeting two sites at once improves the specificity of detection. This lets us to use aggregation not only to characterize functionality of grafted aptamers but also to use this approach as the method of sensing. Nevertheless, there is still need to characterize the density of grafted aptamers and the density of the aptamers functional for interaction that cannot be assessed neither by DLS nor zeta potential.

4.5.3 Characterization of density of total and functional grafted-DNA

Now when the two unconditional criteria (successful grafting and functional aptamers) are fulfilled and gold nanoparticles show good functionality and specificity after functionalization, it is interesting to characterize grafting quantitatively.

In order to characterize the density of grafted molecule on the surface of the gold nano particles we functionalized 80 nm diameter gold particles with thiol modified DNA fluorescently labeled with Rhodamine G6. Nanoparticle concentration was determined sing UV-vis spectroscopy. Nanoparticle-bound oligonucleotides were liberated into solution by addition of DTT, and quantified using fluorescence spectroscopy. The formulas for calculation aptamer grafting density are following:

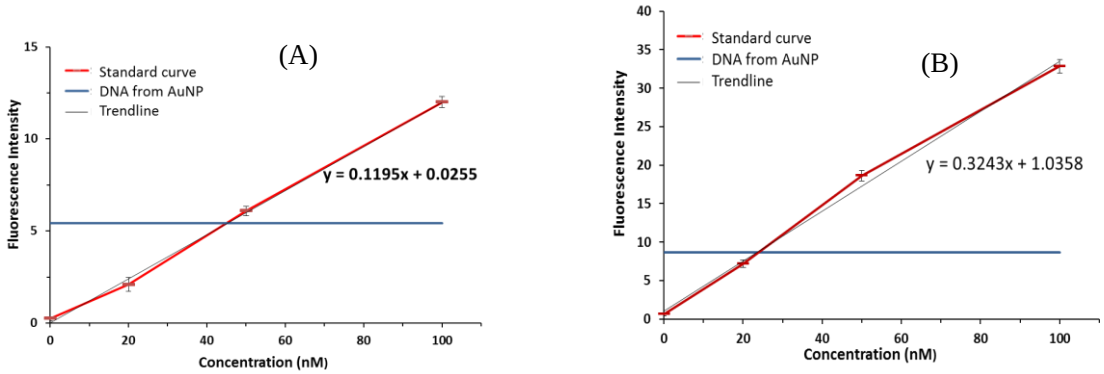

FIGURE 4.14 Standard curve of dependence of fluorescence intensity on concentration of DNA labeled with (A)Rodhamine G6 and (B) Alexa 532. Blue Line corresponds to the concentration of the ssDNA displaced from the surface of gold nanoparticles by 200 µL DTT solution.

The ratio of the fluorescent DNA concentration (C_{DNA}) and AuNP concentration (C_{AuNP}) in the sample, give the number (n) of DNA strands per particle.

$$n = \frac{C_{DNA}}{C_{AuNP}} \tag{4.1}$$

Assuming that nanoparticles are all spherical with defined diameter (d), the surface area of the particle can be calculated.

$$S = \pi d^2 \tag{4.2}$$

Dividing the number of DNA (n) per particle on the surface area (S) of the particle, we obtain the surface density of the DNA coverage (ρ).

$$\rho = \frac{n}{S} = \frac{C_{DNA}}{C_{AuNP}} \times \frac{1}{\pi d^2} \tag{4.3}$$

After calculations we found that 46.1 ±0.5 nM (Fig. 4.14 (A))concentration Rhodamine G6 – labeled DNA was displaced from 0.035 nM gold NP (Abs(550nm)=2.37 O.D.) in 200 µL DTT+PB solution. Meaning that in average 1326 DNA strands were grafted on the surface of each 80 nm diameter particle, which corresponds to the 6.6 x 10^{12} DNA/cm^2 surface density.

On the other hand to verify how many out of grafted DNA were accessible for the interaction DNA-functionalized 80 nm gold nanoparticles where incubated with complementary strand labeled with Alexa 532 fluorophore. Concentration of gold nanoparticle and double stranded DNA liberated after DTT treatment was determined similarly as described above.

Hybridization of the nanoparticle-bound ssDNA with its complementary strand labeled with Alexa532 fluorophore revealed that the concentration of DNA available for hybridization, corresponding to 0.049 nM gold NP (Abs(550nm)=3.34 O.D.), was 22.5 ±0.5 nM (Fig.4.14(B)). That gives us about 460 functional DNA per particle of 80 nm diameter i.e. surface density of functional DNA is 2.3 x 10^{12} DNA/cm^2. The ratio between functional DNA density and DNA grafting density, we get that about only 35% of grafted DNA is accessible for interaction.

Obtained results are in good conformity with the results reported by earlier studies (Hurst et al., 2006), where they investigated effect of spacer, experimental conditions and size of the particles on the density of DNA grafting. Smaller particles where showed to have higher DNA coverage than larger. In addition, taking in account that surface area to volume ratio of particles increases with the decrease of the particle diameter, we can imagine that small particles represent very strong platforms for bio-sensing.

Overall carried out experiments showed how easily can be gold nanoparticles functionalized and characterized. Also the aggregation assay, used to demonstrate aptamer functionality offers opportunities to investigate different points in low cost, which we will discuss later on in this chapter.

4.5.4 Polystyrene nanoparticles direct and indirect assembly

Seeing that gold nanoparticles where so easy to handle and functionalize we decides to investigate other aptamer grafting methods with different chemistry also on the nanoparticles. For this reason, we choose to try functionalization of polystyrene nanoparticles bearing carboxylate moieties on the surface. This choice was made because polystyrene particles offer some interesting properties that are not available for gold particles such as: low density (1,05 g/cm³, compared to gold density 19.30 g/cm³),making them less prone to sedimentation; fluoresce, allowing observing interaction (aggregation) with fluorescence methods; possibility of incorporation of magnetic cores and various surface modification.

We used 100 nm size fluorescent polystyrene nanoparticles with carboxyl groups to explore the amino coupling reaction with amino modified aptamers.

Measurement of the hydrodynamic diameter of the particles with DLS before and after functionalization steps showed increase of average size with 15 nm, indicating successful grafting of the DNA. However results of zeta potential measurement were ambiguous. No significant change was observed between the potentials of particles before and after functionalization,-48±2 and -45±1 mV respectively.

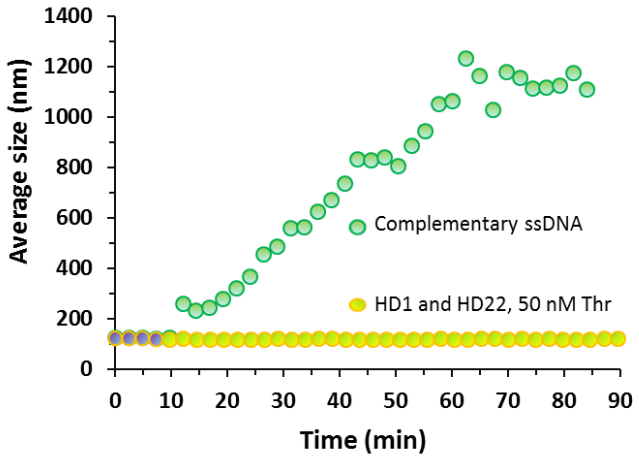

FIGURE 4.15 Aggregation of 100 nm size polystyrene particles functionalized either with complementary ssDNA strands (green) or with HD1 and HD22 aptamers in the presence of 50 nM Thrombin (yellow). First four points correspond to average size of AuNP before introducing particles with complementary strands (green) or in the absence of thrombin (yellow)

To verify DNA grafting quality and functionality, here also we applied aggregation approach. We let the mixture of polystyrene particles functionalized with HD1 and HD22 aptamers to interact with thrombin and consequently form the aggregates. However, contrary to functionalized gold particles, polystyrene particles didn't show any aggregation tendency. The reasons of failing aggregation test can be either unsuccessful functionalization step or alterations of the aptamers folding after the chemical procedure.

To find the underlying causes, we performed experiment of direct aggregation of polystyrene particles functionalized with complementary strands. As it's shown on the fig. 4.15 assembly through the hybridization of complementary strands was successful. These results lead us to think that the surface charge of carboxyl groups on this particular type of particles is perturbing aptamer folding and consequently distract recognition and binding of thrombin.

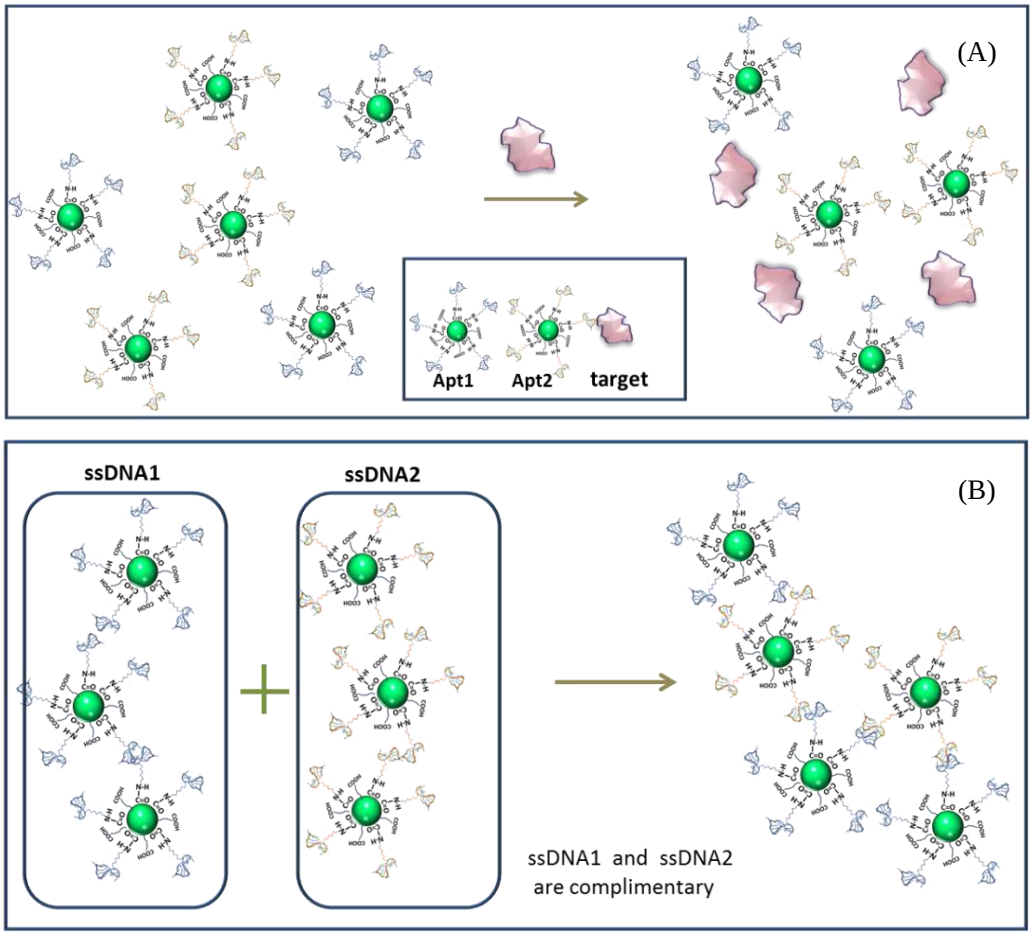

FIGURE 4.16 Illustration of assembly of carboxyl-modified 100 nm size functionalized with amino-terminated (A) aptamers in the presence of thrombin and (B) complementary strands. (A) Presence of thrombin didn't lead to aggregation of aptamer-covered particles. (B) mixing particles functionalized with complementary strands led to hybridization and aggregation.

It would have been interesting to investigate what would be the outcome of the amino coupling reaction if the DNA had carboxyl modification and polystyrene particles had amino terminations. But, having performed functionalization of carboxyl-modified polystyrene with amino-terminated aptamers using various modifications of protocols and still getting unsuccessful conditions for aptamers, no further investigation of polymer functionalization was conducted.

Surfaces that have been chemically functionalized to provide–NH2 or COOH groups for covalent attachment still offer a rather large surface area for adsorption. Hence, unless serious control methods are used, molecules covalently immobilized on such surfaces may represent a minority; hydrophobically adsorbed molecules may comprise the majority. Some studies have shown that immobilization process can significantly alter the biological activity of the reactant; most adsorbed proteins on polystyrene or silicone are partially or largely denatured (Butler, 2000).

4.6 Conclusions

In this chapter we attempted aptamer immobilization on planar surface of gold and polycarbonate and on gold and polystyrene nanoparticles. We used simple characterization tools to investigate successfulness of surface functionalization in different cases.

From point of view of the easiness of functionalization, in both cases, for polycarbonate as well as for gold planar surfaces, aptamer immobilization procedures were one-step and easy to carry out. But qualitative characterization of aptamer grafting with fluorescence microscopy being successful and sufficient for gold surface, was absolutely impossible for polycarbonate surface due to inherent internal fluorescence, existence of which depend from the origin.

Exploring aptamer grafting methods on nanoparticles we investigated thiolated aptamer immobilization on the surface of gold nanoparticles and amino-terminated aptamer immobilization through amino coupling reaction on the carboxyl modified surface of polystyrene particles. Functionalization of gold particles is achieved easily after stepwise titration of salt in the thiolated DNA and AuNP mixture. Surface density of total immobilized and functional immobilized DNA was determined using simple methods as UV-vis spectrometry, Fluorescence spectrometry and DLS. In the case of polystyrene particles, even though measurements of average size confirmed successful grafting of the aptamers on the surface, absence of aggregation in the presence of thrombin indicated that grafted aptamers were not functional. Thus, comparing above discussed two methods, gold nanoparticles show clear advantage over carboxyl modified polystyrene particles, in terms of easiness of functionalization, characterization and the quality of resulting surface.

4.7 References

Ahn, C.H., Choi, J.-W., Beaucage, G., Nevin, J.H., Lee, J.-B., Puntambekar, A., and Lee, J.Y. (2004). Disposable smart lab on a chip for point-of-care clinical diagnostics. Proc. IEEE *92*, 154–173.

Anker, J.N., Hall, W.P., Lyandres, O., Shah, N.C., Zhao, J., and Van Duyne, R.P. (2008). Biosensing with plasmonic nanosensors. Nat. Mater. *7*, 442–453.

Bain, C.D., Troughton, E.B., Tao, Y.T., Evall, J., Whitesides, G.M., and Nuzzo, R.G. (1989). Formation of monolayer films by the spontaneous assembly of organic thiols from solution onto gold. J. Am. Chem. Soc. *111*, 321–335.

Balamurugan, S., Obubuafo, A., Soper, S.A., and Spivak, D.A. (2008). Surface immobilization methods for aptamer diagnostic applications. Anal. Bioanal. Chem. *390*, 1009–1021.

Banica, F.-G. (2012). Chemical Sensors and Biosensors: Fundamentals and Applications (John Wiley & Sons).

BBI solutions 2014 Molar Concentration of Nanoparticles - BBI SolutionsBBI Solutions.

Butler, J.E. (2000). Solid supports in enzyme-linked immunosorbent assay and other solid-phase immunoassays. Methods San Diego Calif *22*, 4–23.

Castelino, K., Kannan, B., and Majumdar, A. (2005). Characterization of grafting density and binding efficiency of DNA and proteins on gold surfaces. Langmuir ACS J. Surf. Colloids *21*, 1956–1961.

Cleland, W.W. (1964). Dithiothreitol, a New Protective Reagent for SH Groups*. Biochemistry (Mosc.) *3*, 480–482.

Demers, L.M., Mirkin, C.A., Mucic, R.C., Reynolds, R.A., Letsinger, R.L., Elghanian, R., and Viswanadham, G. (2000). A Fluorescence-Based Method for Determining the Surface Coverage and Hybridization Efficiency of Thiol-Capped Oligonucleotides Bound to Gold Thin Films and Nanoparticles. Anal. Chem. *72*, 5535–5541.

Diallo, M., Street, A., Sustich, R., Duncan, J., and Savage, N. (2009). Nanotechnology Applications for Clean Water: Solutions for Improving Water Quality (William Andrew).

Dougherty, G.M., Rose, K.A., Tok, J.B.-H., Pannu, S.S., Chuang, F.Y.S., Sha, M.Y., Chakarova, G., and Penn, S.G. (2008). The zeta potential of surface-functionalized metallic nanorod particles in aqueous solution. Electrophoresis *29*, 1131–1139.

Dugas, V., Elaissari, A., and Chevalier, Y. (2010). Surface Sensitization Techniques and Recognition Receptors Immobilization on Biosensors and Microarrays. In Recognition Receptors in Biosensors, M. Zourob, ed. (Springer New York), pp. 47–134.

Esteban Fernández de Ávila, B., Watkins, H.M., Pingarrón, J.M., Plaxco, K.W., Palleschi, G., and Ricci, F. (2013). Determinants of the Detection Limit and Specificity of Surface-Based Biosensors. Anal. Chem. *85*, 6593–6597.

Haiss, W., Thanh, N.T.K., Aveyard, J., and Fernig, D.G. (2007). Determination of Size and Concentration of Gold Nanoparticles from UV–Vis Spectra. Anal. Chem. *79*, 4215–4221.

Hawkins, K.R., and Yager, P. (2003). Nonlinear decrease of background fluorescence in polymer thin-films – a survey of materials and how they can complicate fluorescence detection in μTAS. Lab. Chip *3*, 248–252.

Herne, T.M., and Tarlov, M.J. (1997). Characterization of DNA Probes Immobilized on Gold Surfaces. J. Am. Chem. Soc. *119*, 8916–8920.

Hurst, S.J., Lytton-Jean, A.K.R., and Mirkin, C.A. (2006). Maximizing DNA Loading on a Range of Gold Nanoparticle Sizes. Anal. Chem. *78*, 8313–8318.

Karakouz, T., Vaskevich, A., and Rubinstein, I. (2008). Polymer-coated gold island films as localized plasmon transducers for gas sensing. J. Phys. Chem. B *112*, 14530–14538.

Lalauze, R. (2012). Chemical Sensors and Biosensors (John Wiley & Sons).

Li, Z., Qi, H., Yang, H., Gao, Q., and Zhang, C. (2014). Simple and highly sensitive electrogenerated chemiluminescence adenosine aptasensor formed by adsorbing a ruthenium complex-tagged aptamer on single-walled carbon nanotubes. Anal. Methods *6*, 1317–1323.

Lin, Y.-W., Liu, C.-W., and Chang, H.-T. (2009). DNA functionalized gold nanoparticles for bioanalysis. Anal. Methods *1*, 14–24.

Liu, J., and Lu, Y. (2006). Preparation of aptamer-linked gold nanoparticle purple aggregates for colorimetric sensing of analytes. Nat. Protoc. *1*, 246–252.

Liu, X., Atwater, M., Wang, J., and Huo, Q. (2007). Extinction coefficient of gold nanoparticles with different sizes and different capping ligands. Colloids Surf. B Biointerfaces *58*, 3–7.

Mascini, M. (2009). Aptamers in Bioanalysis (John Wiley & Sons).

McNay, G., Eustace, D., Smith, W.E., Faulds, K., and Graham, D. (2011). Surface-Enhanced Raman Scattering (SERS) and Surface-Enhanced Resonance Raman Scattering (SERRS): A Review of Applications. Appl. Spectrosc. *65*, 825–837.

Mirkin, C.A., Letsinger, R.L., Mucic, R.C., and Storhoff, J.J. (1996). A DNA-based method for rationally assembling nanoparticles into macroscopic materials. Nature *382*, 607–609.

Nimse, S.B., Song, K., Sonawane, M.D., Sayyed, D.R., and Kim, T. (2014). Immobilization Techniques for Microarray: Challenges and Applications. Sensors *14*, 22208–22229.

Nuzzo, R.G., Fusco, F.A., and Allara, D.L. (1987). Spontaneously organized molecular assemblies. 3. Preparation and properties of solution adsorbed monolayers of organic disulfides on gold surfaces. J. Am. Chem. Soc. *109*, 2358–2368.

Opdahl, A., Petrovykh, D.Y., Kimura-Suda, H., Tarlov, M.J., and Whitman, L.J. (2007). Independent control of grafting density and conformation of single-stranded DNA brushes. Proc. Natl. Acad. Sci. U. S. A. *104*, 9–14.

Pavlov, V., Xiao, Y., Shlyahovsky, B., and Willner, I. (2004). Aptamer-Functionalized Au Nanoparticles for the Amplified Optical Detection of Thrombin. J. Am. Chem. Soc. *126*, 11768–11769.

Piruska, A., Nikcevic, I., Lee, S.H., Ahn, C., Heineman, W.R., Limbach, P.A., and Seliskar, C.J. (2005). The autofluorescence of plastic materials and chips measured under laser irradiation. Lab. Chip *5*, 1348–1354.

Song, J., Lau, P.S., Liu, M., Shuang, S., Dong, C., and Li, Y. (2014). A General Strategy to Create RNA Aptamer Sensors Using "Regulated" Graphene Oxide Adsorption. ACS Appl. Mater. Interfaces 140703100132000.

Tamarit-López, J., Morais, S., Puchades, R., and Maquieira, Á. (2011). Oxygen Plasma Treated Interactive Polycarbonate DNA Microarraying Platform. Bioconjug. Chem. *22*, 2573–2580.

Taylor, R.F., and Schultz, J.S. (1996). Handbook of Chemical and Biological Sensors (CRC Press).

Thaxton, C.S., Hill, H.D., Georganopoulou, D.G., Stoeva, S.I., and Mirkin, C.A. (2005). A bio-bar-code assay based upon dithiothreitol-induced oligonucleotide release. Anal. Chem. *77*, 8174–8178.

Tolle, F., and Mayer, G. (2012). Dressed for success – applying chemistry to modulate aptamer functionality. Chem. Sci. *4*, 60–67.

Wittmann, C., and Marquette, C. (2006). DNA Immobilization. In Encyclopedia of Analytical Chemistry, (John Wiley & Sons, Ltd),.

Wu, M., Kempaiah, R., Huang, P.-J.J., Maheshwari, V., and Liu, J. (2011). Adsorption and Desorption of DNA on Graphene Oxide Studied by Fluorescently Labeled Oligonucleotides. Langmuir *27*, 2731–2738.

Zhang, X., Wang, F., Liu, B., Kelly, E.Y., Servos, M.R., and Liu, J. (2014). Adsorption of DNA Oligonucleotides by Titanium Dioxide Nanoparticles. Langmuir *30*, 839–845.

Zhao, W., Brook, M.A., and Li, Y. (2008). Design of gold nanoparticle-based colorimetric biosensing assays. Chembiochem Eur. J. Chem. Biol. *9*, 2363–2371.

Zhou, L., Wang, M.-H., Wang, J.-P., and Ye, Z.-Z. (2011). Application of Biosensor Surface Immobilization Methods for Aptamer. Chin. J. Anal. Chem. *39*, 432–438.

Zimm, B.H., and Bragg, J.K. (1959). Theory of the Phase Transition between Helix and Random Coil in Polypeptide Chains. J. Chem. Phys. *31*, 526–535.

CHAPTER 5. SELF-ASSEMBLY OF APTAMER-FUNCTIONALIZED GOLD NANOPARTICLES ON PLANAR SURFACES

5.1 Introduction

In previous chapter we discussed several surface functionalization methods for their application in bio-sensing. We showed, that gold nanoparticles being, on one hand, simple and effective to functionalize and, on the other hand, easy to manipulate and characterize, represent perfect objects for sensing. We also demonstrated the application of aptamer-functionalized gold nanoparticles for thrombin sensing in liquid phase. But what if instead of using functionalized gold particles in volume we arranged them on surface? This would allow us creating well-characterized gold nanoparticle interface for solid state detection devices. In addition, the arrangement of nanoparticles on the surface also grants us possibility to exploit all those interesting properties that appear only in well order particle arrangements thus facilitating the detection scheme.

Organized colloidal layers and arrays exhibit unique properties that open up new and exciting opportunities in the field of nanotechnology. For example, collective optical, magnetic, electric or transport properties enable novel optical devices, narrow-band optical filters, waveguides, anti-reflecting and self-cleaning coatings, energy storage devices, information carriers, catalysts, highly sensitive chemical, biological, gas and humidity sensors (Edel et al., 2013; Malaquin et al., 2007; Shipway et al., 2000; Velev and Gupta, 2009; Yang et al., 2002).

In our case, using arranged nanoparticles as immobilizers for bio-molecules and electron transfer enhancers would have important added value for the development of a biosensor. Namely, for electrochemical (Orozco et al., 2012) and optical sensing using effects like localized surface plasmon resonance (LSPR) (Sannomiya et al., 2009; Shao et al., 2010), surface-enhanced Raman scattering (SERS) (Cho et al., 2008). Therefore in this chapter, we would like to explore the possibility of arrangement of the aptamer-functionalized gold nanoparticles on solid substrates for integration of reusable biosensors.

5.1.1 Overview of nanoparticle self-assembly on surfaces

Integration of the nanoparticles on the surfaces represents one of the main challenges in the development of the next-generation electronic devices and sensors. The critical step is the capability to direct and control the assembly of nanoparticles (NPs) into distinct patterns and arrays on a variety of substrates. Conventional top-down fabrication methods could be time-consuming and unsuitable for direct handling of nanoparticles. Bottom-up assembly techniques which take advantage of self-assembly processes occurring in fluidic environments to organize particles along desired patterns have been vaunted as promising technologies (Grzelczak et al., 2010).

Self-assembly of nano/micro objects into ordered arrangements on the surface is driven by the interaction forces such as Van der Waals, hydrophobic, electrostatic, capillary, and hydrodynamic forces acting between colloidal particles and/or particles and surface (Whitesides and Grzybowski, 2002). A number of studies have been conducted in order to achieve the control over one or several of these influencing forces and thus drive the "bottom-up" assembly of the colloidal objects on the surface (Mastrangeli et al., 2009). Immobilization of the particles on the surface can be achieved either by chemical or physical attachment (Handbook of nanofabrication 2010).

Chemical approach of particle self-assembly is a powerful approach to obtain a high-quality monolayer or structure of organized layers relying on covalent and non-covalent interactions of linkers covering the surface either of solid support or assembled objects. Different approaches such as, electrostatic self-assembly of molecular layers (SAMs) or functionalization of the object and/or surface with functional groups of alcohol, thiol, amine, acid and azid, can be applied to achieve highly ordered arrangement of particles (Chung et al., 2005; Crespo-Biel et al., 2006; Fendler, 2001; Guo et al., 2005; Liu et al., 2004). The main inconvenience of this approach is that the interaction between ligands is so affine and often irreversible, that the control of particle assembly into regular structures represents a challenge (Mahalingam et al., 2004). However, advanced surface patterning techniques such as nanolithography (dip-pen) and micro contact printing enable attachment of objects on desired areas of desired substrate using the indirect chemical binding forces (Gilles et al., 2011; Grzelczak et al., 2010; O'Brien and Thomas, 2013).

Physical approach of particle self-assembly is driven by physical forces and therefore includes rich selection of methods. It is used to obtain multilayer of particles or thin films. For example under influence of magnetic or electric fields particles can be aligned not only as a monolayer with very strong symmetry but also in the various 1D, 2D or 3D structures. Application of alternating or constant electric field allows manipulation of the assembly through electro-osmotic or electro–chemic effects on various shaped surface (Boccaccini et al., 2010; Hermanson et al., 2001; Krommenhoek and Tracy, 2013; McMullan and Wagner, 2010; Neirinck et al., 2013). The limitation of this method is that it is limited to charged or magnetic particles.

Other efficient techniques for preparing highly ordered, closely packed particle monolayers include the spin-coating method (Ko et al., 2011; Wang and Möhwald, 2004), dip-coating (Ye and Qi 2011), ink-jet (Park and Moon, 2006) etc. which rely on the meniscus force action induced by solvent evaporation.

Another promising set of approaches, exploiting capillary and convective forces in the three-phase contact line of the evaporating colloidal drop, are convective and capillary assembly. These methods are particularly well-suited for the assembly of micro- and nano- particles with good resolution (Malaquin et al., 2007; Velev and Gupta, 2009).

Since at LAAS, we have in possession an instrument for performing convective or capillary assembly, we decided to investigate assembly of DNA-functionalized gold nanoparticles as a monolayer on various substrates through convective assembly. For this reason we discuss the convective assembly in more details below.

5.1.2 Convective assembly of the particles

Self-assembly of colloidal particles driven by convective, capillary and colloidal forces (mostly electrostatic, which being relatively weak in the solution become significant when the solvent is slowly evaporated) leads to uncontrolled or controlled accumulation of the particles on the surface of various characters depending on chosen strategy.

One of the first observed and investigated way to organize particles by capillarity and convection is to spread a thin layer of the particle suspension onto substrate and leave the suspension to dry (Denkov et al., 1992, 1993). Just like in the case of coffee stain which forms ring-like arrays of coffee particles on the border of the drop (Deegan et al., 1997). This is simplest but uncontrolled way to texture a solid surface by particles, in which the choice of a solvent, a size of particles and thermodynamic state could produce different morphologies of NP coverage over large surface.

In further study, increased control on 2D assembly of particles through capillary forces was achieved by dipping the clean wettable surface into the particle suspension and then carefully withdrawing the substrate, similar to Langmuir Blodgett method for thin film formation (Dimitrov and Nagayama, 1996). Withdrawing the substrate created areas of thin films of spread colloids with increased evaporation leading to controlled formation of mono or multilayers of particles. This approach is called convective assembly.

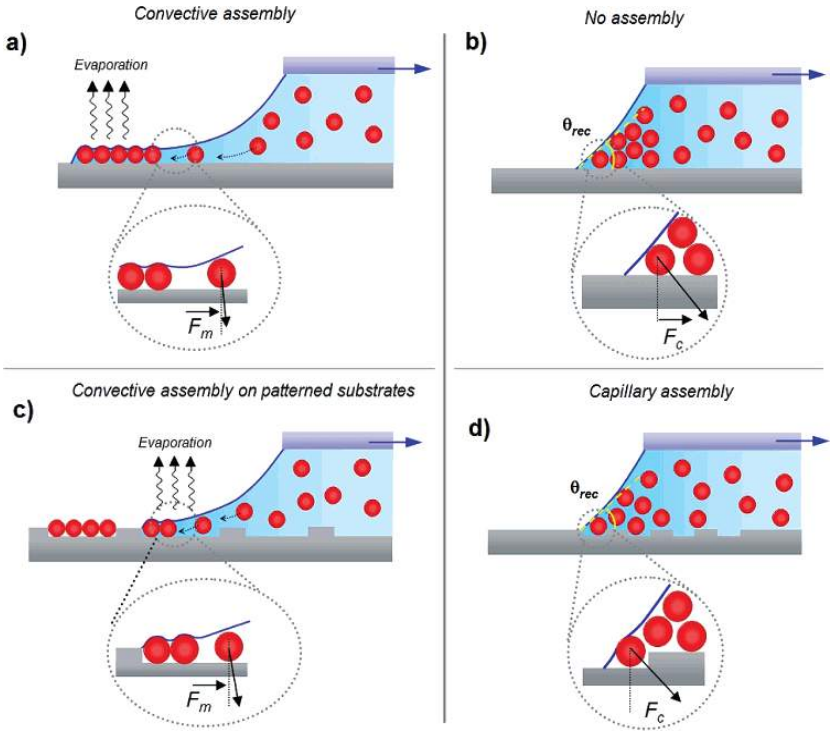

FIGURE 5.1 Assembly mechanisms based on particle confinement at the contact line of a droplet. Convective assembly is obtained on wetting substrates for contact angle values below 20°, where convective flow of solvent induced by evaporation at the contact line of the droplet, leads to the formation of (A) continuous 2D layers of packed particles on flat surfaces or to (C) 2D discontinuous arrangements on patterned surfaces. Capillary assembly takes place for contact angles greater than 20°. While no deposition occurs on flat surfaces (B), the combined effect of geometrical confinement and capillary forces created on patterned substrate can be used to deposit only one or a few particles in organized manner (D).

In later studies, instead of dipping and retracting the substrate, a droplet colloid was spread by a glass spatula (glass slide) over the substrate moving in opposite direction to assembled layer with defined speed (Prevo and Velev 2004; Ormonde et al. 2004; Malaquin et al. 2007). In this way, monolayers of controlled coverage and structure can be produced with the rate regulated by particle concentration or by the implementation of forced convection.

The underlying **mechanism of convective assembly** (Fig. 5.1 (A)) is following: on the wettable surface of substrate the profile of the liquid meniscus close to the contact line of three phases (air, substrate, colloidal drop) leads to a vertical confinement of the suspended particles into a thin film of solvent. The surface contact angle below 20° gives ideal confinement creating the zone of strong evaporation. When the solvent (water) evaporates from the contact-line area, a continuous flux of solvent from the thicker part of the layer is induced to compensate it. This convective flow drives the suspended particles toward the contact line.

The assembly process starts when the thickness of the solvent layer becomes equal to the particle diameter. The combined effects of convective flow and attractive capillary forces, that arise when the top of the particles protrudes from the solvent layer, lead to the formation of extended layers or multilayers of closely packed particles (Fig.5.1 (A)). As the layer of particles grows, the substrate has to be withdrawn together with the already formed layer.

For hydrophobic surfaces the contact angle doesn't allow for particle assembly (Fig. 5.1 (B)) unless capillary forces are enhanced by introducing local distortions i.e. patterns. This assembly is called capillary assembly. Capillary assembly employing hydrophobic patterned surfaces is relevant to the particle assembly on patterned area (Fig.5.1 (D)) and thus allows creation of 1D, 2D or 3D structures (He et al., 2011; Malaquin et al., 2007).

5.1.3 Important parameters for successful convective assembly

In order to achieve our goal of deposition of DNA-functionalized gold nanoparticles on the surface of substrate as an ordered monolayer, we have to take in account all the parameters influencing the assembly. For the steady-state assembly of 2D lattice, Dimitrov and Nagayama proposed a simple equation that describes the solvent flux and the accumulation of the particles in the drying region (Dimitrov and Nagayama, 1996).

$$v_c = \frac{\beta j_e l \varphi}{h(1-\epsilon)(1-\varphi)} \tag{5.1}$$

This equation establishes a relation between the growth velocities (v_c) of the NP layer, porosity (ε), the height of the assembled layer (h) or particle diameter, the volume fraction ratio of the particles in the suspension (φ), a coefficient that relates the solvent velocity to the particle velocity (β) and the evaporation rate of pure water J_e. l represents the ratio of the averaged evaporation rate (J_{evap}) and evaporation rate at any point of the drying region.

This equation identifies three major process parameters that can be used to control the thickness and structure of the assembled layer: the particle volume fraction (φ) the solvent evaporation rate (J_{evap}) and the substrate displacement velocity(v_s). The substrate displacement velocity is experimental parameter is not related to eq. 5.1, however directly influences the morphology of assembled layer. To obtain uniform monolayer at fixed evaporation rate and volume fraction, layer growth velocity v_c has to be equal to substrate displacement velocity v_s so

that the particle consumption due to the layer growth will be exactly compensated by the influx. Increasing the substrate velocity above the natural assembly speeds for a monolayer or, equivalently, decreasing the volume fraction of the suspension will lead to formation of an incomplete layer. Contrary, decreasing the substrate velocity or increasing the volume fraction will result in the formation of multiple layers. But these parameters on their own depend on other parameters. Table 5.1 shows various influencing parameters during experiments, which need to be fine-tuned to obtain desired quality particle layers, summarized in the three groups: (i) External and internal parameters of the experimental platform; (ii) internal parameters of colloid solution; (iii) parameters of the solid support.

Table 5.1 Parameters influencing convective assembly of particles

External and internal parameters of the experimental platform	**Internal parameters of colloid solution**	**Parameters of the solid support**
- Substrate withdrawal velocity - Evaporation rate - Temperature of the support - Humidity	- Size and density of the Particles - Concentration of the particles - Solution composition	- Substrate nature - Surface roughness - Surface hydrophobicity

In our study we investigate majority of these parameters in more details and therefore their roles will be discussed later. However below we want to highlight the importance of the choice of particle size and density.

5.1.3.1 Choice of the particle size

In order to obtain an ordered NP layer, the size of the self-assembling particles has to be selected carefully, considering the chemical composition of the particle, since the density influences the process of the assembly. Studies performed by Qihao HE (He, 2012) on particles of various nature and size (gold, latex, magnetic particle) suggested that in order to obtain ordered assembly there has to be particular correlation of the size of the particles with the density. Large and dense particles tend to sediment on the surface in a random manner before getting deposited by convective (capillary) assembly. On the other hand, small and light particles float and due to Brownian motion diffuse around, that also disturbs controlled assembly.

The dimensionless Peclet (*Pe*) number establishes the relation (eq. 5.2) between convective (gravitational) forces governing sedimentation and thermal diffusion acting on colloid of radius R.

$$P_e = \frac{vR}{D} = \frac{4\pi R^4 \Delta\rho g}{3k_B T} \qquad (5.2)$$

Here v is velocity of sedimentation, D is the constant of thermal diffusion, $\Delta\rho$ is the buoyant density (density difference between colloid and solvent), g is the gravitational acceleration, $k_B T$ is thermal energy. The Peclet number is seen to be the effective gravitational

potential energy difference across a height equal to the particle size, scaled by the temperature (Ramaswamy, 2001; Whitmer and Luijten, 2011).

If for a particle Pe is larger than one, this means that gravitational force is predominant and particles will sediment rapidly. So desired condition for the controlled assembly would be Pe=1, at which sedimentation is contra-balanced by diffusion. For gold np-s, with the density 19.32 g/cm^3, 80 nm particle diameter corresponds to Pe=1. If Pe is smaller than 1, then diffusion will dictate the distribution of particles and in this regime convective assembly is still possible but to certain limits. Convective assembly technique hardly works for the assembly of tiny nanoparticles smaller than 10 nm into monolayered arrays. The limitation is related to the evaporation and convections occurring at a much larger volume than nanoparticle size. As a result, multilayered nanoparticle arrays are usually created (Qian et al., 2012).

5.1.4 **Objective of the study**:

The aim of the study is to investigate feasibility of a monolayer of aptamer-functionalized gold nanoparticles for biosensing interface. For this purpose we explore convective assembly of DNA-capped gold nanoparticles on various substrates and investigate different influencing parameters.

5.2 Experimental

5.2.1 Colloid solution

For the reasons discussed above (Peclet number), **the size** of the gold nanoparticles for assembly was selected to be about **80 nm**, so that Brownian motion of the gold NP and their gravitational force balance each other and let homogenous assembly of NP on the surface.

The functionalization of AuNPs was performed according to classical protocol described in the chapter 4. After functionalization, nanoparticles were resuspended in small amount (50-100 µL) of double-distilled water, to obtain highly concentrated colloidal stock solution. The concentration of the AuNP stock was quantified through absorbance measurement at 550 nm taking in account following relation:

$$C\left(\frac{np}{mL}\right) = \frac{A_{550}(O.D.)}{\epsilon_{550}} N_A \ , \qquad \epsilon_{550} = 6.65 \times 10^{10}\ L \tag{5.3}$$

Further in this chapter, concentration of the gold nanoparticles will be expressed by means of corresponding absorbance at 550 nm.

Before the experiment stock solution with concentration corresponding to absorbance A_{550} = 10-15 O.D. was diluted down to desired experimental concentration in water-surfactant mix. Surfactant tween 20 in various concentrations (0.1, 0.01 and 0.005 %) was used in order to maintain stability of an individual nanoparticle and also alter the surface tension of the colloidal drop.

5.2.2 Parameters of the experimental platform

The experiments of convective assembly of DNA-functionalized nanoparticles were performed on the platform developed at LAAS-CNRS by Mike Genevieve during his PhD work (Geneviève, 2009). The schematic illustration of the setup and description of its working principle are given in the chapter 2. Below we describe important parameters of the assembly experiments.

5.2.2.1 Substrate withdrawal rate

The substrate withdrawal rate is the one of the crucial parameters during the assembly. In order to obtain homogeneous and compact 2D layer of nanoparticles the substrate withdrawal rate has to be equal to the rate of layer formation. The experimental platform limits us to move a substrate with the minimum velocity of **100 nm/s** and therefore the majority of the experiments were performed at this substrate withdrawal rate.

5.2.2.2 Liquid evaporation rate

Evaporation rate is another important parameter, which on its own depends on the **temperature** and the **humidity of the experimental environment**. The platform doesn't allow to control and regulate these parameters automatically; therefore external environmental factors have to be always controlled by an experimenter if possible. For example if the humidity is higher than 45%, it is better not to perform experiment. Also the microscope light is better to be off unless necessary, in order to avoid undesired local heating of support that is inducing changes in various thermodynamic parameters of the assembling system. **The substrate temperature** compared to external environmental conditions has an even higher impact on evaporation. It importantly influences how compact and homogeneous is the NP deposit. We could see the clear difference in the deposition at temperatures of 15, 18 and 22 °C.

5.2.2.3 Glass slide

The edge of a glass slide, used to spread the colloid drop on the substrate, was aligned perfectly parallel to the surface of the substrate so that the distance between them is in the range of **1 mm**. In all cases, right after the injection of the solution, formed meniscus drags the glass slide towards support to achieve the **optimal distance less than 1 µm in heights**. The **glass slide is tilted** relative to the support plane at about **20 degrees**. Although this parameter isn't directly influencing the front of convective assembly, however it plays role on the other side of the glass slide, where the drop of colloid solution is: larger angle exposes larger area of the drop in contact with the air and therefore facilitate unwanted evaporation of the solvent and consequent increase of particle concentration; smaller angel will spread the drop on larger area of the support surface, that might enhance uncontrolled deposition of the nanoparticle due to the sedimentation. For each experiment, glass slide with dimensions of 1 x 1.5 x 0.1 cm was used. To avoid presence of contamination (mostly organic), just before the experiment, glass slides were cleaned with RT2 solution, rinsed with copious amount of distilled water and dried under flux of compressed nitrogen.

5.2.3 Substrate parameters

The nature and **the treatment of the surface** are important parameters that we can adjust. The state of surface charge, roughness, hydrophobicity/hydrophilicity and the behavior of the colloid solution on the liquid-solid interface depend greatly on the nature of the surface. For this reason we used various types of materials and surface-treatment approaches. The hydrophobicity of surface in all cases was assessed by measuring the contact angle between a drop of water and the surface. To show the **effect of the surface nature**, we also used surface of silica treated with Piranha, Chromic acid and HDMS, surface of oxidized Aluminum and PDMS.

5.2.3.1 Silicon surface

At first we worked with **silicon wafer**, which is generally very hydrophilic once oxidized. Further, we used oxidized silica wafers obtained either through dry oxidation, allowing obtaining surface with the contact angles of < 3°, or through wet oxidation. There are few protocols of wet oxidation to obtain highly hydrophilic and well sanitized silicon oxide surfaces:

Treatment of silicon surface with Piranha-HF-Piranha: this treatment represents a chemical attack of the surface with the mix of H_2O_2 and H_2SO_4 in equal volumes. The layer of the oxidized silicon formed after this attack encapsulates all the organic contaminations and impurities on the surface. As the next step the wafer is incubated for 30 minutes in the bath of 5% HF in order to remove oxide layer. At last, the silicon surface is again placed in the Piranha solution to recreate new silica layer. After this treatment the contact angle is about 4° (Fig. 5.2).

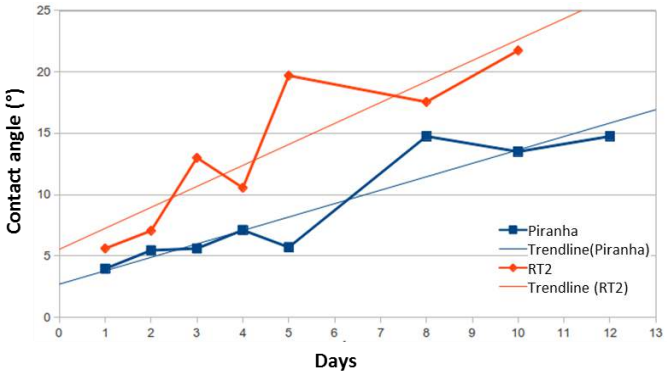

FIGURE 5.2 Dependence of the contact angle of silicon oxide surface on aging after treatment with Piranha (blue squares) and Chromic acid (red dimes)

Treatment of silicon surface with chromic acid: this treatment represents successive cycles of growth and removal of the oxide layer from the wafer surface by means of chromic acid. After this step the contact angle is about 5.3°.

After comparing the results of the treatments with Piranha and chromic acid (Fig.5.2), we saw that piranha yields lower contact angle, which is maintained for longer period than in the case of chromic acid treatment. In addition, piranha treatment allows better control of created oxide layer and is less dangerous. Thus we used the silica substrate treated with Piranha not later than 5 days after the treatment.

Treatment of Silicon with HDMS: for this treatment silicon wafer surface is at first well dehydrated. Then liquid hexamethyldisilazane (HDMS) is dispensed on the wafer using a syringe while the wafer is attached to a vacuum chuck on the spin coater. This treatment makes silicon surface silated, leaving it non-polar and thus hydrophobic.

5.2.3.2 PDMS Surface

Polydimethylsiloxane (PDMS) is formed by mixing elastomer base and the curing agent (mass ratio 10:1). To remove bubbles created during the mixing, PDMS mix is either degased under vacuum for 30 min or degased through several-minute-long centrifugation. Highly viscous but still liquid PDMS is pored over the plane silicon surface placed in the aluminum fold container in order to obtain desired thickness (3-4 millimeters). Then PDMS is cured in the oven at 80 °C for 1 hour. Cured PDMS is carefully peeled off from the substrate with tweezers. PDMS surface unless treated with oxygen Plasma, is highly hydrophobic (contact angle ~ 110°). No additional treatments were conducted for our experiments.

5.2.3.3 Aluminum oxide

Surface of Aluminum oxide was obtained by sputtering of 100 nm aluminum layer on the standard silica wafer. Sputtering is a deposition method, that involves ejecting molecules from source metal by bombarding it with the plasma of an inert gas, and depositing them on to a substrate surface. After surface modification the angle of contact changes from hydrophilic (~5°) to hydrophobic (~ 70 °) in just 4 days (Fig 5.3). Hence, we used additional treatment to make the Aluminum oxide surface less hydrophobic and more stable. The optimal procedure was the UV-Ozone treatment of the surface for 20 min that reduced the contact angle down to 11°, followed by 24 hours aging under Nitrogen gas. The last step resulted in the contact angle of about 34° stable for 5 days following the treatment.

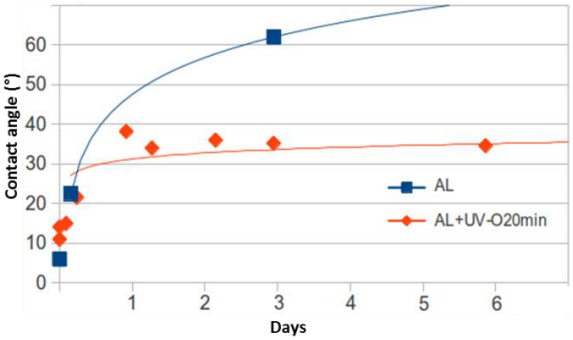

FIGURE 5.3 Dependence of the contact angle of aluminum oxide surface on aging in the case of no treatment (blue squares) and UV-Ozone treatment (red dimes) after sputtering

5.2.4 Characterization of self-assembled AuNPs

In order to analyses the information of assembled particles on the surface we used scanning electron microscopy as the characterization method. Since this method is allowing us to access simultaneously information about the shape, structure, arrangement and distribution of the particles on the surface on several scales (from several mm to several nm).

5.3 Results

5.3.1 Optimization of the support displacement velocity

The very first convective assembly experiment was conducted with gold nanoparticles suspended in PBS buffer, but the presence of the high concentration of the salt led to the formation of the salt crystals on the surface and the deposit was hence irregular. In the next experiment we used a suspension of 80 nm size DNA-functionalized gold particles in pure distilled water with the concentration corresponding absorbance of $A_{550=}$6.3 O.D. The assembly was performed at 21 °C of substrate temperature first with 100 nm/s and then with 300 nm/s substrate displacement velocity. Fig.5.4 shows the SEM image of the assembled layer.

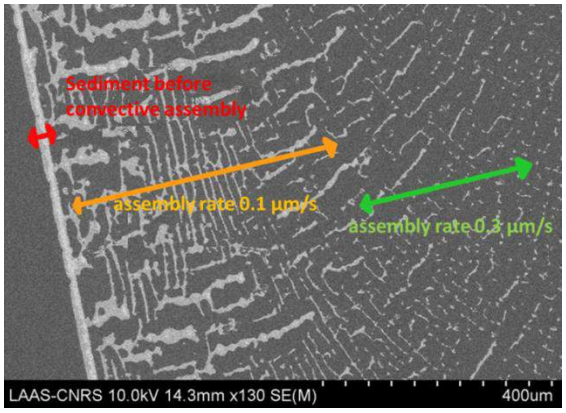

FIGURE 5.4 SEM image of the deposit of 80 nm size DNA-functionalized gold nanoparticles, assembled through convective assembly on the silica oxide surface first with a substrate displacement rate of 0.1 µm/s and then with 0.3 µm/s.

Obviously the deposition in this condition didn't have the homogeneous and compact character. But the assembly at 100 nm/s rate clearly gave better (more dense) coverage of the surface than with 300 nm/s rate. After this, in all further experiments we used support displacement velocity of 100 nm/s. 100 nm/s is the minimum rate allowed by the experimental platform, therefore, in order to diminish the difference between the support displacement and layer formation rate of the particles and thus facilitate homogenous and compact assembly, we had to optimize evaporation and convection parameters.

5.3.2 Optimization of the surfactant concentration

Surface tension of the liquid has the impact on the convection and capillary properties of the colloid and therefore on evaporation rate. Presence of the surfactant reduces free energy of the confining interface, i.e. it diminishes the contact angle between liquid and solid support and helps surface wetting. For this reason we decided to add surfactant Tween 20 in water solution of gold nanoparticles. Tween 20 is a non-ionic detergent, molecules of which have zero total charge. In addition, Tween 20 is also known to facilitate stability of the particles in the solution and prevent their undesired aggregation (Niño and Patino, 1998). We tried several concentration of the Tween 20 namely 0.1, 0.01 and 0.005% water solutions. Obtained results are shown in the Fig. 5.5.

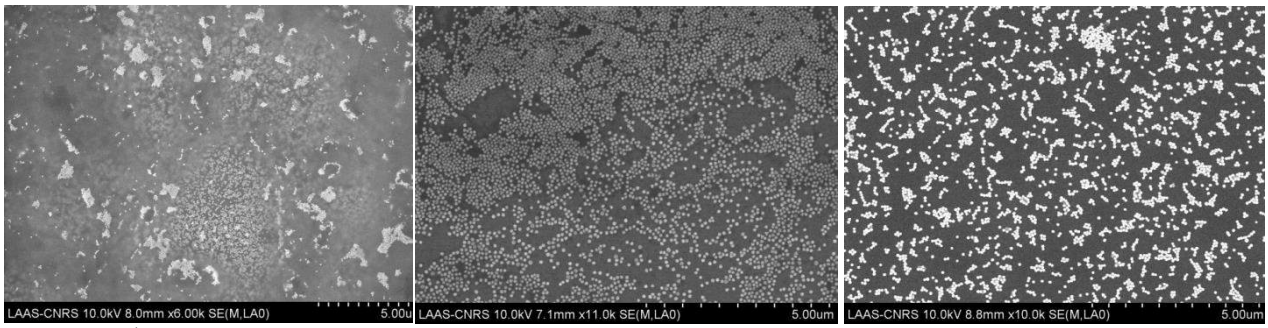

A) 0.1% TWEEN 20 B) 0.01% TWEEN 20 C) 0.005% TWEEN 20

FIGURE 5.5 SEM image of 80 nm diameter DNA-functionalized gold particles with concentration corresponding A_{550}=5.4 O.D. self-assembled through convective assembly on the silicon surface in presence of (A) 0.1, (B) 0.01 and (C)0.005% water solution of TWEEN 20.

The best particle adsorption to the support was observed at 0.01% concentration of the Tween 20 (Fig. 5.5 (B)). At the higher concentration, namely at 0.1% we observed deposition of the AuNP-s in gel-like matrixes (Fig. 5.5 (A)). We could suggest that, since the concentration of the surfactant was higher than the critical micelle concentrations (CMC)[1] of Tween 20 (0.0074% (Kim and Hsieh, 2001)), micelles of Tween 20 molecules could have formed encapsulating a number of gold nps. Thus, 0.01% of Tween 20 was selected for the further experiments.

5.3.3 Optimization of the substrate temperature

The next important parameter for optimization was the substrate temperature. We conducted experiments with the support temperature of 15, 18 and 21 °C.

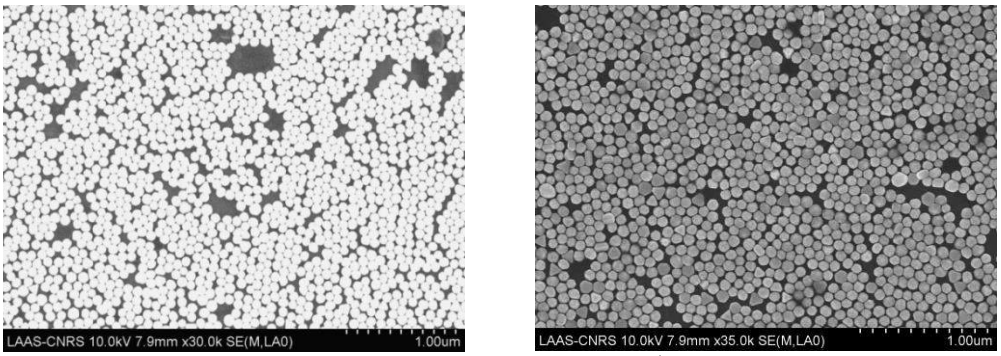

A) T_{sub}= 21°C B) T_{sub}= 18 °C

FIGURE 5.6 SEM image of 80 nm diameter DNA-functionalized gold particles with concentration corresponding A_{550}=10.4 O.D. self-assembled through convective assembly on the silica surface with temperature of (A) 21 °C or (B) 18 °C.

With increased concentrations (A_{550}=10.4 O.D) compared to previous experiments for all temperatures of substrate surface coverage was much more dense. But the density of assembled layer was decreasing with increase of support temperature. Our observations confirm that the higher is a substrate temperature, the larger is the solvent evaporation rate and thus less particles have chance to get recruited at the front line of assembly. At 21 °C the arrangement of the nanoparticles (Fig 5.6 (A)) was less compact than at 18 °C (Fig 5.6 (B)), but further lowering of the support temperature down to 15 °C, led to formation of the multilayer of the particles. In order to

[1] The critical micelle concentration is the concentration of surfactants in bulk above which the micelles start forming.

achieve better control over evaporation rate further convective assembly experiments were performed mostly at 18 °C or at 21 °C.

5.3.4 Optimization of the concentration of Gold NPs

An appropriate nanoparticle concentration was also a crucial factor in this approach, thus requiring optimization. In previous experiments with various concentrations of gold NPs we saw that better assembly was observed for highly concentrated samples ($A_{550} \geq 7\ O.D.$). So we performed assemblies at 18 °C and 21 °C temperature for several different concentrations of gold NPs. The results of these experiments are shown on the Fig.5.7.

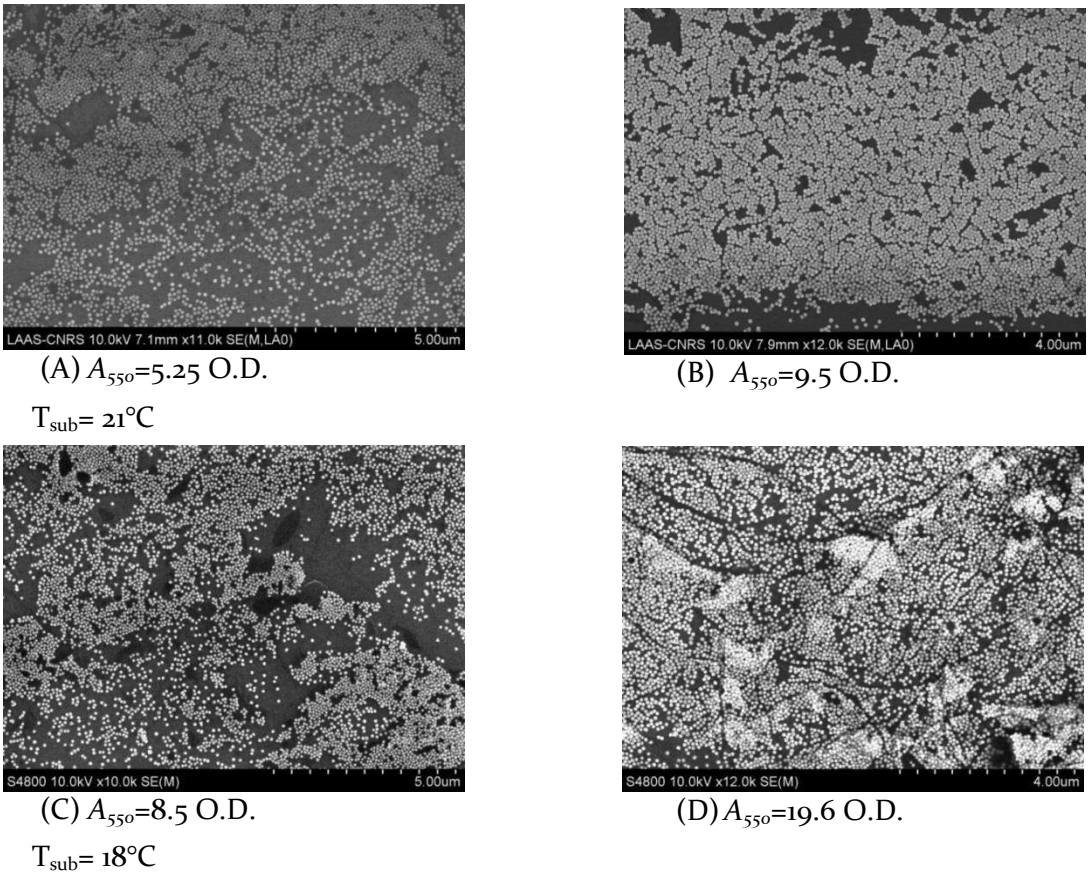

(A) A_{550}=5.25 O.D.

T_{sub}= 21°C

(B) A_{550}=9.5 O.D.

(C) A_{550}=8.5 O.D.

T_{sub}= 18°C

(D) A_{550}=19.6 O.D.

FIGURE 5.7 SEM image of various concentrations of 80 nm Gold deposited on silica surface of (A-B) 21 °C or (C-D)18 °C Temperature through convective assembly.

Results suggest that the higher the temperature, the larger concentration is needed to have compact layer of NPs. For example, at 21 °C compact layer is achieved at particle concentrations higher than 9 O.D. With lowering the temperature a compact layer can be obtained even for concentrations corresponding 8 O.D. absorbance at 550 nm. Concentrations larger than 12 O.D. yield multilayer coverage on the support. Thus when working at support displacement rate of 100 nm/s and support temperature 18-21 °C optimal results are obtained for the particle concentration in range of 8-11 O.D.

5.3.5 Optimization of the substrate contact angle

Above we saw that the convective assembly on the oxidized silicon surface, were the contact angle of the colloid solution with surface about 5° was more or less successful. We decided also to explore the effect of different surface treatment and nature of support on the assembly. For this reason, we conducted experiments also: on the surface of aged silica oxide with high angle of contact (22°); Aluminum oxide surface treated with UV-Ozone (contact angle 34°); silicon oxide surface salinized with HMDS (75°)and PDMS surface (contact angle ~ 110°). The results obtained on surfaces with different nature and contact angle are shown on the Fig.5.8

(A) SiO_2≤3° (B) SiO_2=5° (C) SiO_2=22°

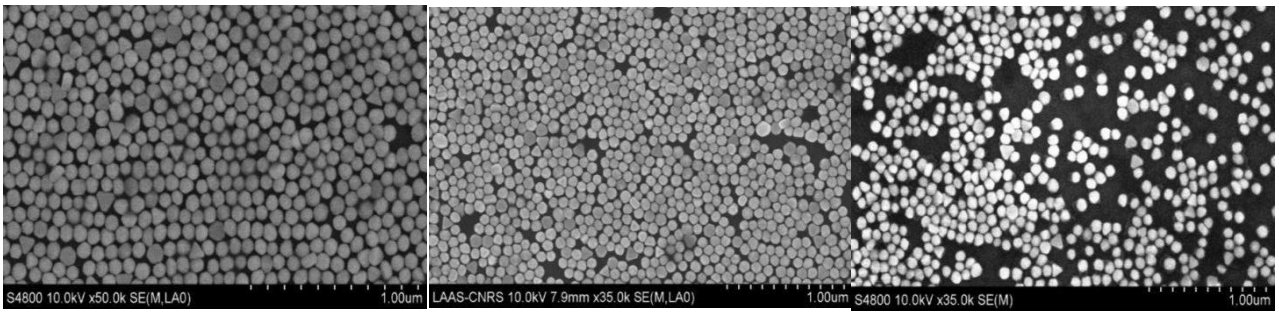

(D) Al_2O_3=35° (E) HMDS=75° (F) PDMS=110°

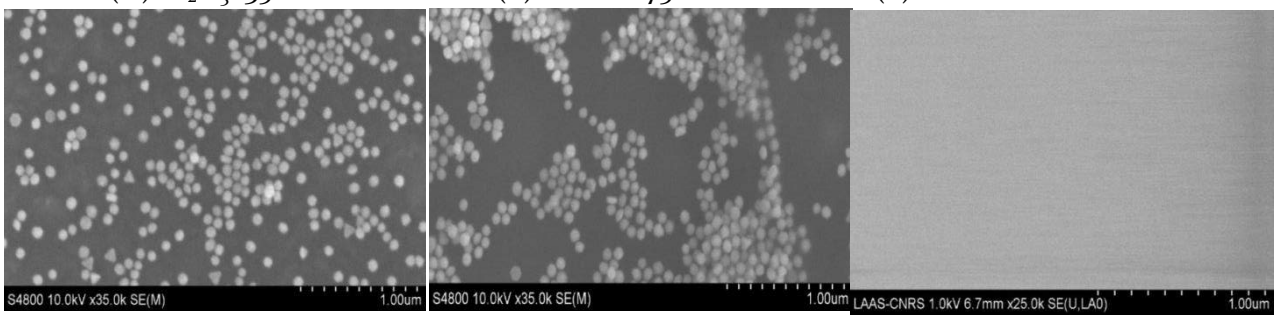

FIGURE 5.8 SEM image of 80 nm gold nanoparticles (Abs_{550}=9.6 O.D.) deposited on various substrates at 18°C substrate temperature.

Successful and homogeneous adsorption of the AuNPs on all scales was observed for all surfaces except for the surfaces of HMDS-treated silica oxide and PDMS (Fig.5.8 (E,F)). In fact, for PDMS no adsorption of nps was observed what so ever. Whereas on HDMS-treated surface particles were distributed non-homogeneously at all levels and particles were assembled randomly into unorganized multilayers. For aluminum oxide (Fig.5.8 (D)) despite the homogeneity, we couldn't achieve compact organization, suggesting necessity of increasing the

concentration of NPs, which was sufficient for homogeneous and compact assembly in the case of low-contact-angle silicon oxide. In the case of aged silica oxide surface, contamination of the surface led to the dense but uncontrolled assembly of the particles into one or several layers (Fig.5.8 (C)). The best results were obtained for the silica oxide surface with contact angle less than 3° (Fig.5.8 (A,B)).

5.3.6 Optimal experimental conditions

After having searched for optimal conditions for monolayer assembly, we performed experiment of A_{550} =10 O.D. gold nanoparticle deposition on silica surface with temperature of 18 °C, and displacement speed of 100 nm/s..

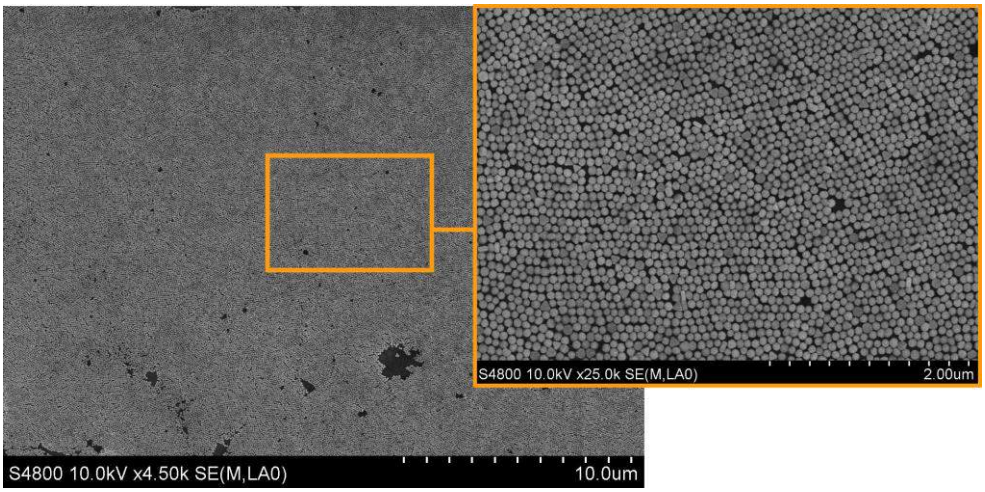

FIGURE 5.9 SEM image of 80 nm gold nanoparticle monolayer assembled on silica surface ($\theta \leq 3°$) at optimized conditions. Substrate displacement rate 100 nm/s, Substrate temperature 18 °C, colloid concentration A_{550} =10 O.D. i.e. $9x10^{10}$ np/mL

Even though, at larger scale residual areas showed lower density of adsorbed particles, overall assembled layer represented homogeneous and compact monolayer. Defect-free surfaces of more than 200 μm^2 can always be identified.

5.3.7 Effect of the second layer

It was interesting to see whether performing the second assembly experiment over the already deposited surface would result into homogeneous second layer. The SEM images of the NP deposit after the first and the second experiments are shown on the Fig 5.10.

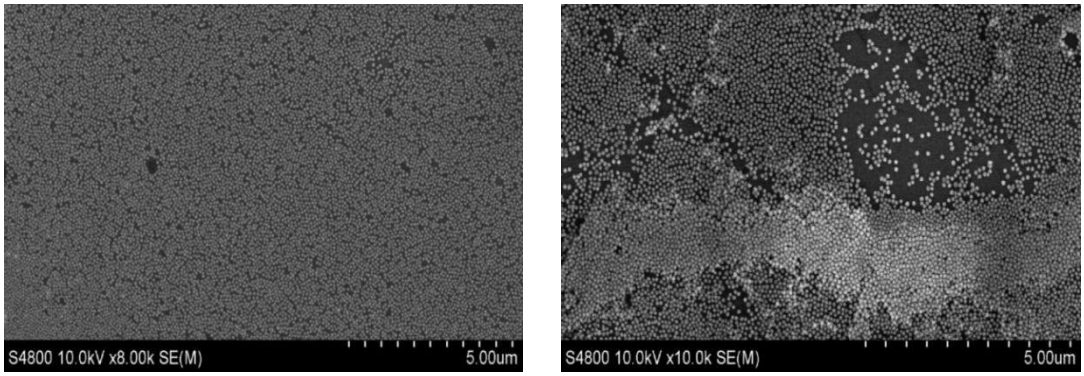

(A) first layer (B) second layer

FIGURE 5.10 SEM image of 80 nm gold nanoparticles (A_{550}=9.2 O.D.) deposited on (A) silica substrate at 18°C substrate temperature or (B) over the already existing gold nanoparticle layer.

The second try didn't appear to leave the surface as homogeneous as it was after the first assembly. We could suggest two main underlying reasons to explain obtained results: either the first layer was destabilized due to wetting upon deposition of second layer; or the presence of the first gold layer changed the regime (conditions) of convective assembly for the second layer. Nevertheless it seems rather complicated to optimize the growth of the multilayer by layer–by-layer convective assembly method.

5.3.8 Effect of the wetting on the assembled layers

Investigation whether wetting of the surface can initiate destabilization of the homogeneously packed NP layer is of crucial importance, not only for the second layer assembly but for main purpose – application of the assembled monolayer as the sensing element platform in biosensor with microfluidics system. Thus we tried to tackle this question by wetting the assembled layer with the drop of water for 5 minutes. SEM pictures showing the surface before and after are showed below.

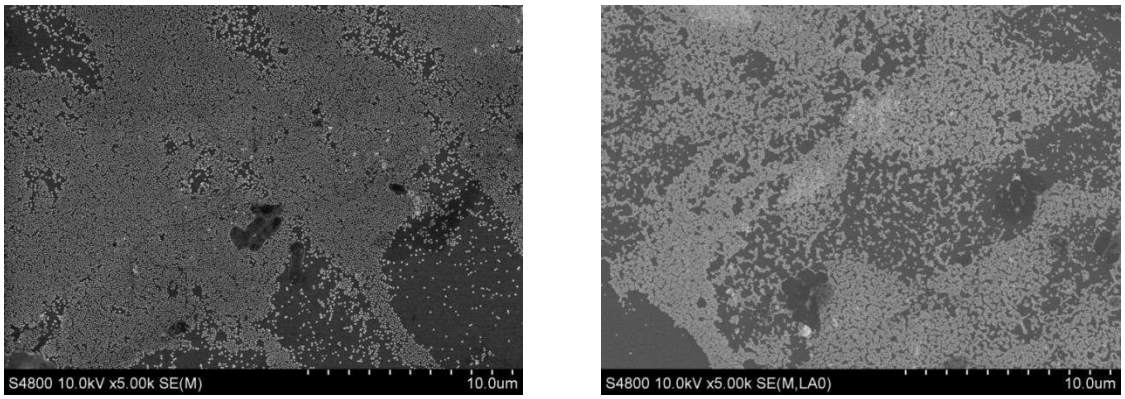

(A) Before wetting (B) After wetting

FIGURE 5.11 SEM image of 80 nm gold nanoparticle layer deposited on silica substrate (A) before and (B) after wetting with water

No obvious changes were observed, no irregular multilayer formation. The measurement of absorbance of the water drop, collected form the surface, didn't give the absorbance signal at the characteristic wavelength for Au colloid, which would be stronger than the error of the

instrument even after concentrating it. Therefore it is difficult to quantify desorption and evaluate the processes ongoing during the wetting with a drop. Further studies of deposit behavior under the flux of liquid (for example in the microfluidic channel), would most probably give a better insight into this phenomena.

5.4 Conclusions

In this study we investigated assembly of the DNA-functionalized gold NPs on the solid substrate through convective assembly, representing a simple and promising self-assembly method. The physics underlying the mechanism of assembly required highly hydrophilic substrate with contact angle less than 20°, and therefore the best results were achieved for silica surface oxidized either by dry or chemical methods (contact angles 3° and 5° respectively). We optimized internal and external experimental parameters such as substrate displacement rate, substrate temperature, concentration of nanoparticles and composition of the solvent to obtain compactly arranged homogeneous monolayer of the assembled gold particles.

The best results for silica substrate moving with the minimal possible 100 nm/s rate were obtained at substrate temperature 18 °C, particle concentrations corresponding absorbance of 10 O.D. at 550 nm in the 0.01% Tween 20 water solution. Assembled gold NP layer was homogeneous in a large area with small defects. Deposited particles didn't show any destabilization and desorption from the surface after wetting it with drop of water.

To summarize, convective assembly of gold nanoparticles is simple and cheap self-assembly strategy, allowing creation of homogeneous nanoparticle monolayer. First results obtained are promising but require further investigation to consider this method for integration of aptamer-functionalized gold nanoparticles in biosensors. Evaluation of stability of the monolayer under the flux of solutions of various compositions would further complement this study. Relative slowness of the process could be speeded up by using suspensions of volatile organic solvents or further increase of volume fraction. Better focus will be required to solve issues of scalability, control, and precision.

5.5 References

Boccaccini, A.R., Keim, S., Ma, R., Li, Y., and Zhitomirsky, I. (2010). Electrophoretic deposition of biomaterials. J. R. Soc. Interface *7*, S581–S613.

Cho, H., Baker, B.R., Wachsmann-Hogiu, S., Pagba, C.V., Laurence, T.A., Lane, S.M., Lee, L.P., and Tok, J.B.-H. (2008). Aptamer-Based SERRS Sensor for Thrombin Detection. Nano Lett. *8*, 4386–4390.

Chung, S.-W., Ginger, D.S., Morales, M.W., Zhang, Z., Chandrasekhar, V., Ratner, M.A., and Mirkin, C.A. (2005). Top-Down Meets Bottom-Up: Dip-Pen Nanolithography and DNA-Directed Assembly of Nanoscale Electrical Circuits. Small *1*, 64–69.

Crespo-Biel, O., Dordi, B., Maury, P., Péter, M., Reinhoudt, D.N., and Huskens, J. (2006). Patterned, Hybrid, Multilayer Nanostructures Based on Multivalent Supramolecular Interactions. Chem. Mater. *18*, 2545–2551.

Deegan, R.D., Bakajin, O., Dupont, T.F., Huber, G., Nagel, S.R., and Witten, T.A. (1997). Capillary flow as the cause of ring stains from dried liquid drops. Nature *389*, 827–829.

Denkov, N., Velev, O., Kralchevski, P., Ivanov, I., Yoshimura, H., and Nagayama, K. (1992). Mechanism of formation of two-dimensional crystals from latex particles on substrates. Langmuir *8*, 3183–3190.

Denkov, N.D., Velev, O.D., Kralchevsky, P.A., Ivanov, I.B., Yoshimura, H., and Nagayama, K. (1993). Two-dimensional crystallization. Nature *361*, 26–26.

Dimitrov, A.S., and Nagayama, K. (1996). Continuous Convective Assembling of Fine Particles into Two-Dimensional Arrays on Solid Surfaces. Langmuir *12*, 1303–1311.

Edel, J.B., Kornyshev, A.A., and Urbakh, M. (2013). Self-Assembly of Nanoparticle Arrays for Use as Mirrors, Sensors, and Antennas. ACS Nano *7*, 9526–9532.

Fendler, J.H. (2001). Chemical Self-assembly for Electronic Applications. Chem. Mater. *13*, 3196–3210.

Geneviève, M. (2009). Assemblage dirigé d'objets à partir de solutions colloïdales.

Gilles, S., Kaulen, C., Pabst, M., Simon, U., Offenhäusser, A., and Mayer, D. (2011). Patterned self-assembly of gold nanoparticles on chemical templates fabricated by soft UV nanoimprint lithography. Nanotechnology *22*, 295301.

Grzelczak, M., Vermant, J., Furst, E.M., and Liz-Marzán, L.M. (2010). Directed Self-Assembly of Nanoparticles. ACS Nano *4*, 3591–3605.

Guo, Q., Sun, X., and Palmer, R.E. (2005). Structural dynamics induced by self-assembled monolayers on Au(111). Phys. Rev. B *71*, 035406.

He, Q. (2012). Développement de procédés micro et nano fluidiques pour la manipulation de micro et nano objets et biomolécules. Université Paul Sabatier - Toulouse III.

He, Q., Sévérac, F., Hajjoul, H., Viero, Y., and Bancaud, A. (2011). Directed assembly of nanoparticles along predictable large-scale patterns using micromolded hydrogels. Langmuir ACS J. Surf. Colloids *27*, 6598–6605.

Hermanson, K.D., Lumsdon, S.O., Williams, J.P., Kaler, E.W., and Velev, O.D. (2001). Dielectrophoretic Assembly of Electrically Functional Microwires from Nanoparticle Suspensions. Science *294*, 1082–1086.

Kim, C., and Hsieh, Y.-L. (2001). Wetting and absorbency of nonionic surfactant solutions on cotton fabrics. Colloids Surf. Physicochem. Eng. Asp. *187–188*, 385–397.

Ko, Y.G., Shin, D.H., Lee, G.S., and Choi, U.S. (2011). Fabrication of colloidal crystals on hydrophilic/hydrophobic surface by spin-coating. Colloids Surf. Physicochem. Eng. Asp. *385*, 188–194.

Krommenhoek, P.J., and Tracy, J.B. (2013). Magnetic Field-Directed Self-Assembly of Magnetic Nanoparticle Chains in Bulk Polymers. Part. Part. Syst. Charact. *30*, 759–763.

Liu, S., Maoz, R., and Sagiv, J. (2004). Planned Nanostructures of Colloidal Gold via Self-Assembly on Hierarchically Assembled Organic Bilayer Template Patterns with In-situ Generated Terminal Amino Functionality. Nano Lett. *4*, 845–851.

Mahalingam, V., Onclin, S., Péter, M., Ravoo, B.J., Huskens, J., and Reinhoudt, D.N. (2004). Directed self-assembly of functionalized silica nanoparticles on molecular printboards through multivalent supramolecular interactions. Langmuir ACS J. Surf. Colloids *20*, 11756–11762.

Malaquin, L., Kraus, T., Schmid, H., Delamarche, E., and Wolf, H. (2007). Controlled Particle Placement through Convective and Capillary Assembly. Langmuir *23*, 11513–11521.

Mastrangeli, M., Abbasi, S., Varel, C., Van Hoof, C., Celis, J.-P., and Bohringer, K.F. (2009). Self-assembly from milli- to nanoscales: methods and applications. J. Micromechanics Microengineering Struct. Devices Syst. *19*.

McMullan, J.M., and Wagner, N.J. (2010). Directed self-assembly of colloidal crystals by dielectrophoretic ordering observed with small angle neutron scattering (SANS). Soft Matter *6*, 5443–5450.

Neirinck, B., Van der Biest, O., and Vleugels, J. (2013). A Current Opinion on Electrophoretic Deposition in Pulsed and Alternating Fields. J. Phys. Chem. B *117*, 1516–1526.

Niño, M.R.R., and Patino, J.M.R. (1998). Surface tension of bovine serum albumin and tween 20 at the air-aqueous interface. J. Am. Oil Chem. Soc. *75*, 1241–1248.

O'Brien, P., and Thomas, P.J. (2013). Nanoscience: Nanostructures through Chemistry (Royal Society of Chemistry).

Orozco, J., Jiménez-Jorquera, C., and Fernández-Sánchez, C. (2012). Electrochemical Performance of Self-Assembled Monolayer Gold Nanoparticle-Modified Ultramicroelectrode Array Architectures. Electroanalysis *24*, 635–642.

Park, J., and Moon, J. (2006). Control of Colloidal Particle Deposit Patterns within Picoliter Droplets Ejected by Ink-Jet Printing. Langmuir *22*, 3506–3513.

Qian, L., Zhai, S., Jiang, Y., and Das, B. (2012). Nanoscale convection assisted self-assembly of nanoparticle monolayer. J. Mater. Chem. *22*, 4932–4937.

Ramaswamy, S. (2001). Issues in the statistical mechanics of steady sedimentation. Adv. Phys. *50*, 297–341.

Sannomiya, T., Sahoo, P.K., Mahcicek, D.I., Solak, H.H., Hafner, C., Grieshaber, D., and Vörös, J. (2009). Biosensing by densely packed and optically coupled plasmonic particle arrays. Small Weinh. Bergstr. Ger. *5*, 1889–1896.

Shao, Y., Xu, S., Zheng, X., Wang, Y., and Xu, W. (2010). Optical Fiber LSPR Biosensor Prepared by Gold Nanoparticle Assembly on Polyelectrolyte Multilayer. Sensors *10*, 3585–3596.

Shipway, A.N., Katz, E., and Willner, I. (2000). Nanoparticle Arrays on Surfaces for Electronic, Optical, and Sensor Applications. ChemPhysChem *1*, 18–52.

Velev, O.D., and Gupta, S. (2009). Materials Fabricated by Micro- and Nanoparticle Assembly – The Challenging Path from Science to Engineering. Adv. Mater. *21*, 1897–1905.

Wang, D.Y., and Möhwald, H. (2004). Rapid fabrication of binary colloidal crystals by stepwise spin-coating. Adv. Mater. *16*, 244–247.

Whitesides, G.M., and Grzybowski, B. (2002). Self-Assembly at All Scales. Science *295*, 2418–2421.

Whitmer, J.K., and Luijten, E. (2011). Sedimentation of aggregating colloids. J. Chem. Phys. *134*, 034510.

Yang, S. m., Míguez, H., and Ozin, G. a. (2002). Opal Circuits of Light—Planarized Microphotonic Crystal Chips. Adv. Funct. Mater. *12*, 425–431.

Ye, X., and Qi, L. (2011). Two-dimensionally patterned nanostructures based on monolayer colloidal crystals: Controllable fabrication, assembly, and applications. Nano Today *6*, 608–631.

(2010). Handbook of Nanofabrication (Academic Press).

CHAPTER 6. GOLD NANOPARTICLE AGGREGATION ASSAY

6.1 Introduction

In the chapter 4, we have demonstrated successful immobilization of aptamers on the surface of gold nanoparticles by monitoring their aggregation, which occurs whenever thrombin mediates the formation of bonds between two functionalized AuNPs. As aggregation requires simultaneous recognition of distinct binding sites of the same molecule, those experiments demonstrated that, gold nanoparticle aggregation not only helped to characterize functionality of the grafted aptamers, but also proved to be specific to the target. Therefore we assume that the observing the kinetics of aggregation we should be able to detect and quantify thrombin. Indeed, different studies based on aggregation of bare or aptamer-capped gold nanoparticles in presence of thrombin, have successfully demonstrated thrombin detection in various concentration ranges (Aaryasomayajula et al.; Chen et al., 2014; Pandana et al., 2008; Pavlov et al., 2004; Peng et al., 2013; Wei et al., 2007; Xia et al., 2010; Zhengping and Zhuo, 2009), (detailed review is made in chapter 1). But we believe that our approach has potential to give more information in low cost. It may be used not only as an assay for detection and quantification of thrombin, but also for understanding the mechanisms of interaction between HD1, HD22 and NU172 aptamers and thrombin or inhibited thrombin as well.

Thus in this chapter we intent to explore the capabilities of the aggregation assay and gather the evidence in support of our beliefs.

6.2 Experimental

6.2.1 Aggregation assay:

Aggregation experiments were performed with Zetasizer Nano S (Malvern technologies, the principle of the method is described in Chapter 2), that allowed to measure average hydrodynamic radius of the aggregate in time-dependent manner. In a typical aggregation assay, aptamer- functionalized gold nanoparticles diluted in PBS buffer to obtain final concentration of particles of 0.1 O.D. corresponding to 1.9 nM concentration aptamers in 100 µL. First the initial size of the NP was measured as the control assuring that there was no aggregation without a protein, and then was introduced a protein (Thrombin, Thrombin-ATIII, Thrombin-HCII, diluted plasma). We used protein stock solutions about 50 to 100 times more concentrated than the final experimental concentration, in order to avoid dilution effect in cuvette. All experiments were performed at room temperature unless indicated.

Aggregation with the range of Thrombin concentration: In order to observe dependence of the aggregation kinetics and maximal average size of the aggregates on the thrombin concentration 4, 8, 16, 32, 64, 128 256 nM Thrombin was titrated into the solution of aptamer-functionalized 20 nm diameter gold nanoparticles.

Interaction of aptamers with thrombin-inhibitor complexes: 50 nM Thrombin was incubated either with ATIII or HCII of 100 nM concentration for 30 minutes at room temperature in order to reach binding equilibrium of thrombin-inhibitor complexes. Thrombin-inhibitor solution was titrated into 80 nm size gold particles. To evaluate whether each of the aptamers could interact with thrombin-inhibitor complex, aggregation experiment was carried out not only with both aptamer mixture but also with each of aptamers separately.

Mechanisms of aptamer-thrombin interactions: In order to understand interaction between aptamers and thrombin we have performed aggregation assay in the presence of only one type of gold particles bearing aptamer (either HD1, HD22 or NU172) and 50 nM thrombin, or 50 nM thrombin preincubated with excess (>1 μM) free HD22 strand. Aggregation of HD22 in the presence of 10-fold diluted, filtered murine plasma in PBS was also performed.

6.3 Results of aggregation assay

6.3.1 Concentration range

First of all, we were interested to investigate possibility of using gold nanoparticle aggregation as a bio sensing assay. For this purpose, we performed aggregation of mixture of 20 nm size HD1-AuNP and HD22-AuNP in the presence of various thrombin concentrations starting from 1 nM up to 1000 nM. Aggregation kinetics was monitored by DLS measuring average hydrodynamic radius of aggregate in time dependent manners. The results are shown on figure 6.1.

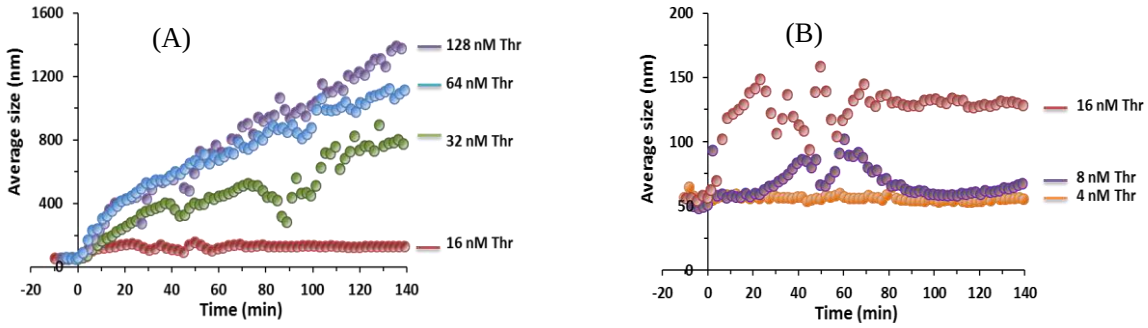

FIGURE 6.1 Aggregation kinetics of 20 nm gold nanoparticles functionalized with HD1 and HD22 in the presence of various concentrations of thrombin

Aggregation was observed starting from 5-8 nM thrombin concentration, thus being lower limit of detection (Fig. 6.1 (B)). With increase of thrombin concentration aggregation speed and the maximum size of aggregate increased and time to reach the signal saturation decreased. Nevertheless, after 256 nM thrombin concentration the size of the maximum aggregate and shape of kinetics didn't change (Fig. 6.2 (A)) and the experiments where automatically stopped by the instrument. It was due to insufficient counts/events, meaning that upon aggregation, aggregates, starting from certain critical size, were sedimenting and leaving suspended only smaller size aggregates in low concentration. Thus the upper limit of this approach was due to sedimentation. Two possibilities can be proposed to overcome this limitation. First, by fine-tuning of initial concentration of gold nanoparticles, namely by decreasing the initial concentration, it will

become possible to push upper limit, but in that case time to reach the signal saturation will increase and effect of natural sedimentation of particles will also become evident. The second option might be the replacement of gold nanoparticles with less dense polymer particles.

Nevertheless we have successfully demonstrated that aggregation assay has a potential to be used for bio-detection. This assay without any optimization already allows measurement of thrombin in the concentration range from 5 to 250 nM, which is relevant to thrombin concentration range in blood. We believe that optimization can further push the detection limits and sensitivity. Furthermore, this assay can be used for other bivalent targets.

6.3.2 Characterization of thermal stability of aptamers

Next, we used aggregation assay to investigate thermal stability of the aggregate and thus thermal stability of each component of aggregation system, namely aptamers and thrombin. Figure 6.2 demonstrates results of thermal denaturation of aggregating system.

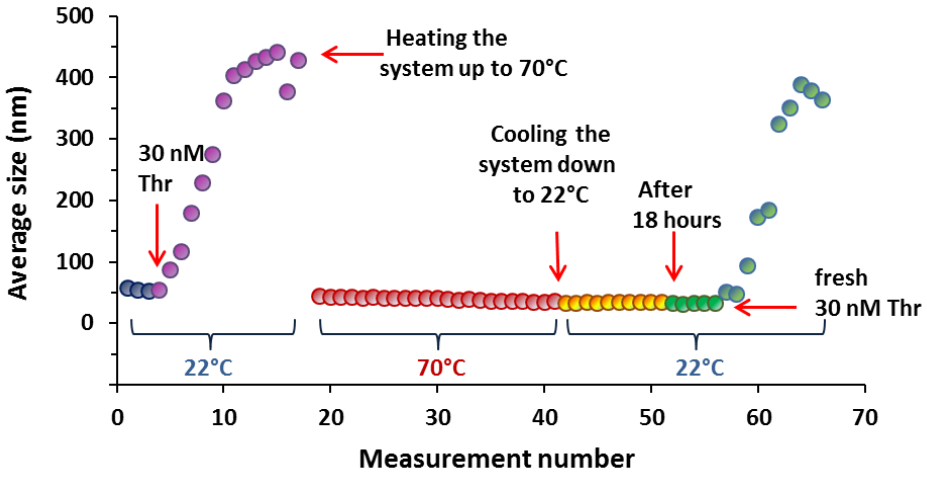

FIGURE 6.2 Effect of themperature on the components of aggregating system. Aggregation of 20 nm HD1-AuNP and HD22-AuNP in the presence of 30 nM thrombin proggressing normally at room themperature, is reversed and aggregates are disassambled following the thermal denaturation of aptamers and thrombin at 70 °C. Cooling down back to room temperature allows refolding of aptamers but not thrombin. Aggregation restarts only after injection fresh thrombin.

We started normal experiment of aggregation of HD1- and HD22-capped 20 nm diameter gold nanoparticles in the presence of 30 nM thrombin, at room temperature (22 °C). After aggregate size reached about 450 nm, we heated up the system up to 70 °C. At this temperature secondary and tertiary structure of aptamers unfolds and thrombin as well undergoes denaturation. Hence, aggregates fall apart. Indeed, the size of the system measured using DLS, decreased back to initial value, indicating disassembly of aggregates due to thermal denaturation of aptamers and linking protein.

After cooling down, back to room temperature, average size was maintained the same as during denaturation. No aggregation was observed, meaning that after thermal denaturation, either thrombin or aptamers didn't return to initial structure (renaturate). It is known that G-quadruplex and duplexes are more stable than double strand but after thermal denaturation they also need more time to return to initial folding, but the folding is always reversible. Keeping this in mind, we measured size of the system, on next day after incubation for 18 hours at room temperature. The size of the system remained unchanged. Since by this time, aptamers should

have already adopted normal aptameric folding, we deduced that reason of failing aggregation process was in thrombin, that after the heating process was irreversibly denaturized and unable to link the aptamers. Titration of fresh 30 nM concentration thrombin, instantaneously induced aggregation with the similar rate as it happened in the begging of the experiment.

Thus, showing that thrombin undergoes irreversible conformational change upon the thermal denaturation contrary to aptamers, which return to their aptameric folding, we propose that thermal denaturation may be considered as the one of the options for surface regeneration in sensor. The advantages, offered by thermal denaturation as surface regeneration method are: no change in buffering condition, less harsh influence on aptamers and the surface, no need of extensive rinsing to remove the cleaning agents. But the time of aptamer refolding after thermal denaturation, representing important point, needs further evaluation and determination.

6.3.3 Mechanisms of aptamer interaction with thrombin

One of the first crystal structures of thrombin and HD1, suggested that HD1 can weakly interact also with exosite II of thrombin (Padmanabhan and Tulinsky, 1996). Other studies as well showed that stoichiometry of thrombin-HD1 interaction is not always one-to-one and therefore HD1 is interacting not only with one site of thrombin (Pagano et al., 2008; Pavlov et al., 2004). Thus, if HD1 can interact with more than one site of thrombin, we should expect to see aggregation of HD1-AuNP in the presence of thrombin without need of HD22[1].

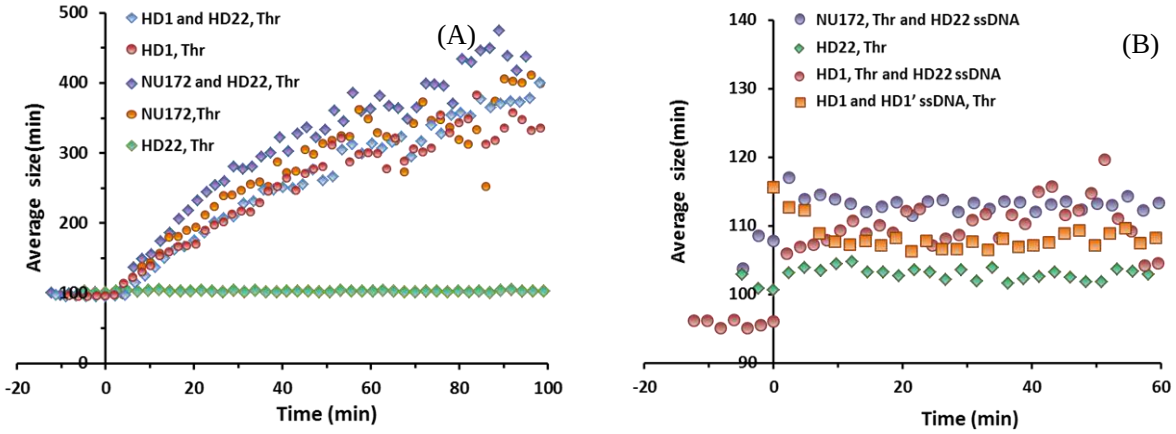

FIGURE 6.3 Measurement of an average hydrodynamic diameter of 80 nm size gold particles functionalized with either HD1, HD22 or NU172 aptamers in the presence of thrombin , thrombin-HD22 complex, thrombin and HD1'. (A)Presence of thrombin induces aggregation with almost similar kinetics in the mixture of HD1-AuNP and HD22-AuNP, Nu172-AuNP and HD22-AuNP, or only HD1-AuNP and only NU172-AuNP but not for only HD22-AuNP. (B) Thrombin complexed with ssHD22, didn't allow binding of neither HD1 nor NU172 to thrombin exositeII and thus didn't lead to particle aggregation. Presence of thrombin doesn't induce the aggregation of HD1-AuNPs hybridized with complementary HD1'.

To verify our assumption we performed aggregation assay for 80 nm size gold particles functionalize with HD1 in the presence of 50 nM Thrombin. Results shown on Fig. 6.3 (A) demonstrate that particle aggregation, comparable with aggregation in standard experiment with

[1] The first experimental evidence of HD1 interaction with several sites of thrombin was demonstrated also through aggregation assay by Pavlov (Pavlov et al., 2004). In their study aggregation of HD1-functionalized gold nanoparticles in the presence of thrombin was monitored with UV-spectroscopy.

HD1-AuNP and HD22-AuNP, occurred even in the absence of HD22-AuNP, confirming that HD1 has more than one binding site on thrombin (Fig.6.4). Similar experiment for only HD22-capped particles didn't show any evidence of aggregation. Slight change of average hydrodynamic diameter of HD22-AuNP with 3±0.5 nm, only indicated the normal 1:1 binding of HD22 with exosite II of thrombin (Fig.6.3).

Further complementing experiments were conducted to clarify whether the second binding site for HD1 was indeed exosite II. We reasoned that the specificity of HD22 binding to thrombin exosite II could be used to block the access to this site by pre-incubation of thrombin with an excess of HD22 for 20 min. This HD22-thrombin complex was then injected into the HD1-AuNP solution, and aggregation did not take place (Fig. 6.3 (B)). Rather the average diameter increased by 15±2 nm, in agreement with the formation of ternary complex between HD1-AuNP, thrombin and HD22 (Fig. 6.5).

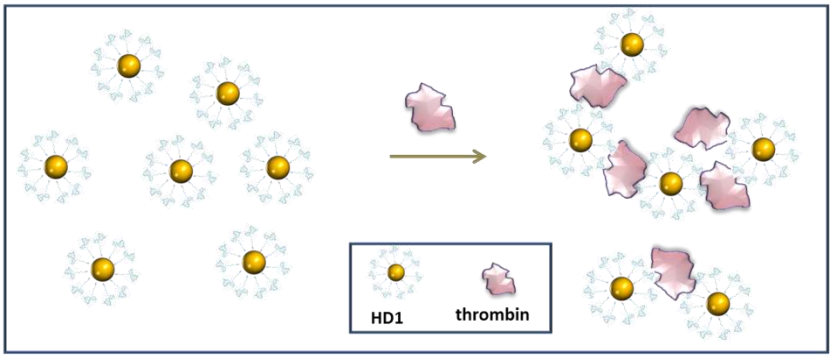

FIGURE 6.4 Aggregarion of HD1-capped gold nanaoparticles in the presence of thrombin, due to HD1 interaction with both binding sites of thrombin

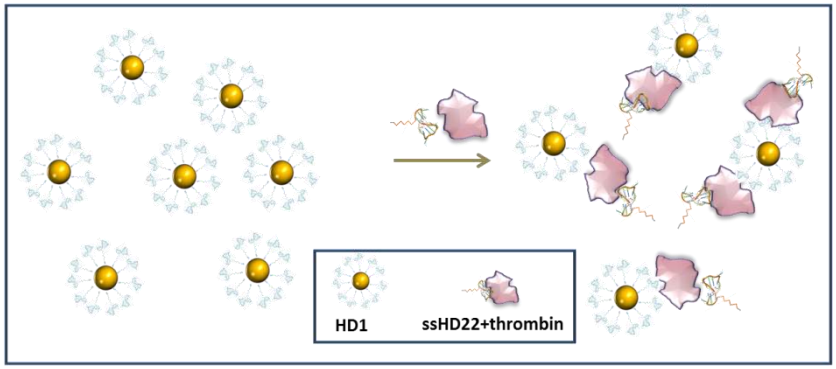

FIGURE 6.5 Interaction of HD1-capped gold nanaoparticles in the presence of thrombin-HD22 complex. HD1 interacts only with thrombin exposite I since exosite II is already occuped by stronger aptamer HD22.

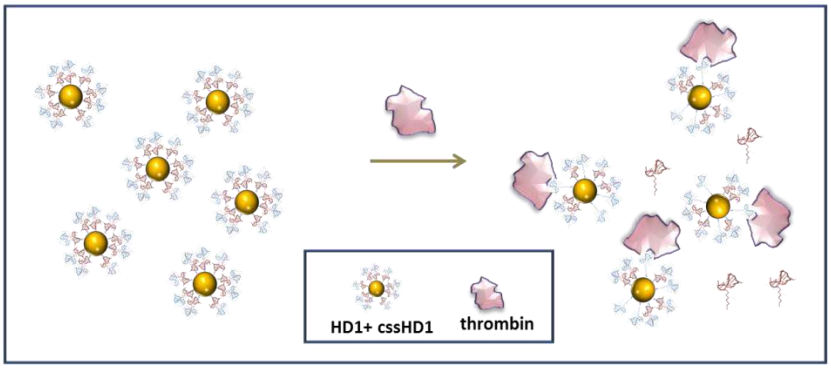

FIGURE 6.6 Interaction of gold nanoparticles bearing HD1 aptamer hybridized to its complementary strand with thrombin. Thrombin exositeI displaces complementray strand and binds HD1 but exositeII being energetically less favorable for binding than complemenatry strand, remains unbound.

From these results we can draw out main conclusion that HD1 has two binding sites with thrombin, one is widely known exosite I and another is exosite II. The arguments are following: Since thrombin having HD22 bound exosite II didn't lead to aggregation of HD1-AuNP, reason can be that covered exosite II was the second site of HD1 binding and only alternative to exosite I;

Affinity of HD1 towards exosite II has to be much more lower than that of HD22, since HD1 couldn't compete and replace HD22 from thrombin-bound state. Therefore we can assume, that in all aggregation experiments with HD1 and HD2-AuNP, aggregation occurs due to HD1 binding only to exosite I and only HD22 interacting with binding exosite II (as it binds stronger), however in the absence of HD22, HD1 can easily access exosite II as well and initiate aggregation. These results were used in Chapter 3 to justify the use of heterogeneous analyte model for HD1.

For estimation the range of the binding energy of HD1 to the exosite I and exosite II of thrombin, we made two experiments. In both experiments HD1-AuNP was incubated with excess of single-stranded DNA complementary (ssHD1') to HD1 to induce hybridization. In one case HD22-AuNP and thrombin was injected and in another case, only thrombin.

In first experiment, with thrombin and HD22-AuNP, the aggregation occurred normally (data not shown), meaning that thrombin competed for binding to HD1-AuNP with ssHD1' and successfully replaced it. From this, it follows, that binding of HD1 to thrombin exosite I is stronger than binding energy to its complementary strand. Indeed the binding energy (free energy) calculated for energy of the HD1 and its complementary HD1' is -29.35 kcal/mol (OligoAnalyzer IDT), whereas the binding energy for HD1 to thrombin exosite I calculated with MD simulations is ranges from -66.73 to -47.03 kcal/mol (Trapaidze et al., 2015).

The second experiment, with only thrombin injected in sample of HD1-AuNP and HD1', no aggregation was observed (Fig. 6.3 (B)), meaning that if thrombin managed to displace HD1' for binding HD1 to exosite I, it didn't succeed in competition with HD1' for binding HD1 to exosite II (Fig.6.6). Thus HD1 binds exosite II with lower energy than -29.35 kcal/mol.

Experiments similar to those for HD1-AuNP, were also performed for 80 nm size particles functionalized with NU172 aptamer, primarily known to bind exosite I of thrombin. Aggregation assay for NU172-AuNP and HD22-AuNP was performed first, that led to formation of aggregates as predicted. Even though there was no implication, for NU172-capped gold particles as well we injected only thrombin, but to our great surprise, similarly to HD1, aggregation did occur (Fig. 6.3 (A)). Suggesting that NU 172 also have also more than one binding sites. Injection of thrombin incubated with ssHD22 similarly to HD1 didn't lead to aggregation revealing that here also exosite II was the second binding site for NU172 (Fig. 6.3. (B)). Experiments with complementary strands weren't performed for NU172.

Globally if we compare normal aggregation, i.e. aggregation in the presence of two aptamers binding different sites of thrombin, with each other and with aggregation in the absence of second aptamer (Fig. 6.3 (A)) we will notice that aggregation kinetics in all cases are almost identical, despite the association constants being different. This justifies that in current experimental conditions aggregation kinetics depends on the diffusion of nanoparticles and not on reaction rates i.e. aggregation is diffusion limited.

The increase of gold nanoparticle concentration, leading to increase of concentration of aptamers in solution could shift aggregation more towards reaction-limited state, but then due to very strong affinity of aptamers to thrombin would lead to very rapid aggregation and consequent sedimentation and we wouldn't be able to see the beginning of the aggregation of slope due to the limitation of instrument requiring up to 3 minutes for one measurement. Contrary, decrease of

concentration of gold nanoparticles would still leave us in the diffusion-limited conditions and in addition full aggregation kinetics would have taken much longer time.

6.3.4 Natural inhibitor-thrombin complex

As we discussed already, thrombin as free protein exists rarely and only for few minutes in plasma. Main natural inhibitors ATIII and HCII present in high concentrations in plasma attack thrombin and deactivate it irreversibly. To verify which impact such complexes can have on aggregation of aptamer-modified gold nanoparticles we performed aggregation assays with 80 nm AuNP capped with HD1 and HD22 and thrombin incubated in excess of either inhibitor. Figure. 6.7 shows the kinetics of interactions.

Knowing that upon binding with inhibitors thrombin undergoes allosteric change and becomes inaccessible for interactions, we didn't expect to have as strong aggregation as just for free thrombin. Indeed, change of the average size of the particles was about 25 nm for both cases when thrombin-ATIII and thrombin-HCII where injected into the mixture of HD1 and HD22 particles. This slight change can be associated either to remnant free thrombin (though, concentration should be very low), to interactions with free inhibitors (existing in excess concentration) or directly to thrombin-ATIII and thrombin-HCII complexes. In addition, it is

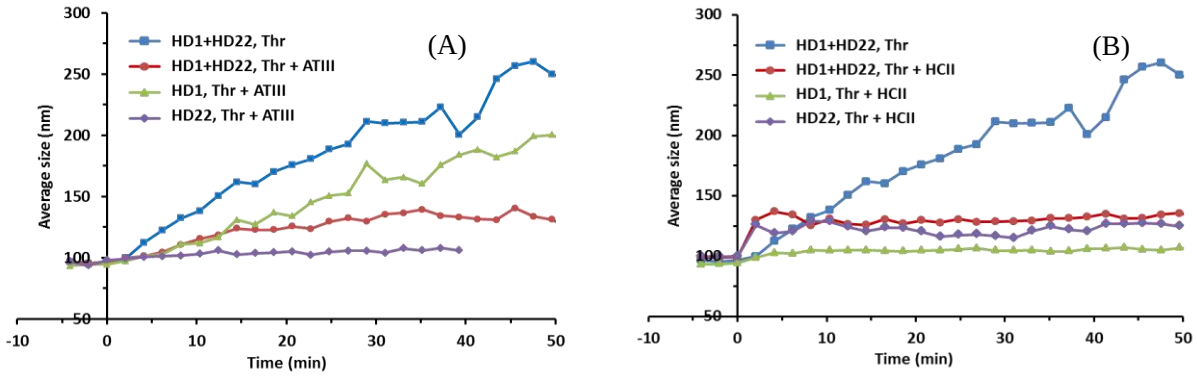

FIGURE 6.7 Kinetics of aggregation of 80 nm size gold particles in the presence of (A) thrombin-ATIII complex or (B) thrombin-HCII complex. Aggregation was performed for mixture containing (red) either type of particles bearing HD1 or HD22, (green) only particles with HD1aptamers, (violet) only particles ith HD22.

important to know, which of the aptamer was involved in interactions.

To find out interacting couple, we inject thrombin-ATIII or thrombin-HCII complexes with only one type of aptamers and observed the aggregation kinetics.

In the case of HD1 aptamer injection of thr-ATIII complex induced slow but significant aggregation trend, whereas with injection thr-HCII initial size of HD1-capped gold particle remained unchanged.

For HD22-functionalized particles, contrary to HD1, no size change was observed after injecting thrombin-ATIII complex. Interaction of HD22 with thrombin-HCII complex however had almost identical aggregation trend as it was observed for HD22 and HD1 mixture.

These results elucidate the reason of observed size change in the HD1 and HD22 mixture. In the case of thrombin–ATIII complex it was HD1 interacting with complex and with thrombin-

HCII interacted HD22. These results seem logical, knowing that ATIII and HCII bind thrombin at its active site, need for docking interaction with thrombin exosites. For docking ATIII partially covers exosite II (Baglin et al., 2002; Li et al., 2004) and HCII occupies exosite I, thus disturbing binding of appropriate aptamers (Holland et al., 2000) Exosite II, partially occupied by ATIII, is not accessible for the specific to this site HD22 but we can presume that smaller HD1 can still bind it with weak nonspecific interaction and this is why the aggregation was observed.

However, our explanation contradicts with the results obtained by SPR (see Chapter 3.), where we saw how did inhibitor deactivate thrombin allosterically upon binding, making binding sites inaccessible for interaction with aptamers. But on the other hand, in the case of SPR experiments, where ligand-receptor interactions occur within a reaction volume close to the solution/solid phase interface, aptamers are not flexible enough, because of being attached to the large surface, there steric interactions (repulsive forces) with other aptamers restrict the interaction with target instead of helping. Whereas in the case of nanoparticles, curvature of bead may help grafted aptamer to stand out and find its interaction site easier with less obstacles. Therefore reaction kinetics, reaction volumes, functional versus actual aptamer concentration and their molecular configuration on planar surface differ significantly that occur in solution or on surface of colloids (Butler, 2000).

To obtain full image it would be interesting also to see the interaction of NPs with ATIII and HCII without complex with thrombin, as in SPR experiments some nonspecific interactions with thrombin aptamers was also revealed.

6.3.5 Plasma

The natural environment for thrombin is plasma. Therefore detection of thrombin must happen in whole or diluted plasma. Of course, interesting would be to investigate behavior of particles in the presence of diluted plasma. For this purpose we injected certain amount of plasma, to achieve 10 times dilution, into the mixture of HD22-AuNP of 80 nm size. We selected HD22, as it interacts with only one site of thrombin and thus cannot aggregate in the presence of thrombin and also because it is less prone to nonspecific interactions compared to HD1 or NU172. Plasma sample was centrifuged and supernatant was passed through the filter to remove all suspended cells and aggregates that could give artefacts in size measurement with DLS method.

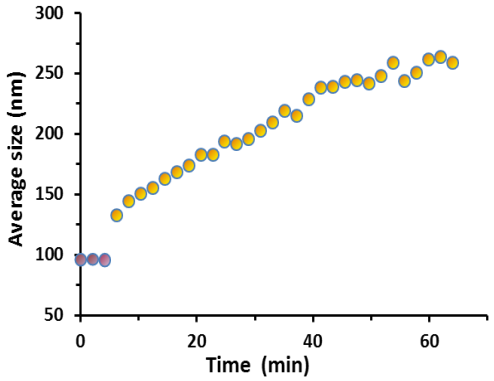

FIGURE 6.8 Aggregation of 80 nm size HD22-AuNPs in the presence of 10 times diluted

Despite the fact that in buffer no aggregation of HD22-AuNP takes place in the presence of thrombin, in 10% plasma (without injection additional thrombin) particles aggregation was initiated. Apparently some plasma proteins managed to interconnect particles and induce aggregation through nonspecific interactions. These results don't give favorable answer for application aggregation assay for thrombin detection in real plasma.

6.4 Conclusions

Aggregation assay allowed investigating not only possibility of thrombin detection in the physiological concentration range of thrombin, but also let us research stability of the thrombin – aptamer structure and mechanisms of interaction of thrombin with aptamers and thrombin inhibitors. HD1 and NU172 showed interaction with thrombin exosite I and weaker interaction with exosite II as well, whereas HD22 showed strong and faithful interaction with exosite II. However in diluted plasma without adding thrombin, even HD22 started aggregation. Thus, we developed assay which gives possibility to observe kinetics of interaction between aptamers and their target protein and to extract information about specificity and selectivity at low cost. Results of conducted experiments once again prove that targeting two sites simultaneously, increases specificity of detection. This assay can readily be used to detect and perform studies on other targets having two interaction sites

6.5 References

Aaryasomayajula, Vishala S. Ramyah, Severs, T., Ghosh, K., DeLong, R., Zhang, X., Talapatra, S., and Wanekaya* , A.K. Assembly of a Dual Aptamer Gold Nanoparticle Conjugate Ensemble in the Specific Detection of Thrombin when Coupled with Dynamic Light Scattering Spectroscopy. J. Nanomedicine Nanotechnol.

Baglin, T.P., Carrell, R.W., Church, F.C., Esmon, C.T., and Huntington, J.A. (2002). Crystal structures of native and thrombin-complexed heparin cofactor II reveal a multistep allosteric mechanism. Proc. Natl. Acad. Sci. *99*, 11079–11084.

Butler, J.E. (2000). Solid supports in enzyme-linked immunosorbent assay and other solid-phase immunoassays. Methods San Diego Calif *22*, 4–23.

Chen, Z., Tan, Y., Zhang, C., Yin, L., Ma, H., Ye, N., Qiang, H., and Lin, Y. (2014). A colorimetric aptamer biosensor based on cationic polymer and gold nanoparticles for the ultrasensitive detection of thrombin. Biosens. Bioelectron. *56*, 46–50.

Holland, C.A., Henry, A.T., Whinna, H.C., and Church, F.C. (2000). Effect of oligodeoxynucleotide thrombin aptamer on thrombin inhibition by heparin cofactor II and antithrombin. FEBS Lett. *484*, 87–91.

Li, W., Johnson, D.J.D., Esmon, C.T., and Huntington, J.A. (2004). Structure of the antithrombin–thrombin–heparin ternary complex reveals the antithrombotic mechanism of heparin. Nat. Struct. Mol. Biol. *11*, 857–862.

OligoAnalyzer IDT Oligo Analyzer.

Padmanabhan, K., and Tulinsky, A. (1996). An Ambiguous Structure of a DNA 15-mer Thrombin Complex. Acta Crystallogr. D Biol. Crystallogr. *52*, 272–282.

Pagano, B., Martino, L., Randazzo, A., and Giancola, C. (2008). Stability and Binding Properties of a Modified Thrombin Binding Aptamer. Biophys. J. *94*, 562–569.

Pandana, H., Aschenbach, K.H., and Gomez, R.D. (2008). Systematic Aptamer-Gold Nanoparticle Colorimetry for Protein Detection: Thrombin. IEEE Sens. J. *8*, 661–666.

Pavlov, V., Xiao, Y., Shlyahovsky, B., and Willner, I. (2004). Aptamer-Functionalized Au Nanoparticles for the Amplified Optical Detection of Thrombin. J. Am. Chem. Soc. *126*, 11768–11769.

Peng, Y., Li, L., Mu, X., and Guo, L. (2013). Aptamer-gold nanoparticle-based colorimetric assay for the sensitive detection of thrombin. Sens. Actuators B Chem. *177*, 818–825.

Trapaidze, A., Bancaud, A., and Brut, M. (2015). Binding modes of thrombin binding aptamers investigated by simulations and experiments. Appl. Phys. Lett. *106*, 043702.

Wei, H., Li, B., Li, J., Wang, E., and Dong, S. (2007). Simple and sensitive aptamer-based colorimetric sensing of protein using unmodified gold nanoparticle probes. Chem. Commun. 3735–3737.

Xia, F., Zuo, X., Yang, R., Xiao, Y., Kang, D., Vallée-Bélisle, A., Gong, X., Yuen, J.D., Hsu, B.B.Y., Heeger, A.J., et al. (2010). Colorimetric detection of DNA, small molecules, proteins, and ions using unmodified gold nanoparticles and conjugated polyelectrolytes. Proc. Natl. Acad. Sci. *107*, 10837–10841.

Zhengping, C., and Zhuo, L. (2009). Novel resonance light scattering testing system for human a-thrombin using gold nanoparticle modified aptamers in sandwich manner.

CHAPTER 7. DIMERIZATION OF THROMBIN APTAMERS

7.1 Introduction

Detection of thrombin as a clinical marker of hemostatic state requires performing biorecognition in the blood or plasma medium, which represent highly complex biological mixtures. Cationic and other aptamer-binding components present in real samples can affect the performance of aptamers. Although thrombin aptamers are characterized with very high affinity towards thrombin, the initial purpose of their selection was their therapeutic application as anticoagulant drug and therefore, for most of thrombin aptamers, the question of selectivity in a complex environment remains unanswered or neglected.

The results of our investigations presented in the third chapter have shown that HD1 or NU172 tend to interact with various nonspecific component of the plasma, compromising specific detection of thrombin. However, high nonspecific background encountered in the case of single-site interaction diagnostic assays, can be efficiently diminished by changing the detection format with double-site interaction. Targeting two sites of thrombin simultaneously, requiring two separate concurrent binding events for signal generation, can provide greater stringency for assay specificity and selectivity.

7.1.1 Simultaneous targeting of non-overlapping sites on the thrombin

Thrombin detection through double-site binding, other than sandwich assays described in the introductory chapter of this thesis, can be achieved as well in two other formats, both requiring simultaneous binding of aptamers on non-overlapping sites of the same thrombin molecules: (i) **assembly of DNA motifs triggered by the dual-binding event**; or (ii) **bivalent aptamer structures (aptadimer)**.

The first approach typically involves two DNA probes, each bearing aptameric sequence for target binding at distinct sites and special DNA sequences, which hybridize or self-assemble into a DNA motif, exclusively after both aptamers simultaneously recognize the same target. Upon assembly, DNA motif generates a signal, detected as an indirect measure of the target (Fig. 7.1).

One of the first reports with two aptamers recognizing different epitopes was reported in 2002 (Fredriksson et al., 2002). Aptamer probes contained also specific sequences which, upon dual-recognition of thrombin, were located in close proximity, enabling complementary connector oligonucleotide to hybridize and link two aptamers. Then the 5' terminus of one aptamer and 3' terminus of another, located next to each other, were ligated with DNA ligase. Ligated sequence was finally detected by real-time PCR (Fig. 7.1 (A)). This strategy allowed detection of picomolar concentration of thrombin. Later a dual-recognition assay that did not require the ligation step was reported (Heyduk and Heyduk, 2005). HD22 aptamer was labeled with fluorescein as the fluorescence donor and HD1 aptamer was labeled with dabcyl as the fluorescence acceptor to form the FRET couple. Simultaneous binding of the two aptamers to the

same thrombin molecule induced FRET effect of between closely located donor-acceptor (Fig. 7.1 (C)). The quantification of the fluorescence signal permitted detection of as low as 50 pM thrombin. More complex, DNA engineering-based approach was proposed by Guisto and colleagues. Rolling circle amplification was used to achieve 30 pM thrombin detection limit (Giusto et al., 2005). For this purpose HD22 aptamer was incorporated into a circular DNA sequence so-called "captamers", whereas HD1 aptamer was connected to the short primer sequence, able to hybridize with the circular DNA. Binding of both aptamers to a thrombin molecule brought the primer to the close proximity with the circular DNA template, promoting hybridization and hence forming a primer for polymerase-mediated extension by the rolling circle amplification reaction (Fig. 7.1 (B)). The products of the amplification reaction were either labeled with intercalating fluorescent dye and fluorescence was measured; or electrochemically labelled nucleoside vinyl-Fc-dUTP was incorporated during the amplification and electrochemical signal was collected from the hybridization with complementary stand on array electrode. One aptamer contained silver nanocluster nucleation sequence and the second a guanine-rich sequence (Li et al., 2012). Aptamers could hybridize through short complementary linker, which would form following the simultaneous recognition of thrombin by two different aptamers (Fig. 7.1 (D)). The formation of DNA duplex structure ensured the proximity of AgNCs with the G-rich sequence, which induced 500-fold enhancement of the red fluorescence of AgNCs and hence allowed thrombin quantification.

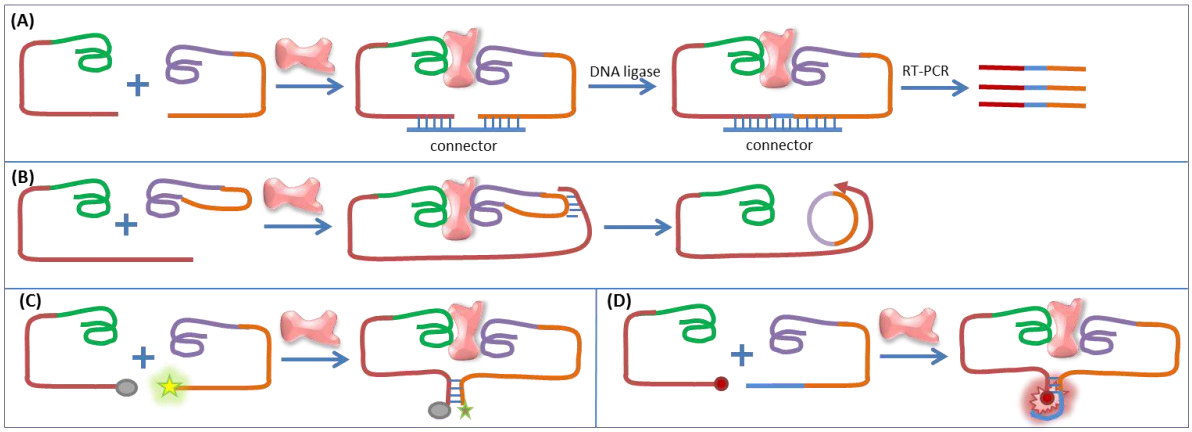

FIGURE 7.1 Detection of thrombin by assembly of DNA motifs triggered by the dual-binding event

While the above reported detection limits prove the high sensitivity, they function only when both aptamer probes are brought together upon binding to the same target molecule, i.e. when tertiary complex aptamer1-thrombin-aptamer2 is formed. This happens when aptamer1-thrombin complex encounters free aptamer2 or vice versa but tertiary complex will not form if aptamer1-thrombin and aptamer2-thrombin complexes meet. To increase the chance of tertiary complex formation thus high concentrations of aptamer probes and long incubation time is needed. Thus, this format offers good selectivity but doesn't enhance the sensitivity of detection and requires time.

Improved sensitivity and less reaction time together with the enhanced specificity is, however, offered by **the second approach - aptamer dimer (aptadimer) format**, in which distinct aptamers are conjugated (Fig. 7.2 (A)) with an optimal linker (Hasegawa et al., 2008;

Müller et al., 2007) or co-hybridized or co-printed on the sensor surface (Fig. 7.2 (B)) with an optimal density (Hianik et al., 2009; Lao et al., 2009). Similar to antibodies bivalent aptamers show enhanced functional affinity so-called avidity[1] effect against thrombin after dimerization. Thrombin binding to one aptamer from dimer increases the likelihood of the interaction with another aptamer due to the local concentration and proximity. Hence sensitivity increases, time to form the complex decreases and captured thrombin remains longer within the complex. Depending on the length, design and the chemical composition of the linker 5 to 200 fold enhancement of functional affinity of various dimers against thrombin have been reported (Ahmad et al., 2012; Hasegawa et al., 2008; Müller et al., 2008; Rakhmetova et al., 2010; Rinker et al., 2008; Tian and Heyduk, 2009).

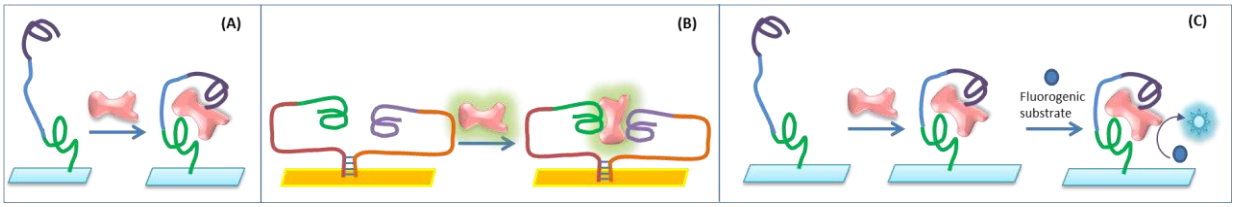

FIGURE 7.2 Thrombin detection with bivalent aptamer

Improved thrombin detection through binding with immobilized aptadimer (Fig. 7.2 (A)), was successfully demonstrated by conventional label-free methods such as electrochemistry, QCM (Hianik et al., 2009), SPR (Hasegawa et al., 2008; Müller et al., 2008; Rakhmetova et al., 2010), AFM (Neundlinger et al., 2011). Although aptamer dimerization has a capacity to allow detection in real samples, thrombin detection assays based on aptadimer haven't been largely investigated. In fact, only two groups have tried to use the aptadimer in the assay for thrombin detection in diluted plasma or serum. First, Lao and colleagues co-printed thrombin aptamers on the surface of microarrays to detect fluorescently labeled thrombin (Fig. 7.2 (B)) in the range of 0.01-10 nM concentration in 10% serum (Lao et al., 2009). Later, Muller and colleagues used aptadimer, immobilized on the surface of the microtiter, to capture thrombin from plasma sample of the real patients (Müller et al., 2011). Captured thrombin was then let to hydrolyze thrombin-specific fluorogenic peptide (Fig. 7.2 (C)). The rate of substrate hydrolysis by captured thrombin was compared to those of standard thrombin concentrations. This approach allowed detection as low as 1 pM concentration of thrombin. Yet the time needed to extract the information about thrombin concentration makes this assay incompatible with the requirements of real-time protein detection.

[1] Avidity, commonly referred to as functional affinity is the accumulated strength of multiple affinities of an individual non-covalent binding interaction, representing combined effect of all affinities participating in the bimolecular interaction, rather than sum of affinities.

7.1.2 Aim of present project

In the present study we aim to take advantage of enhanced interaction specificity, offered by aptamer dimerization, to propose a sensitive and time-efficient strategy to detect thrombin in complex medium. For this purpose, we decided to investigate the possibility of engineering an aptadimer of HD1 and HD22 thrombin aptamers in such a way that binding to target could directly lead to the generation of optically detectable signal. Namely, our approach involves triggering the fluorescence emission through "turn-on" mechanism upon aptamer-thrombin interaction. We intend to use the FRET effect for turning on and off the fluorescence, which is modulated by the proximity of fluorophore and quencher coule, incorporated within the 20-45 bases long linker (Fig. 7.3 (A)). The linker conformation in the absence of a target represents a rigid DNA hairpin composed of a loop and double-helical stem, which keeps FRET couple close to each other. Thus the fluorescence of fluorophore is expected to be quenched very efficiently. Following the capture of the target by aptadimer, complementary stands of the stem dehybridize to allow effective docking of aptamers at corresponding sites of thrombin. As the result, the distance between fluorophore and quencher increases and fluorescence escapes quenching. Such dimer construct theoretically promises a rapid detection both in the liquid phase and at the surface of the solid support. In bulk it can be compatible with mix and read mode, whereas when immobilized on the surface, fluorescence signal generation can be also conjugated with other detection methods such as surface plasmon resonance spectroscopy or imaging, QCM or impedance. Since the linker can be custom-engineered for any aptamer this approach is potentially generic.

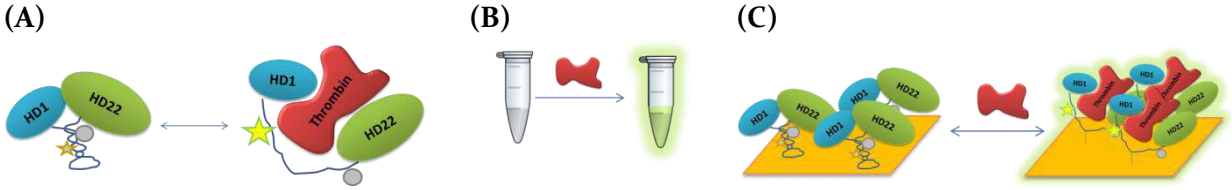

FIGURE 7.3 Illustration of (A) the structure and working principle of the aptadimer; (B) "mix and read" thrombin detection format with aptadimer in liquid phase; and (C) Dual detection of thrombin with fluorescence and a coupled method by the immobilized aptadimer on the surface of electrode, waveguide or quartz crystal.

The implementation of our vision comprises several stages. The first and very crucial step is the engineering the optimal linker i.e. determination of the optimal chemical type, composition, stability, compatibility and length of the linker and positioning of FRET couple (sec. 7.2). The second stage is experimental validation of the action principle, involving the endorsement of successful folding of aptadimer linker into hairpin and stability of the structure (sec 7.4.1). The following step is confirmation of thrombin sensing, finding optimal condition for the experiment (sec 7.4.2-3). The fourth stage concerns specificity of the dimer with non-specific proteins and diluted plasma (sec 7.4.4).

7.2 Dimer construction

Construction of bivalent aptamer dimer, first of all, requires careful selection/design of the linker, especially if the generation of a biorecognition signal is directly dependent on it. The main requirement from the linker is that its presence shouldn't affect aptameric conformation of component aptamers. This question depends on the chemical composition of the linker, which can be either an oligonucleotide or a polymer. Chemical composition also defines whether or not the linker will be flexible; influence (up- or down-regulate) interaction of dimer with target; allow incorporation of functional groups. The length of the linker is also one of the important parameters. It should allow interconnected aptamers reach their optimal positions and orientations for docking and wrapping around their common target easily and effectively.

In the first attempt to create a thrombin aptamer dimer, HD1 and HD22 aptamers were simply interconnected with 15-nucleotide long poly-adenine linker, which demonstrated 3-fold improvement in the affinity over the original monovalent precursors (Müller et al., 2008). Almost simultaneously bivalent thrombin aptamers with 0, 5, 10, 15 and 20 poly-thymine linkers were shown to improve about ten times the apparent affinity (Hasegawa et al., 2008). Subsequently, complex construct of rigid DNA scaffold was used to create multivalent aptamer DNA tiles, with up to 50 fold increase of affinity compared to monovalent aptamers (Rinker et al., 2008). PEG-based 12 and 24 nm length flexible linkers were used to construct bivalent thrombin aptamer allowing 100-fold improvement of initial affinities (Tian and Heyduk, 2009). Based on the assumptions that not only flexibility but also rigidity can influence the enhancement of dimer affinity, instead of designing the linkers Ahmad and colleges selected the optimal scaffold-forming linker from the library of dimers containing HD1 and HD22 aptamers interconnected through 30 bases long combinatorial linker (Ahmad et al., 2012). This way almost 200-fold enhancement of affinity was achieved.

Although selection from combinatorial library of linkers has shown its advantage over design, but the functionality that we want to get from a linker in our case, requires complex designing approach. Other than the concerns about chemical composition and length, the placement of the FRET couple and functioning "on-off" mechanism are also of essential importance. Therefore, we need to design a DNA linker, which contains sufficient number of complementary bases to form a stable stem to keep the construct in closed conformation. But, at the same time, the bonding between the complementary regions should get easily disrupted upon target binding. For this reason we decided to design a linker for our aptadimer, following the set of rules described in next paragraph.

7.2.1 Aptadimer construction rules

The main requirement for any bivalent aptamer is the absence of internal conflict between the linker and the aptamers; however design of an aptadimer also requires fulfillment of few more specific rules:

(I) **The length of the linker** has to be sufficiently long to allow aptadimer wrapping around thrombin.

(II) The stem of the linker has to be composed of complementary regions with desired melting temperature.

(III) Quencher and fluorophore are embedded within the complementary strands of the stem opposite to each other.

(IV) Only Thymine can be internally modified with a quencher and a fluorophore

(V) Loop of the linker has to be stable and limited to 5-to 10 bases

(VI) Linker should have no complementarities with either of aptamer sequences.

(VII) For flexibility linker should contain more thymine bases

Each point will be discussed in following paragraphs.

7.2.2 The linker length

In order to estimate the optimal length of the linker we had to evaluate the distance between two aptamers when docked on the non-overlapping sites on the thrombin surface. For this reason we reconstructed molecular structures of HD1 (4DII pdb) and HD22 (4I7Y pdb) aptamers bound to thrombin using PyMol software (Fig.7.4).

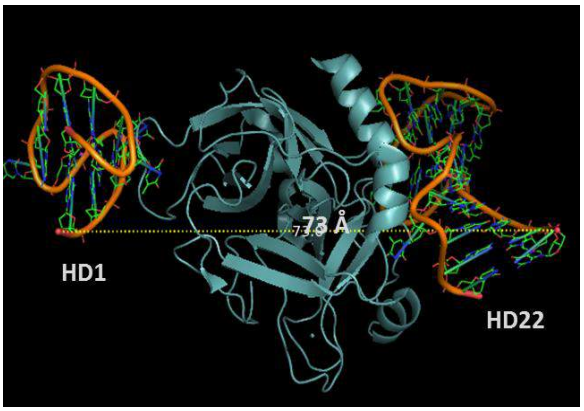

FIGURE 7.4 The measurement of linear distance between 3' and 5' extremities of thrombin–bound HD1 and HD22 aptamers respectively.

Assuming that in our dimer the sequence of HD1 was interconnected by linker with the sequence of HD22, i.e. the aptadimer had following sequence - 5'-**HD1** -3'-5' -*linker* -3'-5'-**HD22**-3', we measured the distance between 3' terminus of HD1 and 5' terminus of HD22. The measured linear distance between the extremities of the aptamers was about 7.3 nm. Taking in account the curvature of the thrombin molecule, diameter of which is about 4.2 nm, we estimated that linker length should be longer than 9-10 nm.

If we consider that one nucleotide size or length, measured between phosphors of neighboring nucleotides, is approximately 0.67 nm, then for 10 nm long linker, at least 15 nucleotides are needed. However, the complexity (functionality) of the stem might require larger number of nucleotides.

7.2.3 Stem of the linker

The stem represents the central player in functionality of the aptadimer. It has to guarantee specific and reversible signal generation upon aptadimer interaction with thrombin. This responsible function is based on dehybridization of complementary regions, bearing fluorophore and quencher, upon binding to target. Thus the complementary regions have to be designed in such way, that in the absence of the target they remain in stable double-strand conformation, which gets easily disrupted upon biorecognition.

One of the characteristic parameters of the double-stranded DNA is the melting temperature, at which thermal agitation overtakes the bonding energy between DNA strands and they denaturate. The higher is the melting temperature of the double-stranded region, the stronger is the bonding. In order to be able to work not only at room temperature but also at body temperature conditions, we decided to seek for the complementary sequences with the melting temperature in the region of 43-48 °C.

First we decided to estimate the number of base pairs needed to form a hairpin with the desired melting temperature. To accomplish this we used the software Oligoanalyzer 3.1 which predicts folding of the secondary structure of given sequence and based on the nearest neighbor method (SantaLucia, 1998) calculates melting temperature of proposed structure. Inputting random complementary sequences of different length containing all types on natural nucleotides, we estimated that complementary sequences of desired melting temperature were about 5 to 7 complementary pairs long. Optimization of stem sequences requires knowledge where exactly the fluorophores will be located and what would be the sequence of the interconnecting loop.

7.2.4 Placement of the fluorophore

In order to realize signal generation the way we had imagined, it is necessary to incorporate fluorophore and quencher within the stem of the linker. But this is only possible if we introduce fluorophore or quencher bearing nucleotide. However not all the FRET couples can be appended to nucleotides within the sequence[1], and with exception of Thymine other nucleotides cannot be internally functionalized[2].

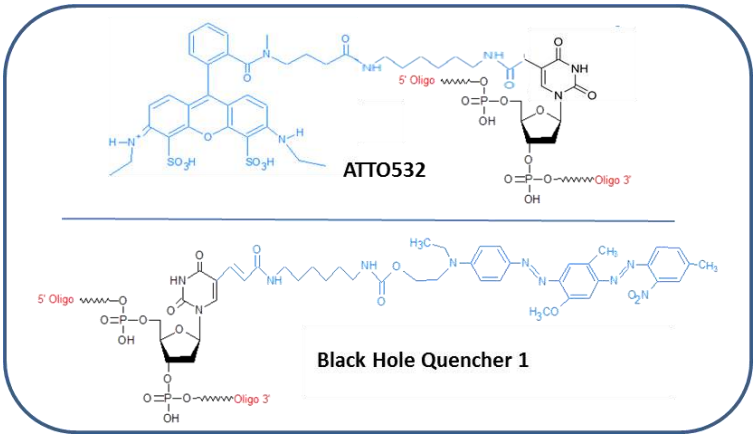

FIGURE 7.5 Illustration of fluorophore ATTO532 and Black Hole Quencher 1 molecules connected to thymine at the 5th position

[1] In common FRET formats fluorophores and quencher are located at the extremities of the sequence, which is not difficult to synthetize.

[2] It should be highlighted that chemical synthesis of oligonucleotides containing two internally modified nucleotides has very low yield. Out of material needed for synthesis of 1000 nmol non-modified sequence only 5 nmol of FRET pair-modified sequence was synthetized.

Thus out of few options as fluorophore ATTO 532 and the corresponding quencher Black Hole Quencher 1 (BHQ1) were selected. These dyes might be incorporated into the DNA by internal modification of thymine at the 5th position (Fig. 7.5).

Although the size of the each dye relative to thymine is several times larger, we neglected this fact and assumed that presence of these dyes wouldn't affect base-pairing of neither the internally modified thymine nor the neighboring nucleotides.

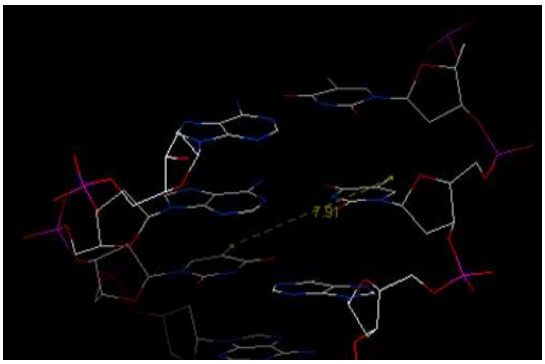

FIGURE 7.6 Visualization of the linear distance between two thymines located in opposite to each other complementary strands and paired with neighboring adenines.

Thus to incorporate FRET couple in the stem we need to have at least one thymine at each complementary region. Moreover thymines have to be located close to each other within the stem to assure the effective quenching of the fluorophore emission.

For example if modified thymines are located opposite to each other paired to each other's neighboring adenine, then the distance between the 5th positions is about 0.8 nm (Fig.7.6).

7.2.5 Design of the Loop

Loop region of the linker has not only the function of interconnecting the complementary parts of the stem, but it also defines the stability of the stem. If the loop is less than 4 nucleotides long then bending of the DNA stand would be difficult. On the other hand long loop introduces additional entropic and enthalpy contributions which might affect the folding of the stem. Therefore we considered a loop with 4 to 10 bases to have the optimal length. Although it is difficult to estimate how the flexibility of the loop and stability of the stem depend on the sequence of the loop, but loop shouldn't have any complementarities neither with aptamers nor with the stem.

7.2.6 Manual design of the linker

After having set the rules, first we started designing the linker manually. Based on our rules, we created initial 25 nucleotides long linker structure containing 7 bps in the stem, 5 nucleotides in loop, and, for 2 and 4 thymines between the rigid stem and HD1 and HD22 aptameric structures respectively for flexible spacing. We run the oligoanalizer software to generate the secondary structure of the aptadimer construct. We checked for the possible internal interference between the stem, the loop, and aptameric sequences and verified the melting temperature of the dimer. According to the results of oligoanalizer, we made alterations in the loop and stem sequences and again generated the secondary structure. We verified again the presence of interfering sequences and folding energy.

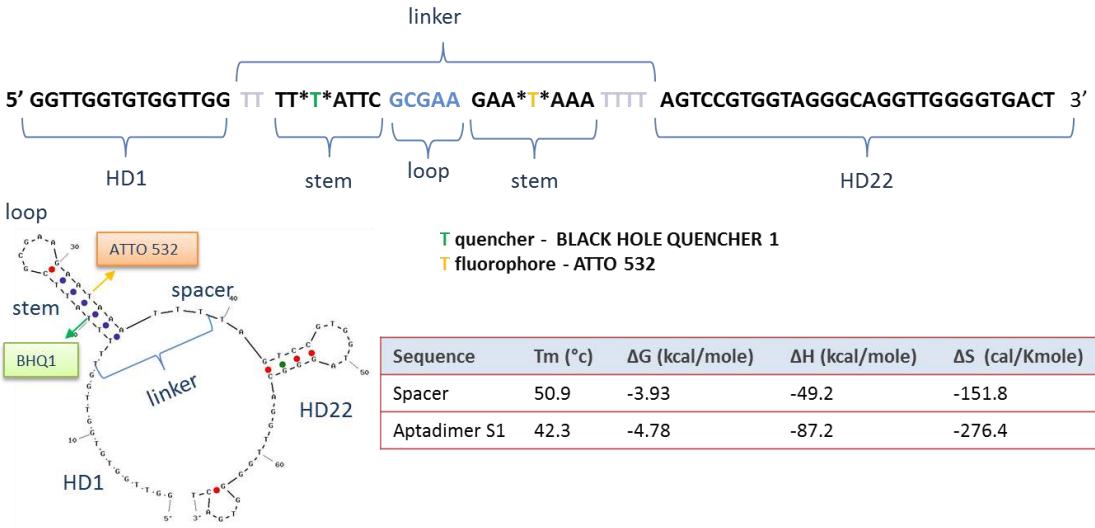

Sequence	Tm (°c)	ΔG (kcal/mole)	ΔH (kcal/mole)	ΔS (cal/Kmole)
Spacer	50.9	-3.93	-49.2	-151.8
Aptadimer S1	42.3	-4.78	-87.2	-276.4

FIGURE 7.7 Primary and secondary structure of manually designed aptadimer S1. Table shows predicted melting temperature and thermodynamic parameters of the spacer and complete structure S1

Thus we made several iteration steps until stable structure of desired melting temperature was obtained. The resulting sequence of the aptadimer and folding of its linker in the secondary structure are shown on the Fig. 7.7. The internally modified thymine bearing Black Hole Quencher was positioned at the 20th position and whereas ATTO 532 appended to the thymine with the 33th position.

7.2.7 Dimer construction by software

Manual selection of the custom spacer, requiring conception of the preliminary structure and then iteration-optimization steps, is relatively time-consuming and subjective process. Therefore to be able to screen the larger variety of possible spacer sequences special software was developed in our group. The algorithm of the software obeys the selection rules described above

```
./Optim_spacer

Choose Input file (0) or Interactive input (1)  :1
Sequence of the first aptamer (use capitals) :GGTTGGTGTGGTTGG
Sequence of the second aptamer (use capitals) :AGTCCGTGGTAGGGCAGGTTGGGGTGACT
Number of bases in each stem strand :8
Number of bases without complementary in each stem strand :6
Number of bases in the loop :8
Number of T spacers on apta1 :0
Number of T spacers on apta2 :0
DNA concentration (in M) :0.001
Na concentration (in M) :0.15
Sort solutions by free energy (0) or melting temperature (1): 1
generated file:
--------------------------------------------------------------------------------
    Sequence        |  dH (kcal/mol) | dS (cal/K.mol) | dG37°C (kcal/mol) | Tm (°C)
--------------------------------------------------------------------------------
CATCGCGAAAAAAAAATCGCGATG        -63.100002      -166.300003     -8.842521       62.696083
CGAAGCTTAAAAAAAAAAGCTTCG        -60.000000      -160.199997     -7.602521       57.147152
CGAAGCTTAAAAAAAAGAAGCTTCG       -60.000000      -160.199997     -7.602521       57.147152
GCGAAGATAAAAAAAAATCTTCGC        -59.700005      -159.599991     -7.502521       56.608650
GCGAAGATAAAAAAAAGATCTTCGC       -59.700005      -159.599991     -7.502521       56.608650
GCGAGAATAAAAAAAAATTCTCGC        -59.700005      -159.599991     -7.502521       56.608650
```

FIGURE 7.8 The software for computational selection of a spacer for given sequences of aptamers.

to help the selection of the optimal spacer. In addition it also evaluates the thermodynamic parameters of each fitting sequence.

The user-friendly, interactive software upon inputting the sequences of the first and second aptamers, the number of complementary bases in stem, the number of nucleotides in the

loop and the number of thymines for each aptamer spacers, generates the possible sequences and arranges them either by the melting temperature or by the free energy change (Fig. 7.8).

The spacer sequence of desired melting temperature was selected and manually evaluated again by Oligoanalyzer. Indeed, no interference between selected spacers and aptameric sequences was revealed (Fig. 7.9).

We came up with the 85 nucleotides long aptadimer sequence with a 41 nucleotides long linker. Linker contained 8 thymine spacers at each extremity, 7 base pairs in stem, and 15 poly-dT loop. Quencher and fluorophore are embedded at the 26th and 47th positions, respectively.

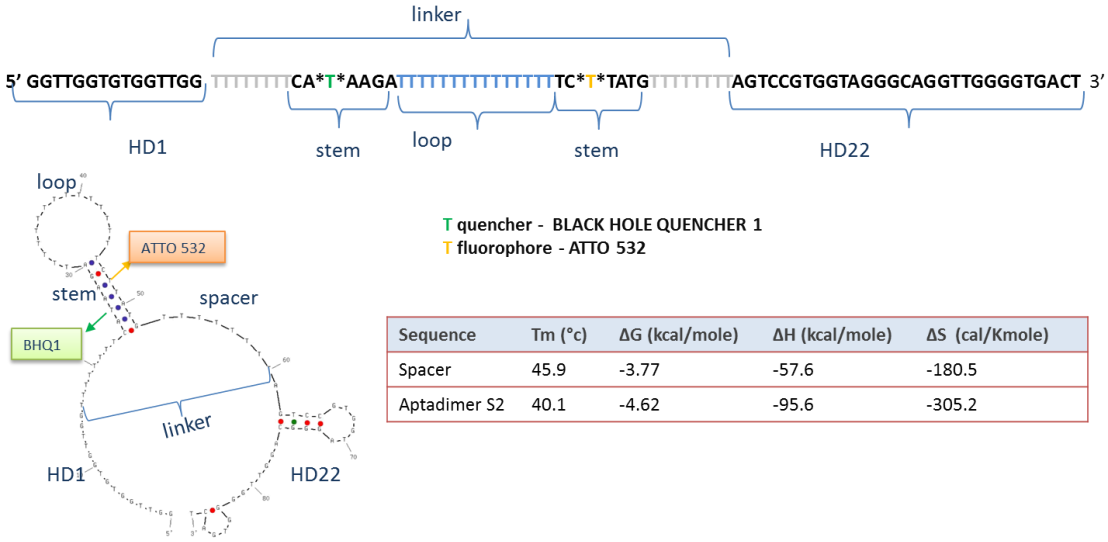

Sequence	Tm (°c)	ΔG (kcal/mole)	ΔH (kcal/mole)	ΔS (cal/Kmole)
Spacer	45.9	-3.77	-57.6	-180.5
Aptadimer S2	40.1	-4.62	-95.6	-305.2

FIGURE 7.9 Primary and secondary structure of computationally designed aptadimer S2. Table shows predicted melting temperature and thermodynamic parameters of the spacer and complete structure S2

We should highlight that development of the software took in total 6 months of laborious work of two master students. Hence the computationally designed aptadimer was created much latter than manually designed one. For this reason and due to time constrains most experiments presented in this study are carried out with manually designed aptamer dimer.

7.3 Experimental

7.3.1 Structure of the dimers

The linkers between HD1 and HD22 aptamers were selected based on compatibility rules and melting temperatures either manually (S1) of by using the software (S2), specially developed for this purpose in our lab. Sequences and specific characterizations are given in the table 7.1.

Table 7.1 Sequences of manually and computationally selected aptadimers	
S1	5' - GGTTGGTGTGGTTGGTTTT*T*ATTCGCGAAGAA*T*AAATTTTAGTCCGTGGTAGGGCAGGTTGGGGTGACT - 3'
	69 bases, linker length 25 bases, 7 complementary bp, loop 5 bases, BHQ1 - dT(20), ATTO532 - dT(33)
S2	5'- GGTTGGTGTGGTTGG TTTTTTTTCA*T*AAGATTTTTTTTTTTTTTTTC*T*TATGTTTTTTTTAGTCCGTGGTAGGGCAGGTTGGGGTGA CT-3'
	89 bases, linker length 45 bases, 7 complementary bp, loop 15 bases, BHQ1- dT(26), ATTO532 –dT(47)

7.3.2 Fluorescence measurements

As FRET pair the fluorophore ATTO532 and the quencher BHQ1 were selected, since they can be internally appended to dT. The maxima for excitation and emission spectrum of ATTO532 are located at 532 and 546 nm, respectively (Fig. 7.10). In our typical experiment, fluorophore was excited at 510 nm and emission range from 520 to 650 was scanned. Integration time was 0.1 s and step was equal to 1 nm.

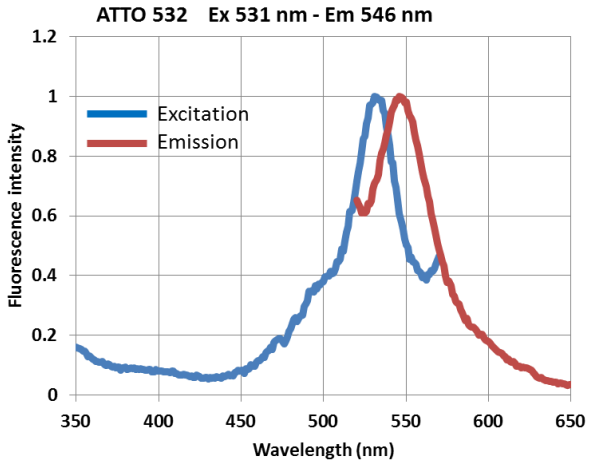

FIGURE 7.10 Excitation and emission spectrum of ATTO532 fluorophore

Fluorescence measurements were made in quartz cuvette. Experiments were typically conducted in the PBS of pH 7.4, containing 10 mM PB (Na2HPO4/ KH2PO4), 145 mM NaCl, 5 mM KCL, 1 mM $CaCl_2$ and 1 mM $MgCl_2$. Dimer structures were kept in 5 μM concentration water solution in the freezer.

Buffer-diluted samples of desired concentrations were prepared in advance or just freshly prior to experiment. In the first case, sample was diluted in PBS buffer, heated in boiling bath and allowed to cool down overnight in adiabatic conditions. In the latter case, the stock water-solution was heated in boiling water-bath then it was freeze-cooled and kept on ice; just before

the measurement the appropriate amount of dimer sample was injected into 5 °C PBS buffer. An appropriate concentration of protein was added after 1 min stabilization.

7.3.3 Endorsement of the structure folding

For the endorsement of successful folding of the linker into double-helix stem configuration, 100 µL of 100 nM concentration S1 structure in PBS was thermally dehybridized and re-hybridized. The system was heated up from room temperature to 60 °C and allowed to cool down with step of approximatively 5 °C.

Chemical denaturation of the stem was accomplished with the stepwise titration of the detergent Triton X-100 with final volumetric concentration from 2 to 8%.

Effect of chemical and thermal denaturation was obtained by heating up and cooling the dimer sample containing 8% detergent.

Folding of S2 structure was verified only by thermal denaturation.

At each point, before taking the absorbance spectra, the system was stabilized for 3 minutes.

7.3.4 Tuning experimental conditions

Interaction of 100 nM S1 construct with equimolar or excess thrombin was performed at room temperature (22 °C), with two different sample preparations. Sample with S1 structure was either prepared in advance (a) or was prepared freshly (f) just before experiment. Absorbance spectra were taken right after thrombin injection, and then after 1 and 3 minutes.

7.3.5 Aptadimer interaction with thrombin

Equimolar and excess thrombin interaction with freshly prepared 300 µL 75 and 10 nM S1 or 50 nM S2 was investigated by temperature scanning mode.

7.3.6 Investigation of aptadimer interaction with the specific and nonspecific targets

Interaction of 300 µL of 50 nM concentration freshly prepared S1 structure with thrombin, prothrombin, excess BSA, and 10% and 1% plasma was examined by measuring the fluorescence in scanning temperature mode. For this reason freshly prepared S1 sample with a titrated protein was heated from 5 °C to 60 °C, with increment of 5 °. After each heating step, the system was allowed to stabilize for 3 min and then the fluorescence was measured.

7.4 Results

7.4.1 Endorsement of aptadimer linker folding into hairpin

As the first step, the folding of the stem of the aptadimer was examined. To verify whether complementary regions have successfully engaged, we decided to induce the dehybridization of stem. If the stem has folded as predicted, then the fluorescence emission of the fluorophore quenched in the double-strand conformation due to the proximity with the quencher, is expected to increase upon dehybridization and subsequent increase in distance between FRET pair.

7.4.1.1 Folding of manually selected linker

First we examined the folding of the manually selected 25 nucleotides long linker of S1 aptadimer. The central part of the linker is the hairpin with 7 bps long double-strand forming region interconnected with 5 nts loop. 3 Thymines at each side of the hairpin serve as flexible spacers between aptameric sequences and the hairpin. Dehybridization of the stem, first, was accomplished thermally, by heating 100 nM concentration **S1** structure in PBS from room temperature till 60 °C and then cooling back to ambient conditions. Thermal de- and re-hybridization of structure was followed by the measurement of the fluorescence emission at 550 nm wavelength. As expected, with the increase of the temperature, intensity of fluorescence emission built up (Fig. 7.11 (A, D)). The drastic increase of the fluorescence intensity was seen starting form 42-45 °C, the melting temperature[1] of the double-stranded stem was located in the temperature region of 45-50 °C as predicted by the software (Fig.7.7). At 60 °C, the fluorescence intensity was increased with about 2.3 fold compared to the fluorescence of the same structure just before denaturation at room temperature. The fluorescence of the sample started to decrease and reached the same level upon cooling the sample down to room temperature, proving that Watson-Crick base pairing again took over the thermal agitation at low temperature and favored re-hybridization of complementary regions of the stem.

After thermal modulation of the stability of the stem region, aptadimer structure was denaturized chemically in presence of nonionic surfactant Triton X-100. Chemical denaturation also induced separation of complementary regions. Titration of increasing concentrations of detergent in sample at room temperature induced the similar effect to thermal denaturation - the intensity of the fluorescence emission augmented drastically (Fig. 7.11 (B, E)). As a result, in presence 0.6% (volume fraction) detergent, increase of fluorescence of about 200% was observed, which didn't increase further at 0.8 % Triton X-100. Thus the detergent effect gave a fluorescence intensity change comparable to that of observed at the maximum of thermal dehybridization. Both pathways of dehybridization lead to the separation of the quencher and the fluorophore with the same degree.

Interestingly, when the sample with the 0.8% Triton X-100, was heated up to 60 °C and cooled back to room temperature, we observed an additional onset in fluorescence emission (Fig. 7.11 (C, F)). Fluorescence intensity at 60 °C was more than 1000% higher compared to the fluorescence of the same sample at room temperature in the absence of detergent.

[1] Melting temperature is the temperature at which half of the DNA is in random coil.

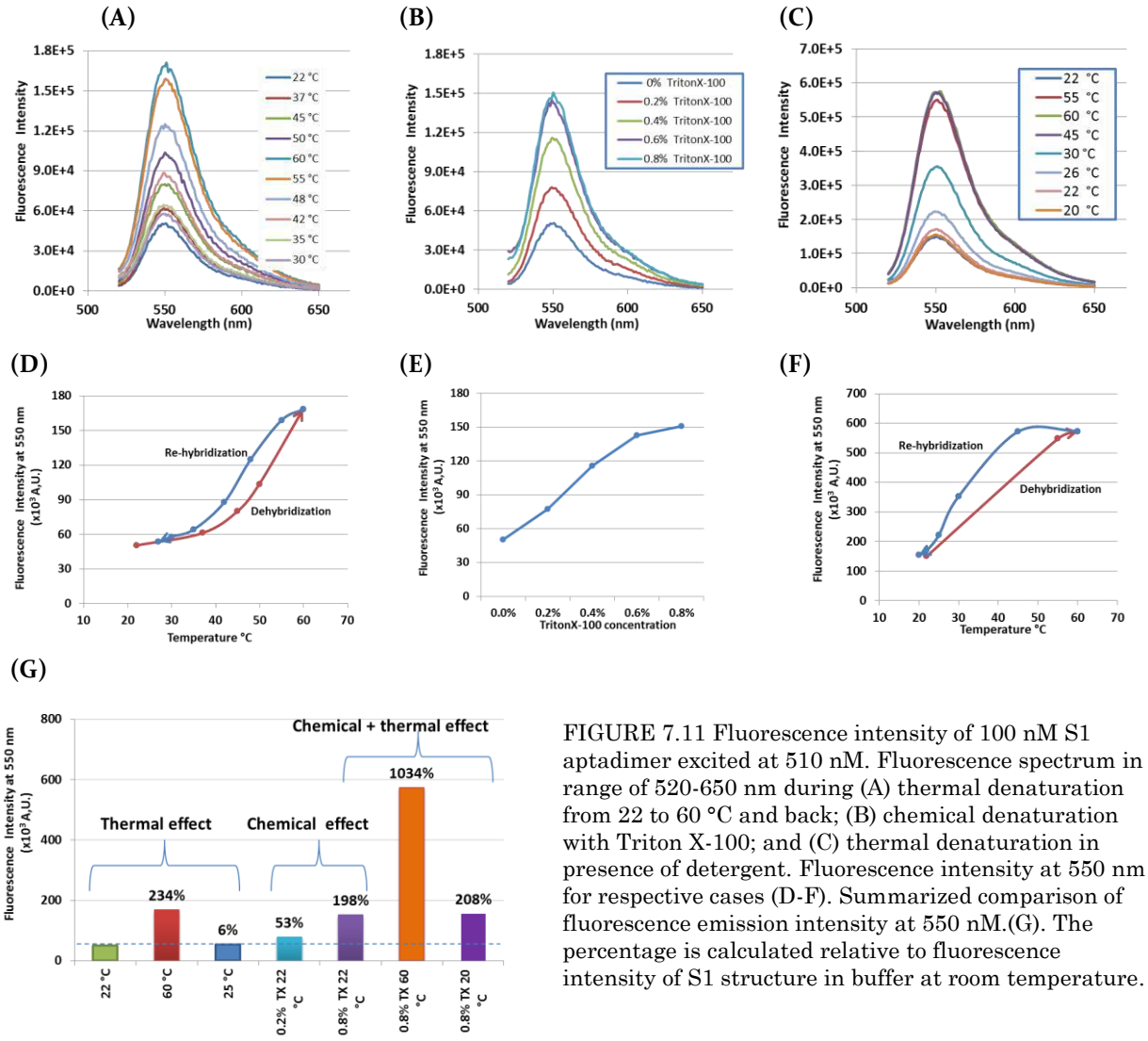

FIGURE 7.11 Fluorescence intensity of 100 nM S1 aptadimer excited at 510 nM. Fluorescence spectrum in range of 520-650 nm during (A) thermal denaturation from 22 to 60 °C and back; (B) chemical denaturation with Triton X-100; and (C) thermal denaturation in presence of detergent. Fluorescence intensity at 550 nm for respective cases (D-F). Summarized comparison of fluorescence emission intensity at 550 nM.(G). The percentage is calculated relative to fluorescence intensity of S1 structure in buffer at room temperature.

This superposed effect of thermal and chemical denaturation was reversible and cooling the sample made the fluorescence emission decrease to the initial level (Fig. 7.11 (G)).

The possible explanation of this reversible extra enhancement might lie in the change of properties of environment upon heating, which influence FRET efficiency. Since FRET efficiency depends not only on distance but also on the orientation of the dipolar moments of FRET donor and acceptor pair and optical density of the medium. The presence of surfactant, on one hand, separates complementary strands increasing the distance between FRET pair and stabilizes fluorophore and quencher orientation enveloping them in micelles; and, on the other hand, it changes the local optical index of the medium. Namely when the temperature of nonionic surfactant increases, the surfactant (especially with the concentration higher than the critical micelle concentration) undergoes phase separation. This point, called cloud point, for Triton X-100 is achieved at 63-69 °C in water (Ruiz et al., 2001). In the presence of a salt, repulsive steric interactions between the surfactant micelles decrease and attractive van der Waals interactions increase, leading to decrease of the cloud point temperature. When phase separation occurs small DNA fragments tend to stay in the surfactant phase. Since the concentration of Triton X-100 in our experiments is much larger than its' critical micelle concentration and the salt concentration is about 150 mM, we can suggest that, our sample reaches cloud point at lower temperature than

60 °C. If it is so, the aptadimer would appear within the detergent phase, where the optical index is different and the orientation of the FRET dipoles is rigidly fixed so that quenching efficiency decreases and therefore fluorescence emission is enhanced.

7.4.1.2 Folding of computationally selected linker

After validating folding of manually selected linker of S1, we examined folding of stem of S2 structure linker of which was selected by software. Similar to S1 structure, S2 also had 7 bps long complementary stem region, but loop contained 14 thymines, and hairpin was flanked at each sides by 8 thymines, making total length of linker equal to 44 nucleotides long. In this case folding of stem in double-strand was endorsed only through thermal denaturation (Fig. 7.12).

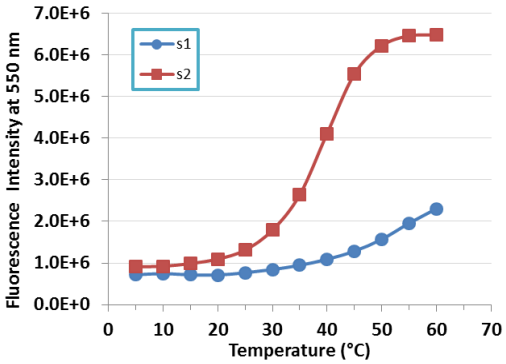

FIGURE 7.12 Thermal denaturation profiles of 75 nM concentration S1 (blue circles) and S2 (red squares) aptadimers in PBS buffer

75 nM concentration of S2 aptadimer in PBS buffer was heated from 5 to 60 °C. Increase of fluorescence emission intensity was observed starting from 25-30 °C and reached the maximum already at 50 °C, in agreement with the expectation that the melting temperature of S2 structure is 40 °C. This melting temperature is slightly lower than that of S1, which can be explained by the fact that the S1 has shorter and more stable loop that has less entropic and enthalpic influence on the double-strand of the stem than in the case of flexible poly dT loop of S2 aptadimer. In other words, it is slightly easier to destabilize the stem interconnected with longer loop than with shorted less flexible loop.

Another interesting observation was the intensity of the fluorescence emission in the state of complete denaturation of the stem. Namely the fluorescence signal was increased to more than 650% compared to initial signal. This corresponds to about 3 fold more intensity than with S1 structure at 60 °C. The reason of such a huge difference between maximum fluorescence signals lies in the position of the fluorophore and quencher. In case of S1, the distance between FRET pair in the linear linker is equal to 12 separating nucleotides i.e. about 8 nm. Whereas in S2 linker quencher-fluorophore are separated with 21 nucleotides, making the linear distance equal to about 14 nm. As it is known the efficiency of the FRET depends on the distance with the inverse 6^{th} power, meaning that quenching efficiency of S1 is about 29 times stronger than that of S2 (See chapter 2). Thus in S1, shorter distance between quencher and fluorophore, doesn't allow release of maximum fluorescence emission whereas in S2 thermal denaturation separates FRET pair on the distance where the quenching effect is diminished. Hence, when examining stability of S1 and S2 aptadimers we found that both structures have well folded stem. S1 has more stable stem than S2, however S2 is able to generate way larger fluorescence emission.

7.4.2 Interaction of dimer with Thrombin

After successful endorsement of linker stem folding, the next point of interest was the validation of the working principle of signal transmission upon thrombin-dimer interaction. For this purpose we decided to allow various concentrations of thrombin to interact with aptadimer at room temperature.

First 100 nM concentration S1 structure in PBS buffer was examined. The stock solution of dimer was prepared in PBS buffer day before the experiment; it was first heated up till 90 °C and then cooled down adiabatically to room temperature overnight. Sample was diluted to desired concentration prior to experiment

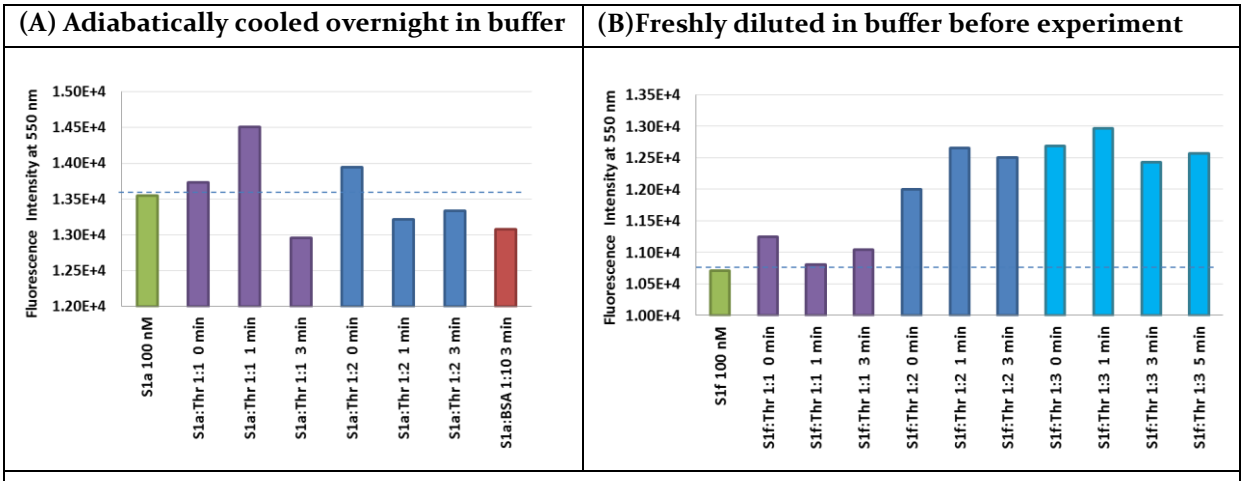

FIGURE 7.13 Effect equimolar, 2 and 3 fold thrombin presence on fluorescence intensity of 100 nM S1 structure prepared (A) by overnight adiabatic incubation or (B) freshly prior to experiment.

Surprisingly, expected enhancement of the fluorescence intensity was not observed upon titration equimolar or excess thrombin for adiabatically cooled samples (Fig. 7.13 (A)). Obtained result didn't give a hint whether thrombin was interacting with the dimer or not. In fact, thrombin could interact with dimer but without having disrupted the stem conformation, in case of interaction with only one of the aptamers. Thus, the reasons for not having an effect of thrombin presence on stem dehybridization could be following: either thrombin was interacting with only one of the aptamers and therefore didn't affect the stability of the stem; or thrombin couldn't open the stem to position itself between the two aptamer for simultaneous docking to form tertiary complex.

In order to elucidate whether the strength of stem folding was causing the problem for simultaneous interaction of both aptamers with thrombin, we decided to affect the stability of the dimer by changing the protocol of sample preparation. Namely, instead of overnight incubation of the dimer in buffered environment, the stock of dimer was prepared in water, which prior to experiment was heated up till 90 °C to destroy all the bonding and was subsequently cooled by placing it on ice. As soon as 100 nM concentration sample was prepared in PBS buffer various (50, 100 and 150 nM) concentrations of thrombin was titrated and fluorescence was measured, leaving very short time for forming the stable double-helical stem.

Interestingly, the change in fluorescence signal obtained (Fig. 7.13 (B)) in these conditions was sufficient to associate it with specific interaction between thrombin and dimer. Obviously, it was stem rigidity objecting the generation of the fluorescence signal and in this conditions

thrombin took advantage over the weaker stem folding to insert itself within dimer. The fluorescence intensity after addition equimolar concentration of thrombin increased with 5% and upon doubling the concentration the increment was about 18% compared to initial fluorescence level. Although the change in fluorescence intensity upon thrombin addition was much smaller compared to the signal observed during thermal denaturation. We suggest, that when dimer wraps around thrombin, diameter of thrombin of 4-5 nm might be insufficient to increase the distance between fluorophore and quencher, so that they remain still in quenching distance and FRET quenching efficiency is still significant.

The stability of the dimer stem depends on the folding of the structure, which in turn depends on the environmental condition, the presence of the salt. In order to show that freshly made sample had weakly stabilized stem than buffer-incubated we performed the thermal denaturation experiment of both samples. For this purpose we scanned the temperature from 5 to 40 °C measuring the fluorescence intensity at 550 nM after each increase of the temperature with a 5 °C step. The result presented in Fig. 7.14 shows that the behavior of thermal profiles of the two structures differs in the region of 5-20 °C. At 5 °C, fluorescence intensity of the freshly prepared sample is significantly larger compared to the incubated sample. However upon increase of the temperature the signal of the fresh sample decreases, finally reaching at 20 °C the similar fluorescence level as the incubated sample.

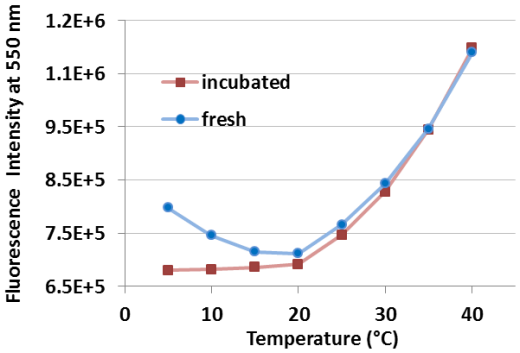

FIGURE 7.14 Thermal profile of fluorescence of 100 nM concentration dimer adiabatically cooled overnight in PBS (red square) of freshly diluted in buffer (blue circle).

This difference in the thermal profiles elucidates the stem folding-associated question. When dimer structure has the salty environment, the overnight incubation favors formation of base-pairing intra- and inter-dimer[1]. Whereas dilution of water stock solution of dimer into the buffer just prior to the experiment (directly low concentration) and low temperature favors formation only the self-folded dimers. Thus the decrease in the fluorescence for freshly prepared samples corresponds to hybridization of complementary regions, which in the absence of salt were not associated, separating quencher and fluorophore from each other. Upon hybridization quencher and fluorophore were set closer to each other. Hence the FRET quenching of fluorescence took place. So we can assume that at 20 °C fresh and incubated samples have formed stems[2]. Thus, in order to detect the interaction between thrombin and the dimer it is better to observe the fluorescence signal of thrombin and freshly prepared aptadimer sample. However, we believe that thrombin can not only insert itself on weaker stem, but it also can affect the global stability of the structure and induce the change in thermal denaturation profile.

[1] The complementary regions of the dimer can form double helix by interacting either with each other (intra), or with complementary regions of another dimer molecule (inter). The chance of forming complex structure with another dimer molecule is low at nanomolar concentration of DNA but increases with the increase of the concentration, for example in stock solution.

[2] For freshly prepared sample we can assume that complementary regions hybridize exclusively with each other, whereas in incubated samples there is higher chance to have inter-molecular dimers with similar fluorescence quenching level, but stronger binding energy.

7.4.3 Interaction of aptadimer with various concentration of thrombin

After showing that thrombin can interact with dimer (both aptamers simultaneously) only if the dimer stem is destabilized, and taking in account that destabilization of the stem folding is dependent on the temperature, we decided to optimize fluorescence signal generation by tuning the temperature. However instead of finding the optimal temperature, we decided to carry out thrombin-aptadimer interaction experiments in thermal scanning regime.

First, the thermal scanning experiments in the presence of freshly prepared 75 nM S1 aptadimer and 75, 150 and 187 nM concentration of thrombin were performed (Fig. 7.15 (A)). The temperature was scanned in the range of 5-55 °C with the increment of 5 °C. Thrombin injected in aptadimer sample just before starting the thermal scanning, already manifested itself in the beginning of the measurement. Namely, instead of decrease of fluorescence intensity in the region of 5-20 °C, which is characteristic to freshly made aptadimer without thrombin, the increase of fluorescence intensity was already observed starting from 10 °C when the thrombin was present. Starting from 20 °C it became already evident that the stem destabilization effect upon thrombin–aptadimer interaction was dependent on thrombin concentration. The slope of the stem dehybridization curve became steeper with the increase of thrombin concentration. The comparison of the fluorescence emission intensity of aptadimer in the presence of various concentrations of thrombin at 30 °C shows already significant differences in the signals. The more thrombin is titrated, the more is the melting curve affected i.e. the stronger is the destabilization effect.

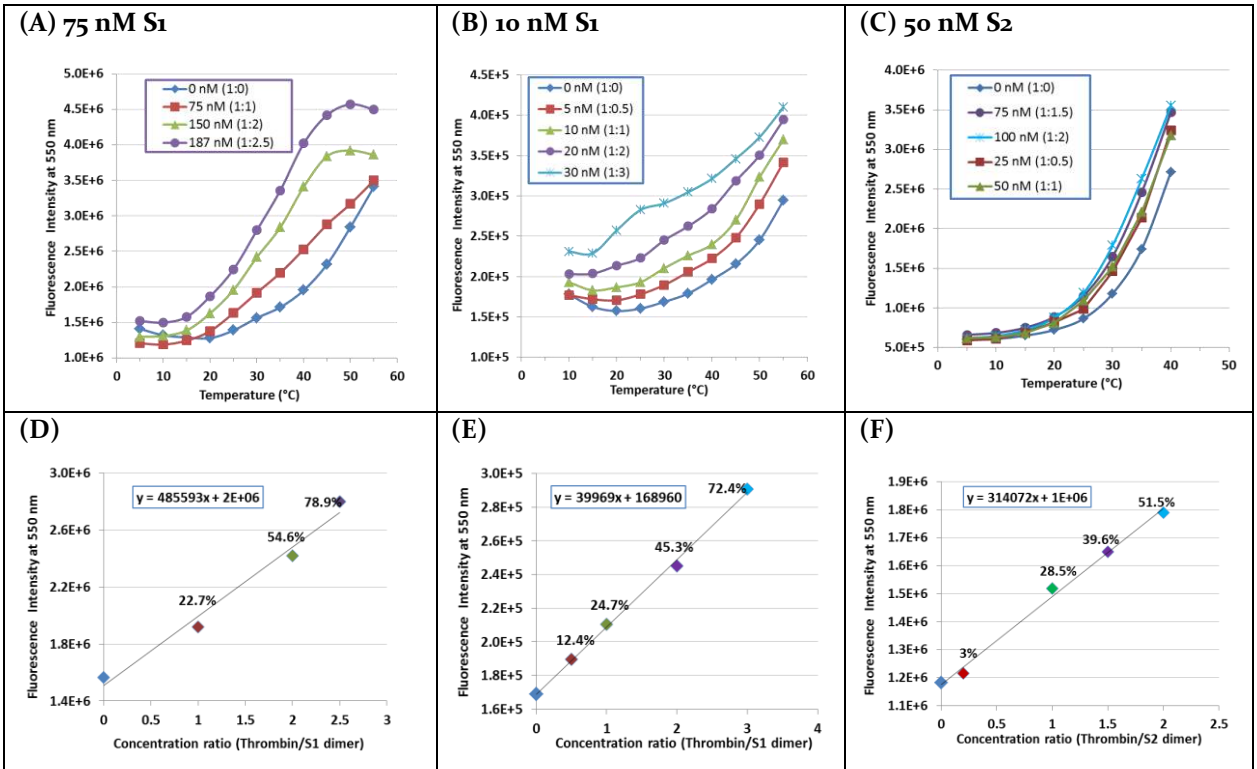

FIGURE 7.15 Thermal denaturation profiles of (A)75 nM S1, (B) 10 nM S1 and (C) 50 nM S2 aptadimers in the presence of various thrombin concentrations. Dependence of fluorescence intensity change of (D) 75 nM S1, (E) 10 nM S1 and (F) 50 nM S2 dimers on the thrombin concentrations at 30 °C. Labels indicate the increment of fluorescence intensity relative to the fluorescence emission of bare dimer structure in the same conditions.

The sensitivity of the fluorimeter machine allowed decreasing of the concentration of fluorescently labeled aptadimer further down. Hence, the second set of experiments now was performed for 10 nM concentration of freshly prepared dimer sample in the presence of 5, 10, 20 and 30 nM concentration of thrombin (Fig. 7.15 (B)). Similarly to the previous experiments, in this case as well, was shown that the shape of the thermal denaturation curve of the stem depends on the concentration of the thrombin. The strength of the fluorescence signal indicated that with the same instrument it is possible to investigate the samples with even lower dimer concentration.

At last we also investigated interaction of freshly prepared 50 nM S2 aptadimer with various concentrations of thrombin (Fig. 7.15 (C)). Although when superposed, it was difficult at first glance to see the difference between the thermal denaturation profiles, however this is only because the change in fluorescence intensifies between closed stem and denatured stem is of larger scale than in the case of S1 structure. If we zoom to only one temperature point, we will be able to see the significant differences between fluorescence intensities of the same structure in the presence of various concentrations of thrombin.

We compared thrombin concentration-dependent changes of the fluorescence to the fluorescence of the bare dimer at 30 °C (Fig. 7.15 (D-F)). This temperature was selected because at this point the stem is still double-stranded for both S1 and S2 structure, the thrombin concentration dependent changes in fluorescence are already significant and the thrombin structure is not denatured. Results reveal that fluorescence signals of the both dimers are sensitive to thrombin, even when thrombin concentration is below than aptadimer concentration. For both aptadimers, interaction with equimolar concentration of thrombin results in 22-30% increase of fluorescence intensity. Furthermore doubling the thrombin concentration leads to increase of fluorescence signal with 45-55% relative to only dimer. Thus, fluorescence response increases linearly with increase of thrombin concentration and it doesn't tend to deviate from the trend even when thrombin exceeds the concentration of aptadimer three times. This fact indicates that, in our experimental conditions[1] the dimer is not getting saturated[2] in the presence of equimolar concentration of thrombin. Complete dimer saturation would require excess thrombin with several fold larger concentration than that of the dimer.

Thus, examining the thermal denaturation profile gave better sensitivity and signal definition than just observation of the fluorescence change at the fixed temperature. We believe that this effect is due to thrombin coordination by the dimer and therefore specific only to thrombin. In order to verify the specificity of the aptadimer we will continue to use the same approach.

[1] 10, 50 or 75 nM concentration of dimer is in the same range of dissociation constants of thrombin aptamers and therefore to affinity of the dimer. The closer the concentration of dimer to the dissociation constant the less thrombin – aptamer pair will be formed at equimolar thrombin concentration.

[2] Under saturation we consider the state of the dimer sample when all the dimers are paired with thrombin.

7.4.4 Interaction of aptadimer with nonspecific proteins

To show that change in fluorescence intensity upon destabilization of the stem is only characteristic of thrombin presence and depends on specific interaction of thrombin and thrombin-sensing regions of aptadimer, we decided to investigate the behavior of the 50 nM S1 aptadimer melting in the presence of prothrombin, serum albumin and diluted plasma.

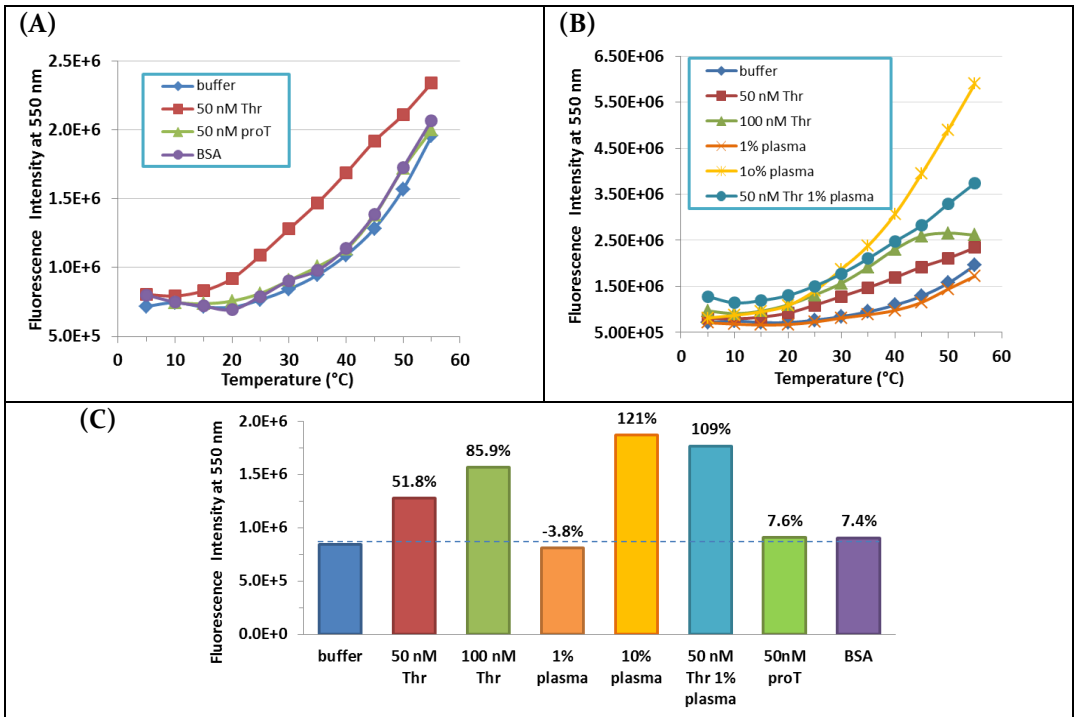

FIGURE 7.16 Thermal denaturation profiles of 50 nM S1 structure in the presence of (A) equimolar prothrombin and excess of BSA; or (B) 100 and 10 fold diluted plasma. (C) Summarized comparison of fluorescence emission intensity at 550 nm and 30 °C. The percentage is calculated relative to fluorescence intensity of only S1 structure in buffer at 30 °C.

Titration of equimolar concentration of prothrombin or excess of BSA didn't induce significant changes in the shape of the stem melting curve and the fluorescence emission intensity at 30 °C was almost identical to that of only dimer. The same result was obtained for the sample with 100 fold diluted murine plasma. Observed results suggested that indeed change of the dimer conformation is specifically dependent on thrombin (Fig 7.16).

However, when the 100 fold diluted murine plasma was spiked with thrombin in equimolar to dimer concentration, observed change in the shape of the curve and the subsequent change in the florescence intensity was comparable of the of 100 nM Thrombin, i.e. the effect was double-enhanced. The enhancement of the fluorescence intensity with more than 120% was observed at 30 °C when 10 fold diluted plasma was introduced in aptadimer sample, indicating that despite the specificity of thrombin-aptadimer interaction, nonspecific interactions still take place with aptamers, affecting the stability of the stem in the similar way as thrombin.

Although the specificity of thrombin detection by means of aptadimer in plasma still remains problematic, preliminary results are promising and further improvement in the dimer structure and assay design give a hope to succeed on this path.

7.4.5 Open questions and encountered problems

This work represents the first attempt to generate smart aptamer dimer for thrombin detection purposes. Being still in the phase of conception, together with the validation of the detection principle, we also faced some problems and open questions that need to be solved and thought on at the following stages of development of the aptadimer-based biosensing. Since the identification of all possible bottle-necks of our approach represents a great and even an essential importance for improving the performance of the dimer, therefore here we intend to highlight open questions, observations, concerns:

1. **Interaction of thrombin with dimer** i.e. how exactly does thrombin interact with dimer:
    a. Can thrombin insert itself within the aptadimer without triggering the fluorescence emission, i.e. without disturbing folding of the stem or changing the distance between the fluorophores? What would be the possible the solution?
    b. How many thrombin molecules can interact with one aptadimer? Can two thrombin molecules simultaneously interact with each of the aptamers of the same dimer? If it is so, what happens with fluorescence signal?
    c. What can be done to assure 1-to-1 interaction between thrombin and aptadimer?
2. Folding of the dimer:
    a. What is the chance of having higher-order complex molecules such as dimer of aptadimers, interconnected with complementary regions? How would this affect interaction with thrombin, the signal generation and the quantification of thrombin concentration? Which approaches could help to examine these questions?
3. **The strength of fluorescence signal**: We performed thrombin-dimer interaction experiments on several instruments. We observed that success of the readout depends on the sensitivity of the fluorimeter. Some instruments allowed sensitive fluorescence measure at 10 nM and even lower concentrations of dimer but required large volume of the sample and we could measure fluorescence signal of only one sample. Whereas other instrument like real time PCR machine, allowed fluorescence detection of several smaller-volume samples (70-100 µL) but required high concentration of the dimer and protein. This point has to be considered when multiplexing the detection.
4. Which additional rules do we need to apply during the design process of the linker in order to get responsive but stable dimers? Should the larger, scaffold-forming sequences be considered as well?
5. It is expensive, time-consuming and difficult to synthetize sufficient concentration of the aptadimer sample with two internally modified nucleotide, would be better to think about approaches like click-chemistry to assemble the dimers with less expensive parts rather than synthetize.

7.5 Conclusions and outlook

In this study we presented our first attempt to design aptamer dimer for recognition and quantification of thrombin. For this purpose, we proposed an integrated approach to design aptadimer structures, which involves the development of new software to predict custom linker sequences obeying defined rules focused on the preservation of aptamer structure and stability. We endorsed dimer folding and confirmed the functionality of aptadimers measuring fluorescence with scanning temperature mode in the presence of specific and nonspecific targets and diluted plasma. The detected specific changes in the fluorescence in presence of thrombin indicated the existence of specific interactions with aptadimer construct.

We believe that this technology is a step forward for developing aptamer-dimer-based sensors, not only for thrombin but also for other targets. This work provides a starting point for merging the principles of DNA nanotechnology with aptameric functions in order to develop specific, performant aptamer-based fluosensors, both for the surface and the volume measurements.

7.6 Acknowledgements

We would like to thank Dr. Serge Mazeres for providing the fluorimeters at video-imaging platform of IPBS-CNRS and for valuable discussions and support in experimental design. We also want to express immense gratitude to Dr. Marie Brut and her students for developing software for dimer spacer prediction.

7.7 References

Ahmad, K.M., Xiao, Y., and Soh, H.T. (2012). Selection is more intelligent than design: improving the affinity of a bivalent ligand through directed evolution. Nucleic Acids Res. 40, 11777–11783.

Fredriksson, S., Gullberg, M., Jarvius, J., Olsson, C., Pietras, K., Gústafsdóttir, S.M., Östman, A., and Landegren, U. (2002). Protein detection using proximity-dependent DNA ligation assays. Nat. Biotechnol. 20, 473–477.

Giusto, D.A.D., Wlassoff, W.A., Gooding, J.J., Messerle, B.A., and King, G.C. (2005). Proximity extension of circular DNA aptamers with real-time protein detection. Nucleic Acids Res. 33, e64–e64.

Hasegawa, H., Taira, K., Sode, K., and Ikebukuro, K. (2008). Improvement of Aptamer Affinity by Dimerization. Sensors 8, 1090–1098.

Heyduk, E., and Heyduk, T. (2005). Nucleic Acid-Based Fluorescence Sensors for Detecting Proteins. Anal. Chem. 77, 1147–1156.

Hianik, T., Grman, I., and Karpisova, I. (2009). The effect of DNA aptamer configuration on the sensitivity of detection thrombin at surface by acoustic method. Chem. Commun. 6303–6305.

Lao, Y.-H., Peck, K., and Chen, L.-C. (2009). Enhancement of Aptamer Microarray Sensitivity through Spacer Optimization and Avidity Effect. Anal. Chem. 81, 1747–1754.

Li, J., Zhong, X., Zhang, H., Le, X.C., and Zhu, J.-J. (2012). Binding-Induced Fluorescence Turn-On Assay Using Aptamer-Functionalized Silver Nanocluster DNA Probes. Anal. Chem. 84, 5170–5174.

Müller, J., Wulffen, B., Pötzsch, B., and Mayer, G. (2007). Multidomain Targeting Generates a High-Affinity Thrombin-Inhibiting Bivalent Aptamer. ChemBioChem 8, 2223–2226.

Müller, J., Freitag, D., Mayer, G., and Pötzsch, B. (2008). Anticoagulant characteristics of HD1-22, a bivalent aptamer that specifically inhibits thrombin and prothrombinase. J. Thromb. Haemost. JTH 6, 2105–2112.

Müller, J., Becher, T., Braunstein, J., Berdel, P., Gravius, S., Rohrbach, F., Oldenburg, J., Mayer, G., and Pötzsch, B. (2011). Profiling of Active Thrombin in Human Blood by Supramolecular Complexes. Angew. Chem. Int. Ed. 50, 6075–6078.

Neundlinger, I., Poturnayova, A., Karpisova, I., Rankl, C., Hinterdorfer, P., Snejdarkova, M., Hianik, T., and Ebner, A. (2011). Characterization of enhanced monovalent and bivalent thrombin DNA aptamer binding using single molecule force spectroscopy. Biophys. J. 101, 1781–1787.

Poniková, S., Tlučková, K., Antalík, M., Víglaský, V., and Hianik, T. (2011). The circular dichroism and differential scanning calorimetry study of the properties of DNA aptamer dimers. Biophys. Chem. 155, 29–35.

Rakhmetova, S.Y., Radko, S.P., Gnedenko, O.V., Bodoev, N.V., Ivanov, A.S., and Archakov, A.I. (2010). Photoaptameric heterodimeric constructs as a new approach to enhance the efficiency of formation of photocrosslinks with a target protein. Biochem. Mosc. Suppl. Ser. B Biomed. Chem. 4, 68–74.

Rinker, S., Ke, Y., Liu, Y., Chhabra, R., and Yan, H. (2008). Self-assembled DNA nanostructures for distance-dependent multivalent ligand–protein binding. Nat. Nanotechnol. 3, 418–422.

Ruiz, C.C., Molina-Bolívar, J.A., Aguiar, J., MacIsaac, G., Moroze, S., and Palepu, R. (2001). Thermodynamic and Structural Studies of Triton X-100 Micelles in Ethylene Glycol–Water Mixed Solvents. Langmuir 17, 6831–6840.

SantaLucia, J. (1998). A unified view of polymer, dumbbell, and oligonucleotide DNA nearest-neighbor thermodynamics. Proc. Natl. Acad. Sci. U. S. A. 95, 1460–1465.

Tian, L., and Heyduk, T. (2009). Bivalent ligands with long nanometer-scale flexible linkers. Biochemistry (Mosc.) 48, 264–275.

OVERALL CONCLUSIONS

The present work was dedicated to investigation of thrombin aptamers and to development of innovative technological bricks which together would drive future advancement in the field of point-of-care devices for continuous monitoring of thrombin in plasma. Real-time detection of free thrombin concentration in blood, has a vital importance for tailoring individual hemostatic or anticoagulant therapy in patients with the risk of developing thromboembolic or hemorrhagic complications

In frame of this Ph.D work, we first tackled fundamental questions of molecular interactions of thrombin aptamers with thrombin, specify towards thrombin in the presence of interfering molecular species such as thrombin precursor prothrombin, thrombin complexes with natural inhibitors ATIII, HCII and A2M, nonspecific molecule serum albumin and complex environment as diluted plasma. Rigorous investigation with surface plasmon resonance revealed that HD1 and NU172 aptamers are interacting not only with exosite I of thrombin, as it was thought before, but also with exosite II and the affinities for both aptamers for both sites are in nanomolar range. These aptamers also demonstrated high affinity towards prothormbin. HD22, on the other hand, showed low nanomolar dissociation constant to thrombin exosite II and no affinity at all to prothrombin. Interestingly none of the aptamers recognized inhibited thrombin, indicating that irreversible binding to its natural inhibitors rendered thrombin exosites inaccessible and allosterically deactivated for interaction with aptamers. Moreover we found out that HD1 is involved in nonspecific interactions with serum albumin. HD1 is unable to identify thrombin in diluted plasma sample, as it gets irreversibly oversaturated by nonspecific interactions even in the presence of nonspecific binding reducing reagent. HD22, on the other hand, didn't show significant interaction patterns neither with BSA nor with diluted plasma in the presence of NSBr. Thus, HD22 proved to be indeed highly affine and specific sensing element for thrombin and showed its advantage over HD1 and NU172 aptamers. These results will have positive impact not only on the field of design of aptasensor for thrombin detection but also on the advancement of basic science.

We also focused our efforts to explore various aptamer immobilization approaches on planar and nanoparticle surfaces of gold and polymer materials. We found that, out of investigated methods, immobilization of thiolated aptamers on gold surface was the easiest and the most efficient functionalization strategies. Immobilized thiolated aptamers were fully functional and the grafting density was optimal for solid state biosensing. Furthermore to achieve nanoscale control of functional aptamer density, we showed advantage of ordered immobilization of DNA-capped nanoparticles on the desired solid support through convective assembly. We investigated the main influencing experimental parameters in order to obtain highly ordered monolayer of aptamer-functionalized 80 nm gold nanoparticles on silica surface for its further application as the part of biorecognition signal transducing element.

Aptamer-modified gold NP-s were also used in aggregation assay, which was first performed to verify functionality of nanoparticle-grafted aptamers. Aggregation of gold

nanoparticles was triggered by simultaneous recognition of the same thrombin molecule by particle-grafted two distinct aptamers. With this assay, we managed not only to detect different concentrations of thrombin (5-500 nM) with good precision, but also to study the thermal stability of the aptamers and their complex with thrombin; and specificity of aptamers towards inhibited thrombin in buffer. In diluted plasma, however aggregation of nanoparticles occurred even in the absence of thrombin, suggesting the presence of nonspecific interactions with aptamers that cannot be controlled or neglected in aggregation assay. Interestingly, results of aggregation assay, showing aggregation of HD1- or NU172-capped gold nanoparticle in the presence of only thrombin helped us to elucidate the real mechanism of HD1 and NU172 interaction with thrombin. These results helped us to apply appropriate fitting model to surface plasmon resonance data and correctly interpret association and dissociation constants of thrombin interaction with HD1 or NU 172. Not only was this assay informative for investigation thrombin-aptamer interactions, but also it promises to be an easy and low-cost tool for detection and characterization any other bivalent target.

Finally we proposed innovative approach of engineering a smart aptadimer of HD1 and HD22 aptamers, allowing detection of thrombin with increased specificity and sensitivity. Aptadimer represents two aptamers interconnected with a nucleic acid spacer, that forms a hairpin with 7 bps. Fluorophore and quencher couple is embedded within this hairpin. In the absence of target, the fluorophore remains quenched, whereas upon capturing the target, fluorescent signal is triggered. Since this strategy requires simultaneous targeting of both binding-sites, it provides an efficient solution for improved thrombin detection, by increasing specificity, selectivity and affinity, and decreasing non-specific interactions. Preliminary tests gave promising results in specific detection of thrombin in 10 times diluted plasma and opened new perspectives for development specific aptamer-based fluosensor both for the surface and the volume measurements. Although further research and development is necessary, this aptadimer technology already offers novel, more powerful approach in detection.

To conclude, the aim of this Ph.D project was achieved. We indeed made big progress in understanding thrombin-aptamer detection problematics and created tools which in near perspective will lead to a successful integration of an aptamer-based thrombin sensor.